Nada är en gemensam institution mellan
Kungliga Tekniska högskolan och Stockholms universitet.

Computational modeling of the lamprey CPG

From subcellular to network level

MIKAEL HUSS

Avhandling som med tillstånd av Kungliga Tekniska högskolan
framlägges till offentlig granskning för avläggande av teknologie doktorsexamen
torsdagen den 14 juni 2007 kl 13.00
i sal FB42, Roslagstullsbacken 21,
AlbaNova, Stockholm.

TRITA-CSC-A 2007:10
ISSN-1653-5723
ISRN KTH/CSC/A--07/10--SE
ISBN 978-91-7178-717-0
© Mikael Huss, maj 2007

Abstract

Due to the staggering complexity of the nervous system, computer modelling is becoming one of the standard tools in the neuroscientist's toolkit. In this thesis, I use computer models on different levels of abstraction to compare hypotheses and seek understanding about pattern-generating circuits (central pattern generators, or CPGs) in the lamprey spinal cord. The lamprey, an ancient and primitive animal, has long been used as a model system for understanding vertebrate locomotion. By examining the lamprey spinal locomotor network, which is a comparatively simple prototype of pattern-generating networks used in higher animals, it is possible to obtain insights about the design principles behind the spinal generation of locomotion.

A detailed computational model of a generic spinal neuron within the lamprey locomotor CPG network is presented. This model is based, as far as possible, on published experimental data, and is used as a building block for simulations of the whole CPG network as well as subnetworks. The model construction process itself revealed a number of interesting questions and predictions which point toward new laboratory experiments. For example, a novel potential role for K_{NaF} channels was proposed, and estimates of relative soma/dendritic conductance densities for K_{CaN} and K_{NaS} channels were given. Apparent inconsistencies in predicted spike widths for intact vs. dissociated neurons were also found. In this way, the new model can be of benefit by providing an easy way to check the current conceptual understanding of lamprey spinal neurons.

Network simulations using this new neuron model were then used to address aspects of the overall coordination of pattern generation in the whole lamprey spinal cord CPG as well as rhythm-generation in smaller hemisegmental networks. The large-scale simulations of the whole spinal CPG yielded several insights: (1) that the direction of swimming can be determined from only the very rostral part of the cord, (2) that reciprocal inhibition, in addition to its well-known role of producing alternating left-right activity, facilitates and stabilizes the dynamical control of the swimming pattern, and (3) that variability in single-neuron properties may be crucial for accurate motor coordination in local circuits.

We used results from simulations of smaller excitatory networks to propose plausible mechanisms for obtaining self-sustaining bursting activity as observed in lamprey hemicord preparations. A more abstract hemisegmental network model, based on Izhikevich neurons, was used to study the sufficient conditions for obtaining bistability between a slower, graded activity state and a faster, non-graded activity state in a recurrent excitatory network. We concluded that the inclusion of synaptic dynamics was a sufficient condition for the appearance of such bistability.

Questions about rhythmic activity intrinsic to single spinal neurons – NMDA-TTX oscillations – were addressed in a combined experimental and computational study. We showed that these oscillations have a frequency which grows with the concentration of bath-applied NMDA, and constructed a new simplified computational model that was able to reproduce this as well as other experi-

mental results.

A combined biochemical and electrophysiological model was constructed to examine the generation of IP_3-mediated calcium oscillations in the cytosol of lamprey spinal neurons. Important aspects of these oscillations were captured by the combined model, which also makes it possible to probe the interplay between intracellular biochemical pathways and the electrical activity of neurons.

To summarize, this thesis shows that computational modelling of neural circuits on different levels of abstraction can be used to identify fruitful areas for further experimental research, generate experimentally testable predictions, or to give insights into possible design principles of systems that are currently hard to perform experiments on.

Sammanfattning

I denna avhandling använder jag datormodellering på flera abstraktionsnivåer för att undersöka egenskaper hos rytmgenererande nervkretsar i ryggmärgen på nejonögat, ett primitivt ryggradsdjur. Nejonögat har länge använts som modellsystem för att förstå hur rörelser (simning i nejonögats fall) alstras av relativt enkla nervkretsar som kallas centrala mönstergeneratorer ("central pattern generators" eller CPG på engelska). Jag har utvecklat en biofysikaliskt baserad datormodell som kan användas till att simulera nervceller i sådana CPG. Modellen innehåller bland annat detaljerad information om kinetiken hos jonkanalerna i cellmembranet. Denna neuronmodell har sedan använts för att undersöka några generella principer för mönstergenerering i ryggmärgen. Bland annat har en storskalig simulation av hela ryggmärgen baserad på neuronmodellen visat att simningsrörelserna kan kontrolleras på ett enkelt men flexibelt sätt, så att aktivering av ryggmärgen nära huvudet är tillräckligt för att styra både framåt- och bakåtsimning. Vi visade i samma studie att ömsesidig inhibition mellan höger och vänster del av ryggmärgen stabiliserar rörelserna och att variation mellan individuella celler gör rörelserna lättare att koordinera. Neuronmodellen användes i en annan studie för att undersöka hur självupprätthållande aktivitet kan uppkomma via synaptiska interaktioner i ett litet excitatoriskt nätverk. En mer abstrakt nätverksmodell visade hur synaptisk dynamik kan leda till bistabilitet mellan ett långsamt och gradvis varierande aktivitetstillstånd och ett snabbt och stereotypt tillstånd. En studie där vi kombinerade experiment och datormodellering visade på några tidigare okända egenskaper för rytmisk aktivitet i enstaka nervceller och ledde till att vi kunde utveckla en matematisk modell som kan förklara experimentella observationer av denna typ av aktivitet. Slutligen konstruerades en hybridmodell bestående av en modell av en biokemisk reaktionsväg (som utmynnar i IP_3-beroende svängningar i kalciumnivån i ryggmärgsceller) och en neuronmodell, så att man kan koppla ihop den biokemiska aktiviteten inuti cellen med den elektriska aktivitet som främst styrs av jonkanaler i cellmembranet.

Acknowledgements

I have had the good fortune to be part of the CBN (formerly SANS) group at KTH. Thanks to all of you. In particular, I thank my supervisors Jeanette Hellgren Kotaleski (main supervisor) and Anders Lansner (co-supervisor), who have been unfailingly helpful and understanding. Thanks also to Sten Grillner, a veritable treasure trove of neuroscience knowledge and anecdotes, and his group at the department of neuroscience at KI, where I have spent part of my time. Some of my work has been done in collaboration with CBN members Fredrik Edin, Alexander Kozlov and Martin Rehn, and KI neuroscience dept. members: former (Kristofer Hallén, Lorenzo Cangiano, Petronella Kettunen, Boris Lamotte d'Incamps) and current (Peter Wallén, Di Wang, Abdeljabbar El Manira, Ebba Samuelsson). Camilla Trané from S3 at KTH was a co-author on one of the papers in the thesis. Credit is also due to other co-authors to papers not included in this thesis: Petter Holme, Karin Nordström, and Hawoong Jeong.

I have learned a lot about science from discussions with current or previous CBN members Örjan Ekeberg, Erik Fransén, Anders Sandberg, Pål Westermark, Christopher Johansson and all of the other PhD and MSc students - sorry about not listing everyone since that would take up half the page! At KI, discussions with Russell Hill and others have enriched my understanding of the lamprey locomotor system.

Some of the people deserving thanks for inspiring me to do research are Joakim Cöster, Rickard Sandberg, Henrik Boström and Lars Asker. I owe old "Molle" friends Erik Arner and Per Lidén thanks for many a pleasant lunch hour. During the last years I have been grateful to Shiro Usui at Riken in Wako-shi, Japan and Beom-Jun Kim at Sungkyunkwan University in Suwon, Korea, for graciously inviting me to their labs. Many thanks also go to Krister Kristensson for providing me with a house to stay in during the Kristineberg Marine Course 2006.

Naturally, a big shout-out to all of my "non-scientific" friends - you know who you are. I know I haven't been in touch much lately because of this thesis ... And deep thanks of course to my family, Lili, Niko and Nova, who saved me from sinking too deep into the scientific bog.

Contents

1 Introduction **1**
- 1.1 Contributions . . . 2
- 1.2 List of articles . . . 3
- 1.3 Articles not in this thesis . . . 3

2 Biological background **5**
- 2.1 Early research on locomotion . . . 5
- 2.2 Central pattern generators . . . 6
- 2.3 The lamprey as a model system for vertebrate locomotion . . . 7
- 2.4 Recurring features of CPGs . . . 9
- 2.5 The lamprey CPG . . . 16
  - 2.5.1 The generation of rhythmic activity . . . 18
  - 2.5.2 Types of CPG neurons . . . 21
  - 2.5.3 Intersegmental coordination . . . 23

3 Computational models in research **25**
- 3.1 What is a (computational) model? . . . 25
- 3.2 What is a computational model good for? . . . 25
- 3.3 Modelling on different levels of description . . . 27
- 3.4 Historical aspects of computational modelling . . . 28
- 3.5 Types of models used in this thesis . . . 29
  - 3.5.1 Compartmental modelling (Hodgkin-Huxley type) . . . 29
  - 3.5.2 Simplified models . . . 30
  - 3.5.3 A biochemical network model . . . 32

4 Research problems addressed **35**
- 4.1 Paper I: A detailed model of a lamprey CPG neuron . . . 35
  - 4.1.1 Motivation . . . 35
  - 4.1.2 Model overview . . . 36
  - 4.1.3 Methodology and practical issues . . . 36
  - 4.1.4 Results . . . 39
  - 4.1.5 Interpretation and caveats . . . 42
- 4.2 Paper 2: Large-scale simulation of intersegmental coordination . . . 43

4.2.1 Motivation 43
4.2.2 Methodology 43
4.2.3 Results 44
4.2.4 Interpretation and caveats 45
4.3 Paper III: Locomotor bouts in hemisegmental networks 46
4.3.1 Motivation 46
4.3.2 Modelling approach 47
4.3.3 Results 48
4.3.4 Interpretation and caveats 49
4.4 Paper IV: Co-existence of a smooth and a stereotypical state 49
4.4.1 Motivation 49
4.4.2 Modelling approach 50
4.4.3 Results 51
4.4.4 Interpretation and caveats 52
4.5 Paper V: An experimentally based model of NMDA-TTX oscillations 53
4.5.1 Motivation 53
4.5.2 Methodology 54
4.5.3 Results 55
4.5.4 Interpretation and caveats 56
4.6 Paper VI: Coupling biochemical and neuronal models 57
4.6.1 Motivation and experimental background 57
4.6.2 Methodology 58
4.6.3 Results 58
4.6.4 Interpretation and caveats 60

5 Conclusions and future work **61**
5.1 Thesis summary 61
5.2 Future work 62
5.3 Closing words 64

Appendix **79**

Chapter 1

INTRODUCTION

The nervous system is a vast and intriguing entity. As a result of hundreds of millions of years of evolution, it has acquired layers upon layers of anatomical and functional components. We are far from understanding the mystery of how human thought and cognition is generated in the brain. An ostensibly simpler part of the central nervous system, the spinal cord, is responsible for generating most of the movements of living organisms. This thesis examines some aspects of neural circuits in the spinal cord of the lamprey - one of the most ancient vertebrates that is still extant. The tool I use for doing so is computational modelling on several different levels.

Since the lamprey is a vertebrate - although a primitive one - it is assumed that some of the knowledge obtained through studying it will be applicable to higher vertebrates, including mammals, and ultimately, humans. With regard to locomotion, it is, together with the *Xenopus laevis* tadpole, the most well-studied vertebrate model system so far, and information from many levels of biology - from single ion channels to swimming behaviour - has been collected. Many of the control principles involved are understood, but interesting questions still remain; I will try to outline some of these in this thesis. In studying the lamprey locomotor system, computational modelling is useful in several ways. First, information from different experimental studies and from different biological levels can be integrated into a coherent framework. Computational modelling can be used to simulate single neurons, locomotor networks, or an entire "virtual lamprey" with muscles and sensory capabilities, swimming in a simulated physical environment. Ultimately, these levels must be reconciled to yield a complete picture. Second, computational modelling can be used to guide new experiments, either by pointing out inconsistencies in the understanding of one of the involved subsystems, or by suggesting novel mechanisms which were not known from previous experiments.

A picture that has emerged over the past decades is that movements are generated using *motor programs* - "a set of muscle commands which are structured

before a movement begins and which can be sent to the muscle with the correct timing so that the entire sequence is carried out in the absence of peripheral feedback" (Marsden *et al.*, 1984). These motor programs are generated by a complicated *motor infrastructure* (Grillner, 2003) involving distributed spinal locomotion modules whose activity patterns can be combined in different ways, depending on the task. The spinal cord itself can thus be seen as a kind of mega-module for generating structured locomotor patterns which can then be dynamically modified according to instructions from the brain in response to changing environmental conditions. It should be added that the spinal cord also contains many of its own fine-tuning mechanisms for adapting the activity patterns in response to incoming sensory data. Not much is known about the identities and locations of locomotor modules in higher vertebrates. In the lamprey, it is easier to isolate and characterize these modules, so that basic principles for their function can be derived and possibly extrapolated to higher vertebrates.

The following exposition assumes that the reader is somewhat familiar with basic components of neurons, like axons, dendrites and synapses, and understands what is meant by e.g. neuronal membrane potential, depolarization, hyperpolarization and action potentials.

1.1. Contributions

- We present a new and biophysically detailed computational model of a generic lamprey locomotor network neuron (Paper I).
- We propose, using simulations, novel central and local control mechanisms for regulating locomotor patterns in vertebrate spinal networks (Paper II)
- We show that reciprocal inhibition, in addition to its role in controlling alternating right-left activity, may also be important for assuring robust control of the swimming pattern in lamprey (Paper II).
- We propose plausible mechanisms underlying “locomotor bouts” in lamprey hemicord preparations (Paper III).
- We propose that synaptic dynamics may be the simplest explanation for the simultaneous existence of different modes of activation in lamprey hemicord preparations (Paper IV).
- We present a simplified conductance-based model that can reproduce the characteristics of NMDA-TTX oscillations in lamprey locomotor neurons and explain novel experimental results derived in the course of the same study (Paper V).
- We present a hybrid model combining a biochemical pathway model of IP_3–mediated intracellular calcium oscillations with an electrophysiological model of a locomotor neuron (Paper VI).

1.2. List of articles

This thesis is based on the following articles.

1. Huss M., Lansner A., Wallén P., El Manira A., Grillner S., and Hellgren Kotaleski J. Roles of ionic currents in lamprey CPG neurons: a modeling study.[1] (2007) *J Neurophysiol* 97, pp. 2696-2711.
2. Kozlov A., Huss M., Lansner A., Hellgren Kotaleski J., and Grillner S. Central and local control principles for vertebrate locomotion. (2007) *Manuscript*.
3. Huss M., Cangiano L., and Hellgren Kotaleski J. Modelling self-sustained rhythmic activity in lamprey hemisegmental networks.[2] (2006) *Neurocomputing* 69, pp. 1097-1102.
4. Huss M. and Rehn M. Tonically driven and self-sustaining activity in the lamprey hemicord: when can they co-exist?[3] (2007) *Neurocomputing* 70, pp. 1882-1886.
5. Huss M., Wang D., Trané C, Wikström M., and Hellgren Kotaleski J. An experimentally constrained computational model of NMDA oscillations in lamprey CPG neurons. (2007) *Manuscript*.
6. Hallén K., Huss M., Kettunen P., El Manira A., and Hellgren Kotaleski J. A model of mGluR-dependent calcium oscillations in lamprey spinal cord neurons.[4] (2004) *Neurocomputing* 58-60, pp. 431-435.

1.3. Articles not in this thesis

The following is a list of peer-reviewed journal articles not included in this thesis.

1. Huss M. and Holme P. Currency and commodity metabolites: Their identification and relation to the modularity of metabolic networks. (2007) *IET Systems Biology*, in press.
2. Huss M. and Nordström K. Prediction of transcription factor binding to DNA using rule induction methods. (2006) *Journal of Integrative Bioinformatics* 3 (online journal, *http://journal.imbio.de/*)
3. Holme P. and Huss M. Role-similarity based functional prediction in networked systems: application to the yeast proteome. (2005) *J R Soc Interface* 2, pp. 327-333.
4. Holme P., Huss M., and Jeong, H. Subnetwork hierarchies of biochemical pathways. (2003) *Bioinformatics* 19, pp. 532-538.

[1] Copyright The American Physiological Society 2007; released as "Free upon publication".
[2] Copyright Elsevier 2006
[3] Copyright Elsevier 2007
[4] Copyright Elsevier 2004

Chapter 2

BIOLOGICAL BACKGROUND

2.1. Early research on locomotion

Up until about a century ago, locomotion - or in more everyday terms, movement from one place to another - was thought to result from chains of reflexes in the spinal cord in response to stimulation of the skin (Philippson, 1905, qtd. in Brown, 1911). For instance, in a walking human, setting down a foot - let's assume the right foot by way of example - on the ground was thought to initiate a sequence of reflexes which would lift the left foot from the ground and perform a cycle of movement by suitably contracting different muscles. When the left foot hit the ground again, a new set of successive reflexes would then cause the right foot to be lifted, and so on. This means that the act of movement would be entirely driven by sensory stimulation in the form of pressure from the ground on the skin of the limbs. However, this picture began to change around 1900. An early key observation was that dogs were able to move their hind legs in a manner reminiscent of walking when held suspended in the air (Freusberg, 1874, qtd. in Brown, 1911). Furthermore, Sherrington (1910) demonstrated that cats and dogs are able to walk even when all sensory nerves are severed from their limbs. Brown (1911) showed conclusively that the mechanism of locomotion in cats could neither be determined by peripheral skin stimuli nor self-generated stimuli intrinsic to the muscles. Sherrington and Brown also showed that locomotor activity can be evoked without input from higher brain centres. Instead, the basic mechanism for the generation of movement is contained within the spinal cord. This was subsequently found to apply to other organisms as well[1]. In other words, locomotion-like activity can be generated purely by neural circuits in the spinal cord, even without any rhythmic stimulation from higher

[1]Maybe not all of them, though. A new study (Song *et al.*, 2007) used gene knockout techniques to find the first apparent example of an organism — the *Drosophila* larva — that seems to need sensory input in order to move. This is in contrast to all other organisms studied so far!

brain centers or from sensory receptors. These neural circuits were later christened "central pattern generators" (see Grillner and Wallén, 1985a, for a review of this concept).

2.2. Central pattern generators

It is important to emphasize that central pattern generators (henceforth abbreviated as CPGs) cannot account for the patterning of movements in a natural setting. What they can do is to generate a kind of template pattern of movement, which is then modified according to sensory input, descending commands from the brain, and so on. Brown's explanation of this point is too eloquent to leave unquoted (Brown, 1911):

> *A purely central mechanism of progression ungraded by proprioceptive stimuli would clearly be inefficient in determining the passage of an animal through an uneven environment. Across a plain of perfect evenness the central mechanism of itself might drive an animal with precision. Or it might be efficient, for instance, in the case of an elephant charging over ground of moderate evenness. But it alone would make impossible the fine stalking of a cat over rough ground. In such a case each step may be somewhat different from all others, and each must be graded to its conditions if the whole progression of the animal is to be efficient.*

The actual identity of the central pattern generator, in terms of the neurons that make it up and their connections to each other, may vary from animal to animal. There is also a slight linguistic ambiguity when using the CPG term - should one regard the spinal motor system as consisting of a single CPG or separate but interacting CPGs (Grillner and Wallén, 1985a)? The appropriate conceptualization may vary from system to system; for instance, some muscles in the locust are thought to be controlled by separate neural circuits, while in other organisms the norm is that circuits are shared, so that overlapping sets of neurons are used in different motor tasks (Pearson, 1993). In the system under study in this thesis — the lamprey — there is good evidence that the swimming CPG can be regarded as continuously distributed over the whole spinal cord. Subnetworks isolated from different parts of the lamprey spinal cord have the ability to generate their own rhythmic activity (Cohen and Wallén, 1980), but there are no strict anatomical borders between distinct subnetworks. It should be noted that CPGs are not only found in the spinal cord; many CPGs for stereotyped motor acts such as breathing and swallowing are located in the brain stem (Grillner, 2006). Also, CPGs are found in invertebrates, which by definition do not even have a spinal cord; some well-studied invertebrate CPGs are the pyloric CPG in the stomatogastric ganglion of the lobster (Marder *et al.*, 2005) and the swimming and crawling CPGs in leech (see De Schutter *et al.*, 2005 and references therein). Thus, CPG is a rather general concept which points to a neural circuit capable of reliably generating a patterned and behaviorally appropriate activity in isolation, no matter the anatomical location of the circuit. Usually,

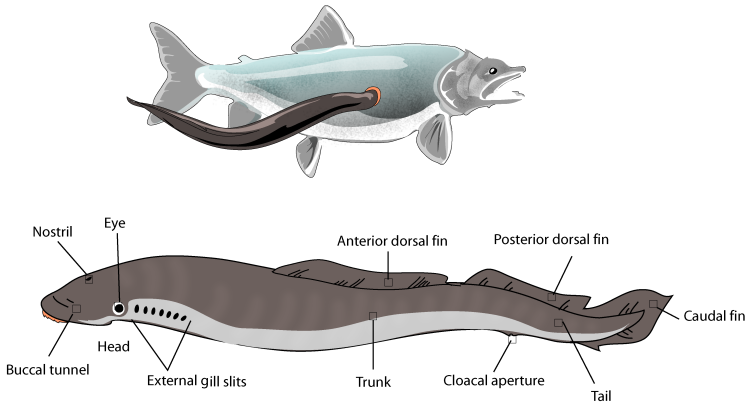

Figure 2.1. *The lamprey feeds on fish by attaching to them with its suction mouth. [Public domain image from Wikimedia Commons.]*

some type of unpatterned (i.e., non-periodic) stimulus is needed to initiate the locomotor-like activity, but it does not determine its shape.

There is also some evidence that CPGs are found in humans (MacKay-Lyons, 2002). For natural reasons, performing experiments to isolate different CPGs in humans are out of the question. Instead, model organisms are used to examine the organization of the locomotor network. It may be noted that descending control from the brain is thought to play a much larger role in humans than in other organisms (MacKay-Lyons, 2002).

2.3. The lamprey as a model system for vertebrate locomotion

The lamprey is a very important model organism for understanding vertebrate motor CPGs (Grillner, 2003). The lamprey is an ancient jawless vertebrate, a cyclostome, which looks similar to an eel. Many species of lamprey exist, but in general they are parasites who feed on host organisms (typically fish) by attaching themselves to the host's body with their round mouths and sucking out body fluids and blood (Fig. 2.1). Lampreys are considered a nuisance in the fishing industry, and fisheries around e.g. the Great Lakes in North America have actively combatted lampreys in their lakes. In some countries, lampreys are considered a delicacy. Indeed, Henry I of England liked to eat lampreys so much that he actually died from ingesting too many of them, or as the saying goes, he died "from a surfeit of lampreys" (Green, 2006).

The lamprey swims with undulating movements produced by a travelling wave of activity that pushes its body through the water. These movements are

generated by spinal CPG networks that coordinate the right and the left sides of the body, so that the muscles on the right and the left side are contracted in an alternating fashion. There is also coordination along the body; during normal swimming, the activity wave starts at the head (the *rostral* end) and propagates toward the tail (the *caudal* end) so that there is a slight time delay between the activation of successive neuronal subcircuits as the wave passes through the body. The reliable propagation of this wave depends on the coordination of these time delays. In a similar manner, the human walking pattern is dependent on a temporally precise sequence of muscle activations.

There are several different reasons to use the lamprey as a model system for locomotion. Perhaps the most important one relates to evolution. The lamprey is, together with the hagfish, the most primitive vertebrate that is still extant. It hasn't evolved much in over 400 million years. This means that the central nervous system (CNS) of the lamprey is likely to be the most primitive version of a CNS that we can examine. Somewhat like a Model T Ford in automobile mechanics, it allows us to look at the simplest known construction for a vertebrate motor system. Furthermore, the lamprey is a good experimental model because its spinal cord is easily accessible to dissection. Because the spinal cord lacks a blood supply, instead being oxygenated from the surrounding cerebrospinal fluid, it can be kept "alive" in an oxygenated chemical bath for several days (Cohen and Wallén, 1980). Motor activity can be elicited in such a preparation by the addition of various chemicals, such as the excitatory amino acids D-glutamate and NMDA (N-methyl-D-aspartate). This form of stimulation is called *bath application* of the chemical in question. The activity observed in response to such stimulation, called "fictive swimming", is similar to activity recorded in an intact, swimming lamprey (Wallén and Williams, 1984) (see Fig. 2.2).

Many important results concerning vertebrate locomotor CPGs have been obtained by studying the lamprey. I will try to outline a few of the results that also hold true for some of the other model organisms examined so far. First, it is useful to know something about the anatomical organization of the lamprey spinal cord. Longitudinally, the spinal cord is divided into about 100 *segments*. These are not strictly defined by any kind of anatomical borders, but rather by the fact that they each send out axons to the same set of *ventral roots* (see below). Transversally, the spinal cord is divided by the midline into two parts; the right and left *hemicords*. Combining the longitudinal and transversal division, we can talk about *hemisegments* - the left and right parts of a single segment. Within each (hemi)segment, there are different kinds of neurons. The sensory neurons transmit information about, for instance, skin pressure and muscle stretching to the central nervous system. The motor neurons send motor commands (in the form of action potentials) to the muscles via axons projecting through the ventral roots, and can therefore be considered the output elements of the motor circuits. Furthermore there are many types of interneurons between the sensory neurons and the motoneurons. More details about these neurons will follow below, after we have considered some common features of CPGs.

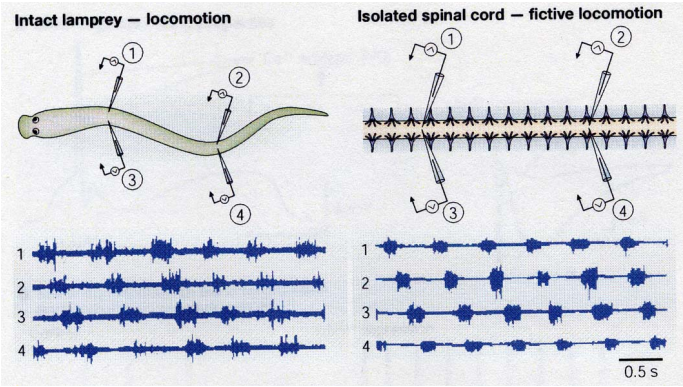

Figure 2.2. *Fictive swimming in lamprey. The same type of electrical activity is recorded from the ventral roots in a live swimming lamprey (left) and in an isolated spinal cord preparation perfused in solution containing stimulating agents (right). The latter type of activity is called fictive swimming. [Adapted by permission from Macmillan Publishers Ltd: Nature Reviews Neuroscience (Grillner, 2003), copyright 2003.]*

2.4. Recurring features of CPGs

It is useful to look at organizational principles known to be important for most or all of the CPGs examined so far. Aside from the lamprey, useful information about CPG organization in vertebrates has been gleaned from e.g. the *Xenopus* frog tadpole (Roberts *et al.*, 1998), cat (Grillner and Zangger, 1979), turtle (Kjaerulff and Kiehn, 1996) and neonatal rat (Mortin and Stein, 1989). For invertebrates, there is a wealth of data from the lobster (Marder *et al.*, 2005), leech (reviewed in De Schutter *et al.*, 2005) and *Clione limacina* mollusc (Arshavsky *et al.*, 1985), among many others. As a sweeping generalization, one might say that invertebrate and vertebrate CPGs are different insofar as invertebrate CPGs tend to have a smaller number of neurons, and that it is easier to identify a distinct function for each of these neurons, while vertebrate CPGs have a more distributed character. However, many of the characteristics of locomotor CPGs are similar across both vertebrate and invertebrate species (Pearson 1993; also cf. chapters 4 and 10 in Stein *et al.*, 1997). Below is a list of features that have been described in many known vertebrate CPGs. Most of them are also found in various invertebrate CPGs. Note that these features are not general in the sense that they are found in *all* vertebrate CPGs — as Pearson (1993) writes, '... CPGs can be assembled in many different ways by using different combinations of basic cellular and synaptic processes in the neurons that make up the CPG network' (p. 267).

The list is purposefully left incomplete, in order to avoid getting bogged down into details, but hopefully it provides a useful reference.

Activation of excitatory amino acid receptors

In living animals, spinal CPGs are activated by a constant and unpatterned (tonic) "input drive" from the brain. In *in vitro* experiments, this drive can be mimicked by applying different kinds of agonists that initiate locomotion. In particular, excitatory amino acids (EAAs) such as glutamate and NMDA can initiate locomotion in vertebrates (Cohen and Wallén, 1980; Poon, 1980). These EAAs can activate the CPGs both via NMDA-, AMPA- (alpha-amino-3-hydroxy-5-methyl-4-isoxazolepropionic acid) and kainate-type glutamate receptors. In the lamprey, either NMDA or D-glutamate can initiate fictive swimming. Bath-applied NMDA is also used as an experimental tool for initiating fictive locomotion in e.g. *Xenopus* embryos and in higher vertebrates such as chick embryo (Barry and O'Donovan, 1987), mouse (Hernandez *et al.*, 1991) and mud puppy (Wheatley and Stein, 1992). Other types of agonists can initiate fictive locomotion in some species: for instance, the dopamine agonist L-DOPA can also evoke locomotor activity in lamprey (Cohen and Wallén, 1980) as well as spinalized cats (Jankowska *et al.*, 1967), 5-HT (serotonin) can induce rhythmic muscle discharges in rabbits (Viala and Buser, 1969), and acetylcholine can cause activation of spinal CPGs in neonatal rats (Smith *et al.*, 1988). However, the excitatory amino acids are fairly generally used receptor agonists for inducing fictive locomotion in a variety of vertebrate species. Note that invertebrates do *not*, in general, seem to have NMDA receptors, so this particular feature is specific to vertebrate motor systems (Mayer and Westbrook, 1987).

Reciprocal inhibition

Arguably the most important design principle used in CPGs is reciprocal inhibition between two subcircuits resulting in alternating activity. This principle was already described by Brown (1911) in the context of cat locomotion. Brown noted that an alternating activity such as one limb being extended while a limb on the opposite side is contracted can be explained by positing a system with a coupled pair of circuits. When one of the circuits (or *half-centers*) is active, it suppresses the other one through inhibiting connections. When the activity is terminated through some process of fatigue (as Brown calls it) the circuit on the opposite side is disinhibited and gets activated, in turn inhibiting the previously active circuit. This cycle is then repeated indefinitely (at least in theory). This conceptual model is called the half-center model.

The half-center model has two central assumptions, and a third assumption that is sometimes included but may regarded as optional. In the half-center model:

1. Reciprocal inhibition between neurons or neuronal circuits is used to ensure alternating activity.
2. Some process of "fatigue" must be posited to explain why the activity of one of the half-centers is eventually terminated.
3. (assumed in most but not all versions) The individual half-centers must not be able to oscillate by themselves.

The "fatigue" process could be due to a variety of mechanisms, including synaptic depression (activity-dependent decrease in synaptic efficacy) or spike frequency adaptation (see Fig. 2.5 and related explanation below). Wang and Rinzel (1992) introduced the concepts of *escape* and *release* to explain different types of activity-terminating mechanisms. These concepts were developed in the context of two mutually inhibitory neurons rather than networks. Escape occurs when a neuron that is being inhibited gets depolarized enough, due to its internal dynamics, to "escape" the inhibition of the opposing cell and cross the voltage threshold required to fire an action potential. Release occurs when the inhibiting neuron terminates its own bursting (for instance, through the build-up of calcium and activation of calcium-dependent potassium channels) and "releases" the opposing neuron so that it can become depolarized and start firing action potentials.

The third criterion, disallowing intrinsically oscillating half-centers, is not always explicitly stated. Given self-oscillating components, the half-center model still explains how alternating activity may arise, although it is no longer necessary for explaining the generation of the rhythmic activity itself.

The first computer simulation using a kind of half-center model seems to have been a study by Reiss (1962), who described both digital and analog simulations in his rather impressive paper. Amongst other things, he noted that the half-center design does not always lead to alternating activity: for some parameter settings, the activity can become synchronized between the half-centers, despite the mutual inhibition, or one of the half-centers may completely suppress the other one. Soon after Reiss' simulations, another modelling study was used to understand the generation of flight patterns in locusts using the half-center concept (Wilson and Waldron, 1968). The first experimental confirmation of the existence of true biological half-center oscillators (defined as fulfilling all three criteria above) was presented by Selverston *et al.* (1983), who investigated cells in the lobster stomatogastric ganglion. By selectively knocking out single neurons in different combinations, Selverston *et al.* showed that there exists a pair of cells that fire action potentials continuously when isolated from each other, but in rhythmic alternating bursts when connected to each other. They also found, however, that there was another type of cell which fired in rhythmic bursts even when isolated - a *pacemaker cell*. Thus this system contains both autonomous and conditional oscillators.

In the lamprey, the half-center principle has been used to understand alternating activity during fictive swimming, when hemisegments in the left and right hemicords alternate so that one side is silent while the other is active. Originally, the reciprocal inhibition was thought to be crucial for rhythm generation, as in the "full" half-center model; today, however, it is thought that the hemicords are able to generate their own rhythmic activity. This will be addressed at length below. Fig. 2.3 shows a conceptual model of how the alternating activity could be achieved in lamprey spinal CPGs: populations of cross-projecting inhibitory interneurons ensure that activity is confined to one hemisegment by inhibiting the other hemisegment while their own hemisegment is active. Excitatory projections within each hemisegment are assumed to activate all types of neuron

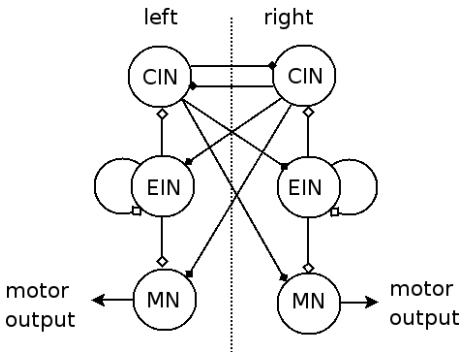

Figure 2.3. *A conceptual "half-center" model of a lamprey spinal cord segment. The midline divides the segment into a left and a right hemisegment. Many cell types are omitted for clarity. EIN = excitatory interneuron, CIN = contralaterally projecting inhibitory interneuron, MN = motoneuron. MN, which directly activate the muscles, are considered to be output elements of the circuit. CIN inhibit all types of neuron on their contralateral side, so that only one of the hemisegments can be "turned on" at a given point in time. EIN provide recurrent excitation to all types of neuron on the same side.*

in the same hemisegment. It should be noted that there are alternative conceptualizations of a segmental lamprey CPG module; a review of such conceptual models can be found in Parker (2006).

Post-inhibitory rebound

Intimately connected to the half-center model is the concept of post-inhibitory rebound, a mechanism whereby a neuron (or a neuronal circuit) which is released from inhibition is activated to a stronger degree than would be expected if it had not been inhibited. This phenomenon, already noted by Sherrington (1910), was shown to be involved in generating patterned motor activity in the *Clione* mollusc (Satterlie, 1985), and subsequently its importance has been stressed in e.g. computational models of *Xenopus* swimming (Roberts and Tunstall, 1990). An inhibited sub-circuit which has the post-inhibitory rebound property is able to "jump-start" its activity as soon as the inhibition from e.g. an opposing neuronal population is lifted, or goes below some threshold level. On the level of a single neuron, post-inhibitory rebound has often been described in terms of inactivating low-voltage activated calcium channels (Matsushima *et al.*, 1993; Tegnér *et al.*, 1997).

Excitatory cores

Many CPGs have been found to contain recurrent excitatory circuits - loops of interconnected neurons where firing activity can be sustained or amplified

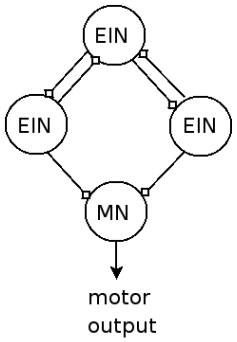

Figure 2.4. *A conceptual "excitatory core" model of a lamprey spinal cord hemisegment. Most types of neuron are omitted for clarity. EIN = excitatory interneuron, MN = motoneuron. Recurrent excitatory connections between EIN generate a rhythm based on single-spike synchronization. The output of the recurrent excitatory network is fed to the MN and subsequently to the muscles.*

through positive feedback. Activity can then be maintained long beyond the end of some transient stimulus to the circuit neurons. This kind of reverberatory circuit could be built using excitatory synaptic transmission or electrical synapses (gap junctions) between the neurons. In *Clione*, both excitatory synaptic transmission and tight electrical coupling between interneurons are involved in generating reverberatory activity (Satterlie, 1985). Excitatory interneurons in *Xenopus* form a similar type of network (Roberts *et al.*, 1995). Interestingly, in *Xenopus*, the motoneurons also feed back onto the interneurons (and to other motoneurons) using (cholinergic) excitatory transmission and electrical coupling, adding another level of re-excitation (Roberts *et al.*, 1998). In both *Clione* and *Xenopus*, alternating activity between the excitatory circuits is thought to be achieved through a combination of cross-inhibition and post-inhibitory rebound. In lamprey, modelling studies suggested that a type of recurrent excitation could be operating in hemisegmental networks (Lansner *et al.*, 1997; Lansner *et al.*, 1998). This prediction was subsequently verified in experiments (Cangiano and Grillner, 2003). Lamprey hemicord preparations are able to generate rhythmic bursting, which is probably mostly due to mutual re-excitation between excitatory interneurons which feed their output to motoneurons (see Fig. 2.4). It has been proposed that networks of this type, called *excitatory cores*, are also found in parts of the cerebral cortex. This is one of many analogies that can be drawn between spinal CPG circuits and cortical networks (Yuste *et al.*, 2005).

Membrane properties

Plateau potentials

Locomotor activity is rhythmic, but what is the source of this rhythmicity? Perhaps over-simplifying a bit, one might contrast two different hypotheses: either the rhythmic activity is an intrinsic property of (some of) the CPG neurons, or the rhythmicity only arises as a consequence of the concerted activity of the connected CPG network. Perhaps, in many cases, the most plausible explanation is a combination of single-cell and network properties (see e.g. Selverston *et al.*, 1983, for a concrete example of a network where both principles are known to operate). In any event, CPG neurons from many different systems display an intrinsic oscillatory property in that they can generate so-called plateau potentials, often when stimulated by bath NMDA application. Such plateau properties have been found in lamprey (e.g. Grillner and Wallén, 1985; Wallén and Grillner, 1987), frog tadpoles (Sillar and Simmers, 1994), turtles (Guertin and Hounsgaard, 1998), neonatal rats (MacLean *et al.*, 1997) and many other organisms. In most cases, the oscillatory activity has been linked to a specific property of NMDA receptors: the magnesium block. When a neuron is resting, or close to its resting potential, its NMDA receptors are typically mostly blocked by magnesium ions (Nowak *et al.*, 1984). This blockage is voltage-dependent, so that when the membrane potential is depolarized, the magnesium ions tend to unbind from the NMDA receptors. These can then pass more (depolarizing) current. In this way the depolarization leads to a self-reinforcing positive feedback loop that causes a quick jump in membrane potential, thereby initiating the plateau potential. Slower hyperpolarizing processes then set in and eventually terminate the plateau potential, taking the cell back to near resting potential, after which the cycle can start again. In some preparations, alternative explanations have been put forward; in turtles, for example, the generation of plateau potentials has been linked to an L-type calcium current rather than the NMDA magnesium block (Guertin and Hounsgaard, 1998). Paper V in this thesis attempts to better characterize plateau potential generation in lamprey CPG neurons.

Transmitter modulation

CPG circuits in both invertebrates and vertebrates are affected by many kinds of chemical modulation through the action of various transmitter substances. This modulation occurs when neuromodulating substances bind to receptors that subsequently activate intracellular biochemical pathways, which in turn can modify membrane properties. Dopamine, 5-HT, acetylcholine and substance P are only a few of the neurotransmitters that have been shown to act in modulating CPG activity. In lamprey, dopamine has complex effects which may differ depending on the type of neuron under modulation (Buchanan, 2001; Svensson, 2003). 5-HT also has diverse effects in lamprey spinal neurons - it has been found to slow down fictive swimming and to reduce the current carried through N-type calcium channels (Hill *et al.*, 2003), but also to presynaptically inhibit neurotransmitter release (Schwartz *et al.*, 2005). Furthermore, it

has been shown to reduce the slow afterhyperpolarization and depress synaptic transmission in three types of segmental interneurons (Biró *et al.*, 2006). γ-aminobutyric acid (GABA) modulation has been found to operate during fictive swimming; for example $GABA_B$ receptor activation is involved in presynaptic inhibition (Alford and Grillner, 1991), presumably through down-regulation of voltage-dependent calcium channels (Grillner, 2003). Substance P increases the frequency of network activity in lamprey through a variety of different effects which may vary between cell types (Parker, 2006). Many other types of neuromodulation, involving e.g. different types of metabotropic glutamate receptors (El Manira *et al.*, 2002; Kettunen *et al.*, 2002), have also been examined in lamprey.

Frequency regulation

Most neurons communicate (in general) by action potentials ("spikes"); in motor systems, motoneurons activate muscles by sending isolated spikes or groups of spikes (bursts). To fine-tune the commands to the muscles, it is then important that the neurons be able to regulate their firing frequency. In spinal motoneurons, repetitive firing is typically controlled by the "slow AHP" (sAHP) following action potentials. During the sAHP, the membrane potential is depressed, usually due to the action of calcium-dependent potassium currents which are activated following the influx of calcium that occurs during an action potential. (In the lamprey, sodium-dependent potassium currents have also been shown to be involved in generating the sAHP (Grillner, 2003)). During the inter-spike interval, the effective calcium concentration decays as calcium is removed from the membrane by different mechanisms. The calcium-dependent potassium channels will therefore get successively less activated, until the depolarization starts to dominate and leads to the next spike. In this way, the sAHP introduces a time delay before the neuron can fire the next spike. The phases of repolarization in a lamprey CPG neuron can be seen in Fig. 2.5a. After the spike has reached its peak, the membrane potential rapidly falls down to a hyperpolarized level. This is called the *fast afterhyperpolarization* (fAHP). It may then, such as in the case shown, display an *afterdepolarization* (ADP), where the membrane potential is briefly depolarized from the fAHP level. This is followed by the more lengthy sAHP, which hyperpolarizes the neuron for a longer time and thus participates in regulating the time that passes until the next spike. Fig. 2.5b illustrates the phenomenon of *spike frequency adaptation*. This means that the interval between spikes successively grows, which can happen because of sAHP summation due to progressive accumulation of calcium (and, in the lamprey, probably also sodium) ions. Many neurotransmitters (for example 5-HT in lamprey; Biró *et al.*, 2006) affect the sAHP, thereby allowing a fine control of the firing frequency. In the lamprey, the sAHP has been linked to the termination of locomotor bursts, first through computational modelling (Grillner *et al.*, 1988; Hellgren *et al.*, 1992) and later using experiments (Hill *et al.*, 1992). Further modelling studies have addressed e.g. the possibility of dynamic sAHP regulation as a crucial factor in pattern generation (Ullström *et al.*, 1998).

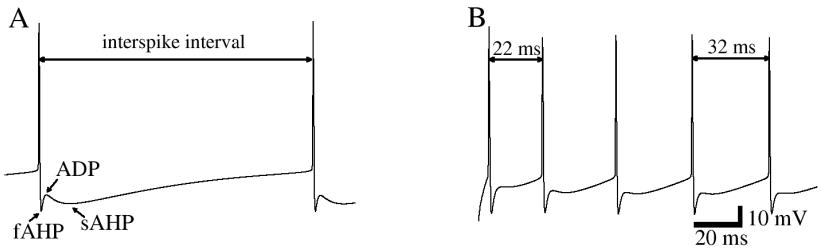

Figure 2.5. *(A) The repolarization phase in the (model) neuron shown here consists of a fast afterhyperpolarization (fAHP), a subsequent afterdepolarization (ADP), and finally a slow afterhyperpolarization (sAHP). (B) Spike frequency adaptation. The firing frequency in this (model) neuron gradually decreases; the first interspike interval is shorter than the following ones.*

Synaptic plasticity and homeostasis

It should not be forgotten that CPG networks are far from static. They contain many adaptive and homeostatic features, of which neuromodulation (mentioned above in connection with membrane properties) is one. As an example of homeostasis, Marder and Prinz (2002) describe experiments where intrinsically bursting cells from lobster CPG networks were removed and plated individually in culture. The neurons then became silent (i.e. they stopped firing), but over the course of three days, they recovered their ability to generate bursting patterns by adjusting the densities of different ion channels. Another type of adaptive change is synaptic plasticity - activity-dependent changes in synaptic efficacy. Virtually all synapses are subject to some kind of dynamic regulation (Zucker and Regehr, 2002). In the lamprey, Parker and Grillner (2000b) described several kinds of short-term synaptic plasticity, including synaptic depression (activity-dependent decrease in synaptic efficacy) between excitatory segmental interneurons and facilitation (increase in efficacy) in synapses from one type of inhibitory interneuron to another type. Also, synapses between excitatory and inhibitory segmental interneurons were sometimes facilitated and sometimes depressed. Later, Parker (2003a) also showed that inputs from excitatory interneurons to motoneurons are usually depressed during spike trains.

2.5. The lamprey CPG

The lamprey is, together with the *Xenopus* embryo, the model system which has shed the most light on detailed cellular and circuit properties of vertebrate CPG networks. Many important experimental findings were first published for the

lamprey: for instance, the importance of excitatory amino acid receptors for locomotion (Cohen and Wallén, 1980) and the presence of intrinsic, NMDA-driven plateau potentials in CPG neurons (Grillner and Wallén, 1985b). Many studies have described e.g. the behaviour of the lamprey CPG in response to neurotransmitters and -modulators (see Svensson *et al.*, 2003, for a good overview), the intersegmental coordination in swimming (see e.g. Matsushima and Grillner, 1990; Matsushima and Grillner, 1992; Sigvardt and Williams, 1996; Tegnér *et al.*, 1993; Williams and Sigvardt, 1994), post-inhibitory rebound (Matsushima *et al.*, 1993; Tegnér *et al.*, 1997), turning behaviour (e.g. Fagerstedt and Ullén, 2001; Fagerstedt *et al.*, 2001), detailed characteristics of membrane currents (e.g. El Manira and Bussières, 1997; Hess and El Manira, 2001; Hess *et al.*, 2007), anatomical organization of the CPG (e.g. Rovainen, 1979; Rovainen, 1983) and many more topics. Also, numerous computational modelling studies, both on a more abstract level (e.g. Buchanan, 1992; Cohen *et al.*, 1982; McClellan and Hagevik, 1997; Williams *et al.*, 1990) and on a more biophysically detailed level (e.g. Grillner *et al.*, 1988; Brodin *et al.*, 1991; Ekeberg *et al.*, 1991; Grillner *et al.*, 1988; Hellgren *et al.*, 1992; Hellgren Kotaleski *et al.*, 1999a; Hellgren Kotaleski *et al.*, 1999b; Lansner *et al.*, 1997; Lansner *et al.*, 1998; Kozlov *et al.*, 2001; Kozlov *et al.*, 2007; Tråvén *et al.*, 1993; Ullström *et al.*, 1998; Wadden *et al.*, 1997; Wallén *et al.*, 1992) have been used to glean even more insights. In addition, neuromechanical models incorporating muscle activation, sensory feedback and water forces have been developed (Ekeberg, 1993; Ekeberg and Grillner, 1999). Physical lamprey robots have also been built by Ayers *et al.* (2000) and Crespi *et al.* (2005). Some of the relevant findings from the studies listed above have been described in the preceding text. Let us now take a somewhat closer look at lamprey CPG networks as they are currently understood.

As mentioned earlier, the spinal cord of the lamprey consists of approximately 100 segments. Figure 2.6 (from Grillner, 2003) shows a graphical representation of some of the relevant components of one segment in the lamprey locomotor network.

The left and right hemisegments are enclosed by boxes. A segment receives input from the so-called command regions, the mesencephalic and diencephalic locomotor regions (abbreviated MLR and DLR) via reticulospinal (RS) neurons in the brainstem (Grillner, 2003). On an even higher level, the basal ganglia modulate the activity of the locomotor command regions. The reticulospinal (RS) neurons synapse on excitatory receptors in the spinal segment. There are also ascending projections from spinal to RS neurons (Kasicki *et al.*, 1989); the interplay between feedforward (RS to spinal) and feedback (spinal to RS) projections has been suggested to dynamically stabilize the motor pattern (Wang and Jung, 2002). The CPG neurons also receive sensory excitatory and inhibitory input from stretch receptors (SR-E and SR-I), also called edge cells. The activity of these cells in response to sensory input can have profound effects on the motor

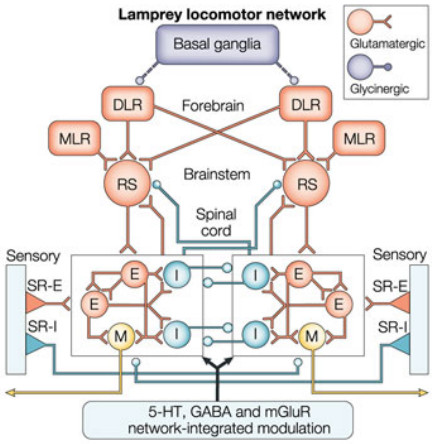

Figure 2.6. *A graphical representation of some important components of the lamprey CPG network. Reticulospinal neurons activate the segmental CPG, which also receives sensory input. The segmental CPG consists of mutually inhibiting hemisegments containing inhibitory and excitatory interneurons. Motoneurons send motor commands to muscles. [Adapted by permission from Macmillan Publishers Ltd: Nature Reviews Neuroscience (Grillner, 2003), copyright 2003.]*

pattern: if they are rhythmically stimulated, the pattern generated by the CPG will be entrained to the stimulation frequency (Grillner, 2003).

The output from the segmental module is the activity of the motoneurons, which project through the ventral roots (not shown) to the muscles. CPG neurons also receive modulatory input, as mentioned earlier.

Before going into details about the types of neuron contained within the segmental networks, let us review some results about rhythm-generation in segmental and hemisegmental spinal preparations.

2.5.1. The generation of rhythmic activity

It has long been known that preparations consisting of just a few spinal segments, down to 1.5 segments (Wallén *et al.*, 1985), can show rhythmic activity in the form of bursts of action potentials, alternating between the left and the right side of the segment. Glycinergic inhibitory transmission was shown to be necessary for the alternation of activity (Alford and Williams, 1989), and contralaterally projecting interneurons (i.e., interneurons that project between opposing hemisegments) are the most likely source of this inhibition. However, from early experimental results it was not clear whether the reciprocal inhibition between hemisegments was a necessary condition for the rhythmic activity to appear, or if it was just a prerequisite for the alternation of activity. One

study (Buchanan, 1999) suggested that the reciprocal inhibition implemented by crossing interneurons was necessary for the generation of rhythmic activity.

However, earlier modelling studies of the lamprey CPG (Lansner *et al.*, 1997; Lansner *et al.*, 1998) had put forward the suggestion that hemisegmental "excitatory cores" could generate the basic rhythmicity, meaning that the cross-connections would modify the rhythm rather than creating it. This prediction led to experimental investigations using a technique where the spinal cord was transected at or close to the midline. These studies showed that rhythmic bursting *can* be induced in hemisegmental preparations, down to a single hemisegment (Cangiano and Grillner, 2003; Cangiano and Grillner, 2005). This means that the crossing inhibition is indeed not required for rhythm generation. In the hemisegmental bursting, of course, there was no alternation between right and left sides, but the bursting pattern observed was linked to segmental bursting by partially transecting the cord in several steps. Two different types of bursting were found in hemisegmental preparations: a fast rhythm (about 2-12 Hz) and a slow rhythm (0.1-0.4 Hz). The faster rhythm was evoked by bath-applied D-glutamate (and in some cases by NMDA as well), and it was this rhythm that was linked to fictive swimming. The experiments showed that the frequency of the rhythm increased as a function of degree of transection, so that pure hemisegments had the fastest rhythm and the pure segments had about 3 to 4 times slower frequencies (Cangiano and Grillner, 2003). The slower rhythm was evoked by NMDA and was dependent on the magnesium block of the NMDA receptor. However, this rhythm took a long time to develop and could not be linked to fictive swimming.

Additional experiments showed that the hemisegmental bursting rhythm could be induced even when glycinergic transmission was blocked – in fact, the frequency of the rhythm was not appreciably changed during these conditions (Cangiano and Grillner, 2003). Therefore it was concluded that hemisegmental EIN, connected into a recurrent network, was the likely source behind the rhythmic bursting. This circuit would then be a kind of excitatory core, as discussed above. As yet, little is known about the interconnections of the EIN in a hemisegment. Cangiano and Grillner (2005) noted that only part of the recorded cells (including EIN) were activated during rhythmic bursting. This finding, considered together with the large variety of EIN cells could mean that there is a continuous recruitment of EIN, or that there are subpopulations of EIN which may be recruited in different contexts. Interestingly, at least two modeling studies had previously suggested that EIN may not be required for rhythm generation in the lamprey locomotor network given reciprocal inhibitory connections between hemisegments (Ijspeert *et al.*, 1999; Jung *et al.*, 1996).

Apart from NMDA and D-glutamate stimulation, a transient electrical current injection was also shown to reliably induce rhythmic bursting in hemisegmental preparations (Cangiano and Grillner, 2003; Cangiano and Grillner, 2005). This is remarkable since the same phenomenon has not been observed in segmental preparations. The rhythmic activity in response to a current injection is self-sustaining: it continues far beyond the extent of the stimulation signal (300 ms), typically lasting for several minutes. This type of self-sustaining bursting is

called a "locomotor bout". An experimental recording of the activity of a neuron during a locomotor bout in a lamprey hemicord preparation is shown in Fig. 2.7.

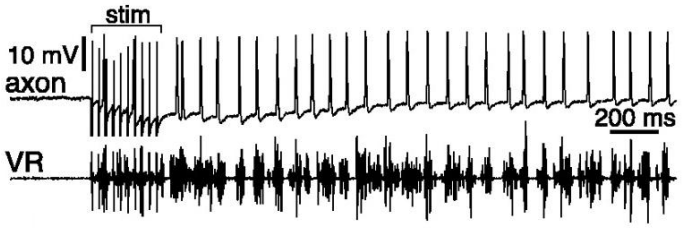

Figure 2.7. *Neuronal activity during a locomotor bout in a lamprey hemicord preparation (modified from Cangiano and Grillner, 2005). The upper trace shows the membrane potential in a neuron, and the lower trace a burst pattern recorded from a ventral root. After an initial current pulse, the neuron continues to spike rhythmically, although at a lower frequency than during the pulse. The neuron's spikes are in phase with the ventral root bursts; it fires only one spike per locomotor burst. [From Cangiano and Grillner (2005). Copyright 2005 by the Society for Neuroscience]*

Interestingly, the activity of individual neurons during locomotor bouts seems to be different from the activity during segmental bursting. During locomotor bouts, neurons almost always fire a single action potential during each bursting cycle. Thus, the burst that is recorded from the ventral roots is in fact a "population burst", composed of single spikes fired at slightly different times (although they are, overall, fairly synchronized). In contrast, in segmental bursting (regular fictive swimming) neurons often fire bursts of spikes (Buchanan and Cohen, 1982; Cohen and Wallén, 1980). A conceptual sketch of the hemisegmental burst as an emergent population burst is shown in Figure 2.8.

Spiking in different EIN is synchronized by fast excitatory (AMPA) synaptic transmission; single MN spike once in each cycle and their population activity is recorded in the ventral roots as a burst. The time between successive spikes in EIN is, according to this model, primarily dependent on their sAHP.

The experimental papers describing locomotor bouts did not contain detailed explanations of the possible mechanisms involved in their generation, although it was noted that AMPA synaptic transmission was necessary (presumably because of their role in synchronizing EIN spiking). In Paper III, we use a network model with realistic model neurons to examine some possible mechanisms.

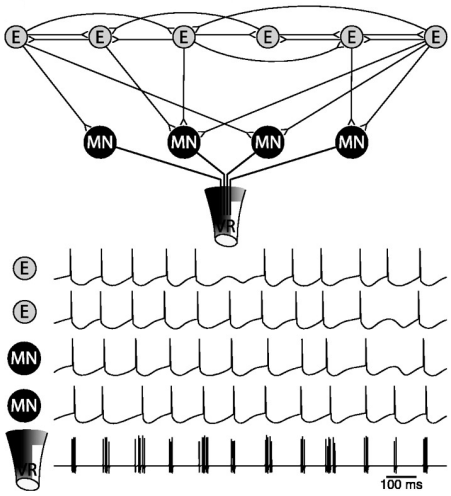

Figure 2.8. *A conceptual sketch of ventral root bursts generated by synchronized single spikes during locomotor bouts in hemisegmental networks. Upper part: Reciprocally connected EIN project to MN, the activity of which is recorded from the ventral roots. Inhibitory cells are not included because they were not necessary for burst generation. Lower part: EIN and MN fire single spikes during a bursting cycle. EIN synchronize their spikes by fast synaptic transmission, and the interspike interval is determined mostly by their sAHP. MN receive input from EIN and spike at slightly different points in time. This leads to the appearance of bursts in a VR recording. [From Cangiano and Grillner (2005). Copyright 2005 by the Society for Neuroscience]*

The self-sustaining bursting in lamprey is faster than EAA-induced bursting (up to 20 Hz or more), which is in itself intriguing – if the network is capable of operating at such high frequencies without external input, why doesn't it go to this high-activity state when it does receive input? This is the question we address in Paper IV.

2.5.2. Types of CPG neurons

The cartoons of the segments and hemisegments shown so far have included three groups of neurons: excitatory and inhibitory interneurons and motoneurons. Thinking in terms of these neuronal groups is sufficient to understand the current conceptual models of rhythm generation, but it should be pointed out that these groups can be partitioned into subtypes of neurons, and that other kinds of neurons are also found in the segmental networks.

Sensory neurons

Sensory cells are not considered to belong to the CPG network *per se*, and therefore they will not be considered from here on. Primary among the known sensory

cells in the lamprey spinal cord are edge cells, which sense the lateral movement of the spinal cord, and dorsal cells, which sense touch and pressure (Parker and Grillner, 1996).

Interneurons

It is useful to divide the spinal interneurons into excitatory and inhibitory interneurons. Excitatory interneurons were characterized in early experimental studies (Buchanan and Grillner, 1987; Buchanan *et al.*, 1989). There are both ipsilateral (i.e., projecting to the same side of the spinal cord) and contralateral (projecting to the opposite part of the cord) types of EIN (Biró *et al.*, 2006). EIN are heterogeneous, with a large spread in properties such as input resistance and firing properties (Buchanan, 1993; Cangiano and Grillner, 2005; Parker and Bevan, 2007).

Inhibitory interneurons can be subdivided into several categories. There are larger contralaterally and caudally projecting interneurons (CCIN) which have been divided into two types (CC1 and CC2 inhibitory interneurons) based on morphological considerations and innervation (Buchanan, 1982). Their number has been estimated to be 10 to 20 per hemisegment (Buchanan, 1982). Moreover, there are smaller contralaterally projecting inhibitory interneurons (ScIN), which are thought to be more numerous - they may make up half of all the 400-600 interneurons estimated to be present in a hemisegment (Ohta *et al.*, 1991). All types of contralaterally projecting inhibitory interneurons are candidates for being part of the segmental CPG network, as they could mediate the reciprocal inhibition responsible for generating alternating activity. However, it is at present unclear what the relative contributions of the larger and less numerous CCIN and the smaller and more numerous ScIN might be (Buchanan, 1999; Parker, 2006).

Small ipsilaterally projecting inhibitory interneurons (SiIN) have also been found (Buchanan and Grillner, 1988). They may not be necessary for the generation of rhythmic activity in a hemisegmental preparation (Cangiano and Grillner, 2003) although they are likely involved in shaping this activity. There is evidence that the inclusion of inhibitory interneurons can make an excitatory network more robust and enable smoother grading of activity (Chance *et al.*, 2002).

One additional type of inhibitory interneuron, the lateral interneuron (LIN) is found in rostral parts of the spinal cord (Buchanan and Cohen, 1982). In some conceptual models (e.g. Buchanan, 2001), these neurons are considered to be part of the segmental CPG network, but there is some evidence to make this unlikely: the LIN have long axonal projections rather than projecting within their own segment, and since they are localized to the rostral part of the spinal cord, they cannot be a general feature of the segmental CPG networks. A modeling study (Hellgren *et al.*, 1992) showed that LIN need not be included in a network model to explain generation of alternating rhythmic activity. Experimental evidence also suggests that rhythmic activity can be elicited in segments from which LINs are absent (Rovainen, 1983).

Finally, giant interneurons (GI) are unusually large cells within the main column of cell bodies (Christensen, 1983). Since GI activity is not correlated to locomotor activity, these cells are not considered to be part of the CPG network.

Motoneurons

The motoneurons can be divided into myotomal motoneurons (MMN), projecting to the muscles, and fin motoneurons (FMN), projecting to the fins (Krause, 2005). These may or may not be considered to be part of the CPG – if motoneurons are considered to be purely output elements that relay the rhythm generated by interneuronal networks, they would strictly speaking not belong to the CPG. This view is supported by early experimental evidence (Wallén and Lansner, 1984). More recently, it was proposed that motoneurons may nevertheless have cholinergic back-projections to interneurons in the CPG in some cases (Quinlan *et al.*, 2004). If so, motoneurons would have to be considered part of the CPG network.

2.5.3. Intersegmental coordination

We have looked in some detail at the neuronal types and rhythm-generating circuitry in segments and hemisegments. But what about the interaction between segments? Research into *intersegmental coordination* in the lamprey CPG has been going on since 1980, when Cohen and Wallén reported that the pattern-generating capability was distributed over the whole spinal cord and that the time delay between segment activations was linearly related to the cycle period. (As mentioned earlier, an activity wave passes through the spinal cord when the lamprey is swimming, and consecutive segments are recruited with a time delay). The *intersegmental phase lag* is equal to this time delay divided by the total locomotor cycle period. Wallén and Williams (1984) reported that during forward swimming, the intersegmental phase lag is approximately constant and equal to about 1% of the total cycle time, independent of locomotor frequency. Thus the absolute time delay is adaptively controlled to match the swimming speed. Similarly, human walking or running requires that muscles are activated in a precise sequence relative to each other, but the actual time that passes between muscle contractions is shorter when we are running faster. Cohen *et al.* (1982) presented the first mathematical model for describing the intersegmental coordination in fictive swimming using coupled limit-cycle oscillators. Later modelling studies using similar coupled-oscillator models led to the conclusions that asymmetric functional coupling between segments was important, with ascending coupling setting the intersegmental phase lags and descending coupling changing the frequency of the coupled oscillators (Williams *et al.*, 1990). Matsushima and Grillner (1990) proposed a conceptual model, "the trailing oscillator hypothesis", in which a local increase in excitability could initiate a traveling wave producing the correct phase lags, even when assuming symmetric coupling. These apparently contradictory hypotheses can in fact be reconciled at least in some respects, and the differences in the conclusions are partially due to the fact that they approach the problem in different ways.

An interesting study that used genetic algorithms to "breed" control networks for lamprey swimming based on Ekeberg's neuro-mechanical model (Ekeberg, 1993) was able to produce the appropriate phase lags over a wide frequency range using a combination of asymmetric coupling and local excitability increases (Ijspeert *et al.*, 1999). Biophysically inspired models, e.g. Wadden *et al.* (1997), Hellgren Kotaleski *et al.* (1999a), Hellgren Kotaleski *et al.* (1999b), were developed accordingly to examine the trailing oscillator hypothesis combined with asymmetric coupling. These models could correctly account for some aspects of intersegmental coordination, but a persistent problem was that the intersegmental phase lag tended to vary with swimming frequency. In Paper II, we present a new simulation model where this problem is rectified, and present a conceptual explanation of how it may be solved by the lamprey spinal CPG.

Chapter 3

COMPUTATIONAL MODELS IN RESEARCH

3.1. What is a (computational) model?

A model can be defined as an object - real or imaginary - which represents another object. For the model to be meaningful, the representing object should share some characteristics with the represented object. If the model is an imaginary construct, it is called an abstract model. Abstract models attempt to represent the important characteristics of the modelled system (so they are usually simplified) and can be used for theorizing within a logical framework. A mathematical model is a special kind of abstract model, and a computational model is really just a mathematical model implemented on a computer.

It should be emphasized that, because of the necessary simplification and abstraction involved in constructing a computational model, as well as the possibility of yet-to-be-discovered information crucial for understanding the modelled system, **a model is never true**. The model should never be confused with the actual system - or as Alfred Korzybski (the inventor of general semantics) put it (Korzybski, 1948):

> *The map is not the territory.*

3.2. What is a computational model good for?

Why, then, should one use computational models to address questions in neuroscience (and other fields)? A very good question, which has many answers.

- Dealing with complexity

Neural systems are so complicated that the human mind could not possibly be able to predict their outputs in response to arbitrary inputs. This means

that computer simulations are helpful in deriving conclusions about the workings of this huge, interconnected system. However, it is also certainly the case that so much remains unknown about the working of the nervous system that we cannot hope to be able to build extremely accurate simulation models of it today. Instead, models must be abstracted to a level appropriate for the specific question being asked. In general, it is desirable to have an explicit question in mind when one starts to construct a model.

- Integrating information about a system

A computational model can work as a platform for unifying disparate experimental data (perhaps from different levels of description; see below) in a consistent manner. This leads to the next point,

- Checking conceptual models and revealing assumptions

Scientists always work with models, though they may not be explicitly stated. Hypotheses about the nervous system are formulated in words, and all neuroscientists probably have an internal model of the workings of the brain or of some subsystem that they are interested in. However, such verbal, qualitative models are necessarily vague and potentially inconsistent. Often, many assumptions are hidden in these models. One of the greatest advantages of a computational model is that it can be used to check the consistency of a conceptual model. When putting down a model in mathematical form, one is forced to make all the assumptions explicit; and when concrete values are assigned to different parameters, it often turns out that some mechanism which sounded plausible in a verbal explanation is in fact impossible or unlikely given the mathematical model. Therefore, a computational/mathematical model can be used as a "sanity check" and as a guide for the experimentalist's intuition.

- Comparing and discovering hypotheses

A computational model can be used either as a hypothesis-testing tool or an exploratory tool. In the former case, a model is used to evaluate hypotheses set forth in advance by a researcher. In a typical scenario, the model's output is compared to some set of experimental data, and the likelihood of each hypothesis being true, given the model, is evaluated. In the exploratory case, little or no data exists to guide the simulations; rather, the model's output is used to look for novel or interesting mechanisms which have not yet been established in experiments. In both cases, the model's output can be used for

- Suggesting fruitful areas for new experiments

Often, revelations of inconsistencies in conceptual models as discussed above also suggests useful experiments needed to resolve the inconsistencies. The ability to guide experimental research is undoubtedly one of the main practical advantages of using computational models. However, if a model is to be helpful in this regard, it is very important that the modelling process be intimately connected to experimental research. In an ideal case, there should be a cycle

of experiments and simulations leading to a gradual refinement of the understanding of the system in question. For example, a puzzling experimental observation could be addressed using a computational model, leading to suggestions about where it would be most fruitful to look for new experimental data. The new results from further experiments are then fed back into the model, making it even more accurate and better suited for suggesting a new batch of experiments. Needless to say, this ideal scenario cannot always be realized, and many simulation studies are performed based on results from the scientific literature without a close connection to bench scientists.

3.3. Modelling on different levels of description

It is not always trivial to decide the level of detail needed in a mathematical-computational model. (The present thesis is a good example of this!) In theory it is easy; as the saying goes, a model should be "as simple as possible, but not simpler". But strictly speaking, this is only true from a mathematical viewpoint. In models of biological systems, it is often convenient to work with models where the components can be mapped to biological entities which can be manipulated in experiments. In such models, some simplicity and mathematical tractability can be sacrificed in favour of biological interpretability.

A biological system can be described on many different levels: genes and biomolecules, cells, tissues, organs, organisms and populations, to name just a few possible levels. On a general level, modelling can be divided into “bottom-up” and “top-down” modelling. In bottom-up modelling, the emphasis is on reductionism: the modeller proceeds from the smallest relevant (but what is relevant?) components and models their interactions, hoping that some emergent phenomenon will appear. In the top-down case, the emphasis is more holistic: the modeller proceeds from the phenomena under study and tries to find the sufficient model components for the phenomena to appear. It is clear that neither of these approaches is usable in all cases. Bottom-up modelling requires considerable information about the properties and interactions of all system components, and there is always an inherent uncertainty about whether all the important components have been included in the model. It is usually necessary to use information from higher levels to decide which components are really needed. Also, it is easy to run into computational constraints: no one today would suggest modelling the brain starting from the level of quantum mechanics.

Top-down models, by contrast, suffer from the fact that an observed phenomenon could be due to any number of combinations of factors; how can we tell whether the one we have found is the right one? Such a model can suggest *sufficient* or *possible* mechanisms for a phenomenon to appear, but it can never say that they are the *actual* ones! Thus, bottom-up modelling usually needs information from higher levels, and top-down modelling needs information from lower levels. A compromise called “middle-out” modelling has been suggested by Brenner (1999). It involves starting from some middle level and working both upwards and downwards. But even here, one will still need in-

formation from both upper and lower levels to be able to start the analysis. In view of these problems, it seems reasonable to work on several different levels in parallel while trying to establish connections between each level as they appear. Research cannot afford to look at one level only, or levels that are too far apart. For instance, few would argue that we could ever understand behaviour simply in terms of biomolecular reactions (or, for example, quantum events occurring during these reactions). That would be like in the story by Plato (in Phaedo, qtd. in Parker, 2006), where Socrates

> *"ridiculed the idea that his behaviour could be explained in mechanistic terms, saying that someone holding this belief would explain his posture in terms of muscles pulling on bones and his speech to the properties of sound, air and hearing, forgetting the true cause of his behaviour; that he had been sentenced to death and chosen to stay".*

3.4. Historical aspects of computational modelling

Computational modelling, of course, dates only as far back as the date of the first usable computers. However, mathematical models have been used throughout history, and computational models are really mathematical models implemented on more efficient calculating devices than e.g. a human brain or abacus. An interesting precursor to today's computer models of biological systems was van der Pol's electrical circuit, which embodied equations for simulating the electrical activity of the heart (van der Pol and van der Mark, 1928). Although van der Pol's model is not implemented in this way today, the underlying "relaxation oscillator" equations are still in active use in many types of dynamical systems research.

One of the first really successful and accurate mathematical models of a complex biological system happened to be born in the field of neuroscience. This was the model of action potential generation developed by Hodgkin and Huxley (1952) using data from the squid giant axon. This model, developed by scientists who did not even have electronic calculators to aid them (instead they used a manual Brunsviga calculator), is astoundingly powerful considering how it was developed. (Or is it actually the case that it is so good because they had to think harder without the "prosthetic brain", the computer?) Even though many refinements of the model have been put forward and new generations of more realistic neuronal models have been developed, the Hodgkin-Huxley model is still a natural benchmark and the canonical starting point for any scientist dealing with computational neuroscience.

Another big step in modeling neurons was the theory of compartmental models by Wilfred Rall (see e.g. Rall, 1962). Borrowing methods from cable theory - mathematical tools originally developed for calculating how telegraph cables transmit messages over the Atlantic - he built up a solid framework for simulating the propagation of electrical current and potential in the dendritic trees of neurons. The division into isopotential compartments developed by Rall can be seen as a spatial discretization of the continuous partial differential equations

governing the current propagation. With Rall's formalism, standard numerical methods can be used to solve a system of ordinary differential equations to simulate the activity of a neuron.

In latter years, many new insights into the behaviour of neurons have yielded ever more detailed and accurate models. In particular, the stochastic nature of ion channel opening has been realized and taken into consideration in many simulations (Diba *et al.*, 2006). However, it is fair to say that the framework developed first by Hodgkin and Huxley and then by Rall is still the dominant one. A recent article (Naundorf *et al.*, 2007) raised some debate as to whether the Hodgkin-Huxley model is still adequate, but the authors' conclusions were later rebutted (McCormick *et al.*, 2007). Be that as it may, the present thesis mostly contains work based on the theories of Hodgkin, Huxley and Rall.

3.5. Types of models used in this thesis

In this thesis, I have used computer modelling of the lamprey's spinal CPG network on different levels, from a biochemical pathway model to a full-scale spinal locomotor network model. The following section gives some conceptual and mathematical background on the components of these models. For single neurons, three kinds of models have been used:

(1) The detailed, conductance-based compartmental model presented in Paper I. This was used to model the full spinal network in Paper II, and a morphologically simplified version of it was used in Paper III.

(2) The Izhikevich neuron model, which is a simple, two-state model based on results from mathematical bifurcation theory. This was used in Paper IV.

(3) A simplified conductance-based model developed by myself to examine plateau generation in single neurons. This model was developed as part of Paper V.

In addition, a mass-action kinetics based model of the biochemical pathway leading from mGluR5 stimulation to IP_3-dependent calcium release into the cytosol was developed. This model was then coupled to an earlier version of neuron model (1), yielding the combined biochemical-neural model described in Paper VI.

3.5.1. Compartmental modelling (Hodgkin-Huxley type)

Neurons contain a range of ion channels; membrane-embedded molecules that allow the passage of certain ions into or out of the cell. The ion channels play a critical role in determining the input-output characteristics of a neuron: how it responds to stimuli and passes on the information it has received. Ion channels exist in other cell types as well, but their role in creating membrane excitability is especially prominent in neurons. The degree of opening of ion channels can be dependent on the neuron's membrane potential, the concentration of some ligand (extra- or intracellular) or even mechanical stretching of the membrane (Kandel *et al.*, 2000). It has been found that lamprey locomotor network neurons

contain a large number of different voltage- and ligand-gated ion channels (see e.g. Grillner, 2003, for a comprehensive overview).

Paper I describes a compartmental model of a neuron, where the ion channels have Hodgkin-Huxley-type kinetics (although with many modifications compared to the original model). Compartmental models are inspired by electrical circuits. Each neuron is represented as a number of connected isopotential compartments. (Isopotential means that the electric potential is the same everywhere within the compartment.) Mathematically, a compartmental model can be viewed as a discretization of the continuous cable equations originally used for modelling branched neural structures (Koch and Segev, 1998). Each compartment can have a unique membrane resistance, axial resistance, capacitance and mix of ionic channels. For more on compartmental models and Hodgkin-Huxley type models of ion channel kinetics, see Koch and Segev (1998).

3.5.2. Simplified models

The Izhikevich model

May authors have proposed simplified models of action potential generation and other neural phenomena, e.g. the FitzHugh & Nagumo model (FitzHugh, 1961) and the Morris-Lecar model (Morris and Lecar, 1981). These models were simplifications of more detailed neuronal models (the original Hodgkin-Huxley model in the FitzHugh-Nagumo case), motivated by plausible mathematical considerations. The idea behind such models is to allow analytical examination of neural phenomena; in particular, these models can be examined in the phase plane since they only have two state variables. The drawback is that the parameters in these models can be hard to map to measurable biological entities; another kind of reduced model which is more easily interpretable in terms of electrophysiology was introduced by Pinsky and Rinzel (1994). Izhikevich (2003) introduced a new abstract model based on mathematical bifurcation analysis. Instead of working by simplifying an existing model, he started by observing that different types of dynamical bifurcations underlie transitions between neural modes of action such as tonic spiking, bursting, post-inhibitory rebound, and so on. By mapping different bifurcations to neural mechanisms he was able to devise a very simple model that, given the appropriate parameter settings, can reproduce most known firing patterns in single neurons. Because the model is not built upon known biological mechanisms, its parameters can be difficult to relate to neuronal components, but it is useful for network simulations because it is easy to implement and large networks can be simulated quickly. The equations for this model are given below.

$$\frac{dv}{dt} = 0.04v^2 + 5v + 140 - u - I \tag{3.1}$$

$$\frac{du}{dt} = a(bv - u) \tag{3.2}$$

In addition to the equations, there is a further "resetting rule": if v = 30 mV, then v is set to c and u is set to $u + d$. Thus, there are four parameters: a and b

from the actual equations, and c and d from the auxiliary rule. I, which appears in the first equation, represents the sum of injected or synaptic currents. The v state variable is to be interpreted as membrane potential, while the u variable is interpreted as the value of some recovery process. By setting a, b, c and d in different ways, neurons with specified firing characteristics can be obtained (Fig. 3.1). For example, $a = 0.02$, $b = 0.2$, $c = -55$ and $d = 4$ yields a model of an intrinsically bursting neuron.

In paper IV we use Izhikevich's model to simulate a hemisegmental network in the lamprey spinal cord in order to understand one of the problems outlined earlier: how an excitatory network with a high recurrent re-excitation capability can nevertheless also function in a slower "tonic" mode where the frequency varies according to the external drive. However, we also added some extra features (described in the paper) to account for the presence of NMDA synapses as well as synaptic facilitation and saturation. The Izhikevich model was chosen because we needed to run a large number of simulations.

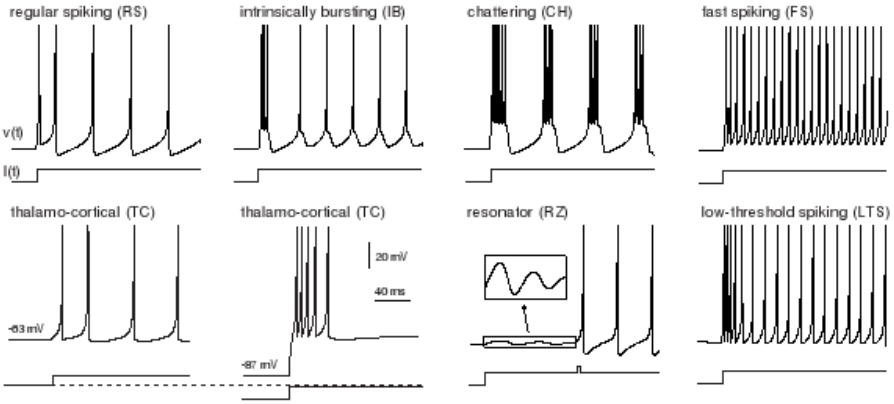

Figure 3.1. *The Izhikevich model is able to mimic different types of neural behaviour depending on how its parameters are set. [Electronic version of the figure and reproduction permissions are freely available at www.izhikevich.com.]*

A simplified conductance-based model

In some cases it is difficult to adapt pre-existing models to a specific modelling task. This was the case in the work described in paper V, where we tried to construct a simplified model of how tetrodotoxin (TTX) resistant NMDA oscillations are generated in lamprey CPG neurons. This type of oscillation arises when synaptic transmission is blocked using TTX, pharmacologically isolating the neurons from each other. When NMDA is applied to such preparations, they sometimes display characteristic plateau potentials.

Such plateau potentials had been simulated in the full detailed model of Paper I, but because of the large number of parameters (particularly with regard to dendritic properties), it was difficult to get an understanding of the conditions under which these oscillations could be produced. In Paper V, we therefore set out to build a model which could be analyzed more easily.

Conceptually, the aim was to develop a "biologically minimal" model of NMDA-TTX oscillations. By this we mean a model that includes biologically meaningful components, like ion channels, although these are modelled in a simplified way. A "mathematically minimal" model would be even more compact in terms of parameters and equations, but it would be more difficult to map the model parameters to experimentally accessible entities in such a model. Our approach was to include only those biological components that are thought to be directly involved in generating and shaping NMDA-TTX oscillations.

The model has two state variables: V (corresponding to membrane potential) and C (corresponding to an effective calcium concentration in a "calcium pool" accessible to calcium-dependent potassium channels within the cell membrane). Since there are only two state variables, successive states of the system can be plotted in a two-dimensional phase plane, which potentially gives some geometric intuition about the system. The ion channels considered were the NMDA channel, a calcium-dependent potassium channel (K_{Ca}), a leak channel, a voltage-dependent potassium channel (K_v), and a voltage-dependent calcium channel (Ca_v), although the last two ones turned out not to be absolutely necessary for generating the NMDA-TTX oscillations. Some of the simplifying assumptions of the model follow:

1. Point neuron assumption: there is no explicit geometry, i.e. dendritic and axonal arbors are disregarded.
2. Steady-state assumption: all ion channel activations are assumed to reach their steady state instantaneously when the membrane potential (or calcium concentration, depending on the ion channel) is changed. This is reasonable since NMDA-TTX oscillations occur on a time scale which is much slower than the internal kinetics of any of the ion channels, as far as is known.
3. The activation of the K_{Ca} channel is directly proportional to the concentration in the Ca^{2+} pool. (Other activation functions such as a Hill function were used, but did not substantially change the simulation results).
4. The influx to the Ca^{2+} pool is a linear function of the calcium currents and the decay term is exponential; thus, no diffusion, buffering or active transport is explicitly modelled.

The full mathematical formulation of the model is found in Paper V.

3.5.3. A biochemical network model

Paper VI discusses a mathematical model of the biochemical pathway that leads from metabotropic glutamate receptor 5 (mGluR5) activation to oscillatory IP_3-mediated Ca^{2+} release in the lamprey (Kettunen *et al.*, 2002). IP_3 and Ca^{2+} bind

to the IP_3 receptor (IP_3R), thus leading to the release of Ca^{2+} from the endoplasmic reticulum to the cytosol. The mathematical model of the biochemical pathway was later connected to a version of the electrophysiological model of Paper I, yielding a combined biochemical-electrophysiological model.

The biochemical pathway model can be divided into two parts: (i) A mass-action kinetics based model of the biochemical reactions leading to the generation of IP_3, and (ii) A model of how IP_3, together with calcium, activates the IP_3 receptor. For part (ii) we used and compared three different mathematical formalisms; see below for details. Part (i), comprising the biochemical reaction pathway from mGluR5 to IP_3, was the same for all versions of part (ii). The whole simulated biochemical pathway as well as a simplified version are shown in Fig. 4.4 in the Results chapter. The reactions and the corresponding equations and parameters are given in the Appendix.

The biochemical pathway was modelled using coupled chemical reactions obeying ordinary mass action kinetics. Suppose we have a reaction of two biochemical species, A and B,

$$A + B \rightleftharpoons AB \tag{3.3}$$

with the forward reaction rate k_1 and the backward reaction rate k_2. Then the rates of change of the concentrations of each species per unit of time, according to mass-action kinetics, are written as

$$\frac{d[A]}{dt} = \frac{d[B]}{dt} = -\frac{d[AB]}{dt} = k_2[AB] - k_1[A][B] \tag{3.4}$$

Some reaction steps were also modelled according to Michaelis-Menten kinetics (Palsson and Lightfoot, 1984), which assumes the following simplified scheme for an enzymatic reaction (note the irreversible second step):

$$E + S \underset{k_b}{\overset{k_f}{\rightleftharpoons}} ES \overset{k_{cat}}{\rightarrow} E + P$$

Here E is the enzyme, S the substrate and P the product, while ES denotes the enzyme-substrate complex. Differential equations are then set up for these reaction steps according to standard mass-action kinetics like above.

The differential equations were specified for each molecular species in the model and the coupled system was solved using XPPAUT (Ermentrout, 2002) and CHEMESIS (Blackwell and Hellgren Kotaleski, 2002).

Three (or two, depending on the viewpoint; see below) different mathematical descriptions for the IP_3R model were used: the "De Young-Keizer model" (De Young and Keizer, 1992), although our implementation uses an equivalent and rescaled version (Li and Rinzel, 1994); the "Li-Rinzel model" (Li and Rinzel, 1994), which is a simplified version of the De Young-Keizer model; and the "Tang-Othmer model" (Tang and Othmer, 1995). The De Young-Keizer model assumes that three independent and equivalent IP_3R subunits are involved in Ca^{2+} release. Each subunit has three binding sites, one for IP_3 and two for Ca^{2+}. One of the Ca^{2+} sites is activating, while the other is inhibitory. Each of the three sites is either occupied or not, so each subunit can be in one of eight

states. Only one of the states (the one where the IP_3 site and the activating Ca^{2+} site are occupied, but not the inhibitory Ca^{2+} site) contributes to Ca^{2+} release, and all three subunits must be in this state for the channel to open (De Young and Keizer, 1992).

The Li-Rinzel model uses time-scale separation to simplify the De Young-Keizer model into a version with only two state variables. The output of the Li-Rinzel model is very similar to that of the De Young-Keizer model; in a qualitative sense they are almost completely equivalent (Li and Rinzel, 1994). We observed extremely similar output using these two models, so I will consider them as equivalent in the following and only report results for the De Young-Keizer version.

The Tang-Othmer model represents a further simplification of the De Young-Keizer model. It allows only certain transitions according to the following schematic:

$$R \leftrightarrow RI \leftrightarrow RIC_+ \leftrightarrow RIC_+C_- \tag{3.5}$$

R denotes an "empty" receptor with no molecules bound, I denotes IP_3, RI denotes a receptor-IP_3 complex, RIC_+ denotes RI with Ca^{2+} bound at the activating site, and RIC_+C_- denotes RI with Ca^{2+} bound at the activating and the inactivating site (Tang and Othmer, 1995). Analogously to the De Young-Keizer model, only the RIC_+ state contributes to Ca^{2+} release.

After the biochemical pathway model was finished, it was integrated into an earlier version of the lamprey CPG neuron model using CHEMESIS. This allowed simulations where changes in intracellular calcium levels resulting from IP_3R activation could have effects upon calcium-sensitive ion channels in the cell membrane, as described in Paper VI.

Chapter 4

RESEARCH PROBLEMS ADDRESSED

In this thesis, computational modelling on different levels of detail has been used to examine various questions about neurons and neuronal circuits in the lamprey spinal CPG network.

4.1. Paper I: A detailed model of a lamprey CPG neuron

4.1.1. Motivation

The aim of the work presented in Paper I was to develop a new, biophysically detailed model of a lamprey CPG neuron, based mainly on published data about different ion channels. The aim of the model was that it should be generic, but possible to adapt for simulating different types of CPG neurons, e.g. EIN, CIN and MN. In earlier modeling work, a compartmental model (Ekeberg *et al.*, 1991) has been used with success to simulate and address hypotheses about the lamprey CPG network. However, at the time when that model was developed, little data existed on e.g. kinetics of ion channels in these neurons; instead, parameters were to a large extent based on estimates from other organisms. Also, many novel types of ion channels have been characterized in lamprey CPG neurons since the publication of the study, for example, a high-voltage-activated, inactivating potassium current, K_t, and two sodium-dependent potassium channels K_{NaF} (F for fast) and K_{NaS} (S for slow). The potential importance of some dendritic conductances has also been recently realized, and the old model, which had a simple dendritic morphology and no active dendritic conductances, was less helpful in this regard. This is particularly important because in recent years, the dissociated cell – where most of the dendritic tree has been removed – has become an important preparation since it is much easier to patch-clamp than an intact cell. The dissociated cell, in many respects, shows different response characteristics compared to the intact neuron. The old model could not account for most of these differences, again because all of its active conductances were

placed on the soma, so that removing the dendritic tree in simulations had minor effects. An additional goal was to examine the effects of using an updated model, instead of the old one, to simulate CPG networks.

4.1.2. Model overview

I will here give a short and superficial overview of the model to make the following presentation easier to follow. The details can be found in Paper I. Fig. 4.1 shows a graphical representation of the morphology of the model neuron. This idealized neuronal geometry was the one we used as default, although other geometries based on reconstructions of actual neurons were also tried. The model has a soma (cell body), a spike-generating zone (the initial segment of the axon) and many dendritic branches. The dendritic compartments are divided into three categories: primary, secondary and tertiary dendrites, corresponding to proximal, medial and distal dendrites - an alternative terminology sometimes used. We include all types of ion channels known to exist in lamprey CPG neurons, a total of 12 types: a voltage-dependent sodium-channel (Na^+), two voltage-dependent potassium channels, one transient (K_t) and one slow (K_s), three voltage-dependent calcium channels (N-type, Ca_N; L-type, Ca_L and a low-voltage activated type, Ca_{LVA}), a bath NMDA channel (NMDA) with associated calcium influx (Ca_{NMDA}), two calcium-dependent potassium channels (K_{CaN} and K_{CaNMDA}), and two sodium-dependent potassium channels, one fast (K_{NaF}) and one slow (K_{NaS}). The NMDA-related channels (NMDA, Ca_{NMDA}, K_{CaNMDA}) are only used when simulating NMDA application. Roughly speaking, Na^+, K_t, and K_{NaF} are related to action potential shape, K_{CaN} and K_{NaS} are related to frequency control, Ca_{LVA} is related to post-inhibitory rebound, and Ca_N and Ca_L are involved in various processes from frequency control to NMDA-TTX oscillations. The role of K_s is still unclear; neither experiments nor simulations have been able to suggest a strong connection between K_s density and a particular function. The conductance densities for the different channels were different in soma, the initial segment and the dendritic compartments.

4.1.3. Methodology and practical issues

Even with the large amount of newly published information on lamprey CPG neurons, there were many practical problems to consider when developing the new neuronal model. For example, how should the parameters be set and how should one evaluate resulting models? There are many different kinds of constraints; for example, measured passive properties, voltage-clamp recordings of individual currents, observed effects of channel blockers, estimates of typical firing frequencies, information about the shape of inter-spike intervals, and so on. Some of these constraints are exemplified below.

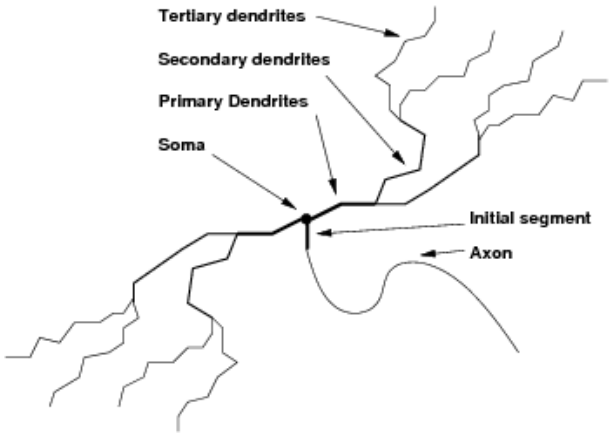

Figure 4.1. *A cartoon of the geometry of the model neuron in Paper I. The different compartments are a soma (cell body), a spike-generating region in the axon (initial segment), and a total of 84 dendritic compartments of different sizes. [Picture created by Alexander Kozlov, 2007]*

Approximate workflow

In practice, the model was built up using roughly the following steps.

- The morphology was loosely based on experimental reconstructions of interneurons, and tuned to match passive characteristics reported by Buchanan (1993).
- Current kinetics for which there was relatively detailed information from dissociated cells were tuned to match the available information so that their conductance density on the somatic compartment could be inferred. (Hess *et al.*, 2007)
- For less well-constrained currents, estimates for somatic densities were made based on more indirect information. (For example, calcium current kinetics and densities were based on El Manira and Bussières, 1997).
- Initial segment channel densities were tuned so that a model dissociated cell would get firing characteristics similar to actual dissociated cells (Hess and El Manira, 2001).
- The remaining channel densities, somatic and dendritic, were set so that different phenomena could be reproduced; for example, sAHP summation in cadmium (Wallén *et al.*, unpublished), shape of sAHP in catechol (Hess and El Manira, 2001) etc.

Many of the steps were, of course, iterated in response to new experimental data, or (most commonly) because changes further down in the chain tended to break constraints that had been fulfilled earlier.

It should be noted that the data was drawn from a variety of different preparations, neuronal types (sometimes unidentified cells); some data were from lar-

val or young adult lampreys, while some were from adult lampreys. It has been implicitly assumed by researchers working on dissociated cells (which usually come from larval or young adult lampreys, due to the difficulty of dissociating cells from mature adults) that current kinetics characterized in these preparations are similar to those that would be found in adult animals. In fact, there are differences between e.g. modulation effects on neurons from lampreys in different life stages, and even between adult animals during different seasons of the year (Parker and Bevan, 2007). This should be kept in mind when extrapolating information from dissociated cells to intact adult cells.

Detour: Automated parameter fitting

It is time for a small detour to discuss the possibility of using automated parameter fitting. One might reasonably ask whether it is not best to design a value function incorporating all the constraints mentioned above, and then to optimize that function using some automated parameter fitting scheme. However, there are a couple of reasons why this is probably not a good idea.

Huge search space First, the number of parameters in the model is large. Even with a supercomputer, it would be practically impossible to search more than a minuscule part of the parameter space in a feasible timeframe. Therefore, the only realistic approach is to tune sub-parts of the system (single ion channel kinetics, for example) independently and then try to fit their respective contributions (i.e. conductances) to the dynamics. After a model has been fully developed, it can be "frozen" for use in network simulations, such as was done in e.g. Paper II. Variation in a population of model neurons can then be simulated by sampling some parameter value of interest (like input resistance) from a distribution centered around the default parameter value.

Hard to design value function Another practical reason is that it can be very difficult to codify the constraints into a value function. For example, how should one weigh the criteria against one another? Is a "correct" behaviour when simulating the application of a certain channel blocker more important than obtaining a realistic sAHP summation curve, for example? If so, how much more important? Also, on the level of a single constraint, it can be hard to formulate the fit mathematically – for instance, action potentials should "look reasonable", which is a non-trivial thing to put down in the form of a mathematical expression. In addition, requiring the model to match e.g. the precise spike timing from a set of experiments is very hard, because different numerical methods (or pseudo-random number generators) can lead to different outputs even for the same model. Here, the ability of a human to evaluate the model as a whole is, in my opinion, indispensable.

A didactic reason A third reason, which is of a somewhat different character, is more about the researcher who works on the problem. Hand-tuning a compartmental model is undoubtedly a hard and frustrating task ("a fool's game"

- Eve Marder, pers. comm.) but on the other hand, it eventually provides the researcher with a good intuition about the model and, by extension, the actual biological system under study. In other words, model-building is also a learning experience. Automated parameter-fitting, by contrast, gives little insight into *why* a certain parameter setting gives a certain behaviour.

Admittedly, a number of good neuronal modelling studies based on automated parameter fitting have been published. For example, Prinz *et al.* (2003) is an interesting paper that shows how a "database" of model neurons can be used to gain insight about overall system properties. (The follow-up study, Prinz *et al.*, 2004, is also a fascinating study which shows how similar behaviour can be generated using completely different network properties.) However, it is important to note that the particular system under study was much better constrained by data, so that the authors varied only eight parameters – also, each parameter was only allowed to take on one of six values, yielding a total of about 1.7 million models. The lamprey CPG neuron model presented here has many more parameters, and this would have lead to a combinatorial explosion.

4.1.4. Results

Here, I choose to divide the results into three different categories: *replication* of experimental results, finding *inconsistencies* in the experimental data or the interpretations of experimental data, and *predictions* to be tested by future experiments. Also, there is a short section of a certain type of *robustness* that the model displays.

Replicating experimental results

One of the most important constraints, and one that was fairly well replicated, was that time courses of a subset of the currents during an imposed action potential waveform should be similar in simulations and in experiments (Paper I, Fig. 2). Firing characteristics of interneurons, as well as the characteristic shapes of fAHPs and sAHPs, were well-reproduced by the model (Paper I, Fig. 3).

The effects of applying channel blockers to dissociated and intact neurons were well replicated at least in a qualitative sense. Thus, the application of cadmium (which blocks Ca^{2+} channels) resulted in repetitive firing where the sAHP has a different shape (Paper I, Fig. 4a); also the sAHP in cadmium was summed in the correct way, that is, depending on frequency of stimulation (Paper I, Fig. 4b). Catechol application to dissociated cells resulted in an inability of the neuron to fire repetitively (Paper I, Fig. 6), while catechol applied to intact neurons resulted in repetitive firing with characteristic, rounded interspike regions (Paper I, Fig. 7). Simulated application of TTX and/or TEA in the presence of NMDA resulted in realistic-looking oscillations for some parameter values (Paper I, Fig. 8).

Finding inconsistencies or hard-to-explain features in experimental data

Running the model, it was found that while action potentials from simulated dissociated cells looked reasonably similar to their experimental counterparts, the spikes from simulated intact cells did not. Specifically, the spikes in simulated intact cells were far too narrow (about 0.5 ms in half-amplitude width) compared to experimental reports (about 1 ms in Hess and El Manira, 2001) and about 2 ms in e.g. Buchanan, 1993). They were in fact about as narrow as in (simulated and real) dissociated cells, which is reasonable given that the kinetics are the same in the model. The only thing that has been added is the dendritic tree, but at least in the model version described in Paper I, the dendritic tree is so electrically compact that it hardly affects the action potential width. Exploratory simulations with a larger dendritic tree showed that the spike could be "smeared out" to slightly less than 1 ms, but not 2 ms. The question is then where this spike broadening comes from. The spike widths for dissociated cells reported in Hess and El Manira (2001), which were well replicated by the dissociated model neuron, were measured in in the absence of calcium currents. However, an added calcium influx would not expected to have such a large impact on the spike width (especially since calcium enters fairly late during the action potential), and indeed it shows no such effect in simulations, even assuming large calcium conductances. One alternative explanation could be that the measured spike widths are different because of different measurement techniques; another is that the dissociated (larval) cells could in fact have different expression levels of some important action-potential related ion channels. Using the model, we could obtain broader spikes (2 ms or more) by reducing the K_t conductance or changing its kinetics, so this may be the most plausible explanation. However, the difference in action potential width is a very interesting possibility for further experimental analysis.

Another interesting question concerns sAHP sizes. Experimental studies have shown that sAHPs tend to be small and relatively constant in size. In the model, by contrast, the sAHP size tended to vary depending on the resting membrane potential and other parameters. Buchanan (2001) noted that one possible explanation of the small and constant sAHPs would be that the resting potential of the neuron is located close to the K^+ reversal potential. Because the currents underlying the sAHP can be modelled as a product of a conductance term and an electromotive force term $(V - E_{rev})$, even a high potassium channel conductance can give rise to a small current if V is close to E_{rev}. However, the generally quoted K^+ reversal potential of -90 mV is quite far from Buchanan's estimate of the mean resting potential (about -78 mV) and even further from other estimates of -70 mV. We were able to obtain realistic-looking sAHPs by instead setting the K^+ reversal potential to -85 mV. However, the sAHP size variation is still larger than observed in experiments so far. It may be that during physiological activity, changes in intra- vs. extracellular K^+ concentration during spiking changes the effective K^+ reversal potential enough to keep a fairly constant sAHP amplitude.

Stauffer *et al.* (2007) gives a thoughtful and historical overview of similar questions in relation to the sAHP in vertebrate interneurons and motoneurons.

Predictions

We derived two main predictions by simulating the model. The first one deals with the somatic and dendritic distribution of K_{Ca} and K_{Na} conductances. It turned out that these ion channels needed to be present in much higher densities (10x) on the dendritic compartments than in the soma to fulfill various experimentally derived criteria. One of these criteria (i) is an (unpublished) observation that dissociated cells tend to have no sAHP, or a very small one. Other criteria used were the observation that intact cells typically have a clear sAHP (ii) and estimates of typical firing frequencies for intact cells, e.g. from Buchanan (1993) (iii). Criterion (i) neatly constrained the sum of somatic K_{Ca} and K_{Na} conductance densities to a maximum value, and (ii)-(iii) gave good constraints on the total dendritic sAHP conductance densities. The relative balance of K_{Ca} and K_{Na} channel densities was tuned according to a fourth criterion: reproducing sAHP summation data with and without cadmium applied (Paper 1, Fig. 4b). Whether the prediction about the relative soma/dendrite densities of K_{Ca} and K_{Na} channels holds true will likely be settled through calcium and sodium imaging experiments underway at the Department of Neuroscience, Karolinska Institutet (Peter Wallén, ongoing research).

The second prediction is about the K_{NaF} current, a fast sodium-dependent potassium current for which no particular function is yet known. The kinetic model for this current was mostly based on fitting the parameters to the current's time course during action potential clamp, with some additional constraints. For example, preliminary evidence shows that disabling the current using substitution of lithium ions for sodium ions in a dissociated cell, while also applying cadmium, should not abolish repetitive firing (Hess *et al.*, unpublished data). Exploratory simulations showed that this current could have a powerful role in frequency-regulation through its (indirect) interaction with calcium and K_{Ca} channels. The K_{NaF} is activated fairly late during an action potential compared to K_t, and is more associated with the action potential's repolarization phase (Hess *et al.*, 2007). This is also the case in the model; K_{NaF} regulates the fAHP to some extent (as does K_t), but its effect is stronger on the following ADP. The size of the ADP can be controlled by changing the K_{NaF} density in the model, particularly if it is changed in the dendrites. A large ADP will lead to a large influx of dendritic calcium and subsequently a powerful K_{Ca} activation, leading to a strong sAHP. This prediction of K_{NaF}'s potentially powerful frequency-regulating role suggests further experimental analysis.

Morphological robustness of the model

To evaluate whether the model would be useful for simulating neurons with different dendritic tree structures – and to check whether the results held true for more natural dendritic tree structures than the rather stylized one we used as default – we ran the model with all parameters fixed on three realistic neuronal morphologies in addition to the one used so far. These morphologies were taken from reconstructions by Buchanan *et al.* (1989), and implemented as compartmental models in GENESIS. It turned out that the specific morphology we used

was not important; all simulated neurons had the same kind of qualitative output, both in terms of spike trains and adaptation (Paper I, Fig. 9) and in terms of other results. Thus, the model is "morphologically robust" – the specific shape of the simulated neuron is not expected to influence the output in a qualitative sense.

In terms of parameter robustness, there are of course some variables which are sensitive to changes. Most notably, the sodium kinetics must not be changed too much or the firing properties are heavily distorted – but this is a common feature of many neural models. We did not make any formal parameter sensitivity analysis in this project, but from experience with the model, the most crucial parameters apart from sodium kinetics seem to be the kinetics of the Ca_N channel. This channel is involved in many phenomena (e.g. sAHP, TTX and/or TEA oscillations, the K_{NaF}-mediated frequency regulation, and so on) and thus changes in its kinetics can lead to large changes in simulation output.

4.1.5. Interpretation and caveats

It should be admitted that with such a large number of adjustable parameters, the predictive value of the model is limited; or at least, the predictions should be taken with a large grain of salt. I view the neuron model primarily as a way to integrate what is known about lamprey CPG neurons, and as a tool for checking the current understanding of different behaviours of the neuron. The model is useful for highlighting discrepancies between experimental data and for pointing out areas which are not well understood. Also, the model is never finished: it should be updated depending on new experimental findings. For example, the NMDA-related part of the model is already known (from Paper V) to be lacking, and should be updated. From a formal point of view it might be claimed that the fitting process should use a "training set" and a "test set" so that the finished model could be independently validated against criteria which were not built into the model to begin with. However – aside from the fact that it is already hard enough to fulfill all criteria with full knowledge! – the goal of this work is not really to build a predictor, but to construct a reasonable implementation of a lamprey CPG neuron as its function is understood today. Therefore it is important to include all the available knowledge. Instead, the independent validation will come from future experiments. They will undoubtedly falsify many of the assumptions in the model, which can then be further improved. It should be noted that the model has also been used with morphologies roughly corresponding to those of motoneurons, although this is not reported in Paper I. The simulation output was then similar to what is shown in the paper, but more consistent with what is known about motoneurons in terms of e.g. firing properties.

4.2. Paper 2: Large-scale simulation of intersegmental coordination

4.2.1. Motivation

The motivations of the work presented in Paper II were twofold: first, we wanted to test the new cell model from Paper I in a network setting, to see whether it offered any additional benefits compared to the previous cell model; and second, we wanted to try to examine and potentially reconcile experimental findings on the subject of intersegmental coordination.

As already mentioned, the problem of intersegmental coordination in the lamprey has been studied for over two decades - see e.g. Matsushima and Grillner (1990), Matsushima and Grillner (1992), Williams and Sigvardt (1994). Early models used coupled phase oscillators as models of the (hemi)cord, starting with Cohen *et al.* (1982) and followed up by e.g. Williams *et al.* (1990) and Sigvardt and Williams (1996). During the 1990s, network models based on more detailed neuronal units started to find use; see e.g. Hellgren Kotaleski *et al.* (1999a), Hellgren Kotaleski *et al.* (1999b), Wadden *et al.* (1997).

One of the problems with the detailed simulation models was that the phase lag could be made constant along the spinal cord, but only for a given frequency; the phase lag tended to be frequency-dependent. In the experimental preparation, however, the phase lag is independent of frequency and approximately constant (with fluctuations around the mean) over the length of the spinal cord during fictive locomotion (Tegnér *et al.*, 1993). We also wanted to resolve this problem in the new network model.

A further sub-goal of the project was to examine the impact of the variability of single cells on network function. This sub-goal became, in due course, the main focus of the work.

4.2.2. Methodology

We used the cell model from Paper I as the basal network unit. Actually, the simulations were also run with the older cell model (Ekeberg *et al.*, 1991), although this is not reported in Paper II. The results were very similar; more on this later. Anatomical and connectivity parameter choices were guided by experimentally obtained estimates as far as possible, although sometimes there was no reliable data available. We made an attempt to collect all published measurements of passive, active and synaptic characteristics in all types of CPG neurons to use as a guideline.

Some runs simulated a hemicord, when only excitatory transmission was assumed, according to the same logic as in Papers III and IV. In simulations of the whole spinal cord, cross-projecting inhibitory interneurons provided inhibitory input to all types of neurons on the contralateral side, as in Fig. 2.3. Apart from connections within their own segment, EIN and CIN neurons also projected to neighbouring (ipsi- or contralateral, respectively) hemisegments, with longer projections in the caudal direction. We did not distinguish between CCIN

and ScIN. ScEIN units were not included. Motoneurons were included as pure output elements from which VR recording-like activity could be plotted. In these virtual VR recordings, MNs were hyperpolarized to avoid spikes for clarity. The model was implemented in SPLIT (Hammarlund and Ekeberg, 1998).

The criteria for a successful model were that it should (i) be able to show fictive locomotion-like activity and (ii) it should have a constant phase lag over some physiological frequency range.

Input to the spinal network was given through bath AMPA activation, and descending locomotor commands were mimicked by current injection to a subset of the spinal (hemi)segments.

4.2.3. Results

The locomotor pattern can be controlled from the head

Interestingly, we found through simulating the network that the phase lag over the whole spinal cord could be controlled by giving locomotor commands (current injections) to only the very rostral part of the simulated spinal cord (the 10 first segments). This was not only true for forward swimming patterns - backward swimming patterns could also be evoked in this way. Backward swimming has recently been described in the lamprey (Islam *et al.*, 2006). In addition, a forward swimming pattern could be dynamically reversed by changing the sign and magnitude of the input current to the rostral part during a simulation. Instead, stimulation to the caudal part could not reverse the locomotor pattern, except in localized circuits in the very caudal part of the spinal cord. This result is due to the inherent asymmetry of the synaptic projections in the lamprey spinal cord: both inhibitory and excitatory interneurons project further in the caudal direction than in the rostral direction.

A novel role for reciprocal inhibition

In addition to the rostral-control principle, another interesting finding shed new light on CPG organization. A simulated hemicord network was able to reverse its pattern dynamically during swimming, but the process was fairly slow and not perfectly stable. In contrast, the full spinal cord with mutual inhibition between hemisegments was able to accomplish the switch swiftly and reliably. Thus, reciprocal inhibition between hemicords may not only be important for achieving an alternating burst pattern, but also for stabilizing and facilitating changes in the direction of locomotion.

The importance of being variable

The neuronal units in the simulation were, as mentioned above, endowed with randomly varying properties (normally distributed around a mean value). This led to a large heterogeneity in e.g. firing properties of individual neurons. Our simulations showed that the inclusion of such variability is not only important

out of considerations about biological realism, but that it is crucial for the function of the simulated network. We realized that it is important to replicate the actual shape of the motoneuronal recordings as seen experimentally. The motoneuronal bursts, in experiments, tend to look like triangle waves (see Fig. 4.2). With a neuronal network of identical units, the bursts instead tend to have an EPSP-like or relaxation oscillator-type shape with a sharp rising phase; only when cellular properties are varied enough does the triangular shape appear. It turns out that an intersegmental phase lag which is relatively frequency-independent can be achieved with triangle-shaped population bursts in simulations, but not with EPSP-like bursts. A conceptual explanation follows (see Fig. 3a,b in Paper II): if one (simplifying) posits some activation threshold that must be crossed in a segment to recruit the next segment, the shape of a burst in each segment matters. With an EPSP-like burst, the threshold will be crossed almost immediately, and the next segment will be recruited. The time delay between segmental activations will always be approximately constant, but as the burst duration varies, the intersegmental phase lag will also vary (because the phase lag is equal to the time delay divided by the total cycle time). By contrast, with triangle-like bursts, activity in the first segment builds up smoothly over time and eventually crosses the threshold. It also decays smoothly and crosses the threshold from the other direction with the same time delay. The actual time taken to cross the threshold is frequency-dependent; but the time-to-peak is always about half of the cycle duration. In this way, the time delay between two consecutive segments is approximately proportional to the total cycle time. This effect was observed in our simulations for a rather broad frequency range.

The principle outlined above in effect means that the segmental circuits can, by themselves, keep the phase lag constant. Our simulations therefore revealed, in addition to the rostral control of the swimming pattern, a local aspect of control which is intrisic to the segmental units. This interplay between centralized and local control allows a flexible yet robust way to control the spinal locomotor pattern.

4.2.4. Interpretation and caveats

As usual, the simulation suggests possible mechanisms, which are not necessarily the actual mechanisms used in nature. Here, the hypotheses put forward are, however, quite intriguing, and should provide ample food for future experiments. I believe it is in cases like this where simulation really comes into its own: when it can put forward elegant and plausible explanations of systems that are hard to probe experimentally.

Comparison between simulations using the older cell model and the newer one showed that the differences were minor, which further suggests that the results are of a general nature. It might be conjectured that even much simpler neuronal model units could be used to achieve the same results. Even though this (unfortunately) means that the added detail of the new cell model

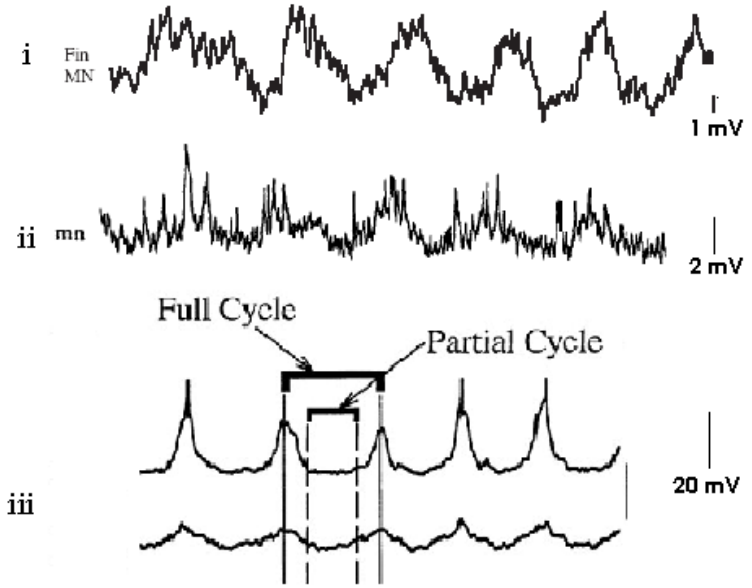

Figure 4.2. *Triangle-like motoneuronal oscillations in lamprey. (i) modified from Mentel* et al. *(2006) [Reproduced with permission from Blackwell Publishing], (ii) modified from Shupliakov* et al. *(1992) [Copyright Wiley-Liss, Inc. 1992; Reprinted with permission of Wiley-Liss, Inc. a subsidiary of John Wiley & Sons, Inc.], and (iii) modified from Buchanan and Kasicki (1999) [Used with permission from Journal of Neurophysiology].*

contributed little to the study of intersegmental coordination, this fact should be interpreted in a positive light: if the phenomena had been dependent on some specific ionic conductance in the new model, the results would, per definition, not have been as general as they now appear.

These simulations used a rather high swimming frequency (3-15 Hz), corresponding approximately to the fast rhythm found in hemisegmental networks (Cangiano and Grillner, 2003). Physiological swimming frequencies in the lamprey vary between 0.1 and 10 Hz at normal swimming speeds (Grillner, 2003), and future simulations should extend the stable range of simulated locomotion correspondingly, downward in the frequency range.

4.3. Paper III: Locomotor bouts in hemisegmental networks

4.3.1. Motivation

As mentioned earlier, it was recently shown that hemisegmental spinal preparations in lamprey can display rhythmic activity in response to both chemical stimulation (using NMDA or D-glutamate) and to a brief electrical stimulation.

The aim of the work described in Paper III was to focus on locomotor bouts; the self-sustained activity arising in hemisegmental networks after a transient electrical pulse. Could the experimentally observed results be replicated and the mechanisms behind them understood?

4.3.2. Modelling approach

Here I outline the assumptions and criteria used to evaluate the output of the model.

Although the experimentally observed locomotor bouts considerably outlast the initial stimulus, they are eventually terminated – usually after a couple of minutes depending on the size of the preparation (Cangiano and Grillner, 2005). The reasons for this termination are not understood; the original paper stated that some unknown activity-dependent process was the likely cause of the termination. Because of this uncertainty, as well as the fact that we were primarily interested in the causes behind the *appearance* of the locomotor bouts, we did not explicitly try to model their termination.

The most important experimentally based criteria that we required the model to fulfill were the following:

1. It should display sustained spiking activity throughout the simulation.
2. The spiking should be organized in bursts [viewed on a network level, since single neurons only spike once per cycle, according to the experimental data].
3. Blocking of AMPA synapses should abolish the spiking activity after the stimulation has ended.

After an inital round of experiments, new experimental data arrived suggesting that locomotor bouts could arise even when NMDA receptors were blocked. We then added a new criterion:

4. Self-sustained activity should be achievable even in the absence of NMDA receptor activation.

The actual model neuron used was the one described in Paper I, but to restrict the computation time, the dendritic tree was simplified to just four large compartments. The somatic and dendritic conductances of K_{CaN} and K_{NaS} channels had to be modified to be able to obtain the same kind of response characteristics as in the full model, but other parameters were unchanged. To introduce some variation in order to avoid unrealistically strong spike synchronization, soma sizes were varied between 50 and 150% of the default value. The number of neurons was varied between 80 and 200. A given pair of neurons was assumed to be connected with a probability of 30%, and synaptic conductances were set so that the mean EPSP amplitude was around 1.5 mV as measured in the soma. AMPA, NMDA, acetylcholine (ACh) and metabotropic glutamate (mGluR) synaptic transmission was assumed. Inhibitory transmission was neglected because strychnine application (which blocks glycinergic transmission) neither abolished rhythmic activity nor increased its frequency in experiments

(Cangiano and Grillner, 2003). In some simulations, axonal delays were neglected; in others, they were randomized between 0 and 20 ms, based on rough estimates from information on mean axonal velocity and anatomy.

4.3.3. Results

Locomotor bouts with and without NMDA

A first round of simulations was performed with 200 neurons endowed with NMDA and AMPA synapses. Somewhat surprisingly, it was easy to achieve realistic-looking locomotor bouts in this network model with a minimum of parameter tuning. The respective importance of NMDA and AMPA is easy to explain: the fast AMPA synaptic component tends to synchronize the spikes of individual neurons, yielding a bursting pattern on a population level, while the slower NMDA component sums and thus creates a tonic synaptic current which is able to carry over the activity until the next action potential.

When new information suggested that NMDA transmission was in fact not required for locomotor bouts, the model was updated with two new synaptic components, both known to be present in lamprey spinal neurons – ACh and mGluR synapses. Using these together with AMPA synapses, it was still possible to get locomotor bouts, but in a slightly different way. ACh synapses were assumed to be slower than AMPA synapses but much faster than NMDA synapses, and they could not in themselves carry the neurons' depolarization over to the next spike. The mGluR synapses were assumed to be extremely slow, and activated at a low level. During the first second of the simulation, the mGluR component, however, could grow strong enough that after a delay, some more sensitive neurons would pass the spiking threshold. The activity of these neurons would then be propagated through the network by AMPA and ACh synapses. The non-instantaneous decay of the ACh component together with the weak but tonically active mGluR component is then enough to keep a neuron sufficiently depolarized to be able to spike again.

With AMPA, NMDA, ACh and mGluR synapses present, the network could show locomotor bouts with less than 90 neurons; if NMDA was removed, up to 150 cells were needed. As in all simulations, the locomotor bouts were organized in bursts with a frequency that fell within the experimentally observed interval.

Finally, the effects of introducing axonal delays were considered. The effects of axonal delays in general are poorly understood, but it is possible that they can be quite important. One of the few modelling papers examining axonal delays, Izhikevich (2006), puts forward a very interesting hypothesis for network self-organization involving an interplay of axonal delays and spike-timing dependent plasticity (STDP). In our model networks, axonal delays neither enhanced nor decreased the ability of a control network (i.e., a network without axonal delays) to display locomotor bouts. However, the spiking pattern became more smeared out, so that the output, while still bursty, was less synchronized. This is in fact more consistent with experimental findings, where the synchrony is not complete (Cangiano and Grillner, 2003).

4.3.4. Interpretation and caveats

Needless to say, the mechanisms suggested by the model need not be the true mechanisms responsible for self-sustaining activity in hemisegmental preparations. What we can learn is that nothing more than the components used in the model need, in principle, be postulated if one wants to explain the phenomenon. Although the model-generated locomotor bouts are quite robust, their robustness would possibly increase even further if one introduced dynamical synapse properties such as facilitation and depression – in experiments, locomotor bouts are found in different hemisegmental preparations with exceptional regularity.

There is also a question of anatomical realism - is 90 neurons with 30% connectivity realistic? It is not known how many excitatory interneurons a hemisegment typically contains; some (uncertain) estimates are "at least 20, probably many more" (Buchanan *et al.*, 1989) and 40-50 (Grillner *et al.*, 2005). 90 neurons would then correspond to about 2-5 hemisegments, which seems reasonable given that several hemisegments are usually needed to elicit locomotor bouts in a preparation (Cangiano and Grillner, 2003). The connection probability is also unknown, though the figure 10% has been used (Kozlov *et al.*, 2007). In the simulations presented here (with no synapse blockers), each neuron would on average receive 27 inputs with a mean EPSP size of 1.5 mV, yielding a total synaptic input of about 40 mV (although the net effect would be smaller due to sublinear EPSP summation because of differences in timing or EPSP shunting). It is interesting to note that Kozlov *et al.* (2007) used a setup where each neuron received input from 39 other cells with a mean EPSP of 1 mV, giving almost exactly the same total synaptic drive. It may be that a certain excitation level in this neighbourhood is needed to sustain the bout. In the *in vivo* network, the cells also seem to receive additional depolarization during this kind of activity; in Kozlov *et al.* (2007), a small additional current injection was necessary for the network to generate the locomotor bouts, and in the simulation discussed here the hyper-slow mGluR component can be said to implement this function. mGluR activation is indeed one of the proposed explanations for the sustained depolarization observed during locomotor bouts (Cangiano and Grillner, 2005).

Finally, the simulation model as presented here had a shortcoming in an aspect not related to the problem it was designed to study. When simulating bath AMPA and/or NMDA activation of the model network, it was discovered that the network would tend to go into an unphysiological high-frequency state, except in a small parameter range of bath EAA concentration. This prompted the investigation in Paper IV.

4.4. Paper IV: Co-existence of a smooth and a stereotypical state

4.4.1. Motivation

As has already been discussed, hemisegmental preparations from the lamprey spinal cord can show rhythmic activity in response to NMDA or D-glutamate

application, and in response to a transient stimulus. D-glutamate application yields a burst rhythm of about 2-12 Hz depending on the concentration of the EAA; NMDA application initially yields the same type of rhythm, after which a slower (0.1-0.4 Hz) rhythm can develop over the course of several hours. In locomotor bouts, there is no frequency dependence on the initial input current magnitude; over a certain threshold, a given preparation shows a stereotypical bursting frequency. The locomotor bout activity discussed in connection with Paper III is fast and robustly observed in experiments, which suggests that the hemisegmental networks contain a high capacity for regenerative self-excitation. Now, if these highly excitable networks are stimulated by bath-applied EAAs, why don't they go to the fast locomotor bout state, or start spiking even faster than in a "regular" locomotor bout? How can a slower, graded activity state ("tonic state") co-exist in the same network with a fast, stereotypical state ("bout state")?

We posited that this must be due to a bifurcation in the dynamics of the network, so that two distinct dynamical modes, reachable via different initial conditions, appear. Thus the phase portrait of the system (with EAA concentration on the x axis and starting frequency on the y axis), for a given EAA concentration level, would contain two fixed points (corresponding to the frequencies of the tonic and bout states, respectively), separated by an unstable fixed point. If the system starts above the frequency of the unstable point, it would then end up in the bout state; otherwise it would end up in the tonic state. In other words, the system would be bistable and sensitive to initial conditions. In the experimental preparation, a sufficiently strong current pulse of the proper duration would send the network to the bout state, but when stimulating it with bath EAA, it would start from a low (or zero) frequency and end up in the tonic state. Armed with this conceptual model, we set out to construct a simple network that could show this qualitative behaviour.

4.4.2. Modelling approach

Since we realized that the generation of the state space diagrams would require a large number of simulation runs, we chose to use the Izhikevich neuron model for the neuronal units. The model from Paper III required around 1 hour per second of simulation time, with the full model requiring even more, on our computers. The parameters of the Izhikevich model were tuned to give reasonable response properties, with f-I curves similar to those measured for lamprey excitatory interneurons (Buchanan, 1993). Inhibitory transmission was again neglected, so the network consisted of recurrently coupled excitatory interneurons. We chose to use 50 neurons with a coupling probability of 30%; each neuron therefore received input from about 15 neurons. The Izhikevich model as originally described has only fast AMPA synapses which are active at their full conductance for a single time step, after which they decay to zero. We added NMDA synapses with a magnesium block and an exponential decay time that was varied in some runs, but the default value was 180 ms. ACh and mGluR synapses were not introduced because we knew that from Paper III that loco-

motor bouts could be modelled by AMPA and NMDA receptors only, and for easier interpretation of the results. Later, dynamical aspects were added to the synapses in the form of facilitation and saturation. Both of these processes were implemented in a simple way: a facilitating synapse was enhanced by a factor 3.5 if it received two spikes within the facilitation window of 50 ms, and a saturating synapse could not sum its activity over 140 single EPSPs.

The AMPA:NMDA maximum conductance ratio was 1:1, but a single EPSP will always be larger in an AMPA synapse (sometimes much larger) due to the magnesium block, which decreases the effective conductance of the NMDA synapse at hyperpolarized potentials. Neurons were assumed to vary in their sizes (this was modelled by multiplying their input by a random normally distributed factor, reflecting natural variation in input resistance) so that their intrinsic firing frequencies were variable. Bath glutamate activation was simulated by adding constant factors to the AMPA and NMDA synaptic conductances.

4.4.3. Results

Our initial runs with static synapses suggested that while either tonic or bout-like activity could be generated by model networks depending on parameter values (specifically, we varied the NMDA decay time constant), these activities could never co-exist in the same network. If the NMDA decay time constant was high, the system would always go to the bout state (because a large tonic depolarization from NMDA synapses would dominate), and if it was too low, the system would go to the tonic state.

Noting that frequency (and cell type) dependent synaptic enhancement and depression have been described in lamprey CPG neurons, we introduced simple versions of synaptic facilitation and saturation as described above. (Depression could also have been included, but turned out to be non-necessary.) With these new synaptic dynamics, we were able to simulate a state diagram where tonic and bout activity states could co-exist. The frequency in the tonic state was smoothly dependent on simulated glutamate level, while the bout state showed a weaker concentration dependence. Note that for the bout state, we only have a single data point from experiments: the case with zero D-glutamate, which can yield a locomotor bout in both experiments and in the model.

A conceptual explanation of why synaptic dynamics yield the desired outcome can be readily formulated. Synaptic facilitation stabilizes the bout state by enhancing the synaptic efficacy as soon as a critical frequency is reached, while at lower frequencies, facilitation will never set in. This enables the tonic state to vary smoothly without leaping to the bout state. However, the facilitation cannot be allowed to run unchecked, because it would eventually lead to tonic high-frequency spiking far beyond the bout frequency. Therefore some mechanism must control that synaptic conductances do not become too large, and this is accomplished by synaptic saturation in the present model. Instead, some form of depression or fatigue could have been used.

Summarizing, our simulations show that two different activity states can co-exist in the same network, given the presence of synaptic dynamics. Similar

results were later reported in a study where the authors examined a homogeneous excitatory network analytically (Barak and Tsodyks, 2007).

Interestingly, after the submission of Paper IV, we found that more than two steady states could coexist in our networks, given that these were given a specific type of connectivity. By constructing a locally clustered network (with dense local and sparse global connections, but the same average connectivity as before) we were able to obtain networks where 1-6 steady states could be reached. Preliminary results indicate that the "new" states, which are always intermediate between the tonic and bout states, appear because the bout state can now be reached in separate, localized parts of the network, without the whole network necessarily becoming activated. The intermediate states therefore represent situations where some parts of the network are in the bout state and other (presumably more isolated) parts are in the tonic state. It is interesting to speculate whether this kind of multistability in a relatively simple network can have any physiological function. It is clear, however, that the connectivity pattern does matter in some cases, and that a random connectivity should not be automatically assumed.

4.4.4. Interpretation and caveats

There are a couple of confounding factors in the interpretation of these results, although they are interesting from a theoretical point of view. Needless to say, the components we found sufficient for network bistability are not necessary the actual components used to accomplish it in the lamprey. Also, it is conceivable that in the tonic, glutamate-stimulated state, the activity takes some time to develop, and the network may have medium time scale compensatory mechanisms that turn down the excitability during this period. By contrast, in the case of electric current application, the network is "taken by surprise", so that the compensatory mechanisms do not have time to develop, thus enabling the highly excitable locomotor bout state. However, this has not been experimentally established.

With regard to parameter values, one may wonder about the unusually large facilitation factor, for instance. While very large facilitation factors have been found in some neurons (Thomson, 2000), this is likely not the case for lamprey CPG neurons (Parker and Grillner, 2000a; Parker, 2003b). Also, the NMDA saturation limit of 140 single EPSPs seems high. However, I believe that the necessity for such values may be connected to an issue discussed above, in connection with Paper III. As was previously mentioned, a tonic depolarization seems to develop during locomotor bouts, and this depolarization was not explicitly modelled here. The high NMDA synaptic currents allowed by our synaptic dynamics may provide the extra depolarizing drive necessary for modelling the experimental system. Also, neurons in the present simulation only receive EPSPs from about 15 other neurons, which is considerably less than in other locomotor bout simulations and leaves each neuron with even less net excitation. The dynamic synaptic parameters may compensate for this.

4.5. Paper V: An experimentally based model of NMDA-TTX oscillations

4.5.1. Motivation

As already mentioned, spinal CPG neurons in the lamprey – as well as other organisms – can display intrinsic rhythmic behaviour in the form of membrane potential oscillations when stimulated by bath-applied NMDA. These oscillations have been examined in the lamprey using tetrodotoxin (TTX), which blocks sodium channels, and thus abolishes action potential propagation. In other words, TTX pharmacologically isolates neurons from each other, so that "pure" NMDA oscillations can be recorded from their cell bodies. NMDA properties are thought to be important for the generation of locomotor activity, possibly as a mechanism for augmenting excitatory synaptic inputs (Grillner *et al.*, 2001). As already mentioned, it is well established that NMDA receptor activity is important for fictive locomotion, and NMDA-TTX oscillations are a useful tool for understanding the properties of NMDA receptors. Fig. 4.3 shows an example of NMDA-TTX oscillations. Refer to Paper V for a detailed conceptual explanation of how they occur.

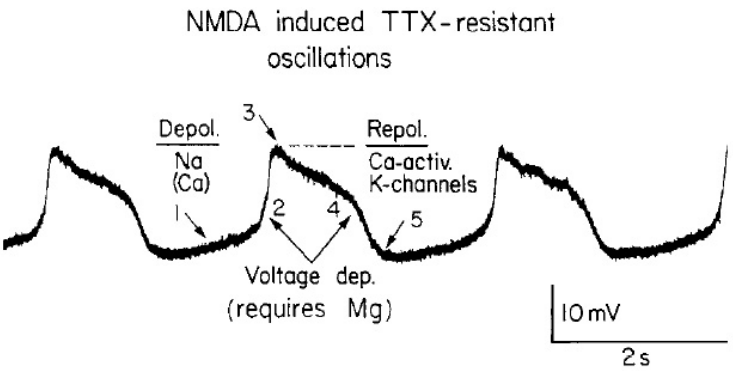

Figure 4.3. *NMDA-TTX oscillations in lamprey CPG neurons. In the depolarizing phase, Na^+ and Ca^{2+} enter through Mg^{2+}-dependent NMDA channels. In the repolarizing phase, K_{Ca} channels restore the membrane potential to a level close to the resting potential. [Reproduced from Wallén and Grillner (1987), Copyright 1987 by the Society for Neuroscience]*

The motivation for the study presented in Paper V arises from the process of modelling the lamprey CPG neuron and from examining previous models. An counterintuitive feature, which has long been known, occurs in simulations using either one of the previously developed cell models (e.g. Tegnér *et al.*, 1998) and the new cell model in Paper I. This feature is that the oscillation frequency

goes down (or sometimes stays constant) as the simulated bath NMDA concentration is increased. This is counter-intuitive because earlier experiments (Brodin *et al.*, 1985) showed that the frequency dependence in fictive locomotion (i.e. without TTX applied) is precisely opposite: higher NMDA concentrations give higher frequencies. It therefore seems natural that NMDA oscillations in TTX should have the same frequency dependence. However, it is difficult to compare the rhythmic activity during fictive locomotion with the NMDA-TTX case for two reasons. During fictive locomotion, the neurons receive phasic synaptic input (Kahn, 1982; Russell and Wallén, 1982) and fire action potentials. Both of these factors could conceivably modify the dynamics enough to yield a different frequency dependence. Our main motivation here was to characterize the frequency-dependence of NMDA-TTX oscillations to resolve this question.

A second motivation, also born out of previous modelling work, was to try to construct a simplified model of NMDA-TTX oscillations to get a better understanding of how and why they appear. Previous models were rather cumbersome to analyze because of the large number of parameters, including morphological and dendritic properties. It was hoped that a simple "point-neuron" model could shed some light on the dynamics of NMDA-TTX oscillations. Of course, we wanted to implement the correct frequency dependence in the model, depending on the experimental results. In order to better be able to construct such a model, we also used new experimental results to try to isolate the NMDA-TTX oscillations to their minimal form, with the least number of necessary components.

4.5.2. Methodology

We began by performing experiments with NMDA and TTX application in CPG neurons from lamprey of different species, with NMDA varied in three (or sometimes more) steps, to examine the frequency dependence of the oscillations. We found that the frequency increased with the NMDA concentration, and based on this result, we constructed different versions of the simplified mathematical model described in chapter 3 (section 3.5.2). In order to better constrain the model, we used previously unpublished experimental results (reported in the paper) examining the effects of various channel blockers. Our simplest NMDA-TTX oscillation model (the "minimal model") is one containing only NMDA channels, K_{Ca} channels and a leak conductance, which may be the only components necessary for generating the oscillations. Note that for simplicity, we did not distinguish between K_{CaN} and K_{CaNMDA} channels, as was done in Paper I. The most complex model, which was constructed for addressing the frequency dependence phenomenon, included two further types of components, voltage-dependent potassium (K_v) channels and voltage-dependent calcium (Ca_v) channels. This model was based on simply keeping the parameters constant in the minimal model and adding equations describing the new channels.

We set up several criteria that a successful model should meet. These were based both on typical characteristics of "normal" NMDA-TTX oscillations, and on information obtained from many types of channel-blocking experiments.

4.5.3. Results

Frequency dependence

The results from the frequency-dependence experiments showed that the frequency was indeed increased when the NMDA concentration was increased from 100 to 200 μM, as in fictive locomotion. The frequency was in some cases more than doubled when going from 100 to 200 μM. The qualitative results were consistent over all preparations. I will call this type of frequency dependence "positive", and the opposite case – slower frequencies for increasing NMDA concentrations – "negative" frequency dependence. Except for the information about the frequency dependence, a further interesting fact was that the length of the plateau seemed not to increase much for higher NMDA concentrations. Plateau lengthening at high NMDA levels was thought to be the probable reason for the simulated decrease in frequency at high NMDA levels in previous models. From visual inspection of the recordings, it was instead the inter-plateau interval that was changed (=shortened) when NMDA concentration was increased.

Model evaluation and sensitivity analysis

We defined a set of criteria that a successful model should be able to fulfill. Note that all of these criteria are defined for a g_{nmda} range $[g^{min}_{nmda}\ 2 \cdot g^{min}_{nmda}]$ where g^{min}_{nmda} is the (approximate) minimum g_{nmda} value that yields oscillations. We chose this interval because the experiments were done from 100 to 200 μM concentrations, and oscillations were not observed for concentrations below 100 μM; so the experiments can roughly be said to characterize a range of approximately $[g^{min}_{nmda}$ $2 \cdot g^{min}_{nmda}]$.

- The frequency dependence should be correct (higher NMDA concentration gives higher frequency).
- The frequency should be within the experimentally observed range (0.05-1 Hz).
- The amplitude should be within the experimentally observed range (10-40 mV).
- There should be little plateau lengthening.
- Blocking K_v channels should give rise to larger-amplitude oscillations.
- Blocking both K_v and Ca_v channels should still allow "regular" NMDA-TTX oscillations.
- Increasing (depolarizing) the resting membrane potential should result in faster oscillations with reduced amplitude.

The model we developed was able to fulfill all the desired characteristics. Moreover, it turned out to be very robust to parameter changes, according to the sensitivity analysis we performed. In fact, by only changing a single parameter at a time, we were unable to obtain a model showing the negative frequency dependence. By changing parameters in appropriate ways, one can obtain oscillations that resemble those found in a range of different experiments.

Why didn't the old model work?

The final question to answer, then, was why the old models based on Brodin *et al.* (1991) (e.g. Tegnér *et al.*, 1998) couldn't show the positive frequency dependence. I will call the family of models based on Brodin *et al.* (1991) "the old model" from now on. As the sensitivity analysis indicated, obtaining the negative frequency dependence in our new model was not a matter of simply changing one parameter. By comparing the output of our newly developed model to the old model, we discovered a combination of two modifications that yielded the negative frequency dependence in the new model. Running a version of the old model with K_v and Ca_v channels blocked – leaving just NMDA, K_{Ca} and leak channels, as in our minimal model– we discovered that it then had a positive frequency dependence, but that it generated NMDA-TTX oscillations with an exaggerated amplitude (>50 mV) where the plateau was at -20 mV. Substituting the magnesium block function used in the old model into our minimal model, the same thing happened - large-amplitude plateaus at around -20 mV. In spite of the difference in complexity of the models, they thus showed qualitatively similar behaviour in this case. Further simulations showed that the given magnesium block function induces a bistability where the model neuron must have either no oscillations or large-amplitude oscillations. From this we derived a prediction: that the magnesium block function (the steady-state I-V relation) of lamprey CPG neurons may be substantially different from what has been assumed. Changing the magnesium block was by itself not sufficient for switching the frequency dependence in our new model. By comparing the relative magnitudes of parameters in the old and new models, we found that the older model had a relatively much higher K_v conductance. By increasing this parameter substantially in the new model, when using the "old" magnesium block function, the frequency dependence on NMDA concentration became negative.

4.5.4. Interpretation and caveats

An important fact to keep in mind when extrapolating from NMDA-TTX oscillations to behaviour is that it is uncertain how well the bath-applied NMDA approximates the input to neurons under physiological conditions. *In vivo*, NMDA receptors are activated transiently rather than tonically; on the other hand, NMDA synapses tend to sum their activity, and given strong input from e.g. the reticulospinal system, it may be that summing results in a more or less tonic NMDA receptor activation, maybe close to the saturation limit of the receptor. Also, the fact that there are no action potentials complicates the interpretation of how the NMDA-TTX oscillations can be related to normal locomotor activity. Nevertheless, experiments (and simulations) of NMDA-TTX oscillations are valuable, because they offer a somewhat simplified model system where e.g. ion channel properties can be studied. They give insight into the workings of the NMDA receptor - insights which may then be used to better understand the network through thought experiments or simulations. The work presented in Paper V must of course be interpreted in the light of the numerous simplifications and assumptions made. However, I believe that these simplifications are not critical,

and that the model captures much of the essence of the NMDA-TTX oscillations. It is to be hoped that this study can offer some further guidance for future work where NMDA receptors are modelled. Finally, this project was the only one in the thesis where the ideal feedback loop of experiments and modelling was fully realized.

4.6. Paper VI: Coupling biochemical and neuronal models

4.6.1. Motivation and experimental background

Calcium permeable ion channels and calcium-dependent potassium channels control a large part of a lamprey locomotor neuron's behaviour (Bacskai *et al.*, 1995); working in tandem with the calcium-dependent potassium currents, they control phenomena such as firing frequency adaptation, post-inhibitory rebound and burst termination.

Calcium can enter the cell through (at least) N-, L-, and P/Q-type calcium channels (all high-voltage activated), low-voltage activated calcium channels, and NMDA channels. It seems that at least some pathways involving calcium are segregated, so that (for example) only calcium that has entered through N and P/Q type calcium channels activate the sAHP-determining K_{Ca} channel in the lamprey (Wikström and El Manira, 1998). It has been suggested that there are "microdomains" where different types of ion channels are co-localized in close proximity and where effective calcium concentrations become extremely high due to the microdomain's small volume (Goldberg *et al.*, 2003). In addition to entry from the exterior through ion channels, calcium can also come into the cytoplasm by leaving intracellular stores in the endoplasmic reticulum (ER), a specialized subcellular structure primarily involved in the synthesis of proteins and lipids (Alberts *et al.*, 1994).

Recent experiments in lamprey locomotor neurons (Kettunen *et al.*, 2002) showed that intracellular calcium release occurs in these neurons and is the result of a cascade initiated by glutamate binding to the metabotropic glutamate receptor 5 (mGluR5) and culminating in the activation of inositol (1,4,5)-trisphosphate receptor (IP_3) receptors (IP_3R) in the ER. IP_3 is a so-called second messenger molecule which mediates the release of Ca^{2+} ions from the ER into the cytoplasm (Hamada *et al.*, 2002).

The IP_3-dependent increase in the intracellular calcium level is oscillatory, which is a consequence of the kinetics of the IP_3 receptor (see below). The oscillations are very slow - with a period of 30-200 seconds, they are definitely on a different time scale than spiking or locomotor network bursting.

The IP_3 receptor is a tetrameric ion channel that releases Ca^{2+} from intracellular stores in response to IP_3 binding (Hamada *et al.*, 2002). The degree of opening of the channel is influenced by both IP_3 and Ca^{2+} concentration. IP_3 is always needed for the channel to open, but it is itself not sufficient for channel opening. Ca^{2+} acts as a co-agonist at low concentrations, which results in a positive feedback loop: cytoplasmic Ca^{2+} helps open the IP_3R, which in turn releases more Ca^{2+} into the cytoplasm (Miyakawa *et al.*, 2001). However, Ca^{2+} is also a

repressor of IP_3R function at high concentration (Hamada *et al.*, 2002). Thus the IP_3R has a bell-shaped dependence on Ca^{2+} concentration - at low values it is not activated enough and at high values it is repressed, so an intermediate value gives the highest activation, at least during steady state conditions.

The goals of the project described in Paper VI was, on one hand, to create a detailed biochemical model of the reaction pathway starting with mGluR5 activation and ending in IP_3-mediated Ca^{2+} release, and on the other hand, to couple this biochemical model to (the then current version of) the electrophysiological model of Paper I.

4.6.2. Methodology

A plausible reaction pathway between mGluR5 activation and Ca^{2+} release was posited, guided by experimental results from Kettunen *et al.* (2002). Fig. 4.4 contains a graphical representation of the model; numbers refer to reactions (see Appendix). A very brief summary of the pathway follows:

- mGluRs are activated by glutamate molecules binding to them.
- Activated mGluRs activate G proteins. These are normally coupled to guanosine diphosphate (GDP), but upon activation GDP is exchanged for guanosine triphosphate (GTP) and the G protein separates into two parts, G_α and $G_{\beta\gamma}$.
- The G_α proteins activate phospholipase C (PLC); PLC turns off G_α, so there is a negative feedback in this step.
- PLC produces IP_3 through hydrolysis of phosphatidylinositol 4,5-biphosphate (PIP2).
- IP_3 activates the IP_3 receptor. The receptor opens its channel and releases Ca^{2+}. Ca^{2+} upregulates PLC activity, so there is a positive feedback from Ca^{2+} to PLC.

Kinetic parameters for the reactions involved were estimated from the literature; since such data is scarce, values from different systems were used. Some of the parameters were adjusted to yield output more similar to that observed in the lamprey experiments. The reaction network was simulated by running coupled ordinary differential equations as described in the previous chapter, first using the XPPAUT package and then using the CHEMESIS extension to the GENESIS neuronal modeling software. Finally, the CHEMESIS implementation was coupled to the electrophysiological neuron model using functions in CHEMESIS and GENESIS.

4.6.3. Results

Even with the high level of uncertainty in parameter values, we were able to obtain IP_3-mediated calcium oscillations in the biochemical model using either type of kinetic model for the IP_3 receptor. However, the fit to data was not ideal:

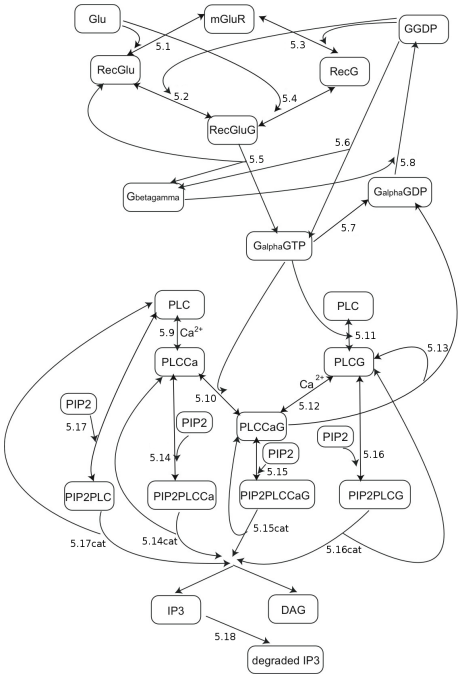

Figure 4.4. *A graphical representation of the simulated biochemical pathway connecting mGluR5 activation to IP_3- and calcium-mediated calcium oscillations. The numbers refer to equations in the model. Single arrows symbolize irreversible reactions; double arrows symbolize reversible reactions. [Picture created by Kristofer Hallén, 2002 and modified by Mikael Huss, 2007.]*

the De Young-Keizer model of the IP_3R was better at approximating the shape of the oscillations, while the Tang-Othmer model gave more realistic frequencies. A simulated replication of an experiment from Kettunen *et al.* (2002) yielded a dynamical behaviour very similar to the experimental one using the De Young-Keizer model, but not using the Tang-Othmer model. In this experiment, glutamate was added in double pulses. The calcium oscillations had a pattern where the first glutamate application step resulted in steady oscillations until the glutamate was removed, after which one truncated calcium pulse appeared before the calcium concentration returned to baseline. When glutamate was applied in a second step, the calcium oscillations started again with an amplitude that was slightly enhanced compared to the previous glutamate step. These features were all faithfully replicated by our biochemical model with the De Young-Keizer IP_3R. Although the time scale was different between the simulation and the experiment, the oscillation frequency was nevertheless within the experimental range as reported in Kettunen *et al.* (2002).

The activation of mGluR5 receptors leads to slow intracellular calcium oscillations (f=0.005-0.033 Hz; Kettunen *et al.*, 2002) which, if present during

fictive swimming, cause the swimming rhythm to slow down. How the rhythm is slowed down is not yet known. In Paper VI, we hypothesized that the intracellularly released calcium could activate calcium-dependent potassium channels and thereby hyperpolarize the cell, ultimately leading to a slowed-down locomotor rhythm. To test this idea, we combined the model of the glutamate-induced, IP_3-mediated calcium oscillations with the previously developed locomotor neuron model described in Paper I. This hybrid model showed that our proposed mechanism was feasible. Preliminary experiments indicate that the hyperpolarization is not mediated by potassium channels in the soma, since the somatic resting potential is not affected by the oscillations (El Manira, personal communication). However, as our generic neuron model has pointed out (Paper I), the soma probably has a very low density of K_{Ca} current in comparison to the dendritic tree, which means that the major contribution to a potential Ca^{2+}-mediated hyperpolarization would come from dendritic K_{Ca} currents. It is not yet known from experiments whether the dendrites are hyperpolarized during IP_3-mediated Ca^{2+} oscillations.

4.6.4. Interpretation and caveats

Given the scarcity of data on kinetic parameters for the included reactions, the results are of course highly speculative. The model output, in some respects, is a good match for experimental results, but the components of the pathway should be better characterized before one can claim a good quantitative description of the phenomenon. The work in Paper VI should be regarded as a tentative attempt to tie together the levels of biochemistry and electrophysiology. The predictions of the combined model may, in the future, be tested and used as a starting point for further research.

Chapter 5

CONCLUSIONS AND FUTURE WORK

5.1. Thesis summary

In this thesis, I have examined different aspects of pattern generation in the lamprey spinal cord through computational modelling. As a starting point for detailed network simulations, we constructed a generic model of a spinal CPG neuron based as far as possible on published experimental data. This model served as a building block of a large-scale simulation of the whole spinal CPG, where three important results emerged: that the rostral part of the spinal cord can control the phase lag during forward and backward swimming, that individual segments can keep phase lags constant if the individual neurons have sufficient variation in their firing properties, and that reciprocal inhibition may be crucial for achieving reliable dynamic control of the swimming pattern. The latter finding is particularly interesting in that reciprocal inhibition was already known to be an important control principle in locomotion; our results thus suggest that reciprocal inhibition (like many other features of biological systems) is "multi-tasking" - it controls both alternation of activity and robustness of pattern generation.

Interesting results about the rhythm-generating capabilities of relatively small hemisegmental networks have emerged during recent years. The segmental CPG network in lamprey can, in view of these results, be considered to have the same organization as in the half-center model, but with half-centers capable of generating their own rhythmic activity. We used network simulations - both abstract and detailed ones - to address questions about how the self-sustaining activity in hemisegmental networks comes about, and how it can co-exist with a smoothly graded activity mode. The results suggested that known features of lamprey CPG neurons and networks are sufficient to explain these phenomena.

Rhythmic activity is not always a network property - intrinsic NMDA-driven oscillations are found in CPG neurons from lamprey as well as other species. In order to understand more about the properties of these oscillations, we per-

formed a combined experimental and computational study which culminated in the construction of a relatively simple model that can reproduce and explain many of the experimental findings. We were also able to suggest why earlier models of the same oscillations failed to reproduce the new experimental data emanating from our study.

Receptor-mediated modulation is an ubiquitous feature of neurons. This modulation takes place through the action of biochemical pathways triggered by receptor activation. We constructed a model able to simulate this kind of modulation by merging a biochemical pathway model with an electrophysiological neuron model. With this type of model, one can address interesting questions about neuromodulation, although in our paper it was ultimately difficult to proceed with the exploratory modelling without extensive further experimentation.

5.2. Future work

Many interesting questions remain about the lamprey CPG network. Some of the questions I would like to see addressed in future work are the following.

- How is the hemisegmental rhythm connected to the segmental rhythm?

Assuming that the electrically activated hemicord preparation is representative of hemicord preparations under other conditions, the hemisegmental rhythm appears to be generated by synchronization of neurons that spike only once per cycle (Cangiano and Grillner, 2005). By contrast, during rhythmic activity recorded from segmental preparations (or the full spinal cord), neurons often fire many spikes at low frequency on top of a depolarized plateau during a locomotor cycle. The segmental rhythm is 3-4 times slower on average, and the fast rhythm in hemicord preparations - which was shown by Cangiano and Grillner (2003) to be linked to fictive swimming - has not been observed to go below 2 Hz, while the segmental rhythm can be as slow as 0.1 Hz. It thus seems that the hemisegmental and segmental rhythms represent different dynamical modes. It would be interesting to further investigate how the inhibitory (and maybe excitatory) cross-connections promote this putative shift in dynamics.

- What is the role of the slow, NMDA-dependent rhythm in hemisegmental networks?

Cangiano and Grillner (2003) found, in addition to the fast rhythm which was related to fictive swimming, a slower (0.1-0.4 Hz) type of rhythmic activity which was dependent on NMDA. This rhythm could not be connected to fictive swimming. It would be interesting to examine this rhythm further. Is it nevertheless linked to low-frequency segmental bursting, even though this could not be shown in experiments? Also, how is the slow hemisegmental rhythm generated? It is known that it is magnesium-dependent, but the long time required for the rhythm to develop suggests that there may be additional slow activity-dependent effects involved.

- What is the role of ipsilateral inhibitory transmission?

Small inhibitory interneurons that project within hemisegments have been characterized, but found not to be involved in generating the hemisegmental rhythm (Cangiano and Grillner, 2003). Nevertheless, they might be important for other reasons. New simulations and experiments could address their putative role in e.g. allowing smooth grading of rhythmic activity. A computational study of cortical circuits (Lundqvist *et al.*, 2006) also showed that adding ipsilateral inhibition to an excitatory network can lead to physiologically realistic-looking bursting activity. It could be hypothesized that in the lamprey, the ipsilateral inhibition is more important in segmental bursting than in hemisegmental bursting, and that it could be involved in shaping the depolarized plateaus seen during fictive swimming. These have, so far, proved hard to model, since the spiking frequency on the plateaus tends to become unrealistically high in the models.

- Why are action potentials in dissociated neurons and intact neurons different?

As mentioned earlier, the generic neuron model in Paper I cannot account for the very significant differences in action potential width between dissociated and intact neurons. As new measurement techniques become available, it may be possible to acquire more accurate measurements. If the differences persist, it would be interesting to see whether this is a question of developmental differences (dissociated cells are usually from larval lampreys and intact cells usually from adult ones). In general, it would be interesting to extensively compare characteristics of ionic currents in larval and adult lamprey neurons.

- What is the recruitment pattern of excitatory interneurons during fictive locomotion?

It has long been known that the speed and strength of movements is graded in animals using a "size-recruitment principle", whereby motoneurons of increasing size (decreasing input resistance) are gradually recruited into the active pool (Kandel *et al.*, 2000). In contrast, interneuronal recruitment has been harder to study and therefore results are scarce (Bhatt *et al.*, 2007). Are all excitatory interneurons (for example) active during locomotor activity, or is only a subset recruited at a given time? At least during locomotor bouts in lamprey, only part of the EIN network was found to be active (Cangiano and Grillner, 2005), and similar results were obtained in an earlier study in *Xenopus* (Sillar and Roberts, 1993). However, Bhatt *et al.* (2007) reported that during escape responses in zebrafish, essentially all EINs are active both during slow and fast movements. The grading of movement strength is instead accomplished by varying the firing intensity in individual neurons. It would be interesting to examine the recruitment pattern and changes in firing intensity (if any) of lamprey EINs during fictive locomotion. Also, as our preliminary results on multistability in excitatory networks (see end of Section 4.4.3) suggest, the connectivity of a network can have consequences. It would therefore also be interesting to know more about the synaptic connectivity pattern of EINs and try to relate it to neuronal recruitment.

In addition, countless questions about adaptive properties such as synaptic plasticity and neuromodulation can be asked.

5.3. Closing words

Even though the lamprey is considered a "primitive" vertebrate, its spinal locomotor circuits have turned out to be quite sophisticated and adaptable, and are rewarding as an object of study. The work described in this thesis has made me appreciate the efforts that have gone into understanding this model system for locomotion. I have also found CPG research as a whole to be a rich and fascinating field. In the beginning, I probably underestimated both the experimental and theoretical challenges faced by researchers in this field.

Computational biology, including computational neuroscience, is still at an early stage of development. Coming years and decades will undoubtedly provide progress in leaps and bounds through e.g. data standardization and database integration, new theoretical formalisms for describing biological processes, and of course, more powerful computing systems. When it comes to the modelling process itself, I have found that it is essential to have a clear question in mind when starting to develop a computational model, and to connect the model firmly to experimental research. As mentioned earlier, the ideal case is one where simulations and experiments interact in a mutually beneficial loop. It is perhaps significant for my development as a computational modeller that it was the last project performed for this thesis (the work presented in Paper V) where the interplay between modelling and experiments was the strongest.

Bibliography

ALBERTS, B., BRAY, D., LEWIS, J., RAFF, M., ROBERTS, K. AND WATSON, J. D., *Molecular biology of the cell*, Garland, New York, 3rd edition, **1994**.

ALFORD, S. AND GRILLNER, S., The involvement of $GABA_B$ receptors and coupled G-proteins in spinal GABAergic presynaptic inhibition, *J Neurosci*, 11(12):3718–3726, **1991**.

ALFORD, S. AND WILLIAMS, T. L., Endogenous activation of glycine and NMDA receptors in lamprey spinal cord during fictive locomotion, *J Neurosci*, 9(8):2792–2800, **1989**.

ARSHAVSKY, Y. I., BELOOZEROVA, I. N., ORLOVSKY, G. N., PANCHIN, Y. V. AND PAVLOVA, G. A., Control of locomotion in marine mollusc *Clione limacina*. III. On the origin of locomotory rhythm, *Exp Brain Res*, 58(2):273–284, **1985**.

AYERS, J., WILBUR, C. AND OLCOTT, C., Lamprey robots, *Proceedings of the international symposium on aqua biomechanisms*, **2000**.

BACSKAI, B. J., WALLÉN, P., LEV-RAM, V., GRILLNER, S. AND TSIEN, R. Y., Activity-related calcium dynamics in lamprey motoneurons as revealed by video-rate confocal microscopy, *Neuron*, 14(1):19–28, **1995**.

BARAK, O. AND TSODYKS, M., Persistent activity in neural networks with dynamic synapses, *PLoS Comp Biol*, 2(3):e35, **2007**.

BARRY, M. AND O'DONOVAN, M. J., The effects of amino acids and their antagonists on the generation of motor activity in the isolated chick cord, *Dev Brain Res*, 433(2):271–276, **1987**.

BHATT, D. H., MCLEAN, D. L., HALE, M. E. AND FETCHO, J. R., Grading Movement Strength by Changes in Firing Intensity versus Recruitment of Spinal Interneurons, *Neuron*, 53(1):91–102, **2007**.

BIRÓ, Z., HILL, R. H. AND GRILLNER, S., 5-HT Modulation of Identified Segmental Premotor Interneurons in the Lamprey Spinal Cord, *J Neurophysiol*, 96(2):931–935, **2006**.

BLACKWELL, K. T. AND HELLGREN KOTALESKI, J., *Neuroscience Databases: a Practical Guide*, chapter Modeling the dynamics of second-messenger pathways, Kluwer Academic Publishers, Norwell, MA, **2002**.

BRENNER, S., Theoretical biology in the third millennium, *Philos Trans R Soc Lond B Biol Sci*, 354(1392):1963–1965, **1999**.

BRODIN, L., GRILLNER, S. AND ROVAINEN, C. M., N-methyl-D-aspartate (NMDA), kainate and quisqualate receptors and the generation of fictive locomotion in the lamprey spinal cord, *Brain Res*, 325(1-2):302–306, **1985**.

BRODIN, L., TRÅVÉN, H. G., LANSNER, A., WALLÉN, P., EKEBERG, Ö. AND GRILLNER, S., Computer simulations of N-methyl-D-aspartate receptor-induced membrane properties in a neuron model, *J Neurophysiol*, 66(2):473–484, **1991**.

BROWN, G. T., The intrinsic factors in the act of progression in the mammal, *Proc Roy Soc London*, 84(572):308–319, **1911**.

BUCHANAN, J. T., Identification of interneurons with contralateral, caudal axons in the lamprey spinal cord: synaptic interactions and morphology., *J Neurophysiol*, 47(5):961–975, **1982**.

BUCHANAN, J. T., Neural network simulations of coupled locomotor oscillators in the lamprey spinal cord, *Biol Cybern*, 66(4):367–374, **1992**.

BUCHANAN, J. T., Electrophysiological properties of identified classes of lamprey spinal neurons, *J Neurophysiol*, 70(6):2313–2335, **1993**.

BUCHANAN, J. T., Commissural interneurons in rhythm generation and intersegmental coupling in the lamprey spinal cord, *J Neurophysiol*, 81(5):2037–2045, **1999**.

BUCHANAN, J. T., Contributions of identifiable neurons and neuron classes to lamprey vertebrate neurobiology, *Prog Neurobiol*, 63(4):441–466, **2001**.

BUCHANAN, J. T. AND COHEN, A. H., Activities of identified interneurons, motoneurons, and muscle fibers during fictive swimming in the lamprey and effects of reticulospinal and dorsal cell stimulation, *J Neurophysiol*, 47(5):948–960, **1982**.

BUCHANAN, J. T. AND GRILLNER, S., Newly identified 'glutamate interneurons' and their role in locomotion in the lamprey spinal cord, *Science*, 236(4799):312–314, **1987**.

BUCHANAN, J. T. AND GRILLNER, S., A new class of small inhibitory interneurones in the lamprey spinal cord, *Brain Res*, 438(1-2):404–407, **1988**.

BUCHANAN, J. T., GRILLNER, S., CULLHEIM, S. AND RISLING, M., Identification of excitatory interneurons contributing to generation of locomotion in lamprey: structure, pharmacology, and function, *J Neurophysiol*, 62(1):59–69, **1989**.

BUCHANAN, J. T. AND KASICKI, S., Segmental distribution of common synaptic inputs to spinal motoneurons during fictive swimming in the lamprey, *J Neurophysiol*, 82(3):1156–1163, **1999**.

CANGIANO, L. AND GRILLNER, S., Fast and slow locomotor burst generation in the hemispinal cord of the lamprey, *J Neurophysiol*, 89(6):2931–2942, **2003**.

CANGIANO, L. AND GRILLNER, S., Mechanisms of rhythm generation in a spinal locomotor network deprived of crossed connections: the lamprey hemicord, *J Neurosci*, 25(4):923–935, **2005**.

CHANCE, F. S., ABBOTT, L. F. AND REYES, A. D., Gain modulation from background synaptic input, *Neuron*, 35(4):773–782, **2002**.

CHRISTENSEN, B. N., Distribution of electrotonic synapses on identified lamprey neurons: a comparison of a model prediction with an electron microscopic analysis, *J Neurophysiol*, 49(3):705–716, **1983**.

COHEN, A. H., HOLMES, P. J. AND RAND, R. H., The nature of the coupling between segmental oscillators of the lamprey spinal generator for locomotion: a mathematical model, *J Math Biol*, 13(3):345–369, **1982**.

COHEN, A. H. AND WALLÉN, P., The neuronal correlate of locomotion in fish. "Fictive swimming" induced in an in vitro preparation of the lamprey spinal cord, *Exp Brain Res*, 41(1):11–18, **1980**.

CRESPI, A., BADERLSCHER, A., GUIGNARD, A. AND IJSPEERT, A. J., AmphiBot I: an amphibious snake-like robot, *Rob Auton Syst*, 50(4):163–175, **2005**.

DE SCHUTTER, E., EKEBERG, Ö., HELLGREN KOTALESKI, J., ACHARD, P. AND LANSNER, A., Biophysically detailed modelling of microcircuits and beyond, *Trends Neurosci*, 28(10):562–569, **2005**.

DE YOUNG, G. W. AND KEIZER, J., A single-pool inositol 1,4,5-trisphosphate-receptor-based model for agonist-stimulated oscillations in Ca^{2+} concentration, *Proc Natl Acad Sci U S A*, 89(20):9895–9899, **1992**.

DIBA, K., KOCH, C. AND SEGEV, I., Spike propagation in dendrites with stochastic ion channels, *J Comput Neurosci*, 20(1):77–84, **2006**.

EKEBERG, Ö., A combined neuronal and mechanical model of fish swimming, *Biol Cybern*, 69:363–374, **1993**.

EKEBERG, Ö. AND GRILLNER, S., Simulations of neuromuscular control in lamprey swimming, *Philos Trans R Soc Lond B Biol Sci*, 354(1385):895–902, **1999**.

EKEBERG, Ö., WALLÉN, P., LANSNER, A., TRÅVÉN, H., BRODIN, L. AND GRILLNER, S., A computer based model for realistic simulations of neural networks. I. The single neuron and synaptic interaction, *Biol Cybern*, 65(2):81–90, **1991**.

EL MANIRA, A. AND BUSSIÈRES, N., Calcium channel subtypes in lamprey sensory and motor neurons, *J Neurophysiol*, 78(3):1334–1340, **1997**.

EL MANIRA, A., KETTUNEN, P., HESS, D. AND KRIEGER, P., Metabotropic glutamate receptors provide intrinsic modulation of the lamprey locomotor network, *Brain Res Brain Res Rev*, 40(1-3):9–18, **2002**.

ERMENTROUT, B., *Simulating, analyzing and animating dynamical systems: a guide to XPPAUT for researchers and students*, SIAM, Philadelphia, **2002**.

FAGERSTEDT, P., ORLOVSKY, G. N., DELIAGINA, T. G., GRILLNER, S. AND ULLÉN, F., Lateral turns in the lamprey. II. Activity of reticulospinal neurons during the generation of fictive turns, *J Neurophysiol*, 86(5):2257–2265, **2001**.

FAGERSTEDT, P. AND ULLÉN, F., Lateral turns in the lamprey. I. Patterns of motoneuron activity, *J Neurophysiol*, 86(5):2246–2256, **2001**.

FITZHUGH, R., Impulses and physiological states in theoretical models of a nerve membrane, *Biophys J*, 1:445–466, **1961**.

FREUSBERG, A., Reflexbewegungen beim Hunde, *Pflueger's Archiv fuer die gesamte Physiologie*, 9:358–391, **1874**.

GOLDBERG, J. H., TAMAS, G., ARONOV, D. AND YUSTE, R., Calcium microdomains in aspiny dendrites, *Neuron*, 40(4):807–821, **2003**.

GREEN, J., *Henry I. King of England and Duke of Normandy*, Cambridge University Press, 1st edition, **2006**.

GRILLNER, S., The motor infrastructure: from ion channels to neuronal networks, *Nat Rev Neurosci*, 4(7):573–586, **2003**.

GRILLNER, S., Biological pattern generation: The cellular and computational logic of networks in motion, *Neuron*, 52(5):751–766, **2006**.

GRILLNER, S., BUCHANAN, J. T. AND LANSNER, A., Simulation of the segmental burst generating network for locomotion in lamprey, *Neurosci Lett*, 89(1):31–35, **1988**.

GRILLNER, S., MARKRAM, H., DE SCHUTTER, E., SILBERBERG, G. AND LEBEAU, F. E., Microcircuits in action–from CPGs to neocortex, *Trends Neurosci*, 28(10):525–533, **2005**.

GRILLNER, S. AND WALLÉN, P., Central pattern generators for locomotion, with special reference to vertebrates, *Annu Rev Neurosci*, 8:233–261, **1985**a.

GRILLNER, S. AND WALLÉN, P., The ionic mechanisms underlying N-methyl-D-aspartate receptor-induced, tetrodotoxin-resistant membrane potential oscillations in lamprey neurons active during locomotion, *Neurosci Lett*, 60(3):289–294, **1985**b.

GRILLNER, S., WALLÉN, P., HILL, R., CANGIANO, L. AND EL MANIRA, A., Ion channels of importance for the locomotor pattern generation in the lamprey brainstem-spinal cord, *J Physiol*, 533(Pt 1):23–30, **2001**.

GRILLNER, S. AND ZANGGER, P., On the central generation of locomotion in the low spinal cat, *Exp Brain Res*, 34(2):241–261, **1979**.

GUERTIN, P. A. AND HOUNSGAARD, J., NMDA-induced intrinsic voltage oscillations depend on L-type calcium channels in spinal motoneurons of adult turtles, *J Neurophysiol*, 80(6):3380–3382, **1998**.

HAMADA, K., MIYATA, T., MAYANAGI, K., HIROTA, J. AND MIKOSHIBA, K., Two-state conformational changes in inositol 1,4,5-trisphosphate receptor regulated by calcium, *J Biol Chem*, 277(24):21115–21118, **2002**.

HAMMARLUND, P. AND EKEBERG, Ö., Large neural network simulations on multiple hardware platforms, *J Comput Neurosci*, 5(4):443–459, **1998**.

HELLGREN, J., GRILLNER, S. AND LANSNER, A., Computer simulation of the segmental neural network generating locomotion in lamprey by using populations of network interneurons, *Biol Cybern*, 68(1):1–13, **1992**.

HELLGREN KOTALESKI, J., GRILLNER, S. AND LANSNER, A., Neural mechanisms potentially contributing to the intersegmental phase lag in lamprey. I. Segmental oscillations dependent on reciprocal inhibition, *Biol Cybern*, 81(4):317–330, **1999**a.

HELLGREN KOTALESKI, J., LANSNER, A. AND GRILLNER, S., Neural mechanisms potentially contributing to the intersegmental phase lag in lamprey.II. Hemisegmental oscillations produced by mutually coupled excitatory neurons, *Biol Cybern*, 81(4):299–315, **1999**b.

HERNANDEZ, P., ELBERT, K. AND DROGE, M. H., Spontaneous and NMDA evoked motor rhythms in the neonatal mouse spinal cord: an in vitro study with comparisons to in situ activity, *Exp Brain Res*, 85(1):66–74, **1991**.

HESS, D. AND EL MANIRA, A., Characterization of a high-voltage-activated I_A current with a role in spike timing and locomotor pattern generation, *Proc Natl Acad Sci U S A*, 98(9):5276–5281, **2001**.

HESS, D., NANOU, E. AND EL MANIRA, A., Characterization of Na^+-activated K^+ currents in larval lamprey spinal cord neurons, *J Neurophysiol*, 97(5):3484–3493, **2007**.

HILL, R. H., MATSUSHIMA, T., SCHOTLAND, J. AND GRILLNER, S., Apamin blocks the slow AHP in lamprey and delays termination of locomotor bursts, *Neuroreport*, 3(10):943–945, **1992**.

HILL, R. H., SVENSSON, E., DEWAEL, Y. AND GRILLNER, S., 5-HT inhibits N-type but not L-type Ca^{2+} channels via 5-HT_{1A} receptors in lamprey spinal neurons, *Eur J Neurosci*, 18(11):2919–2924, **2003**.

HODGKIN, A. L. AND HUXLEY, A. F., A quantitative description of membrane current and its application to conduction and excitation in nerve, *J Physiol*, 117(4):500–544, **1952**.

IJSPEERT, A. J., HALLAM, J. AND WILLSHAW, D., Evolving swimming controllers for a simulated lamprey with inspiration from neurobiology, *Adapt Beh*, 7(2):151–172, **1999**.

ISLAM, S. S., ZELENIN, P. V., ORLOVSKY, G. N., GRILLNER, S. AND DELIAGINA, T. G., Pattern of motor coordination underlying backward swimming in the lamprey, *J Neurophysiol*, 96(1):451–60, **2006**.

IZHIKEVICH, E. M., Simple model of spiking neurons, *IEEE Trans Neural Networks*, 14(6):1569–1572, **2003**.

JANKOWSKA, E., JUKES, M. G., LUND, S. AND LUNDBERG, A., The effect of DOPA on the spinal cord. 5. Reciprocal organization of pathways transmitting excitatory action to alpha motoneurones of flexors and extensors, *Acta Physiol Scand*, 70(3):369–388, **1967**.

JUNG, R., KIEMEL, T. AND COHEN, A., Dynamic behavior of a neural network model of locomotor control in the lamprey, *J Neurophysiol*, 75(3):1074–1086, **1996**.

KAHN, J. A., Patterns of synaptic inhibition in motoneurons and interneurons during fictive swimming in the lamprey, as revealed by Cl^- injections, *J Comp Physiol*, 147(2):189–194, **1982**.

KANDEL, E. R., SCHWARTZ, J. H. AND JESSELL, T. M., *Principles of Neural Science*, McGraw-Hill, New York, 4th edition, **2000**.

KASICKI, S., GRILLNER, S., OHTA, Y., DUBUC, R. AND BRODIN, L., Phasic modulation of reticulospinal neurones during fictive locomotion and other types of spinal motor activity in lamprey, *Brain Res*, 484(1-2):203–216, **1989**.

KETTUNEN, P., KRIEGER, P., HESS, D. AND EL MANIRA, A., Signaling mechanisms of metabotropic glutamate receptor 5 subtype and its endogenous role in a locomotor network, *J Neurosci*, 22(5):1868–1873, **2002**.

KJAERULFF, O. AND KIEHN, O., Distribution of networks generating and coordinating locomotor activity in the neonatal rat spinal cord in vitro: a lesion study, *J Neurosci*, 16(18):5777–5794, **1996**.

KOCH, C. AND SEGEV, I. (editors), *Methods in neuronal modeling*, MIT Press, 2nd edition, **1998**.

KORZYBSKI, A., *Science and sanity: an introduction to non-aristotelian general semantics*, International Non-Aristotelian Library Publ. House, Lakeville, Conn., 3rd edition, **1948**.

KOZLOV, A., HELLGREN KOTALESKI, J., AURELL, E., GRILLNER, S. AND LANSNER, A., Modeling of substance P and 5-HT induced synaptic plasticity in the lamprey spinal CPG: consequences for network pattern generation, *J Comput Neurosci*, 11(2):183–200, **2001**.

KOZLOV, A. K., LANSNER, A., GRILLNER, S. AND HELLGREN KOTALESKI, J., A hemicord locomotor network of excitatory interneurons: a simulation study, *Biol Cybern*, 96(2):229–243, **2007**.

KRAUSE, A., *Generation of locomotor activity in fin motoneurons of the lamprey during "fictive locomotion"*, Ph.D. thesis, Germany: University of Köln, **2005**.

LANSNER, A., EKEBERG, Ö. AND GRILLNER, S., Realistic modeling of burst generation and swimming in the lamprey, in *Neurons, networks, and motor behavior*, pp. 165–171, The MIT Press, **1997**.

LANSNER, A., HELLGREN KOTALESKI, J. AND GRILLNER, S., Modeling of the spinal neuronal circuitry underlying locomotion in a lower vertebrate, *Ann N Y Acad Sci*, 860:239–249, **1998**.

LI, Y.-X. AND RINZEL, J., Equations for $InsP_3$ receptor-mediated $[Ca_i^{2+}]$ oscillations derived from a detailed kinetic model: a Hodgkin-Huxley like formalism, *J Theor Biol*, 166:461–473, **1994**.

LUNDQVIST, M., REHN, M., DJURFELDT, M. AND LANSNER, A., Attractor dynamics in a modular network model of neocortex, *Network*, 17(3):253–276, **2006**.

MACKAY-LYONS, M., Central pattern generation of locomotion: a review of the evidence, *Phys Ther*, 82(1):69–83, **2002**.

MACLEAN, J. N., SCHMIDT, B. J. AND HOCHMAN, S., NMDA receptor activation triggers voltage oscillations, plateau potentials and bursting in neonatal rat lumbar motoneurons in vitro, *Eur J Neurosci*, 9(12):2702–2711, **1997**.

MARDER, E., BUCHER, D., SCHULZ, D. J. AND TAYLOR, A. L., Invertebrate central pattern generation moves along, *Curr Biol*, 15(17):R685–99, **2005**.

MARDER, E. AND PRINZ, A. A., Modeling stability in neuron and network function: the role of activity in homeostasis, *Bioessays*, 24(12):1145–1154, **2002**.

MARSDEN, C. D., ROTHWELL, J. C. AND DAY, B. L., The use of peripheral feedback in the control of movement, *Trends Neurosci*, 7(7):253–257, **1984**.

MATSUSHIMA, T. AND GRILLNER, S., Intersegmental co-ordination of undulatory movements–a "trailing oscillator" hypothesis, *Neuroreport*, 1(2):97–100, **1990**.

MATSUSHIMA, T. AND GRILLNER, S., Neural mechanisms of intersegmental coordination in lamprey: local excitability changes modify the phase coupling along the spinal cord, *J Neurophysiol*, 67(2):373–388, **1992**.

MATSUSHIMA, T., TEGNÉR, J., HILL, R. H. AND GRILLNER, S., GABAB receptor activation causes a depression of low- and high-voltage-activated Ca^{2+} currents, postinhibitory rebound, and postspike afterhyperpolarization in lamprey neurons, *J Neurophysiol*, 70(6):2606–2619, **1993**.

MAYER, M. L. AND WESTBROOK, G. L., The physiology of excitatory amino acids in the vertebrate central nervous system, *Prog Neurobiol*, 28(3):197–276, **1987**.

MCCLELLAN, A. D. AND HAGEVIK, A., Descending control of turning locomotor activity in larval lamprey: neurophysiology and computer modeling, *J Neurophysiol*, 78(1):214–228, **1997**.

MCCORMICK, D. A., SHU, Y. AND YU, Y., Neurophysiology: Hodgkin and Huxley model still standing?, *Nature*, 445(7123):E1–E2, **2007**.

MENTEL, T., KRAUSE, A., PABST, M., EL MANIRA, A. AND BÜSCHGES, A., Activity of fin muscles and fin motoneurons during swimming motor pattern in the lamprey, *Eur J Neurosci*, 23(8):2012–2026, **2006**.

MIYAKAWA, T., MIZUSHIMA, A., HIROSE, K., YAMAZAWA, T., BEZPROZVANNY, I., KUROSAKI, T. AND IINO, M., Ca^{2+}-sensor region of IP_3 receptor controls intracellular Ca^{2+} signaling, *EMBO J*, 20(7):1674–1680, **2001**.

MORRIS, C. AND LECAR, H., Voltage oscillations in the barnacle giant muscle fiber, *Biophys J*, 35(1):193–213, **1981**.

MORTIN, L. I. AND STEIN, P. S., Spinal cord segments containing key elements of the central pattern generators for three forms of scratch reflex in the turtle, *J Neurosci*, 9(7):2285–2296, **1989**.

NAUNDORF, B., WOLF, F. AND VOLGUSHEV, M., Neurophysiology: Hodgkin and Huxley model still standing? (reply), *Nature*, 445(7123):E2–E3, **2007**.

NOWAK, L., BREGESTOVSKI, P., ASCHER, P., HERBET, A. AND PROCHIANTZ, A., Magnesium gates glutamate-activated channels in mouse central neurones, *Nature*, 307(5950):462–465, **1984**.

OHTA, Y., DUBUC, R. AND GRILLNER, S., A new population of neurons with crossed axons in the lamprey spinal cord, *Brain Res*, 564(1):143–148, **1991**.

PALSSON, B. O. AND LIGHTFOOT, E. N., Mathematical modelling of dynamics and control in metabolic networks. I. On Michaelis-Menten kinetics, *J Theor Biol*, 111(2):273–302, **1984**.

PARKER, D., Activity-dependent feedforward inhibition modulates synaptic transmission in a spinal locomotor network, *J Neurosci*, 23(35):11085–11093, **2003**a.

PARKER, D., Variable properties in a single class of excitatory spinal synapse, *J Neurosci*, 23(8):3154–3163, **2003**b.

PARKER, D., Complexities and uncertainties of neuronal network function, *Philos Trans R Soc Lond B Biol Sci*, 361(1465):81–99, **2006**.

PARKER, D. AND BEVAN, S., Modulation of Cellular and Synaptic Variability in the Lamprey Spinal Cord, *J Neurophysiol*, 97(1):44–56, **2007**.

PARKER, D. AND GRILLNER, S., Tachykinin-mediated modulation of sensory neurons, interneurons, and synaptic transmission in the lamprey spinal cord, *J Neurophysiol*, 76(6):4031–4039, **1996**.

PARKER, D. AND GRILLNER, S., The activity-dependent plasticity of segmental and intersegmental synaptic connections in the lamprey spinal cord, *Eur J Neurosci*, 12(6):2135–2146, **2000**a.

PARKER, D. AND GRILLNER, S., Neuronal mechanisms of synaptic and network plasticity in the lamprey spinal cord, *Prog Brain Res*, 125:381–398, **2000**b.

PEARSON, K. G., Common principles of motor control in vertebrates and invertebrates, *Annu Rev Neurosci*, 16:265–297, **1993**.

PHILIPPSON, M., L'autonomie et la centralisation dans le système nerveux des animaux, *Tray Lab Physiol Inst Solvay (Bruxelles)*, 7:1–208, **1905**.

PINSKY, P. AND RINZEL, J., Intrinsic and network rhythmogenesis in a reduced Traub model for CA3 neurons, *J Comput Neurosci*, 1(1-2):39–60, **1994**.

VAN DER POL, B. AND VAN DER MARK, J., The heartbeat considered as a relaxation oscillation, and an electrical model of the heart, *Phil Mag*, Suppl 6:763–775, **1928**.

POON, M., Induction of swimming in lamprey by L-DOPA and amino acids, *J Comp Physiol A*, 136(4):377–344, **1980**.

PRINZ, A. A., BILLIMORIA, C. P. AND MARDER, E., Alternative to hand-tuning conductance-based models: construction and analysis of databases of model neurons, *J Neurophysiol*, 90(6):3998–4015, **2003**.

PRINZ, A. A., BUCHER, D. AND MARDER, E., Similar network activity from disparate circuit parameters, *Nat Neurosci*, 7(12):1345–1352, **2004**.

QUINLAN, K. A., PLACAS, P. G. AND BUCHANAN, J. T., Cholinergic modulation of the locomotor network in the lamprey spinal cord, *J Neurophysiol*, 92(3):1536–1548, **2004**.

RALL, W., Theory of physiological properties of dendrites, *Ann N Y Acad Sci*, 96:1071–1092, **1962**.

REISS, R. F., A theory and simulation of rhythmic behaviour due to reciprocal inhibition in small nerve nets, *Proceedings of AFIPS Spring Joint Computer Conference*, 21:171–194, **1962**.

ROBERTS, A., SOFFE, S. R., WOLF, E., YOSHIDA, M. AND ZHAO, F. Y., Central circuits controlling locomotion in young frog tadpoles, *Ann N Y Acad Sci*, 860:19–34, **1998**.

ROBERTS, A. AND TUNSTALL, M. J., Mutual re-excitation with post-inhibitory rebound: a simulation study on the mechanisms for locomotor rhythm generation in the spinal cord of *Xenopus* embryos., *Eur J Neurosci*, 2(1):11–23, **1990**.

ROBERTS, A., TUNSTALL, M. J. AND WOLF, E., Properties of networks controlling locomotion and significance of voltage dependency of NMDA channels: simulation study of rhythm generation sustained by positive feedback, *J Neurophysiol*, 73(2):485–495, **1995**.

ROVAINEN, C. M., Neurobiology of lampreys, *Physiol Rev*, 59(4):1007–1077, **1979**.

ROVAINEN, C. M., Identified neurons in the lamprey spinal cord and their roles in fictive swimming, *Symp Soc Exp Biol*, 37:305–330, **1983**.

RUSSELL, D. F. AND WALLÉN, P., On the control of myotomal motoneurones during "fictive swimming" in the lamprey spinal cord in vitro, *Acta Physiol Scand*, 117(2):161–170, **1982**.

SATTERLIE, R. A., Reciprocal inhibition and postinhibitory rebound produce reverberation in a locomotor pattern generator, *Science*, 229(4711):402–404, **1985**.

SCHWARTZ, E. J., GERACHSHENKO, T. AND ALFORD, S., 5-HT prolongs ventral root bursting via presynaptic inhibition of synaptic activity during fictive locomotion in lamprey, *J Neurophysiol*, 93(2):980–988, **2005**.

SELVERSTON, A. I., MILLER, J. P. AND WADEPUHL, M., Neural mechanisms for the production of cyclic motor patterns, *IEEE Trans Systems, Man and Cybernetics*, SMC-13(5), **1983**.

SHERRINGTON, C. S., Flexion-reflex of the limb, crossed extension-reflex, and reflex stepping and standing, *J Physiol*, 40(1-2):28–121, **1910**.

SHUPLIAKOV, O., WALLÉN, P. AND GRILLNER, S., Two types of motoneurons supplying dorsal fin muscles in lamprey and their activity during fictive locomotion, *J Comp Neurol*, 321(1):112–123, **1992**.

SIGVARDT, K. A. AND WILLIAMS, T. L., Effects of local oscillator frequency on intersegmental coordination in the lamprey locomotor CPG: theory and experiment, *J Neurophysiol*, 76(6):4094–4103, **1996**.

SILLAR, K. T. AND ROBERTS, A., Control of frequency during swimming in *Xenopus* embryos: a study on interneuronal recruitment in a spinal rhythm generator, *J Physiol*, 472:557–572, **1993**.

SILLAR, K. T. AND SIMMERS, A. J., 5HT induces NMDA receptor-mediated intrinsic oscillations in embryonic amphibian spinal neurons, *Proc Biol Sci*, 255(1343):139–145, **1994**.

SMITH, J. C., FELDMAN, J. L. AND SCHMIDT, B. J., Neural mechanisms generating locomotion studied in mammalian brain stem-spinal cord in vitro, *FASEB J*, 2(7):2283–2288, **1988**.

SONG, W., ONISHI, M., JAN, L. Y. AND JAN, Y. N., Peripheral multidendritic sensory neurons are necessary for rhythmic locomotion behavior in *Drosophila* larvae, *Proc Natl Acad Sci U S A*, 104(12):5199–5204, **2007**.

STAUFFER, E. K., MCDONAGH, J. C., HORNBY, T. G., REINKING, R. M. AND STUART, D. G., Historical reflections on the afterhyperpolarization-firing rate relation of vertebrate spinal neurons, *J Comp Physiol A*, 193(2):145–158, **2007**.

STEIN, P. S. G., GRILLNER, S., SELVERSTON, A. AND STUART, D. G. (editors), *Neurons, networks, and motor behavior*, Computational Neuroscience, The MIT Press, **1997**.

SVENSSON, E., *Modulatory effects and interactions of substance P, dopamine and 5-HT in a neuronal network*, Ph.D. thesis, Stockholm, Sweden: Karolinska Institutet, **2003**.

SVENSSON, E., WIKSTRÖM, M. A., HILL, R. H. AND GRILLNER, S., Endogenous and exogenous dopamine presynaptically inhibits glutamatergic reticulospinal transmission via an action of D_2-receptors on N-type Ca^{2+} channels, *Eur J Neurosci*, 17(3):447–454, **2003**.

TANG, Y. AND OTHMER, H. G., Frequency encoding in excitable systems with applications to calcium oscillations, *Proc Natl Acad Sci U S A*, 92(17):7869–7873, **1995**.

TEGNÉR, J., HELLGREN-KOTALESKI, J., LANSNER, A. AND GRILLNER, S., Low-voltage-activated calcium channels in the lamprey locomotor network: simulation and experiment, *J Neurophysiol*, 77(4):1795–1812, **1997**.

TEGNÉR, J., LANSNER, A. AND GRILLNER, S., Modulation of burst frequency by calcium-dependent potassium channels in the lamprey locomotor system: dependence of the activity level, *J Comput Neurosci*, V5(2):121–140, **1998**.

TEGNÉR, J., MATSUSHIMA, T., EL MANIRA, A. AND GRILLNER, S., The spinal GABA system modulates burst frequency and intersegmental coordination in the lamprey: differential effects of $GABA_A$ and $GABA_B$ receptors, *J Neurophysiol*, 69(3):647–657, **1993**.

THOMSON, A. M., Molecular frequency filters at central synapses, *Prog Neurobiol*, 62(2):159–196, **2000**.

TRÅVÉN, H. G., BRODIN, L., LANSNER, A., EKEBERG, Ö., WALLÉN, P. AND GRILLNER, S., Computer simulations of NMDA and non-NMDA receptor-mediated synaptic drive: sensory and supraspinal modulation of neurons and small networks, *J Neurophysiol*, 70(2):695–709, **1993**.

ULLSTRÖM, M., HELLGREN KOTALESKI, J., TEGNÉR, J., AURELL, E., GRILLNER, S. AND LANSNER, A., Activity-dependent modulation of adaptation produces a constant burst proportion in a model of the lamprey spinal locomotor generator, *Biol Cybern*, 79(1):1–14, **1998**.

VIALA, D. AND BUSER, P., The effects of DOPA and 5-HTP on rhythmic efferent discharges in hind limb nerves in the rabbit, *Brain Res*, 12(2):437–443, **1969**.

WADDEN, T., HELLGREN, J., LANSNER, A. AND GRILLNER, S., Intersegmental coordination in the lamprey: simulations using a network model without segmental boundaries, *Biol Cybern*, 76(1):1–9, **1997**.

WALLÉN, P., EKEBERG, Ö., LANSNER, A., BRODIN, L., TRÅVÉN, H. AND GRILLNER, S., A computer-based model for realistic simulations of neural networks. II. The segmental network generating locomotor rhythmicity in the lamprey, *J Neurophysiol*, 68(6):1939–1950, **1992**.

WALLÉN, P. AND GRILLNER, S., N-methyl-D-aspartate receptor-induced, inherent oscillatory activity in neurons active during fictive locomotion in the lamprey, *J Neurosci*, 7(9):2745–2755, **1987**.

WALLÉN, P., GRILLNER, S., FELDMAN, J. L. AND BERGELT, S., Dorsal and ventral myotome motoneurons and their input during fictive locomotion in lamprey, *J Neurosci*, 5(3):654–661, **1985**.

WALLÉN, P. AND LANSNER, A., Do the motoneurones constitute a part of the spinal network generating the swimming rhythm in the lamprey?, *J Exp Biol*, 113:493–497, **1984**.

WALLÉN, P. AND WILLIAMS, T. L., Fictive locomotion in the lamprey spinal cord in vitro compared with swimming in the intact and spinal animal, *J Physiol*, 347(1):225–239, **1984**.

WANG, H. AND JUNG, R., Variability analyses suggest that supraspino-spinal interactions provide dynamic stability in motor control, *Brain Res*, 930(1-2):83–100, **2002**.

WANG, X.-J. AND RINZEL, J., Alternating and synchronous rhythms in reciprocally inhibitory model neurons, *Neural Comp*, 4(1):84–97, **1992**.

WHEATLEY, M. AND STEIN, R. B., An *in vitro* preparation of the mudpuppy for simultaneous intracellular and electromyographic recording during locomotion, *J Neurosci Methods*, 42(1-2):129–137, **1992**.

WIKSTRÖM, M. A. AND EL MANIRA, A., Calcium influx through N- and P/Q-type channels activate apamin-sensitive calcium-dependent potassium channels generating the late afterhyperpolarization in lamprey spinal neurons, *Eur J Neurosci*, 10(4):1528–1532, **1998**.

WILLIAMS, T. L. AND SIGVARDT, K. A., Intersegmental phase lags in the lamprey spinal cord: experimental confirmation of the existence of a boundary region, *J Comput Neurosci*, 1(1-2):61–67, **1994**.

WILLIAMS, T. L., SIGVARDT, K. A., KOPELL, N., ERMENTROUT, G. B. AND REMLER, M. P., Forcing of coupled nonlinear oscillators: studies of intersegmental coordination in the lamprey locomotor central pattern generator, *J Neurophysiol*, 64(3):862–871, **1990**.

WILSON, D. M. AND WALDRON, I., Models for the generation of the motor output pattern in flying locusts, *Proc IEEE*, 56:1058–1064, **1968**.

YUSTE, R., MACLEAN, J. N., SMITH, J. AND LANSNER, A., The cortex as a central pattern generator, *Nat Rev Neurosci*, 6(6):477–483, **2005**.

ZUCKER, R. S. AND REGEHR, W. G., Short-term synaptic plasticity, *Annu Rev Physiol*, 64:355–405, **2002**.

APPENDIX

This appendix contains a specification of the biochemical pathway model used in Paper VI, as well as some comments on parameter modifications to the three original IP_3 receptor models used in the same paper.

I first give the reactions for the modelled system of biochemical reactions, followed by the XPP code used to simulate the system. This code illustrates how the differential equations are formulated for the reactions, and it shows the parameter values used.

The equations and parameter values for the three IP_3R models can be found in the papers by Li and Rinzel (1994) and Tang and Othmer (1995). (We use a re-scaled version of the De Young-Keizer model, described in Li and Rinzel, 1994.) In each case, one parameter value was modified to improve the model's fit to data. These modifications are explained in the concluding section of the Appendix.

Some of this material was written by Kristofer Hallén.

Biochemical reactions

Abbreviations are explained below.

$$mGluR + Glu \underset{k_{1b}}{\overset{k_{1f}}{\rightleftharpoons}} RecGlu \tag{5.1}$$

$$GGDP + RecGlu \underset{k_{2b}}{\overset{k_{2f}}{\rightleftharpoons}} RecGluG \tag{5.2}$$

$$GGDP + mGluR \underset{k_{3b}}{\overset{k_{3f}}{\rightleftharpoons}} RecG \tag{5.3}$$

$$Glu + RecG \underset{k_{4b}}{\overset{k_{4f}}{\rightleftharpoons}} RecGluG \tag{5.4}$$

$$RecGluG \underset{k_{5b}}{\overset{k_{5f}}{\rightleftharpoons}} G\alpha GTP + G\beta\gamma + RecGlu \tag{5.5}$$

$$GGDP \underset{k_{6b}}{\overset{k_{6f}}{\rightleftharpoons}} G\alpha GTP + G\beta\gamma \tag{5.6}$$

$$G\alpha GTP \underset{k_{7b}}{\overset{k_{7f}}{\rightleftharpoons}} G\alpha GDP \tag{5.7}$$

$$G\alpha GDP + G\beta\gamma \underset{k_{8b}}{\overset{k_{8f}}{\rightleftharpoons}} GGDP \tag{5.8}$$

$$Ca + PLC \underset{k_{9b}}{\overset{k_{9f}}{\rightleftharpoons}} PLCCa \tag{5.9}$$

$$G\alpha GTP + PLCCa \underset{k_{10b}}{\overset{k_{10f}}{\rightleftharpoons}} PLCCaG \tag{5.10}$$

$$PLC + G\alpha GTP \underset{k_{11b}}{\overset{k_{11f}}{\rightleftharpoons}} PLCG \tag{5.11}$$

$$Ca + PLCG \underset{k_{12b}}{\overset{k_{12f}}{\rightleftharpoons}} PLCCaG \tag{5.12}$$

$$PLCCaG \underset{k_{13b}}{\overset{k_{13f}}{\rightleftharpoons}} G\alpha GDP + PLCCa \tag{5.13}$$

$$PIP2 + PLCCa \underset{k_{14b}}{\overset{k_{14f}}{\rightleftharpoons}} PIP2PLCCa \overset{k_{15cat}}{\rightarrow} IP_3 + DAG + PLCCa \tag{5.14}$$

$$PIP2 + PLCCaG \underset{k_{15b}}{\overset{k_{15f}}{\rightleftharpoons}} PIP2PLCCaG \overset{k_{16cat}}{\rightarrow} IP_3 + DAG + PLCCaG \tag{5.15}$$

$$PIP2 + PLCG \underset{k_{16b}}{\overset{k_{16f}}{\rightleftharpoons}} PIP2PLCG \overset{k_{17cat}}{\rightarrow} IP_3 + DAG + PLCG \tag{5.16}$$

$$PIP2 + PLC \underset{k_{17b}}{\overset{k_{17f}}{\rightleftharpoons}} PIP2PLC \overset{k_{18cat}}{\rightarrow} IP_3 + DAG + PLC \tag{5.17}$$

$$IP_3 \underset{k_{18b}}{\overset{k_{18f}}{\rightleftharpoons}} degradedIP_3 \tag{5.18}$$

Abbreviations

GαGTP	α subunit of G protein bound to GTP, active
GαGDP	α subunit of G protein bound to GDP, inactive
G$\beta\gamma$	$\beta\gamma$ subunits of G protein
GGDP	G protein bound to GDP, inactive.
Glu	Glutamate
mGluR	metabotropic glutamate receptor
PLC	Phospholipase Cβ
PLCCa	Ca^{2+} bound to PLC
PLCG	G bound to PLC
PLCCaG	Ca^{2+} and G bound to PLC
RecG	G protein bound to mGluR
RecGlu	Glu bound to mGluR
RecGluG	G protein and Glu bound to mGluR

```
#ode file for XPPAUT
#Biochemical signalling model
#Kristofer Hallén 021104, modified by Mikael Huss May 03

dmGluR/dt=-mGluR*Glu*k1f+R_Glu*k1b-GDP*mGluR*k5f+R_G*k5b

# Two glutamate pulses
Glu=heav(T)-heav(T-480)+heav(T-660)

#R_Glu Glutamate bound to mGluR
dR_Glu/dt=mGluR*Glu*k1f-R_Glu*k1b-GDP*R_Glu*k3f+R_Glu_G*k3b\
+R_Glu_G*k6f-GT*betagamma*R_Glu*k6b

#GT=Galpha*GTP
dGT/dt=-GT*k2f+GD*k2b+GDP*k15f-GT*betagamma*k15b+R_Glu_G*k6f\
-GT*betagamma*R_Glu*k6b-GT*PLCCa*k9f+PLCCa_G*k9b-PLC*GT*k11f+PLC_G*k11b

#GD=Galpha*GDP
dGD/dt=GT*k2f-GD*k2b-GD*betagamma*k16f+GDP*k16b+PLCCa_G*k10f-GD*PLCCa*k10b

#GDP=The whole G protein complex.
dGDP/dt=-GDP*k15f+GT*betagamma*k15b+GD*betagamma*k16f-GDP*k16b\
-GDP*R_Glu*k3f+R_Glu_G*k3b-GDP*mGluR*k5f+R_G*k5b

#betagamma part of G protein
dbetagamma/dt=GDP*k15f-GT*betagamma*k15b-GD*betagamma*k16f+GDP*k16b\
+R_Glu_G*k6f-GT*betagamma*R_Glu*k6b

#G protein and glutamate bound to mGlur
dR_Glu_G/dt=GDP*R_Glu*k3f-R_Glu_G*k3b+Glu*R_G*k4f-R_Glu_G*k4b\
-R_Glu_G*k6f+GT*betagamma*R_Glu*k6b

#G protein bound to mGluR
dR_G/dt=-Glu*R_G*k4f+R_Glu_G*k4b+GDP*mGluR*k5f-R_G*k5b-R_G*antag*k17f+block_R_G*k17b

dPLC/dt=-Ca*PLC*k7f+PLCCa*k7b-PLC*GT*k11f+PLC_G*k11b-PLC*PIP2*k19f+PP*k19b\
+PP*k19cat

#Ca bound to PLC
dPLCCa/dt=Ca*PLC*k7f-PLCCa*k7b-GT*PLCCa*k9f+PLCCa_G*k9b\
+PLCCa_G*k10f-GD*PLCCa*k10b-PIP2*PLCCa*k13f+PPCa*k13b+PPCa*k13cat

dIP3/dt=-IP3*k8f+PPCa*k13cat+PPCa_G*k14cat+PP*k19cat+PP_G*k18cat

#Ca and G protein bound to PLC
dPLCCa_G/dt=GT*PLCCa*k9f-PLCCa_G*k9b-PLCCa_G*k10f+GD*PLCCa*k10b\
```

```
+Ca*PLC_G*k12f-PLCCa_G*k12b-PIP2*PLCCa_G*k14f+PPCa_G*k14b+PPCa_G*k14cat

#G protein bound to PLC
dPLC_G/dt=PLC*GT*k11f-PLC_G*k11b-Ca*PLC_G*k12f+PLCCa_G*k12b+PP_G*k18cat\
-PLC_G*PIP2*k18f+PP_G*k18b

dPIP2/dt=0

#PLC, PIP2 and Ca bound
dPPCa/dt=PIP2*PLCCa*k13f-PPCa*k13b-PPCa*k13cat

#PLC, PIP2, G protein and Ca bound
dPPCa_G/dt=PIP2*PLCCa_G*k14f-PPCa_G*k14b-PPCa_G*k14cat

#dantag/dt=-R_G*antag*k17f+block_R_G*k17b
dantag/dt=0

dblock_R_G/Dt=R_G*antag*k17f-block_R_G*k17b

#PLC_G_PIP2
dPP_G/dt=PLC_G*PIP2*k18f-PP_G*k18b-PP_G*k18cat

#PLC_PIP2
dPP/dt=PLC*PIP2*k19f-PP*k19b-PP*k19cat

#Pang Sternweis 1990 Rat brain
init GDP=1
#Bhalla, scaled up from från Mahama and Linderman
init mGluR=0.3
#Smrcka 1991, bovine brain.
init PLC=0.04
#Normal intracellular calcium conc
init Ca=0.1
init PIP2=20
#Bhalla: 'antagonist-receptor binding is weak', 0
init antag=0
#init Glu=1
#IP3
init IP3=1

par k1f=0.8 k1b=1
par k2f=0.0133 k2b=0
par k3f=0.006 k3b=0.0001
par k4f=0.0625 k4b=0.1
par k5f=3.85 k5b=0.05
#Mukhopadhyay et al 1999.
```

```
par k6f=1.8 k6b=0
par k7f=3 k7b=1
par k8f=2.5
par k9f=25.2 k9b=1
par k10f=1.6667 k10b=0
par k11f=2.52 k11b=1
par k12f=30 k12b=1
par k13f=2.52 k13b=40 k13cat=10
par k14f=160 k14b=640 k14cat=160
par k15f=0.0001 k15b=0
par k16f=6 k16b=0
par k17f=60 k17b=0.01
par k18f=75 k18b=300 k18cat=75
par k19f=0.625 k19b=10 k19cat=2.5
```

IP_3R model parameters

In the Li-Rinzel model, the $d2$ parameter was lowered to 0.5μM to make the receptor sensitive to the IP_3 concentration levels in the model.

In the version of the De Young-Keizer model that we used, described in Li and Rinzel (1994), the $b2$ parameter, which is analogous to $d2$ in the Li-Rinzel model, was scaled down by the same factor for the same reason.

In the Tang-Othmer model, the k_{-1} parameter was increased to 220 s^{-1} to make the receptor sensitive for the appropriate IP_3 concentration levels. The new value is well within the physiological range.

Papers

Paper I

J Neurophysiol 97: 2696–2711, 2007.
First published February 7, 2007; doi:10.1152/jn.00528.2006.

Roles of Ionic Currents in Lamprey CPG Neurons: A Modeling Study

Mikael Huss,[1,2] Anders Lansner,[1] Peter Wallén,[2] Abdeljabbar El Manira,[2] Sten Grillner,[2] and Jeanette H. Kotaleski[1,2]

[1]*School of Computer Science and Communication, Royal Institute of Technology, Stockholm, Sweden; and* [2]*Department of Neuroscience, Nobel Institute for Neurophysiology, Karolinska Institutet, Stockholm, Sweden*

Submitted 17 May 2006; accepted in final form 2 February 2007

Huss M, Lansner A, Wallén P, El Manira A, Grillner S, Kotaleski JH. Roles of ionic currents in lamprey CPG neurons: a modeling study. *J Neurophysiol* 97: 2696–2711, 2007. First published February 7, 2007; doi:10.1152/jn.00528.2006. The spinal network underlying locomotion in the lamprey consists of a core network of glutamatergic and glycinergic interneurons, previously studied experimentally and through mathematical modeling. We present a new and more detailed computational model of lamprey locomotor network neurons, based primarily on detailed electrophysiological measurements and incorporating new experimental findings. The model uses a Hodgkin–Huxley-like formalism and consists of 86 membrane compartments containing 12 types of ion currents. One of the goals was to introduce a fast, transient potassium current (K_t) and two sodium-dependent potassium currents, one faster (K_{NaF}) and one slower (K_{NaS}), in the model. Not only has the model lent support to the interpretation of experimental results but it has also provided predictions for further experimental analysis of single-network neurons. For example, K_t was shown to be one critical factor for controlling action potential duration. In addition, the model has proved helpful in investigating the possible influence of the slow afterhyperpolarization on repetitive firing during ongoing activation. In particular, the balance between the simulated slow sodium-dependent and calcium-dependent potassium currents has been explored, as well as the possible involvement of dendritic conductances.

INTRODUCTION

The lamprey CNS has widely served as a model system of the neural basis of vertebrate locomotion. There are fewer neurons in the lamprey than in higher vertebrates and the motor activity underlying locomotion can be maintained in the isolated spinal cord for days (Grillner et al. 2000, 2003). The core of the lamprey spinal central pattern generator (CPG) consists of ipsilaterally projecting glutamatergic neurons and contralaterally projecting glycinergic neurons (Buchanan et al. 1982, 1987; Grillner 2003). One tool for investigating the lamprey CPG, in addition to the experimental approach, has been extensive modeling at different levels of abstraction (Grillner et al. 2001). Both biophysical single-cell and network models of the lamprey spinal CPG were previously described (see, e.g., Ekeberg et al. 1991; Grillner et al. 1988; Hellgren et al. 1992; for more abstract types of models also see Buchanan 1992; McClellan and Hagevik 1997; Williams 1992). Different aspects of the local spinal network were previously simulated using Hodgkin–Huxley types of models, including its modulation by sensory feedback, activation by supraspinal structures, and coordination along the spinal cord (Brodin et al. 1991; Ekeberg et al. 1991; Hellgren et al. 1999a,b; Kozlov et al. 2001; Tegnér et al. 1998, 1999; Tråvén et al. 1993; Ullström et al. 1998; Wadden et al. 1997; Wallén et al. 1992). Understanding such systems at the neuronal network level is very demanding because of the complexity of the dynamic interactions within and between neurons. Therefore to examine the possible architecture of cellular and synaptic properties that lead to an experimentally shown phenomenon, computer simulations are powerful tools of analysis. Detailed models of various cell types are necessary building blocks for such network simulations. These detailed models need to have a good grounding in electrophysiology, especially ion channel kinetics. Over the last years, new experimental data have become available that require an updated mathematical description for adequate simulation studies (see, e.g., Cangiano et al. 2002; Hess and El Manira 2001, 2002; Wallén et al. 2003, 2005; Hess et al. 2007). Improved models should also make it possible to address some previously unanswered questions and to put forth hypotheses about the inner workings of the single lamprey spinal neuron. This article presents a computational model of a lamprey spinal cord neuron based on new experimental data.

The closest analogue to our work is a computational model of the CPG neuron in the *Xenopus* frog embryo (Dale 1995a). Like the lamprey, *Xenopus* is an important model system for studying vertebrate motor pattern generation. The swimming CPGs in the two systems share a number of similarities. In both *Xenopus* and lamprey, the segmental CPG is thought to consist of recurrent excitatory networks coupled by reciprocal inhibition and the voltage-dependent properties of *N*-methyl-D-aspartate (NMDA) receptors have a key role in pattern generation (Grillner 2003; Roberts and Tunstall 1990; Roberts et al. 1995). In the *Xenopus* embryo, electrophysiological properties and ionic currents are well characterized (see, e.g., Dale 1995b; Kuenzi and Dale 1998). Other computational models of neurons participating in pattern-generating networks have furthermore been created for many invertebrate systems, for instance, in the stomatogastric ganglion of the lobster (Buchholtz et al. 1992) and the cardiac ganglion of the leech (Nadim et al. 1995; Olsen et al. 1995).

As in the nervous systems of most animal phyla, the lamprey spinal cord contains, among others, three basic types of neurons: sensory neurons, motor neurons, and interneurons. The focus of this study was to develop a generic model of lamprey spinal CPG neurons. This model (which is summarized in Table A1 and equations in the APPENDIX) can be implemented

Address for reprint requests and other correspondence: J. Hellgren Kotaleski, Nobel Institute for Neurophysiology, Department of Neuroscience, Karolinska Institutet, SE 17177, Stockholm, Sweden (E-mail: jeanette.hellgren@ki.se).

The costs of publication of this article were defrayed in part by the payment of page charges. The article must therefore be hereby marked "*advertisement*" in accordance with 18 U.S.C. Section 1734 solely to indicate this fact.

0022-3077/07 $8.00 Copyright © 2007 The American Physiological Society

Downloaded from jn.physiology.org on May 9, 2007

on different morphologies, depending on the type of spinal neuron one seeks to simulate. No systematic study comparing the kinetics and densities of specific ionic currents in different CPG neuron classes has been carried out, but different lamprey spinal CPG neurons show quite similar behavior in some respects (Biró et al. 2006; Buchanan 1993, 2001; Hu et al. 2002; Wallén and Grillner 1987). For example, a study characterizing various properties of identifiable lamprey spinal neurons (Buchanan 1993) found that properties that depend largely on active ionic conductances, such as action potential amplitude and width as well as the size of the slow afterhyperpolarization (sAHP), were similar between different classes of neurons, suggesting similar mechanisms for generation of the spike and sAHP. Our generic cell model will therefore be used as a basis when simulating the various cell types involved in the lamprey CPG circuits.

However, there are still many possible sources of variability both within and between classes of spinal neurons. For instance, variability in soma size and number of dendritic branches lead to a variability in a number of measured cell properties such as rheobase and input resistance (Buchanan 1993). Also, spiking frequencies and postsynaptic potential amplitudes were found to show a marked variability in motoneurons and various classes of interneurons (Parker and Bevan 2007). In view of this variability, it would be difficult or impossible to construct a model that could reproduce all published experimental results with a fixed parameter set, even for a single class of CPG neuron. However, the present model can reproduce most important cell behaviors qualitatively and sometimes quantitatively.

The role of certain ionic currents cannot be addressed experimentally in some cases, although simulations can be used to predict their roles and suggest new experiments. Results of this kind are described and discussed herein. Work on incorporating this new cell model into a hemisegmental CPG network model is in progress and will be reported elsewhere.

METHODS

Model specification

The cell model is a compartmental model implemented using the GENESIS neural simulator (Bower and Beeman 1998). Passive properties and ion channel kinetics and distributions are described in the following sections.

Cell morphology

Spinal neurons in the lamprey CPG are found in a large variety of shapes and sizes. For example, interneurons typically have a much smaller cell body and dendritic tree than those of motoneurons (compare, e.g., Buchanan et al. 1989, 2001; Wallén et al. 1985). Our ionic current models (see following text) can be implemented on different cell morphologies. For illustration, we use a morphology herein that gives the model neuron an input resistance and rheobase close to mean values reported for two different types of interneuron in the lamprey spinal cord (Buchanan 1993). We used the five filled interneurons from Buchanan et al. (1989) as guidance, but the model we will use to illustrate the results is not strictly based on any of these, being instead an idealized version that has typical values for soma dimensions, rheobase, and input resistance. For purposes of comparison, we constructed three other model neurons (see *Effects of changes in the morphology*), each one based closely on one of the filled cells with dendritic compartments representing each branch shown in the reconstructions in the original paper (Buchanan et al. 1989). The "default" model has 86 compartments, 84 of them dendritic (Fig. 1). All compartments are modeled as cylinders. The soma compartment has a length of 20 μm and a diameter of 20 μm, which gives a membrane area within the range observed for interneuron somata (Buchanan 1982; Buchanan et al. 1989). A separate compartment represents the axon initial segment; it is 50 μm long with a diameter of 5 μm. This representation of the axon is inspired by the work described in Colbert and Pan (2002) and it allowed reasonable densities of ionic conductances (see APPENDIX). There are two primary dendrites, each branching out to two secondary dendrites, which in turn branch out into two tertiary dendrites each. The three levels of dendrites correspond to proximal, medial, and distal dendrites, respectively. Each of these is in turn divided into two, four, and eight compartments, respectively [resulting in $(2 \times 2) + (4 \times 4) + (8 \times 8) = 84$ dendritic compartments]. The size of the dendritic tree can be varied to mimic different types of spinal neurons. In the parameter set presented here, primary dendrites are 90 μm long with 5-μm diameter; the secondary dendrites are 150 μm long with 3-μm diameter; and the tertiary dendrites are 240 μm long with 2-μm diameter. The ratio of the dendritic surface area to the somatic is thus about 16, which is slightly less than that estimated for mammalian motoneurons (Lüscher and Clamann 1995).

We also simulated dissociated cells because some experimental data were available for such cells only, which largely lack dendrites. The dissociated cells used in the experiments were motoneurons, contralaterally and caudally projecting interneurons (CCINs), or unidentified neurons from larval or young adult lampreys. A dissociated cell is modeled in the same way as the default model interneuron, but with all dendritic branches removed; only the soma and the axon initial segment are retained.

Passive membrane parameters

All passive parameters are identical for each compartment. The specific membrane resistance is 1 Ωm^2, the axial resistance is 1 Ωm, and the specific capacitance is 0.01 F/m^2. The resting membrane potential was usually set to -78 mV, the mean value reported for CC, EIN, and LIN neurons according to Buchanan (1993), except when examining the effects of varying the membrane potential or simulating experiments, in which case the model's resting potential was set to the same value as in the experiment.

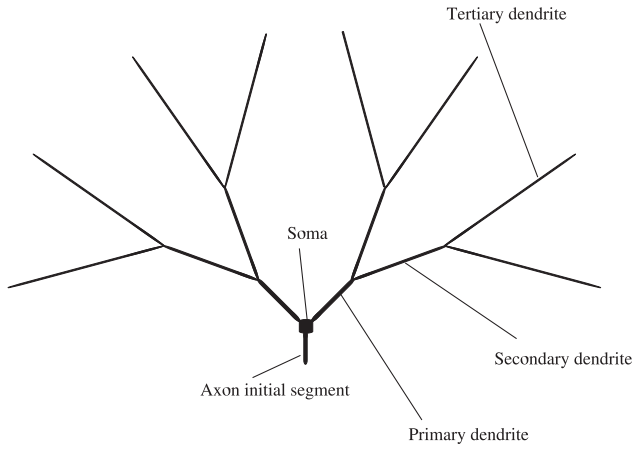

FIG. 1. Graphical representation of the morphology of the "default" cell model.

Downloaded from jn.physiology.org on May 9, 2007

Ion current kinetics

Ion current kinetics—at least for those ion currents involved in action potential generation and termination—do not seem to vary significantly across different types of lamprey locomotor neurons (Buchanan 1993, 2001). For instance, the action potentials of different types of cells have remarkably similar amplitudes and durations. The voltage threshold for action potential generation also does not vary appreciably between cell types (Buchanan 1993, 2001). In building the model, data from different preparations were used. Thus we used information obtained from experiments on motoneurons, inhibitory interneurons, excitatory interneurons, and unidentified neurons. Sometimes these were dissociated cells; for example, kinetic data on the K_t, K_{NaF}, Ca_N, Ca_L, and Ca_{LVA} (see Table A1 for definitions of notation) currents were measured in dissociated cells from larval and young adult lampreys.

Lamprey spinal cord neurons were recently shown to contain a larger number of distinct ion channels types than previously known (see, e.g., Hess and El Manira 2001, 2002; Wallén et al. 2005; Hess et al. 2007). Importantly, three novel currents were experimentally characterized: one transient, high-voltage–activated, inactivating A-type potassium current (hereafter referred to as K_t) and two sodium-dependent potassium currents (K_{Na}), which will be denoted as K_{NaF} (F for fast) and K_{NaS} (S for slow). Furthermore, more quantitative data were obtained on the other types of currents, that is Na^+, K_s, and subtypes of Ca^{2+} currents.

Kinetic parameters for the ion channel models, along with the equations used, can be found in Table A1 in the APPENDIX and are also further described in RESULTS.

Ion conductance distribution

The soma densities of the various conductances are as follows (all in S/m^2): Na^+ 320, K_s 40, K_t 50, K_{NaF} 50, K_{NaS} 5.2, Ca_N 80, Ca_{LVA} 0, Ca_L 4, K_{CaN} 60.

The low-voltage–activated Ca^{2+} (Ca_{LVA}) conductance was set to zero in the soma because experimental evidence suggests that the Ca_{LVA} current is usually not expressed in dissociated cells, where most of the dendritic tree has been removed. El Manira and Bussières (1997) found that, in dissociated larval neurons, no motoneurons and only 19% of unidentified spinal neurons expressed this type of current. For adult cells, Ca_{LVA} currents were consistently found in intact preparations of both motoneurons and unidentified spinal neurons (Matsushima et al. 1993). This could mean that the Ca_{LVA} current is usually present in the dendritic tree but not in the soma, as we have assumed here; however, an alternative explanation is that Ca_{LVA} could be differently expressed in larval and adult neurons.

In the initial segment, the densities are (in S/m^2): Na^+ 20,000, K_t 6,000. The reasons for the differences between these values and the somatic Na^+ and K_t conductance densities are given in the APPENDIX and in the DISCUSSION. For dissociated cells, the conductance densities in the soma and axon were the same as those for the intact neuron model.

The densities of the various ion conductances in the dendrites are (in S/m^2): Na^+ 320, K_s 40, K_t 20, K_{NaF} 150, K_{NaS} 52, Ca_N 80, Ca_{LVA} 575, Ca_L 2, K_{CaN} 600.

NMDA, Ca_{NMDA}, and K_{CaNMDA} conductances are included, in the soma and dendrites, if bath NMDA activation is simulated. For the densities, see *NMDA-induced oscillations* in RESULTS. For simplicity, all dendritic compartments have the same density of each ion channel. In cases where the dendritic density of an ion conductance differs from the somatic one, a modification was made to better fit the model to an experimental observation. Rationales for these modifications can be found in the APPENDIX.

RESULTS

In this section, we compare the behavior of the model neuron to that seen in real neurons under various experimental conditions and discuss different phenomena that the modeling process has revealed.

The single action potential in intact and dissociated cells

The model can address possible consequences of using dissociated cells as an experimental preparation and how results from those can be extrapolated to intact cells. Figure 2*A* shows two sample somatic action potentials generated by the model: one intact cell with the default parameters and one with parameters corresponding to a dissociated cell. The action potentials were induced by simulating current injection for 2 ms (the period of stimulation is indicated in the figure). The action potential is initiated earlier in the "dissociated" model cell than in the "intact" model cell because the dissociated model cell has a higher input resistance resulting from its lack

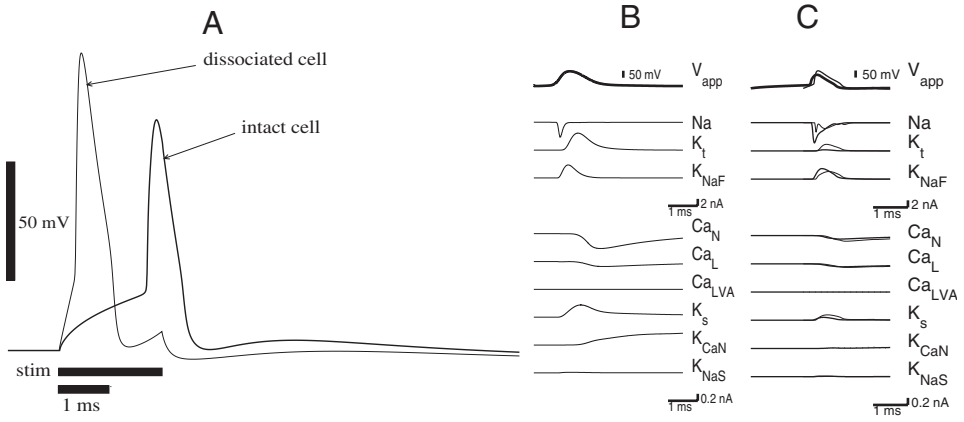

FIG. 2. Action potentials (APs) and ion currents in the soma of model cells. *A*: voltage traces of APs generated by the "intact" model cell, including dendrites (thicker line) and by the model dissociated cell, which has no dendrites (thinner line). Period of stimulation is indicated by the bar marked "stim." Note that the AP starts earlier in the dissociated cell because of the difference in input resistance. Also, in agreement with experimental results, the amplitude of the AP in the dissociated cell is larger than that in the intact cell. *B*: time courses and magnitudes of different ionic currents in the soma of the model dissociated cell in response to a simulated AP-like waveform (shown with a bold line topmost in the picture) used in an experimental study to measure different currents (Hess et al. 2007). This waveform was used to tune current parameters in the model. *C*: resulting time courses and magnitudes of different ionic currents in the soma of model cells after a spontaneous AP in an intact cell with dendrites (thicker line) and in a dissociated cell (thinner line).

Downloaded from jn.physiology.org on May 9, 2007

of a dendritic tree. The action potential of the intact model cell, apart from being initiated later, also has a smaller amplitude. This is in accordance with experiments: in intact cells, the action potential tends to reach +20 mV or so, whereas dissociated cell action potentials can reach +60 mV (Hess and El Manira 2001). Interestingly, experiments also show that the action potential width varies strongly between dissociated and intact cells—the half-amplitude width was around 0.5 ms in dissociated cells and around 1 ms in intact cells in one study (Hess and El Manira 2001). At present, the reason for this discrepancy is unclear. The action potentials generated by our model's default settings agree with the former value, both in simulated intact cells and simulated dissociated cells. Our model cannot account for the discrepancy with the present settings: the action potential can be made broader by changing, e.g., the Na^+ or K_t dynamics (for example, by changing the activation time constant of the K_t current in the model, we can make the model generate action potentials with a duration around 1 ms), but then the model does not give the right behavior for dissociated cells. It is possible that the measured differences in action potential duration can (at least partly) be attributed to the different measurement techniques (patch-clamp in dissociated cells and sharp electrodes in intact cells).

An alternative explanation might be that in intact cells, the passive load imposed on the soma by the dendritic tree tends to widen the action potential. This effect can also be observed to a certain degree in our simulations when the dendritic branches are made thicker, longer, or more numerous (not shown). Finally, it is conceivable that the K_t kinetics, measured in neurons from larval and young adult lampreys, might be different from that found in neurons of adult lampreys. Figure 2*B* shows the activation of various currents in the soma during a simulated action-potential–like waveform in a dissociated cell. The simulated voltage waveform is displayed with a bold line. This voltage signal was previously used as a voltage command in an experimental study (Hess et al. 2007) where the contributions of various ionic currents were dissected out in dissociated larval lamprey neurons. The results from that study were used to tune somatic ionic current densities in this model, particularly those most important for action potential generation (Na^+, K_{NaF}, K_t). Thus the traces from Fig. 2*B* are similar to the experimentally obtained traces (see Fig. 6 in Hess et al. 2007). Figure 2*C* predicts the resulting time courses and magnitudes of the same currents in a model intact and dissociated cell when the action potential is generated by the neuron itself in response to a brief current injection instead of being imposed on the cell as a voltage command. Current traces are shown with a bold line for the model intact cell and with a thinner line for the model dissociated cell. The Na^+, K_t, and K_{NaF} are the most important ones for determining the shape of the action potential, which is reflected in the plots of current activations in the dissociated cell. For the intact cell, however, the K_t current is much less activated than Na^+ and K_{NaF} (see following text). Other currents are activated to a lesser degree, in many cases with a delay compared with the three currents mentioned earlier. The K_{NaS} current, for instance, is activated with such a delay and is present at such a low somatic density that it is hardly activated during this simulation. Note that the Ca_{LVA} current is not activated at all because it is present only in the dendrites in the model, as explained in METHODS.

Repetitive firing characteristics: role of Ca^{2+}- and Na^+-dependent K^+ currents

The slow afterhyperpolarization (sAHP) is very important for determining a neuron's repetitive firing characteristics. Example sAHPs are magnified in *insets* in Fig. 3*A*. The main factor—at least during low-frequency stimulation of the cell—determining the amplitude and shape of the sAHP is a calcium-dependent potassium current that is activated by calcium entering through high-voltage–activated calcium channels, mainly N-type calcium channels (Ca_N) (Wikström and El Manira 1998), but there is also an sAHP component that is not abolished by cadmium application and is thus not sensitive to calcium (Cangiano et al. 2002). Previous experiments showed that this potassium current is instead dependent on sodium ion influx to the cell (Wallén et al. 2003, 2005). This slow sodium-dependent potassium current accounts for roughly 20–50% of the sAHP size, depending on the activity of the cell. It is not known whether this channel is activated solely by the sodium ion concentration, or by both sodium ion concentration and voltage. In the model, we couple it to a "sodium pool" with slow dynamics (decay time constant = 50 ms). This simplified

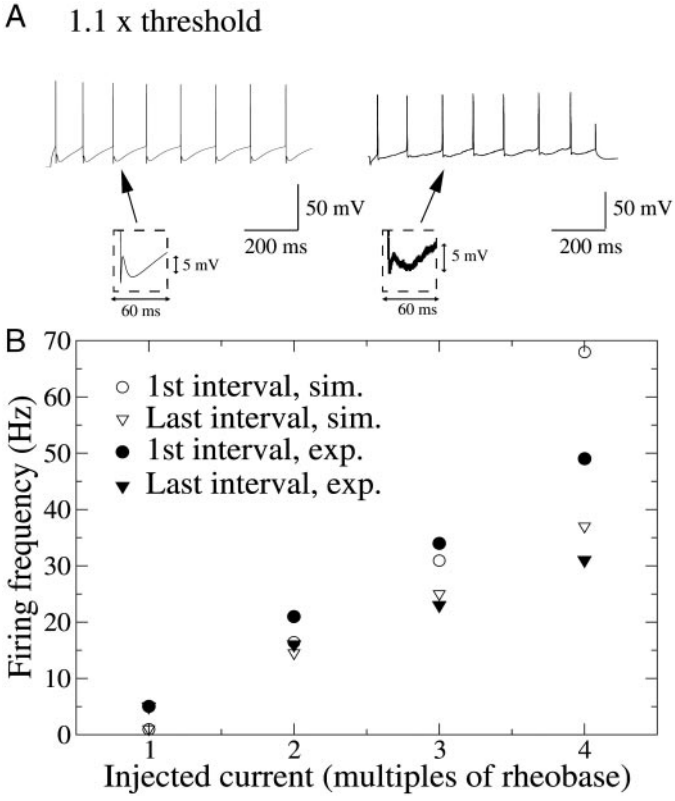

FIG. 3. Firing characteristics in model spinal neurons. *A*: response of a simulated spinal neuron and a real unidentified lamprey spinal neuron to a continuous injected current. Current is slightly above threshold for repetitive firing (0.5 nA in the simulated cell; 1.5 nA for the real cell). *Insets*: magnifications of the slow afterhyperpolarization (sAHP). *B*: current–frequency curves for simulated spinal neurons and experimental data for interneurons (estimated from Buchanan 1993; Fig. 9*A*). Current injection is normalized to rheobase to facilitate comparison between experimentally obtained and simulated results. Circles (hollow for simulation, filled for experiments) show the instantaneous frequency (reciprocal of the duration) of the first interspike interval, whereas the triangles (hollow for simulation, filled for experiments) show the steady-state frequency (measured as the reciprocal of the duration of the last interspike interval during a 1-s current pulse).

Downloaded from jn.physiology.org on May 9, 2007

model (see APPENDIX for more details) is sufficient to reproduce much of the available experimental data.

The sAHP is much smaller in dissociated cells than in intact cells, or even absent. Because the sAHP is the main determinant of the firing frequency—and it is mediated by K_{CaN} and K_{NaS} channels—it is reasonable to believe that these channels could be present in the dendritic tree. To obtain a model that had typical-looking sAHPs in intact model cells and small or no sAHPs in dissociated model cells, these currents were included in the dendritic tree at tenfold the somatic density. The very high firing frequencies observed in one study on dissociated larval cells (Hess and El Manira 2001) also required a high density of Na^+ and K_t current in the initial segment (see APPENDIX for further details).

Figure 3*A* shows the responses simulated for a model intact spinal neuron (*left*) and a real unidentified spinal adult neuron (*right*) for a current injection level slightly above the current threshold for repetitive firing. The sAHP region is shown magnified in an *inset* for both cases. Figure 3*B* shows the current–frequency relationship of the model neuron, both for the first interspike interval and for the steady-state interspike interval (last interval). Experimental values, estimated from Fig. 9*A* in Buchanan (1993), are shown in the same plot. We used data for interneurons because the instantiation of our model used here has passive characteristics resembling those of interneurons. Current–frequency curves for motoneurons can also be well reproduced by the model, given that the soma size and extent of the dendritic tree are increased in the model to match the passive characteristics of real motoneurons (not shown). The injection current is normalized to rheobase for ease of comparison. In the physiologically relevant range shown, it is apparent that the correspondence of the steady-state firing rates between the experiments and the simulations is fairly good. The first interspike interval—although fairly well reproduced by the model at low current-injection strengths—becomes too high at very high levels of injected current. This is because, in the simulation, such strong injection currents tend to lead to a doublet spike in a simulated soma of relatively small size such as the one used here. Figure 4 shows simulated and experimentally recorded spike trains when calcium channels have been blocked. The recordings were performed on an unidentified neuron and we compare the results with a simulated trace from a model spinal interneuron. In the experiment, calcium channels were blocked using cadmium. Figure 4*A* shows the response in an unidentified neuron and a simulated spinal neuron when cadmium was applied, blocking all high-voltage–activated calcium channels. The stimulation was just strong enough to yield repetitive firing in both the experiment and the simulation. The shape of the sAHP, which is now mediated by K_{NaS} only, was noticeably altered compared with the case with intact Ca^{2+} channels (compare Figs. 3 and 4; the *insets* in each figure show magnifications of the regions of interest). Although the shape of the interspike region is similar in both cases (lacking the "dip" that is seen in the control case), the time course of the early phase of the sAHP is faster in the simulation. This difference can be explained by the fact that the experimental recording was obtained from a larger cell (rheobase >1 nA), and additional simulations using a cell with larger soma and more extensive dendritic tree yielded a time course more nearly similar to the one observed experimentally, with the shape retained (not shown).

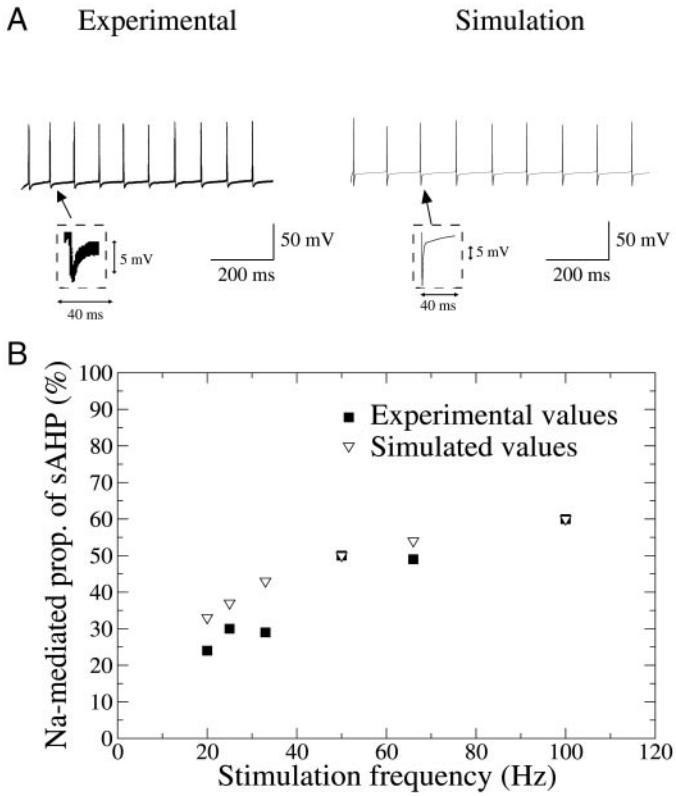

FIG. 4. K_{NaS}, the slow AHP, and spiking frequency. *A*: spike trains from unidentified central pattern generator (CPG) neurons (*left*) and simulated spinal neurons (*right*) in response to a constant-current injection close to the firing threshold (1.5 nA for the unidentified CPG neuron, 0.5 nA for the simulated spinal neuron) when high-voltage–activated calcium channels have been blocked, so that Ca_L, Ca_N, and K_{CaN} currents are not activated. In the experimental case, this was accomplished by adding cadmium. With Ca^{2+} channels blocked, the sAHP size could be determined solely by the K_{NaS} current. *Insets*: magnifications of the relevant regions, which may be compared with the sAHP magnifications in Fig. 3*A*. *B*: K_{NaS}-mediated proportion of the sAHP varies with the frequency of the stimulation imposed on the cell. Experimental values are black squares; simulated values are white triangles. At higher stimulation frequencies, the K_{NaS} part of the sAHP becomes comparatively larger.

Previous experiments showed that the part of the sAHP contributed by the K_{NaS} current grows as the firing frequency of the cell is increased (Wallén and Grillner 2003), suggesting that this current becomes important at high firing frequencies. This effect is replicated in the model. Figure 4*B* illustrates how the K_{NaS} part of the sAHP varies when spike trains of different frequencies are induced in the cell. The higher the imposed spike frequency, the larger the K_{NaS}-mediated part of the sAHP becomes. This is the result of a slower dynamics in the K_{NaS} part.

Catechol-sensitive currents: K_t and K_{NaF}

After having introduced the basic factors involved in action potential generation and firing frequency control in lamprey CPG neurons, we now describe in more detail how the fast K currents K_t and K_{NaF} influence the shape of both action potentials and slow AHPs. We begin by considering the K_t current, for which there is more experimental evidence. The K_t

Downloaded from jn.physiology.org on May 9, 2007

current, a fast-inactivating transient potassium current, is thought to be the main determining factor of action potential width in motoneurons, contralaterally and caudally projecting interneurons (CCINs) and unidentified spinal neurons (Hess and El Manira 2001). A change in the K_t current's activation time constant in our model can change the width without having a large effect on the rising phase or amplitude (results not shown). The K_t current can be blocked by catechol. In *Xenopus*, two high-voltage–activated conductances (I_{Kf} and I_{KNa}) that are blocked by catechol also affect action potential width, although they do not seem to be as important for normal locomotor pattern generation as the K_t in lamprey (Kuenzi and Dale 1998).

Figure 5 shows some characteristics of our model K_t current. The half-activation value is at around 0 mV and the time constant of activation is rapid compared with the time constant of inactivation. The recovery of inactivation curve suggests that most of the K_t channels are available again only 2–4 ms after an action potential has occurred. These kinetic parameters were measured in dissociated cells and, when they are used in our model, they yield action potentials with a half-amplitude width of nearly 0.5 ms both in the dissociated cell model and in the intact cell model.

In addition to the sAHP-related K_{Na} current, a faster sodium-dependent potassium current (here called K_{NaF}) was also previously described in lamprey spinal neurons (Hess and El Manira 2002; Hess et al. 2007). Like K_t, this current can be blocked by catechol (Hess and El Manira 2002; Hess et al. 2007). The activation and inactivation properties of this current were found to be similar to those of the Na^+ current (Hess and

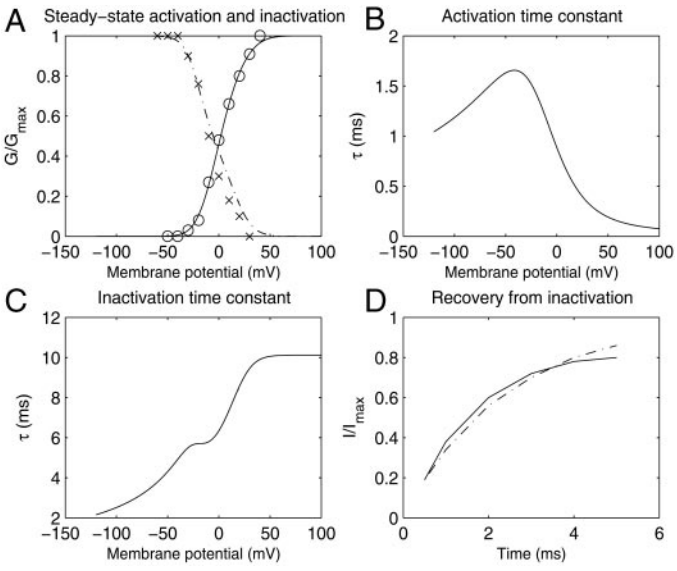

FIG. 5. Kinetics of the modeled K_t current. *A*: curves of normalized steady-state activation and inactivation for K_t as a function of voltage. Circles are experimentally observed steady-state activation values; crosses are experimentally observed steady-state inactivation values (Hess and El Manira 2001; Hess and El Manira 2007). Solid line is the steady-state activation function used in the model; the dash–dotted line is the steady-state inactivation function. *B*: time constant of activation used in the model. *C*: time constant of inactivation used in the model. *D*: recovery from inactivation as a function of time. Solid line represents experimentally observed values; the dotted line represents values generated by the model for voltage steps from $V_m = -120$ mV.

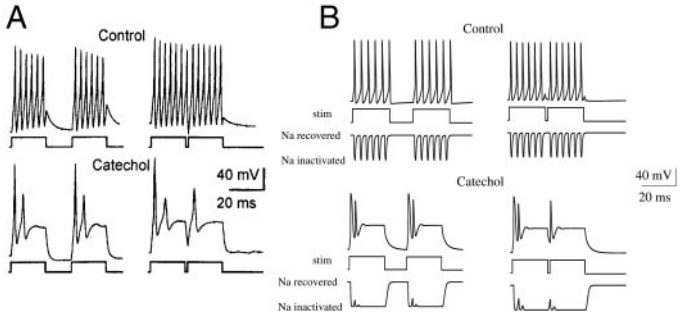

FIG. 6. K_t promotes repetitive firing in the absence of calcium by facilitating Na^+ current recovery from inactivation. *A*: experimental recordings from a double-voltage step experiment (Hess and El Manira 2001). Current is injected in two steps separated by a longer (*left*) or shorter (*right*) pause. Calcium channels are blocked in all experiments. Control cells fire repetitive APs. Cells treated with catechol (blocking K_t and K_{NaF} channels) fire one or 2 action potentials and fail to fire repetitively. *B*: simulated experiments with the model cell. Protocols are the same as in *A* and blocking a current was here modeled by decreasing its conductance to 3% of the original value. Here, the value of the Na^+ inactivation variable is plotted for each of the 4 experiments. In the simulated experiments with catechol, Na^+ fails to recover from inactivation between APs.

El Manira 2002; Hess et al. 2007), i.e., the K_{NaF} "mirrors" the Na^+ current. One interpretation of this is that K_{NaF} channels are activated by a localized sodium ion pool with fast turnover. Rapid influx into this pool of Na^+ ions during an action potential would then activate K_{NaF} in proportion to the sodium current and a rapid decay of the local concentration would explain the transient character of the K_{NaF} current. According to this reasoning, a fast sodium pool was used in simulating the current here, as described in the APPENDIX.

Applying catechol to a dissociated lamprey spinal neuron results in a wider action potential and an inability of the cell to fire repetitively in the absence of calcium influx. It was suggested (Hess and El Manira 2001) that catechol blocks the K_t channels, leading to a failure of Na^+ channels to properly recover from inactivation. Figure 6 shows the response of a real cell (reproduced from Hess and El Manira 2001) and a model neuron to a double-step protocol where the cell is stimulated by injected current for 20 ms, after which the injected current is removed for 2 and 13 ms, respectively, before another current step is applied for 20 ms. The procedure is done in the presence and absence of catechol, resulting in a total of four experiments. We repeated these experiments (described in Hess and El Manira 2001) in the model, where we have direct access to the activation and inactivation state of the Na^+ current. These experiments were performed on dissociated cells, both in the real cells and in the simulation. At the time of the experimental study, the existence of the K_{NaF} current, which is also blocked by catechol, was not known, so the observed effects were attributed solely to the absence of K_t. We used simulations with our model to see whether blocking only K_t is sufficient to explain the results or whether K_{NaF} has to be blocked as well. The simulations suggest that blocking only K_t currents in a model dissociated cell is sufficient to reproduce the observed results because blocking both K_t and K_{NaF} gives a result that is practically identical to blocking only K_t. (Note, however, that the effects of blocking K_{NaF} in addition to K_t are prominent when simulating experiments an intact cell; more on this subsequently follows in connection with Fig. 7.) As can be seen, when the K_t current is intact, the

Downloaded from jn.physiology.org on May 9, 2007

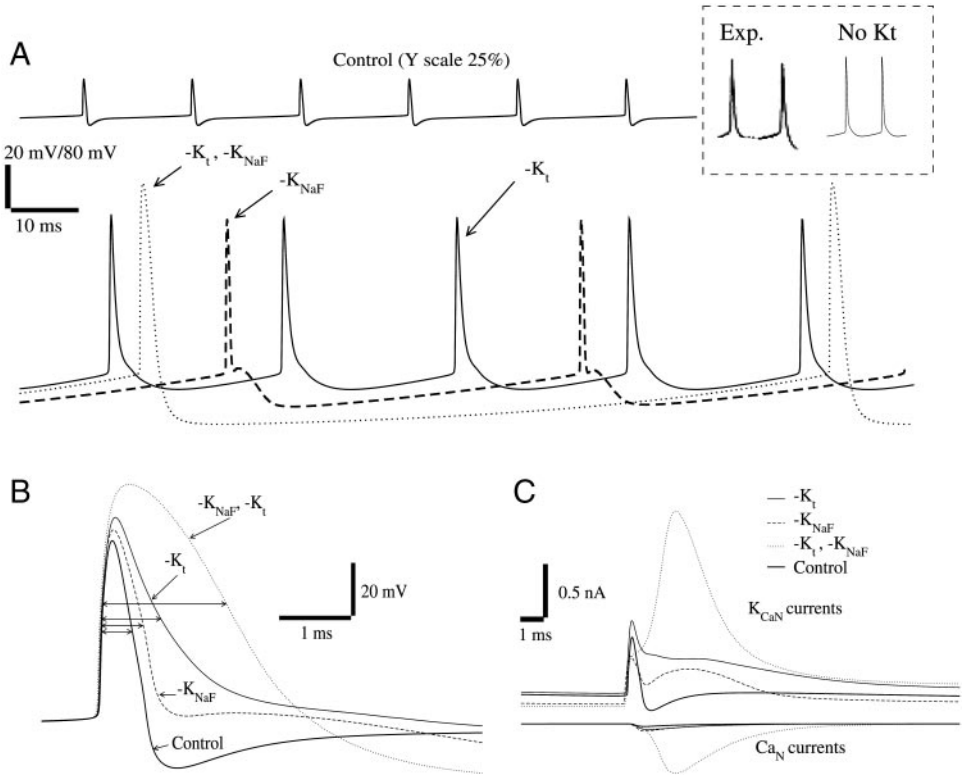

FIG. 7. Repetitive firing when K_t and/or K_{NaF} currents are blocked. Notation "$-K_t$" stands for "K_t blocked" in all the legends and in figure text. *A*: voltage trace of spikes and AHPs in simulations where K_t and/or K_{NaF}, or none of them, were blocked. Simulated stimulation strength was 2 nA. Control case is shown separately, at the *top* of the figure, for clarity. *Inset*, *top right corner*: for purposes of comparison, the interspike interval (with the characteristic rounded AHP) in an experimental recording from the intact spinal cord (*left*, modified from Hess and El Manira 2001) and a smaller version of the larger voltage trace with K_t blocked shown in this figure (*right*). Blocking one or both of the K^+ currents has a significant effect on the shape of the sAHP between spikes. *B*: magnification of an AP from *A*. Blocking one or both of the K^+ currents results in a broadened spike. Double-headed arrows show the spike width at the half-amplitude of each AP, measured from the AP peak to the resting level. *C*: Ca_N and K_{CaN} currents in a primary dendritic compartment during the action potentials shown in *B*. Dendritic currents are shown because the effects of K_{NaF} blockage are most prominent in the dendrites in the model. Broadened APs lead to increased calcium influx and subsequently larger amplitudes of K_{CaN} currents.

cells fire action potentials in rapid succession, but when catechol is applied (corresponding to setting K_t and/or K_{NaF} conductances to a few percent of the original value in the model), the cells stop firing after two spikes. In our replicated version of the experiment using the model, we also plotted the magnitude of the Na^+ current's inactivation state variable. It can be seen from the plot that this variable fails to return to its original value between action potentials when the K_t and K_{NaF} currents are absent.

The experiments just described were performed in dissociated cells in the absence of calcium. When catechol is applied in the intact spinal cord, without blocking calcium channels, the cells are still able to fire repetitively, but their AHPs lose their biphasic look with one fast AHP and one slow AHP and instead show a single AHP with a rounded shape (Hess and El Manira 2001). Because catechol can block both K_t and K_{NaF}, this effect could be attributed to the absence of either or both of these currents. We therefore used a model neuron to examine the effects of blocking just one or both of the currents during repetitive firing (Fig. 7). In Fig. 7*A*, simulations with a strong applied injection current (2 nA) are shown where K_t, K_{NaF}, or both are blocked. For reference, a control trace is shown at the top of the figure with spikes scaled to 25% size for clarity. The spike frequency in the control trace is high but comparable to the frequency in the control case of the experiment we replicate (Hess and El Manira 2001). It is apparent that blocking only K_t is sufficient to obtain the rounded sAHP. Part of an experimental trace (modified from Hess and El Manira 2001) is shown in an *inset* alongside with part of a simulation where only K_t was blocked. When only K_{NaF} is blocked, there is a small fast AHP followed by a slight afterdepolarization (ADP), after which follows a large sAHP. When both K_t and K_{NaF} are blocked, there is no fast AHP or ADP but a very large sAHP. Looking at the action potential shapes, blocking either K_t or K_{NaF} in isolation seems to increase the spike width. Figure 7*B* therefore shows a magnification of action potentials from Fig. 7*A*; these were superimposed for clarity. Apparently, in the model, blocking K_t or K_{NaF} leads to a broader spike, although the effect of blocking K_t is stronger. When both are blocked, there is a supralinear effect that leads to a much broader spike. Double-headed arrows mark out the half-amplitude width of each action potential. The differences in spike width would be expected to lead to changes in calcium influx during the action potential and subsequent changes in K_{Ca} currents activated by the calcium that has entered. Figure 7*C* shows Ca_N and K_{CaN} current time courses and amplitudes during the action potentials in Fig. 7*B*. [We plot only N-type calcium channels because calcium entering through these channels is the main activator of K_{CaN} channels; there is also a small effect from calcium influx through P/Q-type channels (Wikström and El Manira 1998), although we have neglected this effect in our model.] Because dendrites have a much higher density of K_{CaN} channels than soma, we plotted currents from a primary dendritic compartment to see the effects more clearly. Also, because the activation of K_{CaN} currents here dominated that of the other sAHP-mediating current, K_{NaS}, we plot only Ca_N and K_{CaN} currents. As expected, the differences in spike width are reflected by changes in resulting dendritic K_{CaN} currents. Comparing the current time courses with the voltage traces in Fig. 7*A* suggests that the rounded shape of the sAHPs mainly reflects the activity of the K_{CaN} current.

NMDA oscillations

Because our cell model is constructed to be useful in a network simulation, it is important that, in addition to the

Downloaded from jn.physiology.org on May 9, 2007

voltage- and concentration-gated ion channels described earlier, the ligand-gated ion channel mechanisms are accurate as well. Earlier experimental studies of the lamprey CPG showed that a tonic activation of NMDA receptors may give rise to intrinsic voltage oscillations in intact spinal neurons. Several variations of these NMDA-induced oscillations were examined experimentally and computationally (see, e.g., Brodin et al. 1991; Grillner and Wallén 1985). Experimental studies on single cells extensively described tetrodotoxin (TTX)- and TTX + tetraethylammonium (TEA)-resistant NMDA-induced oscillations (Grillner and Wallén 1985; Wallén and Grillner 1987). We simulated these types of oscillations using our model. Although NMDA-induced oscillations are robustly observed in intact adult neurons where synaptic transmission has been blocked by TTX application, we have so far not observed them in dissociated larval neurons (El Manira and Hill, unpublished observations). This could mean that the dendrites (which are largely missing from the dissociated cells) are needed to generate NMDA oscillations or it could be attributed to developmental differences between the larval and adult life stages. Additional experiments using multiphoton imaging are under way to examine the calcium transients resulting from different kinds of activation, including bath NMDA application. These experiments will likely clarify the distribution of NMDA channels over the cell. Our main purpose concerning NMDA dynamics was to make sure that the model can generate NMDA-induced oscillations with different distributions of NMDA channels. This was found to be the case: depending on how the conductances are set, the model can generate oscillations with NMDA channels on soma only, dendrites only, or both on soma and dendrites. In this section and in the following one we show sample output from a parameter setting where NMDA, Ca_{NMDA}, and K_{CaNMDA} channels were present on both soma and dendrites. The densities were set differently in soma and dendrites. Soma densities were: NMDA = 30× bath NMDA concentration; Ca_{NMDA} = 2× bath NMDA concentration; K_{CaNMDA} = 0.175 [all in S/m^2; NMDA concentration in arbitrary units (au)]. Dendrite densities were: NMDA = 5× bath NMDA concentration; Ca_{NMDA} = 1× bath NMDA concentration; K_{CaNMDA} = 1.75 (all in S/m^2; NMDA concentration in au).

TTX oscillations

With NMDA present while action potentials are being abolished by administering TTX to block sodium channels, one sees a characteristic type of NMDA-mediated oscillation (Grillner and Wallén 1985). The depolarized plateaus in these oscillations often have a stereotyped shape, with a small Ca^{2+}-dependent depolarization in the beginning and a slowly declining phase that is suddenly terminated, whereupon the potential quickly drops toward the trough potential (Fig. 8*A*). This interplateau state is triggered when enough calcium has entered through the open NMDA-receptor channels to terminate the depolarized plateau through the activation of hyperpolarizing K_{CaNMDA} channels. The length of the interplateau phase is likely determined by the time it takes for the accumulated calcium to be removed. When a certain depolarizing potential threshold is crossed (determined by the voltage range where the magnesium block of the NMDA channel starts to be removed), a self-reinforcing loop between membrane potential and NMDA channel activation rapidly takes the neuron to a depolarized potential. TTX oscillations are usually 10–25 mV in amplitude (Wallén and Grillner 1985). See Tegnér et al. (1998) for a more detailed description of the possible mechanisms behind these TTX oscillations. Figure 8*A* shows experimentally recorded and simulated TTX oscillations, whereas Fig. 8*B* shows the sizes of various currents during one of the simulated plateaus. NMDA, Ca_{NMDA}, and K_{CaNMDA} currents dominate, although there is also a fairly large Ca_L component. Sometimes, variations on the theme are seen and many TTX-resistant oscillations seem to be "broken up" or to have internal

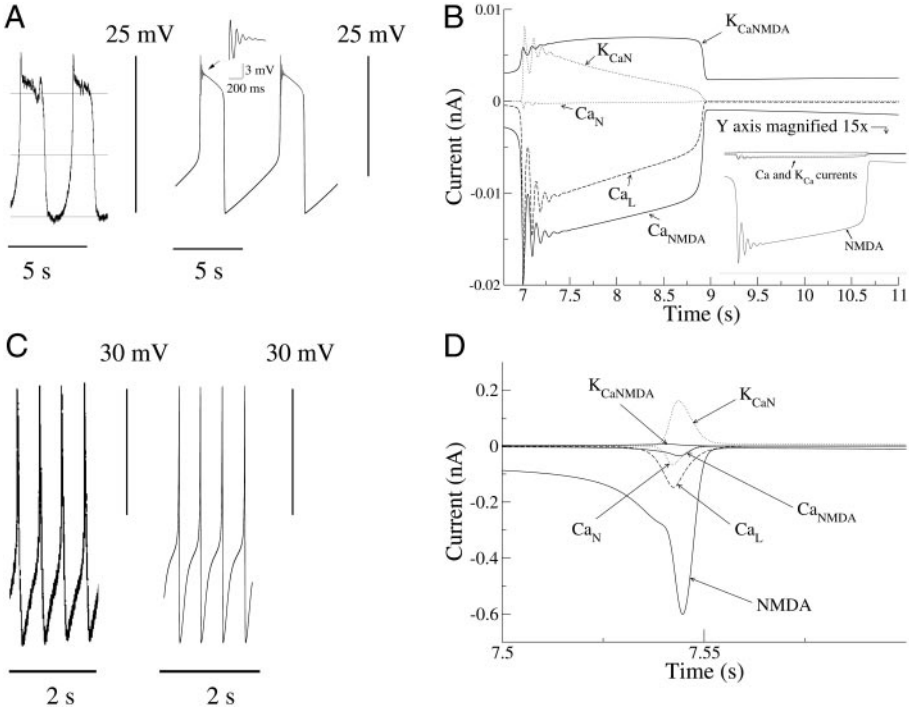

FIG. 8. Various types of *N*-methyl-D-aspartate (NMDA)–induced oscillations. *A*: NMDA-induced oscillations in the presence of tetrodotoxin (TTX), which blocks Na^+ channels. *Left*: experimental recording. *Inset*: magnification of the small-amplitude oscillations at the beginning of a plateau. *Right*: simulation [bath NMDA concentration was 0.7 (a.u.) and the resting potential was −70 mV]. *B*: somatic currents activated during the simulated NMDA-induced oscillations in the presence of TTX (same as *A*, *right*). Because the NMDA current is much larger than the other currents, it has been omitted in the plot. Relative magnitude of NMDA current compared with the other currents is shown in the *inset*; the *y*-scale is 15-fold larger in this *inset* than in the main plot. *C*: NMDA-induced oscillations in the presence of TTX and tetraethylammonium (TEA), which blocks K_s and K_t channels. *Left*: experimental recording. *Right*: simulation [bath NMDA concentration was 0.65 (a.u.) and resting potential was −70 mV]. *D*: somatic currents activated during the simulated NMDA-induced oscillations in the presence of TTX and TEA (same as *C*, *right*).

Downloaded from jn.physiology.org on May 9, 2007

oscillations within them (see, e.g., Grillner and Wallén 1985). These internal oscillations (examples of which are shown in an *inset* to Fig. 8*A*) are, in the model, dependent on the dynamics of the Ca_N and K_{CaN} channels. Both the "regular" TTX-resistant oscillations and the "irregular" ones can be mimicked by the model by varying relevant parameter values (not shown). In Fig. 8*B*, the NMDA current has been omitted from the main figure because it is so large compared with the other currents; a smaller version of the main plot with a different *y*-scale (zoomed out 15 times) is shown in an *inset* to give an idea of the amplitude proportions of NMDA versus other currents.

TEA + TTX–resistant oscillations

When in addition to TTX, TEA is applied, blocking both the K_s and K_t channels, the oscillations dramatically change their character, becoming much shorter in duration (Grillner and Wallén 1985). As a result of insufficient hyperpolarization, the calcium channels remain open and large amounts of calcium ions flow into the cell as Ca_N, Ca_L, and NMDA currents depolarize the membrane potential. The cell has time to reach a much more depolarized level before the influx of calcium activates enough calcium-dependent potassium channels to pull the potential back to hyperpolarized levels again. TEA + TTX oscillations can have amplitudes >60 mV. Figure 8*C* shows an experimental recording (modified from Grillner and Wallén 1985) and a simulation of TEA + TTX oscillations. Figure 8*D* shows the degree of activation of different currents during one oscillation period from the simulation.

Effects of changes in the morphology

The results shown so far were obtained with the "default" model described in METHODS. To find out how modifying the model neuron's morphology affects its properties, we constructed compartmental models by closely modeling three of the filled cells shown in Buchanan et al. (1989). All simulations previously described for the default model were run using these "reference" model cells and all results were qualitatively confirmed for each cell: simulated channel blockers (Cd^{2+}, catechol) had the same effects as described earlier, NMDA-induced TTX and TTX + TEA oscillations were present, and so forth. Despite the qualitative robustness of the cellular properties, there were slight quantitative differences in spiking properties such as adaptation. For conciseness, we limit ourselves to showing the variations in spike trains resulting from current injections at two levels. The reconstructed cells (modified from Buchanan et al. 1989) are shown together with graphical representations of the corresponding compartmental models in Fig. 9, *B–D*, whereas 9*A* shows the default model for ease of comparison. The lengths and widths of the dendritic branches in the graphical representations correspond to those used in the compartmental models.

The geometric orientation of the branches is arbitrary from the perspective of the compartmental model, but they were plotted with orientations roughly corresponding to those of the original reconstructed neurons. Axon collaterals are indicated with a dashed line. The neuron marked "Reference cell 1" is from Fig. 3*C* in Buchanan et al. (1989), whereas cell 2 is from Fig. 3*D* and cell 3 is from Fig. 7 in the same paper. The current densities of the default model were kept constant. The resulting input resistance values for the three new model neurons were 64, 52, and 98 MΩ for cells 1, 2, and 3, respectively. The current injection level needed to elicit an action potential was 0.29, 0.33, and 0.19 nA, respectively. Figure 9 compares spike trains generated by the default model and the three compartmental models based on the filled neurons. Two spike trains are shown for each model cell: one generated in response to a simulated 0.5-nA current injection and one generated in response to a simulated 1.5-nA current injection. Note that the current injection levels were constant and thus not normalized to rheobase. The lower current-injection level, 0.5 nA, is roughly 1.5- to 2.5-fold the rheobase of the model cells, whereas the higher level is roughly five- to sevenfold rheobase. All three model cells fired spike trains not unlike those generated by the default model. However, there were slight differences in the firing frequency and the degree of adaptation between the model neurons. Thus at the lower injection level, clear adaptation where the last interspike interval is noticeably longer than the first one is seen for the default cell and reference cell 2 (see *C3*), whereas the adaptation is only slight in reference cell 1 (see *B3*). Reference cell 3 displays no noticeable adaptation at this current-injection level (see *D3*). At the higher injection level, all cells show adaptation, although it is strongest in the default cell and cell 2 (*C4*): the first interspike interval is very short and is followed by a longer interval, after which the interval length settles down to a steady state.

The spike trains of reference cell 2 seem most similar to the default model cell, which may partly reflect that these cells have similar rheobase (0.33 and 0.35 nA, respectively) and input resistance (52 and 49 MΩ, respectively.) However, these factors are not sufficient to explain all differences in spiking between the neurons: for example, reference cell 2 shows faster firing than reference cell 3 at the lower injection level (compare *B3* and *C3*) but slower firing at the higher injection level (compare *B4* and *C4*), suggesting that differences in the dendritic tree morphology resulted in different slopes of the steady-state frequency–current (*f–I*) curves in these cells.

The differences in the initial adaptation between the model neurons can be partly explained as follows. Spike-frequency adaptation is a transient phenomenon and, because the current injection is delivered to the soma, the soma size will be an important factor in determining the first interspike interval. As dendritic currents become activated with a slight delay, they will successively have a larger influence on the interspike interval. In our example simulations, the cells that show the strongest initial adaptation are both cells with a relatively small soma. [Note also that the injection current (1.5 nA) is very high: almost fivefold rheobase for these neurons.] If the other two cells are injected with a sufficiently strong current, they will also respond with a similarly strong adaptation. Simulations where soma and dendrite sizes were varied while retaining the total membrane area of the cells (not shown) confirmed that the preceding explanation is essentially correct with respect to the simulated cells—that is, an increase in soma size with concomitant reduction in dendrite size to preserve total surface area leads to smaller adaptation. Moreover, simulations with passive dendrites (all active conductances set to zero) yielded the same outcome, which shows that the observed phenomenon was not an artifact arising from the implicit

Downloaded from jn.physiology.org on May 9, 2007

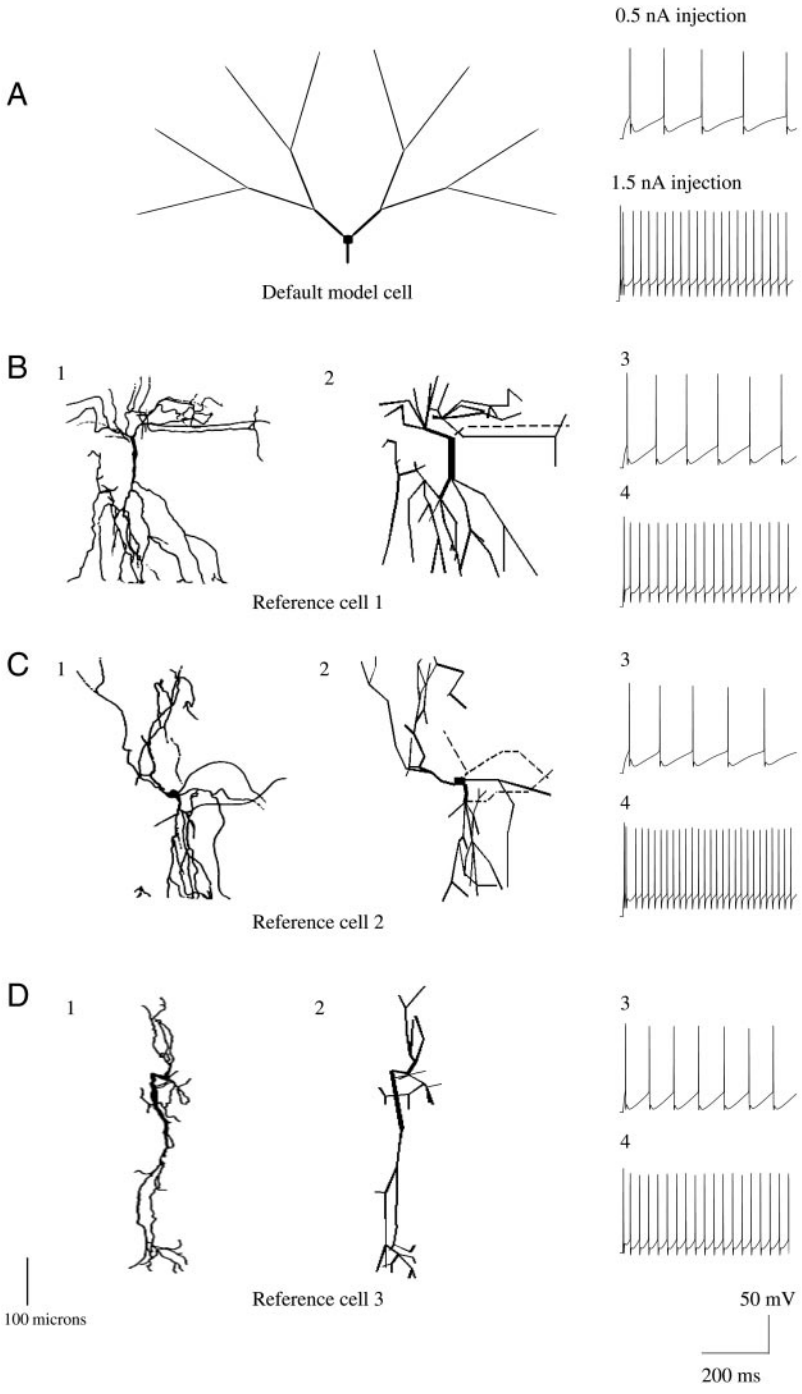

FIG. 9. Effects of changing the morphology of model cells. *A*: graphical representation of the default model cell and its response to current injections of 0.5 and 1.5 nA. *B–D*: experimentally obtained reconstructions of EIN cells (1) and graphical representations of their corresponding compartmental models (2) as well as their responses to the same simulated stimulation protocols; 0.5-nA current injection is in each case indicated by (3) and the 1.5-nA injection by (4). Reference cell 1 is modified from Buchanan et al. (1989) (Fig. 3*C*), whereas reference cell 2 is from Fig. 3*D* and reference cell 3 is from Fig. 7 in the same paper. Scale bar next to *D1* is valid for all graphical representations. Dendritic branches of the model cells were plotted so that they roughly resemble those of the original reconstructed neuron, although their actual geometric orientations are arbitrary in the compartmental model. Axon collaterals (not explicitly simulated) are indicated by dashed lines in the model neurons. Several long axon collaterals were removed from the image of reconstructed cell 3 to improve legibility. Scale bars below *D4* are valid for all traces showing the response to injected current.

changes in dendritic conductances resulting from changing the dendritic surface area.

In summary, firing properties show considerable robustness in a qualitative sense with some quantitative variability.

DISCUSSION

A new model of a lamprey locomotor network neuron has been constructed. Although previous models (e.g., Ekeberg et al. 1991) were biophysically detailed, channel kinetics were based mostly on adapting ion channel models from other organisms to fit experimental traces. The present model is to a large extent based on voltage-clamp and other types of experiments on real lamprey neurons. It incorporates several types of ionic currents not present in previous models (K_t, K_{NaF}, K_{NaS}), which in itself represents a significant improvement. Although previous models contained only one high-voltage–activated calcium current, the present model has two (Ca_N and Ca_L), which have both been identified in lamprey, and both have kinetic parameters consistent with experimental results (El Manira and Bussières 1997). The new model can reproduce many experimental results that were not addressable before, such as effects of applying catechol. The separation of the high-voltage–activated calcium current into Ca_N and Ca_L also led to simulated TTX-resistant oscillations with characteristics

Downloaded from jn.physiology.org on May 9, 2007

more consistent with those seen in experiments. In the previous models, the dendritic tree was purely passive, whereas in actual lamprey spinal neurons several types of active conductances are thought to be located there. The new model allows an examination of the distribution of such conductances across the neuron, leading for example to the hypothesis presented in this paper about K_{CaN} and K_{NaS} channels being present at significantly higher densities in the dendritic tree than in the soma. In the same vein, the present model reproduces experimentally observed differences between dissociated cells and intact cells. Previous models such as that proposed by Ekeberg et al. (1991) did not yield a realistic dissociated cell when the dendritic tree was removed. Because the dissociated cell is an important experimental preparation, the model needs to be able to give a good description of it.

One important use of the model is as a "check" of the soundness of our experimentally based understanding of the single lamprey CPG neuron. The model can provide a tool to study the currents underlying the neuron's electrical activity by showing the simulated amplitudes and time courses of selected currents during various types of activity, as well as following manipulation of some of the model components (see, e.g., Figs. 2 and 6–8). In this way insights into the functional roles of recently characterized ion channels in the lamprey CPG can be achieved. For example, the importance of K_t for action potential repolarization and width in this system suggested by Hess and El Manira (2001) is supported by the model. K_t is classified as an "A-type" current—a fast, inactivating potassium current. In general, the kinetics of A-type currents varies depending on the cell type (Birnbaum et al. 2004). Suggested functional roles of this current depend on the activation threshold (see, e.g., Surmeier et al. 1989). The typical role of A-type currents, which are activated at more hyperpolarized levels, below the neuron's spiking threshold, is to act as a kind of brake or damper, so that the onset of an action potential is delayed (Hille 2001). In lamprey CPG neurons, the A-type current is activated at a high membrane potential. It repolarizes the neuron after an action potential and thereby frees the Na^+ channels from inactivation, making the neuron ready for another spike. A repolarizing function of an A-type current was also previously found in other systems (Storm 1987; Surmeier et al. 1989). In the context of the operation of the lamprey locomotor CPG network, it was shown that the K_t current affects the number of action potentials per locomotor cycle and the regularity of the locomotor rhythm (Hess and El Manira 2001).

The interplay between Na^+ and K_t allowed very high spiking frequencies in one study of dissociated cells in which calcium had been blocked (so that K_{Ca} currents are absent) (Hess and El Manira 2001). To reach the spiking frequencies found in those experiments, our model had to include Na^+ and K_t channels in the axon initial segment at a much higher density than the somatic one. Several computational models also found it necessary to have much higher sodium channel densities in the initial segment. A good discussion of these issues can be found in Stuart et al. 1999. Because the Na^+ and K_t currents are present on the initial segment in such high densities in the model, the initial segment component of these currents seems to be more important for action potential generation than the somatic component. If instead enough K_t channels are placed on the soma to fully repolarize the action potential, the resulting somatic K_t current becomes much larger than experimental data suggest. The K_t current is, in general, considerably less activated in the soma of an intact cell than in a dissociated cell (see Fig. 2*C*). The reason is that the maximum somatic potential reached during a spike in an intact cell is only +15 to +20 mV, whereas it can be up to +60 mV in a dissociated cell (Hess and El Manira 2001). K_t is a high-voltage–activated current that reaches its maximum conductance only at +40 mV or so (Hess and El Manira 2001). Because the activation kinetics is also faster at more depolarized levels, the difference in the resulting current amplitude will be considerable.

The model also throws light on firing-frequency characteristics of the lamprey CPG neuron. It predicts that differences in firing frequency and sAHP size between dissociated and intact neurons may be explained by a high density of K_{CaN} and K_{NaS} currents (tenfold the somatic density) in the dendritic tree. In addition, it shows that a simplified model of the K_{NaS} current is sufficient to explain many of the relevant experimental results on sodium-mediated sAHPs and the relative contribution of a calcium-dependent versus a sodium-dependent component (Wallén and Grillner 2003). As described earlier slow K_{Na} channels (K_{NaS}) in the lamprey seem to regulate the sAHP, firing frequency, and adaptation together with K_{Ca}. The relative importance of K_{Na} increases with activation frequency. K_{Na} channels were also found in other parts of the nervous system (Dryer 1994; Yuan et al. 2003). They were suggested to play a role in such phenomena as the regulation of neural excitability and firing patterns and modulation of the action potential waveform (see, e.g., Dryer 1994). As in the lamprey, a K_{Na} current was also previously found to affect the sAHP amplitude in neocortical intrinsically bursting neurons (Franceschetti et al. 2003). In that study, it was also shown that K_{Na} channels can give rise to rhythmic bursting, an effect seen in our model as well if the K_{NaS} conductance is sufficiently increased (not shown). As in lamprey CPG neurons, a slow K_{Na} current was shown to be involved in adaptation in V1 neurons (Wang et al. 2003).

The preceding results suggest various functional roles of the different currents in the lamprey CPG neurons and can form a basis for comparison with the *Xenopus* embryo model, a model system that was experimentally and computationally investigated in detail (see Dale and Kuenzi 1997). Interestingly, neurons in these two spinal cord CPGs use many of the same classes of ionic currents, but these currents seem to differ in their functional and/or electrophysiological characteristics between the two model systems. Here differences in developmental stages might, however, play a role. Here we will make a short comparison of what is known about the functional roles of ionic currents in *Xenopus* versus lamprey. In *Xenopus* embryo spinal neurons, Ca^{2+} currents are necessary for repetitive firing (Dale and Kuenzi 1997), whereas in lamprey spinal neurons, repetitive firing persists in cadmium for both dissociated and intact cells (Hess and El Manira 2001; Wallén, personal communication). Both the *Xenopus* embryo and the lamprey contain currents described as A-type–like; however, they seem to differ in their functional significance because Dale and Kuenzi (1997) state that the *Xenopus* A-type current is probably highly inactivated during locomotor activity and was thus omitted from their mathematical model of a *Xenopus* neuron. Like the lamprey CPG neuron, the *Xenopus* embryo

Downloaded from jn.physiology.org on May 9, 2007

CPG neurons contain potassium currents that control action potential width. In *Xenopus* these currents are a type of delayed rectifier (I_{Kf}) and a fast sodium-dependent potassium current (I_{KNa}), whereas experiments in the lamprey showed the K_t current to be essential. Our simulations suggest that K_{NaF} could also be of importance (see Fig. 7). These findings would in themselves suggest that the lamprey K_t and K_{NaF} could be analogous to the *Xenopus* I_{Kf} and I_{KNa}. However, there are notable differences between these pairs of currents in the two model systems. For instance, the lamprey K_t, in addition to controlling action potential width, is important for enabling repetitive firing by controlling the action potential repolarization, which is not the case for the *Xenopus* I_{Kf} and I_{KNa} (Kuenzi and Dale 1998). In *Xenopus* a slow potassium current, I_{Ks}, controls and decreases a cell's firing frequency (Kuenzi and Dale 1998), whereas calcium- and sodium-dependent potassium (K_{Ca}, K_{Na}) currents preferentially regulate firing frequency and adaptation in the lamprey CPG, although a slower delayed rectifier is also present. Calcium-dependent potassium channels also exist in *Xenopus* and are involved in a rundown of activity in the CPG (Dale and Kuenzi 1997), a phenomenon occurring over much longer timescales than spike-frequency adaptation in lamprey neurons. Comparing the fast sodium-dependent currents in the two organisms, we note that the activation of *Xenopus* I_{KNa} channels depends on both voltage and the level of Na^+ ions that enter primarily through leak channels and excitatory synaptic channels; Na^+ influx during action potentials does not give an appreciable effect except during repetitive firing (Dale and Kuenzi 1997). In contrast, the lamprey K_{Na} channels (both the fast and slow types) are noticeably activated after a single action potential (Cangiano et al. 2002; Hess and El Manira 2002; Wallén et al. 2005). In summary, although many of the same current classes seem to be present in both model systems, the currents generally have different roles.

A common criticism of this type of model is that simulation results are sensitive to parameters, and that data are too variable to constrain the model. This is a valid concern, and to show that our generic model gives qualitatively similar (although quantitatively variable) output when the morphology is varied, we constructed three reference model neurons closely based on filled cells from Buchanan et al. (1989), which is the most comprehensive study of excitatory interneurons in the lamprey CPG so far. Simulations using these morphologies showed that the results herein (roles of various currents, effects of simulated channels blockers, appearance of NMDA-induced oscillations in TTX and/or TEA, etc.) still hold true in each of the model cells, although there were slight quantitative differences in the spike trains resulting from given current injection levels. The functional implications of this kind of variability will be further examined in network simulations. There are previous results suggesting that variability in properties such as rheobase and sAHP size (which controls adaptation) can lead to an enhanced robustness and increased working range of locomotor pattern generation (Hellgren et al. 1992).

Another type of variability likely to be important for pattern generation is found on the synaptic level. For example, excitatory synapses between excitatory interneurons and motoneurons or crossed-caudal (CC) interneurons can be either facilitating or depressing (Parker 2000, 2003), whereas inhibitory synapses from small inhibitory interneurons are depressing in motoneurons and facilitating in CC interneurons (Parker 2000). Different cell types can be differently modulated by neuromodulators; for example, substance P has opposite effects on the postinhibitory rebound in inhibitory interneurons and motoneurons (Svensson 2003). This synaptic and modulatory variability will be considered in the network simulations based on this cell model.

Some of the model's predictions suggest new experiments to confirm or falsify them. For instance, the prediction of much higher densities of K_{Ca} and K_{Na} currents in the dendrites suggests a closer look at Na^+ and Ca^{2+} transients in dendrites and how they are connected to the activity of the neuron. Experiments measuring such transients using multiphoton imaging are under way. Further, although not illustrated herein, the model predicts that slightly counterintuitively, the frequency of TTX oscillations should decrease as the applied-bath NMDA level is increased. This prediction is currently being tested experimentally.

In future work, we plan to search for putative new roles for ion channels when the model is used in a network context, such as an interneuron network inside a central pattern generator module.

APPENDIX

Kinetic parameters for the ion channel equations

The equations referred to in Table A1 are listed below.

The equation used to calculate the ionic current through each channel is given in the first column in Table A1. This equation always involves a maximum conductance and a reversal potential. In most cases, it also involves one or sometimes two activation (or inactivation) variables, which vary between 0 and 1 and may be voltage or concentration dependent. In the case of the voltage-dependent (in)activation variables, the following equation holds

$$\frac{dx}{dt} = \alpha_x(V)(1 - x) - \beta_x(V)x \tag{A1}$$

where x is the name of the (in)activation variable (m, h for the Na^+ current, for example). In two cases—the Ca_N channel and the Ca_L channel—the following (completely equivalent) equation was used instead

$$\frac{dx}{dt} = \frac{x_\infty - x}{\tau_x(V)} \tag{A2}$$

Here, x is again the name of the (in)activation variable (m and h for Ca_N and q for Ca_L). This formalism was used here because it was the preferred format in the original paper describing the Ca_N current model (Booth et al. 1997).

The equations determining the value of the (in)activation variable in the voltage-dependent case are thus expressed either in terms of α_x and β_x (corresponding to opening and closing rates) or in terms of x_∞ and τ_x (corresponding to steady-state value and time constant). These variables, in turn, are dependent on further parameters A, B, and C. When the equation for the (in)activation variable is expressed in terms of α_x and β_x, the following equations are used to determine these

$$y(V) = \frac{A(V - B)}{1 - \exp\left(\frac{B - V}{C}\right)} \tag{A3}$$

Downloaded from jn.physiology.org on May 9, 2007

TABLE A1. *Ion current kinetics*

Current Type	E_{rev}, V	Variable	Equations	*A*	*B*	*C*
Fast sodium current (Na^+)[1]	0.050	α_m	A*1*, A*3*	0.6×10^6 *; 2×10^6 **	−0.043*; −0.053**	0.001
$I_{Na} = g_{Na} \times m(V)^3 \times h(V) \times (V - E_{rev})$		β_m	A*1*, A*4*	0.18×10^6 *; 0.6×10^6**	−0.052*; −0.062**	0.020
		α_h	A*1*, A*4*	75×10^3*; 50×10^3**	−0.046*; −0.054**	0.001
		β_h	A*1*, A*5*	6×10^3*; 4×10^3**	−0.042*; −0.050**	0.002
Fast, transient potassium current (K_t)[2]	−0.085	α_m	A*1*, A*3*	1.8×10^5	0.027	0.014
$I_{Kt} = g_{Kt} \times m(V)^3 \times h(V) \times (V - E_{rev})$		β_m	A*1*, A*4*	0.58×10^4	0.044	0.006
		α_h	A*1*, A*4*	3.33×10^3	0.019	0.006
		β_h	A*1*, A*5*	99	−0.0185	0.0076
Slow, persistent potassium current (K_s)[3]	−0.085	α_n	A*1*, A*3*	1.44×10^3	−0.03	0.002
$I_{Ks} = g_{Ks} \times n(V) \times (V - E_{rev})$		β_n	A*1*, A*4*	1.1×10^3	0.0474	0.002
Fast, sodium-dependent potassium current	−0.085	α_z, β_z	A*11*, A*12*	6,000	0.1	—
(K_{NaF})[4]		Pool	A*9*	5×10^{11}	0.15×10^{-3}	—
$I_{KNaF} = g_{KNaF} \times z([Na]) \times (V - E_{rev})$						
Slow, sodium-dependent potassium current	−0.085	α_z, β_z	A*10*	—	0.1	—
(K_{NaS})[5]		Pool	A*9*	3×10^9	0.05	—
$I_{KNaS} = g_{KNaS} \times z([Na]) \times (V - E_{rev})$						
N-type calcium channel (Ca_N)[6]	0.050	m	A*2*, A*8*	0.004	−0.015	−0.0055
$I_{CaN} = g_{CaN} \times m(V)^2 \times h(V) \times (V - E_{rev})$		h	A*2*, A*8*	0.3	−0.035	0.005
L-type calcium channel (Ca_L)[7]	0.050	q	A*2*, A*8*	0.003	−0.025	−0.005
$I_{CaL} = g_{CaL} \times q(V) \times (V - E_{rev})$						
Low-voltage-activated calcium channel	0.050	α_m	A*1*, A*3*	0.02×10^6	−0.058	0.0045
(Ca_{LVA})[8]		β_m	A*1*, A*4*	0.05×10^6	−0.061	0.0045
$I_{CaLVA} = g_{CaLVA} \times m(V)^3 \times h(V) \times (V - E_{rev})$		α_h	A*1*, A*4*	0.1	−0.063	0.078
		β_h	A*1*, A*5*	0.03×10^3	−0.061	0.0048
N-type calcium-dependent potassium	−0.085	z	A*10*	—	5×10^{-7}	—
channel (K_{CaN})[9]		Pool	A*9*	1.25×10^5	0.030	—
$I_{KCaN} = g_{KCaN} \times z([Ca_N]) \times (V - E_{rev})$						
Bath-NMDA-gated channel (NMDA)[10]	0.0	α_p	A*1*, A*6*	700	0†	0.017
$I_{NMDA} = g_{NMDA}$ ($NMDA_{bath}$) $\times p(V) \times (V - E_{rev})$		β_p	A*1*, A*7*	10.08	0	0.017
Calcium through NMDA channels	0.020	α_p	A*1*, A*6*	700	0.008†	0.017
(Ca_{NMDA})[11]		β_p	A*1*, A*7*	10.08	0.008	0.017
$I_{CaNMDA} = g_{CaNMDA}(NMDA_{bath}) \times p(V) \times (V - E_{rev})$						
NMDA calcium-dependent potassium	−0.085	z	A*10*	—	5×10^{-7}	—
channel (K_{CaNMDA})[12]						
$I_{KCaNMDA} = g_{KCaNMDA} \times z([Ca_{NMDA}]) \times (V - E_{rev})$		Pool	A9	1.25×10^5	2	—

[1]Parameters based on fitting to reproduce spike trains in dissociated cells under various conditions. [2]Parameters based on data from Hess and El Manira (2001). [3]Parameters based on fitting to unpublished voltage-clamp data. [4]Parameters based on data from Hess et al. 2007. [5]Parameters based on fitting to experimental data in Wallén and Grillner (2003). [6]Parameters based on voltage-clamp data in El Manira and Bussières (1997). [7]Parameters based on voltage-clamp data in El Manira and Bussières (1997). [8]Parameters based on Tegnér et al. (1997). [9]Parameters based on fitting to experimental results from Wallén and Grillner (1987, 2003). [10]Parameters from Brodin et al. (1991). [11]Parameters from Brodin et al. (1991). Parameters modified from Brodin et al. 1991. *Refers to soma and dendrites. ** Refers to axon initial segment.

for the opening rates (α) of the activation variables

$$y(V) = \frac{A(B - V)}{1 - \exp\left(\frac{V - B}{C}\right)} \quad \text{(A4)}$$

for the closing rates (β) of the activation variables and opening rates for inactivation variables, and

$$y(V) = \frac{A}{1 + \exp\left(\frac{B - V}{C}\right)} \quad \text{(A5)}$$

for the closing rate of the inactivation variables. In these equations, $y(V)$ stands for either $\alpha_x(V)$ (opening rate) or $\beta_x(V)$ (closing rate).

For the NMDA and Ca_{NMDA} currents, slightly different equations for α_x and β_x were used, following Brodin et al. (1991)

$$\alpha(V) = A \exp\left(\frac{V - B}{C}\right) \quad \text{(A6)}$$

$$\beta(V) = A \exp\left[-\left(\frac{V - B}{C}\right)\right] \quad \text{(A7)}$$

In the Ca_N and Ca_L cases, where the activation and (for Ca_N) inactivation variables were expressed in x_∞ and $\tau(x)$, the following equations determine these values [note that $\tau(x)$ is constant]

$$\tau(x) = A \quad x_\infty = \frac{1}{1 + \exp\left(\frac{V - B}{C}\right)} \quad \text{(A8)}$$

Not all ion channels were voltage dependent. In some cases, the concentration of some ion determined the activation level of the

Downloaded from jn.physiology.org on May 9, 2007

channels. The model includes sodium- and calcium-dependent channels. To model these concentration-dependent channels, we introduced intracellular "pools" with a characteristic influx rate and time constant of removal. The ion concentration $[C_i]$ in the pools increases proportionally to the size of inward currents carried by the ion type in question, and decays according to the time constant of removal

$$\frac{d[C_i]}{dt} = A_i I_i - \frac{[C_i]}{B_i} \quad (A9)$$

where A_i is the pool's influx rate of sodium, I_i is the sodium or calcium current, and B_i is the pool's time constant of decay.

Both in the sodium and the calcium case, we used two different pools ("fast" and "slow"), the concentration in which determined the activation rates of the two sodium-dependent potassium channels (K_{NaF} and K_{NaS}) and the two calcium-dependent potassium channels (K_{CaN} and K_{CaNMDA}), respectively. Each of these pools, naturally, can have different A and B values.

For most of the concentration-dependent currents (K_{NaS}, K_{CaN}, and K_{CaNMDA}), we let the activation variable be an instantaneous function of the ion concentration. For K_{NaF}, however, it was found that a better fit to experimental data could be achieved if the activation variable had fast internal dynamics so that it reached its equilibrium value after a brief delay instead of instantaneously.

Thus for K_{NaS}, K_{CaN}, and K_{CaNMDA}, the activation is determined by an instantaneous function

$$z = \frac{[C_i]}{[C_i] + B_i} \quad (A10)$$

Here, $[C_i]$ is the ion concentration in the relevant pool and B_i is a parameter describing the half-activation concentration of the pool. B_i need not be the same in separate pools containing the same ion type (such as in the fast and slow Ca^{2+} pools).

For K_{NaF}, the activation is instead determined by

$$\frac{dz}{dt} = \alpha_z([Na^+])(1 - z) - \beta_z([Na^+])z \quad (A11)$$

where α_z and β_z are determined through

$$\alpha_z = A\frac{[Na^+]}{[Na^+] + B} \quad \beta_z = A\left(1 - \frac{[Na^+]}{[Na^+] + B}\right) \quad (A12)$$

where A is a delay factor that determines the time constant of the process and B is the half-activation concentration in the fast Na^+ pool. These equations yield a steady-state value $z_\infty = [Na^+]/([Na^+] + B)$ for z (so the steady-state value is the same as the instantaneous value from *Eq.* A9), and this value is approached with a time constant of $1/A$.

Sources of parameter values

The Na^+ current model was adapted from a previous cell model but modified to better replicate results from experiments performed after the publication of that paper (Ekeberg et al. 1991). For the initial segment, the kinetics is slightly different from the somatic kinetics (refer to Table A1 for the values). These differences in kinetics were added to obtain a better fit to the time course of sodium activation observed during action potential clamp on larval lamprey neurons (Hess et al. 2007). The K_t model was based on voltage-clamp data (Hess and El Manira 2001) from larval and young adult neurons. It is notable that in the initial segment, Na^+ and K_t conductances are needed in high densities (62.5 and 120 times soma density, respectively) to satisfy a constraint derived from experiments; in the presence of a calcium blocker, the lamprey locomotor network neuron should be able to spike indefinitely in response to a sustained current pulse up to ≥7 nA (Hess and El Manira 2001). This constraint cannot be satisfied by increasing the somatic Na^+ and K_t conductances because that would violate other constraints derived from action potential clamp studies (see Fig. 2*B*). The K_s model was fitted to voltage-clamp data from larval neurons (Hess and El Manira, unpublished data) in combination with constraints from pharmacological experiments (Hess and El Manira 2001).

Modeling of the K_{NaF} current was based on results from action potential clamp experiments (Hess and El Manira 2002; Hess et al. 2007), whereas the K_{NaS} model was based on experiments that used different protocols to examine this current's influence on the sAHP (Wallén and Grillner 2003). For both the Ca_N and the Ca_L current, we had partial data (from El Manira and Bussières 1997), but not enough data points to do a good fit in terms of selecting an activation gate formalism. In that paper, different Ca^{2+} currents in larval dissociated cells were separated from each other by the use of specific channel blockers. This allowed us to infer some characteristics of Ca_N and Ca_L currents. In the case of Ca_N, we borrowed the m^2h formalism and the equation formats from a study done on turtle neurons (Booth et al. 1997). The m^2h gate formalism was also used to model inactivating HVA currents in Köhr and Mody (1991). This formalism allowed a good fit to those data points that we do have. In the case of Ca_L, we know from El Manira and Bussières 1997 that it is not inactivated (or very slowly inactivated). We therefore selected a formalism with just one activation gate. This allowed a good fit of the equations to those data points presented in that paper.

In contrast to the other ion channels in this paper, the parameters are given in terms of steady-state activation and activation time constant, also the preferred format in Booth et al. (1997). Data from El Manira and Bussières (1997) were also used to estimate the effective calcium reversal potential (+50 mV) used here; this value, which may seem unusually low, was estimated from a current–voltage (*I–V*) curve in the paper. The Ca_L channel does not contribute to calcium influx into the fast calcium pool. We finally checked the qualitative consistency of our HVA Ca^{2+} ion channel models with results presented in Hill et al. (2003), which contains additional data about the *I–V* relationship of the total HVA current in dissociated spinal neurons. The kinetics for the low-voltage–activated calcium channel are taken directly from a previous modeling study (Tegnér et al. 1997) with one modification: the $C_{\alpha h}$ parameter was multiplied by a factor of 10. This was because in the original article, the relevant phenomenon [postinhibitory rebound, a phenomenon found in motoneurons and unidentified spinal neurons, thought to be mediated by Ca_{LVA} channels (Matsushima et al. 1993; Tegnér et al. 1997)] that we sought to reproduce in our model was demonstrated from a holding potential of −54 mV. In our model, the spiking threshold is around −56 mV, so a holding potential of −54 mV cannot be achieved. The adjustment in $C_{\alpha h}$ was necessary to obtain rebound spiking at a more hyperpolarized holding potential (−58 mV). The Ca_{LVA} conductance was set to zero in the soma, as discussed in METHODS, but using a nonzero value for the somatic conductance does not change any results presented here qualitatively, although the model neuron gets slightly more excitable. The NMDA, Ca_{NMDA}, and K_{CaNMDA} channel models were modified from a previous lamprey neuron model (Brodin et al. 1991). For example, the slow pool kinetics was changed to better reproduce experimental results. Some of the current densities were modified from the soma to the dendritic tree. Importantly, the K_{CaN} and K_{NaS} currents are present at tenfold higher densities in the dendritic tree, as described in the text. This was necessary to reconcile the considerable differences in sAHP size between intact and dissociated cells; information on the frequency dependency of sAHP summation (Fig. 4*B*) was also taken into consideration when setting these parameter values. The Ca_{LVA} density, which is zero in the soma because this current is thought to be located exclusively in the dendritic tree (Hu et al. 2002), was set to a value that allows postinhibitory rebound (see above). The K_{NaF} density was increased and the Ca_L density was reduced from the somatic level to obtain more typical-looking ADPs (afterdepolariza-

Downloaded from jn.physiology.org on May 9, 2007

tions). The K_t density was decreased because keeping it at the somatic level tended to destabilize TTX-resistant NMDA oscillations.

ACKNOWLEDGMENTS

We thank Dr. Russell Hill for helpful suggestions on this manuscript.

GRANTS

This project was supported by European Union Grants QLG3-CT-2001-01241 ("Microcircuits") and IST-001917 ("Neurobotics") and Swedish Science Council Grants VR-M 3026, VR-M 5974, VR-M 5706, and VR-NT 3861.

REFERENCES

Birnbaum SG, Varga AW, Yuan L, Anderson AE, Sweatt JD, Schrader LA. Structure and function of Kv4-family transient potassium channels. *Physiol Rev* 84: 803–833, 2004.

Biró Z, Hill RH, Grillner S. 5-HT modulation of identified segmental premotor interneurons in the lamprey spinal cord. *J Neurophysiol* 96: 931–935, 2006.

Booth V, Rinzel J, Kiehn O. Compartmental model of vertebrate motoneurons for Ca^{2+}-dependent spiking and plateau potentials under pharmacological treatment. *J Neurophysiol* 78: 3371–3385, 1997.

Bower JM, Beeman D. *The Book of GENESIS. Exploring Realistic Neural Models with the GEneral NEural SImulation System* (2nd ed.). New York: Springer-Verlag, 1998.

Brodin L, Tråvén HGC, Lansner A, Wallén P, Ekeberg Ö, Grillner S. Computer simulations of *N*-methyl-D-aspartate receptor-induced membrane properties in a neuron model. *J Neurophysiol* 66: 473–483, 1991.

Buchanan JT. Identification of interneurons with contralateral, caudal axons in the lamprey spinal cord: synaptic interactions and morphology. *J Neurophysiol* 47: 961–975, 1982.

Buchanan JT. Neural network simulations of coupled locomotor oscillators in the lamprey spinal cord. *Biol Cybern* 66: 367–374, 1992.

Buchanan JT. Electrophysiological properties of identified classes of lamprey spinal neurons. *J Neurophysiol* 70: 2313–2325, 1993.

Buchanan JT. Contributions of identifiable neurons and neuron classes to lamprey vertebrate neurobiology. *Prog Neurobiol* 63: 441–466, 2001.

Buchanan JT, Grillner S. Newly identified "glutamate interneurons" and their role in locomotion in the lamprey spinal cord. *Science* (*Wash DC*) 236: 312–314, 1987.

Buchanan JT, Grillner S, Cullheim S, Risling M. Identification of excitatory interneurons contributing to generation of locomotion in lamprey: structure, pharmacology, and function. *J Neurophysiol* 62: 59–69, 1989.

Buchholtz F, Golowasch J, Epstein I, Marder E. Mathematical model of an identified stomatogastric ganglion neuron. *J Neurophysiol* 67: 332–339, 1992.

Cangiano L, Wallén P, Grillner S. Role of apamin-sensitive K_{Ca} channels for reticulospinal synaptic transmission to motoneuron and for the afterhyperpolarization. *J Neurophysiol* 88: 289–299, 2002.

Colbert CM, Pan E. Ion channel properties underlying axonal action potential initiation in pyramidal neurons. *Nat Neurosci* 5: 533–538, 2002.

Dale N. Kinetic characterization of the voltage-gated currents possessed by Xenopus embryo spinal neurons. *J Physiol* 489: 473–488, 1995a.

Dale N. Experimentally derived model for the locomotor pattern generator in the Xenopus embryo. *J Physiol* 489: 489–510, 1995b.

Dale N, Kuenzi FM. Ion channels and the control of swimming in the Xenopus embryo. *Prog Neurobiol* 53: 729–756, 1997.

Dryer SE. Na^+ activated K^+ channels: a new family of large-conductance ion channels. *Trends Neurosci* 17: 155–160, 1994.

Ekeberg Ö, Wallén P, Lansner A, Tråvén H, Brodin L, Grillner S. A computer based model for realistic simulations of neural networks. I. The single neuron and synaptic interactions. *Biol Cybern* 65: 81–90, 1991.

El Manira A, Bussières N. Calcium channel subtypes in lamprey sensory and motor neurons. *J Neurophysiol* 78: 1334–1340, 1997.

Franceschetti S, Lavazza T, Curia G, Aracri P, Panzica F, Sancini G, Avanzini G, Magistretti J. Na^+-activated K^+ current contributes to post-excitatory hyperpolarization in neocortical intrinsically bursting neurons. *J Neurophysiol* 89: 2101–2111, 2003.

Grillner S. The motor infrastructure: from ion channels to neuronal networks. *Nat Rev Neurosci* 4: 573–586, 2003.

Grillner S, Buchanan J, Lansner A. Simulations of the segmental burst generating network for locomotion in lamprey. *Neurosci Lett* 89: 31–35, 1988.

Grillner S, Cangiano L, Hu G, Thompson R, Hill R, Wallén P. The intrinsic function of a motor system—from ion channels to networks and behavior. *Brain Res* 886: 224–236, 2000.

Grillner S, Wallén P. The ionic mechanisms underlying N-methyl-D-aspartate receptor-induced, tetrodotoxin-resistant membrane potential oscillations in lamprey neurons active during fictive locomotion. *Neurosci Lett* 60: 289–294, 1985.

Grillner S, Wallén P, Hill R, Cangiano L, El Manira A. Ion channels of importance for the locomotor pattern generation in the lamprey brainstem-spinal cord. *J Physiol* 533: 23–30, 2001.

Hellgren J, Grillner S, Lansner A. Computer simulation of the segmental neural network generating locomotion in lamprey by using populations of network interneurons. *Biol Cybern* 68: 1–13, 1992.

Hellgren Kotaleski J, Grillner S, Lansner A. Neural mechanisms potentially contributing to the intersegmental phase lag in lamprey I: segmental oscillations dependent on reciprocal inhibition. *Biol Cybern* 81: 317–330, 1999a.

Hellgren Kotaleski J, Lansner A, Grillner S. Neural mechanisms potentially contributing to the intersegmental phase lag in lamprey II: hemisegmental oscillations produced by mutually coupled excitatory neurons. *Biol Cybern* 81: 299–315, 1999b.

Hess D, El Manira A. Characterization of a high-voltage-activated I_A current with a role in spike timing and locomotor pattern generation. *Proc Natl Acad Sci USA* 98: 5276–5281, 2001.

Hess D, El Manira A. A fast potassium current activated by sodium entry during the action potential in lamprey spinal neurons. Program No. 546.1. *2002 Abstract Viewer/Itinerary Planner.* Washington, DC: Society for Neuroscience, 2002, Online.

Hess D, Nanou E, El Manira A. Characterization of Na^+-activated K^+ currents in larval lamprey spinal cord neurons. *J Neurophysiol* [Feb 28, 2007; 10.1152/jn.00742.2006].

Hill RH, Svensson E, Dewael Y, Grillner S. 5-HT inhibits N-type but not L-type Ca^{2+} channels via 5-HT1A receptors in lamprey spinal neurons. *Eur J Neurosci* 18: 2919–2924, 2003.

Hille B. *Ion Channels of Excitable Membranes* (3rd ed.). Sunderland, MA: Sinauer, 2001.

Hu G, Biró Z, Hill RH, Grillner S. Intracellular QX-314 causes depression of membrane potential oscillations in lamprey spinal neurons during fictive locomotion. *J Neurophysiol* 87: 2676–2683, 2002.

Köhr G, Mody I. Endogenous intracellular calcium buffering and the activation/inactivation of HVA calcium currents in rat dentate gyrus granule cells. *J Gen Physiol* 98: 941–967, 1991.

Kozlov A, Hellgren Kotaleski J, Aurell E, Grillner S, Lansner A. Modeling of substance P and 5-HT induced synaptic plasticity in the lamprey spinal CPG: consequences for network pattern generation. *J Comp Neurosci* 11: 183–200, 2001.

Kuenzi FM, Dale N. The pharmacology and roles of two K^+ channels in motor pattern generation in the *Xenopus* embryo. *J Neurosci* 18: 1602–1612, 1998.

Lipowsky R, Gillessen T, Alzheimer C. Dendritic Na^+ channels amplify EPSPs in hippocampal CA1 pyramidal cells. *J Neurophysiol* 76: 2181–2191, 1996.

Lüscher HR, Clamann HP. Relation between structure and function in information transfer in spinal monosynaptic reflex. *Physiol Rev* 2: 299–312, 1995.

Matsushima T, Tegnér J, Hill RH, Grillner S. $GABA_B$ receptor activation causes a depression of low- and high-voltage-activated Ca^{2+} currents, postinhibitory rebound, and postspike afterhyperpolarization in lamprey neurons. *J Neurophysiol* 70: 2606–2619, 1993.

McClellan AD, Hagevik A. Descending control of turning locomotor activity in larval lamprey: neurophysiology and computer modeling. *J Neurophysiol* 78: 214–228, 1997.

Nadim F, Olsen ØH, De Schutter E, Calabrese RL. Modeling the leech heartbeat elemental oscillator: I. Interactions of intrinsic and synaptic currents. *J Comp Neurosci* 2: 215–235, 1995.

Olsen ØH, Nadim F, Calabrese RL. Modeling the leech heartbeat elemental oscillator: II. Exploring the parameter space. *J Comp Neurosci* 2: 237–257, 1995.

Parker D. Variable properties in a single class of excitatory spinal synapse. *J Neurosci* 23: 3154–3163, 2003.

Parker D, Bevan S. Modulation of cellular and synaptic variability in the lamprey spinal cord. *J Neurophysiol* 97: 44–56, 2007.

Parker D, Grillner S. The activity-dependent plasticity of segmental and intersegmental synaptic connections in the lamprey spinal cord. *Eur J Neurosci* 12: 2135–2146, 2000.

Downloaded from jn.physiology.org on May 9, 2007

Roberts A, Tunstall MJ. Mutual re-excitation with post-inhibitory rebound: a simulation study on the mechanisms for locomotor rhythm generation in the spinal cord of Xenopus embryos. *Eur J Neurosci* 2: 11–23, 1990.

Roberts A, Tunstall MJ, Wolf E. Properties of networks controlling locomotion and significance of voltage dependency of NMDA channels: simulation study of rhythm generation sustained by positive feedback. *J Neurophysiol* 73: 485–495, 1995.

Rovainen CM. Physiological and anatomical studies on large neurons of central nervous system of sea lamprey (*Petromyzon marinus*). II. Dorsal cells and giant interneurons. *J Neurophysiol* 30: 1024–1042, 1967.

Storm JF. Action potential repolarization and a fast after-hyperpolarization in rat hippocampal pyramidal cells. *J Physiol* 385: 733–759, 1987.

Stuart G, Spruston N, Hausser M. (Editors). *Dendrites.* New York: Oxford Univ. Press, 1999.

Surmeier DJ, Bargas J, Kitai ST. Two types of A-current differing in voltage-dependence are expressed by neurons of the rat neostriatum. *Neurosci Lett* 103: 331–337, 1989.

Svensson E. *Modulatory Effects and Interactions of Substance P, Dopamine and 5-HT in a Neuronal Network* (PhD thesis). Stockholm, Sweden: Karolinska Institutet, 2003.

Tegnér J, Grillner S. Interactive effects of the $GABA_B$ergic modulation of calcium channels and calcium-dependent potassium channels in lamprey. *J Neurophysiol* 81: 1318–1329, 1999.

Tegnér J, Hellgren-Kotaleski J, Lansner A, Grillner S. Low-voltage-activated calcium channels in the lamprey locomotor network: simulation and experiment. *J Neurophysiol* 77: 1795–1812, 1997.

Tegnér J, Lansner A, Grillner S. Modulation of burst frequency by calcium-dependent potassium channels in the lamprey locomotor system: dependence of the activity level. *J Comput Neurosci* 5: 121–140, 1998.

Tråvén HGC, Brodin L, Lansner A, Ekeberg Ö, Wallén P, Grillner S. Computer simulations of NMDA and non-NMDA receptor-mediated synaptic drive: sensory and supraspinal modulation of neurons and small networks. *J Neurophysiol* 70: 695–708, 1993.

Ullström M, Hellgren Kotaleski J, Tegnér J, Aurell E, Grillner S, Lansner A. Activity dependent modulation of adaptation produces a constant burst proportion in a model of the lamprey spinal cord locomotor generator. *Biol Cybern* 79: 1–14, 1998.

Wadden T, Hellgren J, Lansner A, Grillner S. Intersegmental coordination in the lamprey: simulations using a network model without segmental boundaries. *Biol Cybern* 76: 1–9, 1997.

Wallén P, Ekeberg Ö, Lansner A, Brodin L, Tråvén H, Grillner S. A computer-based model for realistic simulations of neural networks. II. The segmental network generating locomotor rhythmicity in the lamprey. *J Neurophysiol* 68: 1939–1950, 1992.

Wallén P, Grillner S. N-Methyl-D-aspartate receptor-induced, inherent oscillatory activity in neurons active during fictive locomotion in the lamprey. *J Neurosci* 7: 2745–2755, 1987.

Wallén P, Grillner S. One component of the slow afterhyperpolarization in lamprey neurons is mediated by a Na^+ activated K^+ current. Program No. 53.2. *2003 Abstract Viewer/Itinerary Planner.* Washington, DC: Society for Neuroscience, 2003, Online.

Wallén P, Grillner S, Feldman JL, Bergelt S. Dorsal and ventral myotome motoneurons and their input during fictive locomotion in lamprey. *J Neurosci* 5: 654–661, 1985.

Wallén P, Robertson B, Bhattacharjee A, Kaczmarek LK, Grillner S. K_{Na} channels of the slack subtype underlie the non-Ca component of the slow AHP in lamprey spinal neurons. Program No. 152.5. *2005 Abstract Viewer/Itinerary Planner.* Washington, DC: Society for Neuroscience, 2005, Online.

Wang X, Liu Y, Sanchez-Vives MV, McCormick DA. Adaptation and temporal decorrelation by single neurons in the primary visual cortex. *J Neurophysiol* 89: 3279–3293, 2003.

Wikström MA, El Manira A. Calcium influx through N- and P/Q-type channels activate apamin-sensitive calcium-dependent potassium channels generating the late afterhyperpolarization in lamprey spinal neurons. *Eur J Neurosci* 10: 1528–1532, 1998.

Williams TL. Phase coupling by synaptic spread in chains of coupled neural oscillators. *Science* 258: 662–665, 1992.

Yuan A, Santi CM, Wei A, Wang Z, Pollak K, Nonet M, Kaczmarek L, Crowder CM, Salkoff L. The sodium-activated potassium channel is encoded by a member of the *Slo* gene family. *Neuron* 37: 765–773, 2003.

Downloaded from jn.physiology.org on May 9, 2007

Paper II

Central and local control principles for vertebrate locomotion

Alexander Kozlov[1,2], Mikael Huss[1,2], Anders Lansner[1], Jeanette Hellgren Kotaleski[1,2] and Sten Grillner[2]

[1]*School of Computer Science and Communication, Royal Institute of Technology, Lindstedtsv. 3, S-100 44 Stockholm, Sweden*

[2]*Nobel Institute for Neurophysiology, Department of Neuroscience, Karolinska Institutet, S-171 77 Stockholm, Sweden*

The central nervous system of vertebrates is organized in a modular fashion, such that individual modules can independently execute sophisticated motor programs. The control of such autonomous modules must, however, be achievable in a flexible way. At the same time the inherent functions of the modules need to adjust appropriately. For instance, in many vertebrates, stable locomotor activity can be generated by autonomous central pattern generators (CPGs) located in the spinal cord without the need for sensory feedback or higher brain centres for shaping details. However, it is not fully understood how the control of locomotion and coordination along the spinal cord is achieved. Here we investigate the spinal locomotor network of the lamprey with the aim of describing a simple and biologically feasible way to flexibly control the locomotor pattern for swimming. Our results highlight the importance of variability in individual neuron response properties. We show, using a biophysically detailed, full-scale computational model of the spinal locomotor CPG network, that the direction and speed of the locomotor pattern could be controlled from only the very rostral part of the spinal cord. At the same time, the propagation delay between the spinal segments can be

adjusted by the local networks. This maintains the structure of the locomotor pattern, and thus the shape of the body, independent on the frequency of swimming. Our full-scale simulations suggest a novel, simple and plausible mechanism for control of motor coordination. We also show that the reciprocal inhibition between the right and left sides of the spinal cord allows for faster and more reliable control of this coordination. This suggests a novel function for the inhibition in addition to its previously well-studied role in supporting alternating left-right motor activity. Our study thus points towards simple and general principles for achieving goal-directed locomotor behaviour in vertebrates and invertebrates. The crucial role of neuronal variability suggests that population properties are important targets of evolution.

The lamprey swims by undulating movements produced by a traveling wave of activity that pushes its body forward through the water. A similar traveling wave can be produced in an *in vitro* spinal cord preparation[1]. The spinal cord consists of about 100 segments, and the spinal locomotor network coordinates motoneuron bursting activity in the right and the left sides of the body through reciprocal inhibition between hemisegments. It has been found that the average delay between the bursts in consecutive spinal segments is about 1% of the activity cycle during forward swimming, and that this relative lag is, to a first approximation, independent of locomotor frequency[2]. Propagation of the wave can also be reversed, such as during backward swimming[3]. Many studies have addressed these questions, both experimentally and using computational models[4, 5, 6, 7, 8, 9, 10]. The existence and stability of the travelling wave in a distributed network has been studied extensively in chains of autonomous oscillators. The role of asymmetric longitudinal synaptic projections in achieving uniform swimming patterns has also been established. However, in all models so far, the apparent frequency-independence of the phase lag was either assumed from

the start or relied on a specific hypothetical control strategy. Initiation and maintainance of backward swimming remains unresolved too. It has long been disputable whether a rostral or caudal activation can elicit it and, particularly, how can it be implemented in reality.

Here, we use a full-scale simulation of the whole lamprey spinal CPG to pinpoint mechanisms underlying a flexible and biologically feasible control of locomotion direction as well as coordination along the spinal cord as an emergent property of the distributed spinal neural network. Each neuron is modelled in a biophysically detailed manner and the synaptic connections are set based on experimental data (see Fig. 1 and Methods). Simulations suggest that locomotion direction (i.e. forward or backward swimming) along the entire spinal cord can be flexibly controlled in a simple manner from the very rostral part of the spinal cord corresponding to only 1/10-th of its length. During these circumstances the spinal CPG network is intrinsically able to adjust the phase lag along the cord at the segmental level. The importance of variability in cellular properties is highlighted as a prerequisite for this local control. A novel role for reciprocal inhibition is also proposed.

As the locomotor wave moves from the head towards the tail during forward swimming in lamprey, successive caudal segments are recruited with a delay (Fig. 2a, left panel). The relative duration of this delay, compared to the period of the locomotor cycle, is called the phase lag. During backward swimming, the wave moves in the opposite direction[3] (Fig. 2a, right panel).

Our simulated network produces alternating locomotor-like output in excitatory (E) and inhibitory (I) interneuron populations on both the left and right sides of the spinal cord (Fig. 2b). In Fig. 2c, intersegmental phase lag is shown as a function of the intensity of current injected to ten rostral segments. To explore the role of reciprocal inhibition, we modeled both the whole spinal cord and a hemi-spinal cord network, the

hemicord, where no inhibition from the contralateral side was allowed. As one can see in Fig. 2c, the dynamic range is much wider in the full cord than in the hemicord, suggesting that the reciprocal inhibition between hemisegments is important for reliable and efficient control of the swimming pattern. Stimulation of only the rostral part of the network yields positive as well as negative phase lag, depending on the sign and strength of the injection, meaning that both forward and backward swimming patterns can be generated (Fig. 2d).

Under the simulated conditions, neurons fired no more than one spike per activity cycle, so the observed pattern was shaped by population bursts due to the spike synchronization and cell recruitment in interneuronal populations[11]. To reflect the variability found among neurons in lamprey spinal networks[12, 13], we built the network using normally distributed values for single-cell properties (compare Fig. 1d). This yielded triangle-like bursting output patterns in simulated motoneurons (Fig. 3a, solid line), similar to many experimentally obtained motoneuron recordings[14, 15, 16]. The model motoneurons integrate output from E populations on the length of the excitatory projections but are hyperpolarized to avoid spikes. The `triangular' shape of their membrane potential with characteristic gradual rise and decay phases is typical for the population bursts in the simulated inhomogeneous network and this feature is observed in a wide frequency range. For comparison, sharper and more distinct bursts, close in their shape to single excitatory post-synaptic potentials (EPSP), were obtained using homogeneous parameter values (Fig. 3a, dotted line). Previous biophysically detailed models had more intensively firing units and displayed square pulse, or relaxation oscillator-like, locomotor bursts[9, 10].

The triangle-wave shape suggests a way for segments to adaptively control the intersegmental phase lag locally (Fig. 3b). Assuming some threshold for the activity level a segment has to reach before it can effectively recruit the next segment, a

triangle-type burst reaches the threshold after a delay which is proportional to the cycle duration. The intersegmental phase lag, as a relative time delay, can therefore be preserved at an approximately constant level when the frequency is varied. An EPSP- or square pulse-like burst, in contrast, crosses the interaction threshold almost immediately upon being induced. This should lead to an approximately constant absolute time delay between the activation of subsequent segments. The intersegmental phase lag will therefore vary proportionally to the oscillation frequency.

Consistent with theoretical predictions, the intersegmental coordination was near perfect between 3 and 15 Hz, with the homogeneous network being closer to a completely uncoordinated set-up (Fig. 3c). This frequency range corresponds to the fast rhythm observed in the experiments on fictive locomotion.

In simulations where a rostral command was applied during stable forward swimming activity, the full simulated network was able to rapidly change, or even reverse, its locomotor pattern in response to the command (Fig. 3d, upper panel). In a simulated hemicord, the pattern can also be reversed, but the process is much slower (Fig. 3d, lower panel) and it is also less stable (not shown). An overall perceived quality of the pattern , e.g. constancy of the intersegmental phase lag along the body, is lower in the hemicord too (Fig. 3d). This confirms the above conclusion that the reciprocal inhibition between hemicords is crucial in the model for achieving reliable control.

In summary, our simulation study has revealed plausible central and local mechanisms for the control of the lamprey swimming locomotor pattern. The rostral part of the CPG network can efficiently determined the direction of movement, while local intrinsic properties allow an adaptive coordination of the intersegmental phase lag. We show that simulating a distribution of neuronal parameters is crucial for achieving a proper coordination without central control. In addition, our study highlights the importance of reciprocal inhibition for facilitating the control of the locomotor pattern.

This is a novel potential function of the reciprocal inhibition in addition to its more recognized role in allowing alternating activity between antagonist muscle groups.

Methods

Neuron populations. Populations of E and I cells are simulated using an 86-compartment model of the spinal interneuron[17]. In total there are 6000 E cells and 4000 I cells in the simulation. Cells are placed randomly within a narrow band, 2mm wide, 0.25mm thick, and 100mm long. Cell populations are activated by application of AMPA to the bath solution modeled as permanent opening of a fraction of the AMPA channels[11] (30% in most simulations and 18-70% in Fig. 3c where the frequency of oscillations is varied). Poisson distributed noise with mean intensity of 200 spikes per second is applied uniformly to all cells through AMPA synapses with 1 nS conductance.

Network model. Synaptic connectivity for the cell populations is shown in Fig. 1e,f. Models for the excitatory (AMPA and NMDA) and inhibitory (Glyc) synapses are based on previously used values[18] with synaptic conductances g_{syn}^{AMPA} =0.5 nS, g_{syn}^{NMDA} =0.25 nS, and g_{syn}^{Glyc} =0.5 nS, and other parameters set according a previous study[19]. Synaptic sites are spread uniformly over the cell surface, with 38 inputs per cell. Synapses are distributed uniformly along the axons. Axons extend a length corresponding to 4 segments rostrally and 8 segments caudally for the E cells, and 5 segments rostrally and 15 segments caudally for the I cells. The total synaptic delay is calculated for each connection according to the distance between the connected interneurons and the mean conduction velocity of 0.7m/s for E cells and 1m/s for I cells.

Parameter variability. We use the normal distribution for the parameter values assigned individually in the simulation, if not mentioned otherwise. The Gaussian function is truncated at 1/4 and 4 times the mean value, with the standard deviation of 0.5 being used. The normal distribution is applied to the cell's compartment area, the

decay time constant and the influx rate of the ionic pools, as well as the axonal conduction velocity.

Simulation environment. Calculations are performed using a specialized library for parallel simulations of biophysically detailed large-scale neural networks, SPLIT[20]. The simulation platform is Lenngren, a 442 CPU Linux super-computer with 3.4 GHz 'Nocona' Xeon processors at the Center for Parallel Computers, Royal Institute of Technology, Stockholm, Sweden**.**

References

1. Grillner, S. The motor infrastructure: from ion channels to neuronal networks. *Nat. Rev. Neurosci*. **4**, 573-586 (2003).

2. Wallén, P. & Williams, T. Fictive locomotion in the lamprey spinal cord in vitro compared with swimming in the intact and spinal animal. *J. Physiol.* **346**, 225–239 (1984).

3. Islam, S. S., Zelenin, P. V., Orlovsky, G. N., Grillner, S. & Deliagina, T. G. Pattern of motor coordination underlying backward swimming in the lamprey. *J. Neurophysiol.* **96**, 451–460 (2006).

4. Matsushima, T. & Grillner, S. Intersegmental co-ordination of undulatory movements – a “trailing oscillator” hypothesis. *Neuroreport* **1**, 97–100 (1990).

5. Matsushima, T. & Grillner, S. Neural mechanisms of intersegmental coordination in lamprey: local excitability changes modify the phase coupling along the spinal cord. *J. Neurophysiol.* **67**, 373–388 (1992).

6. Sigvardt, K. A. & Williams, T. L. Effects of local oscillator frequency on intersegmental coordination in the lamprey locomotor CPG: theory and experiment. *J. Neurophysiol.* **76**, 4094–4102 (1996).

7. Cohen, A. H., Holmes, P. J. & Rand, R. H. The nature of the coupling between segmental oscillators of the lamprey spinal generator for locomotion: a mathematical model. *J. Math. Biol.* **13**, 345-369 (1982).

8. Williams, T. L., Sigvardt, K. A., Kopell, N., Ermentrout, G. B. & Remler, P. M. Forcing of coupled nonlinear oscillators: studies of intersegmental coordination in the lamprey locomotor central pattern generator. *J. Neurophysiol.* **64**, 862-871 (1990).

9. Hellgren Kotaleski, J., Grillner, S. & Lansner, A. Neural mechanisms potentially contributing to the intersegmental phase lag in lamprey. I. Segmental oscillations dependent on reciprocal inhibition. *Biol. Cybern.* **81**, 317-330 (1999).

10. Hellgren Kotaleski, J., Grillner, S. & Lansner, A. Neural mechanisms potentially contributing to the intersegmental phase lag in lamprey. II. Hemisegmental oscillations produced by mutually coupled excitatory neurons. *Biol. Cybern.* **81**, 299-315 (1999).

11. Kozlov, A. K., Lansner, A., Grillner, S. & Hellgren Kotaleski, J. A hemicord locomotor network of excitatory interneurons: a simulation study. *Biol. Cybern.* **96**, 229-243 (2007).

12. Buchanan, J. T. Electrophysiological properties of identified classes of lamprey spinal neurons. *J. Neurophysiol*. **70**, 2313-2325 (1993).

13. Cangiano, L. & Grillner, S. Mechanisms of rhythm generation in a spinal locomotor network deprived of cross connections: the lamprey hemicord. *J. Neurosci.* **25**, 923-935 (2005).

14. Shupliakov, O., Wallén, P. & Grillner, S. Two types of motoneurons supplying dorsal fin muscles in lamprey and their activity during fictive locomotion. *J. Comp. Neurol.* **321**, 112-123 (1992).

15. Wallén, P., Shupliakov, O. & Hill, R. H. Origin of phasic synaptic inhibition in myotomal motoneurons during fictive locomotion in the lamprey. *Exp. Brain Res.* **96**, 194-202 (1993).

16. Buchanan, J. T. & Kasicki, S. Segmental distribution of common synaptic inputs to spinal motoneurons during fictive swimming in the lamprey. *J. Neurophysiol.* **82**, 1156-1163 (1999).

17. Huss, M., Lansner, A., Wallén, P., El Manira, A., Grillner, S. & Hellgren Kotaleski, J. Roles of ionic currents in lamprey CPG neurons: a modeling study. *J. Neurophysiol.* **97**, 2696-2711 (2007).

18. Tråvén, H. G., Brodin, L., Lansner, A., Ekeberg, Ö., Wallén, P. & Grillner, S. Computer simulations of NMDA and non-NMDA receptor-mediated synaptic drive: sensory and supraspinal modulation of neurons and small networks. *J. Neurophysiol.* **70**, 695-709 (1993).

19. Kozlov, A., Hellgren Kotaleski, J., Aurell, E., Grillner, S. & Lansner, A. Modeling of substance P and 5-HT induced synaptic plasticity in the lamprey spinal CPG: consequences for network pattern generation. *J. Comput. Neurosci.* **11**, 183-200 (2001).

20. Hammarlund, P., & Ekeberg, Ö. Large neural network simulations on multiple hardware platforms. *J. Comput. Neurosci.* **5**, 443-459 (1998).

Correspondence and requests for materials should be addressed to S.G. (sten.grillner@neuro.ki.se).

Figure legends

Figure 1. Full-scale simulation of the spinal locomotor network of lamprey. **a**, Multi-compartment model of the spinal interneuron. Diameters are exaggerated by a factor of 4 for visibility. **b**, Population of interneurons. The cell in the center is shown in green. **c**, Distribution of interneurons along the spinal cord. Dendrites and axons are not shown. Longitudinal scale is compressed by a factor of 10. The spinal network consists of two symmetric parts on both sides of the midline (pink plane). A 10-segment long hemicord population is encircled to show the scale. **d**, Mean firing rate as function of the somatic current injection (thick line). The shaded area shows maximum variation of the spike frequency in the simulated population. **e**, **f**, Organization of the synaptic connections in the transverse (**e**) and longitudinal (**f**) sections of the spinal cord. Caudally directed projections dominate. Excitatory neurons (E) project ipsi-laterally, e.g. their axons do not cross the midline, and inhibitory neurons (I) project contra-laterally in the simulation.

Figure 2. Control of the direction of swimming. **a**, Pattern of neuron activity for the forward and backward swimming in specified segments on one side of the spinal cord. **b**, Activity in four simulated populations, the left and right E and I interneurons. Dots correspond to the spikes in single neurons. Neurons are ordered in rostro-caudal direction according to the arrows. **c, d**, Controlling the intersegmental phase lag by the rostral command. Somatic current injection is applied to interneurons in the first 10 segments, with linear decay (**c**, inset). The magnitude of the intersegmental phase lag varies continuously with the current injection for both the hemi-spinal cord and full cord networks (**c**). Only left E population of the full cord network is shown (**d**).

Figure 3. Intersegmental coordination of neural activity. **a**, Intensity of neural activity in a hemisegment, measured as subthreshold depolarization in motorneurons, for homogeneous network and network with distributed parameters. **b**, In the

inhomogeneous network, the time delay *d* between the beginning of the depolarization and the crossing of the synaptic interaction threshold between the segmental populations scales linearly with the cycle duration *T*. **c**, Intersegmental phase lag as function of oscillation frequency. The relation for homogeneous network is close to linear, $y=kx$ (thick dashed line). The parameter variability in the inhomogeneous network changes this dependence to a near constant relation, $y=const$ (thick solid line). Shaded area shows the range of adaptation of the intersegmental delay. **d**, Dynamics of the intersegmental phase lag during transition from the forward to backward swimming pattern in the simulated full cord and hemicord inhomogeneous networks. The command is applied at the time interval shown with the thick solid line above the spike raster plots. Simulations start with random initial conditions.

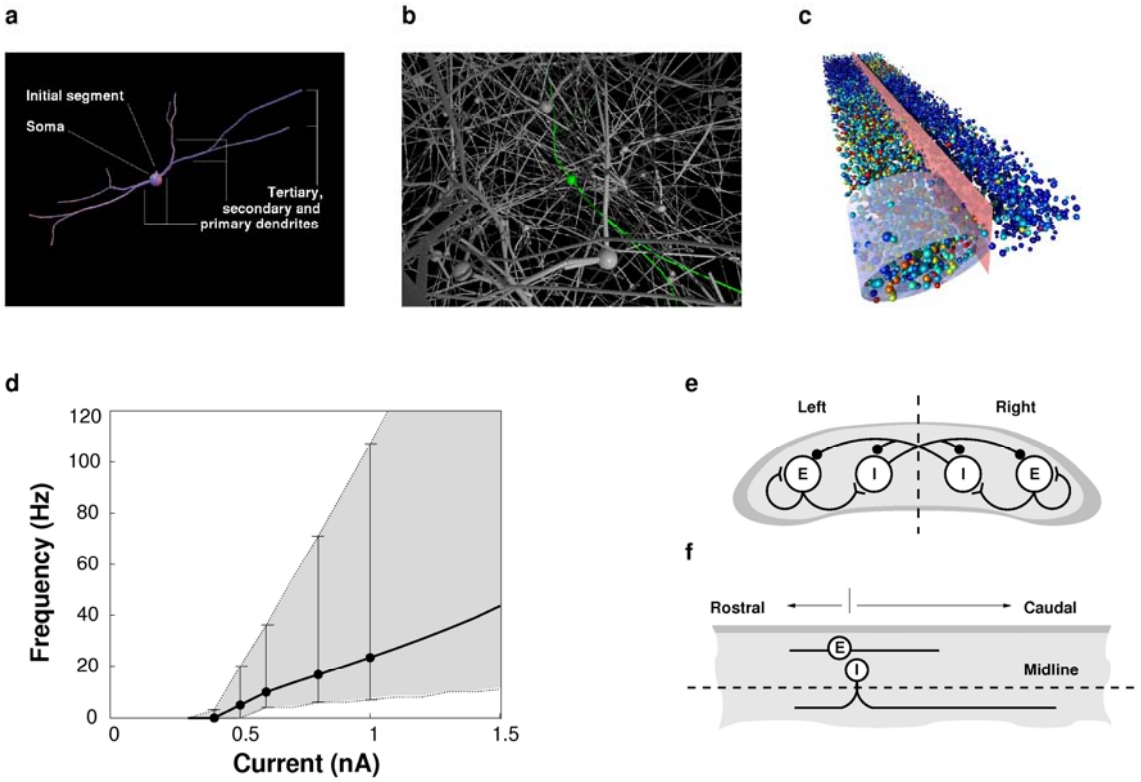
a
Initial segment
Soma
Tertiary, secondary and primary dendrites
b
c
d
Frequency (Hz)
120
100
80
60
40
20
0
0
0.5
1
1.5
Current (nA)
e
Left
Right
E
I
I
E
f
Rostral
Caudal
E
I
Midline

Figure 1.

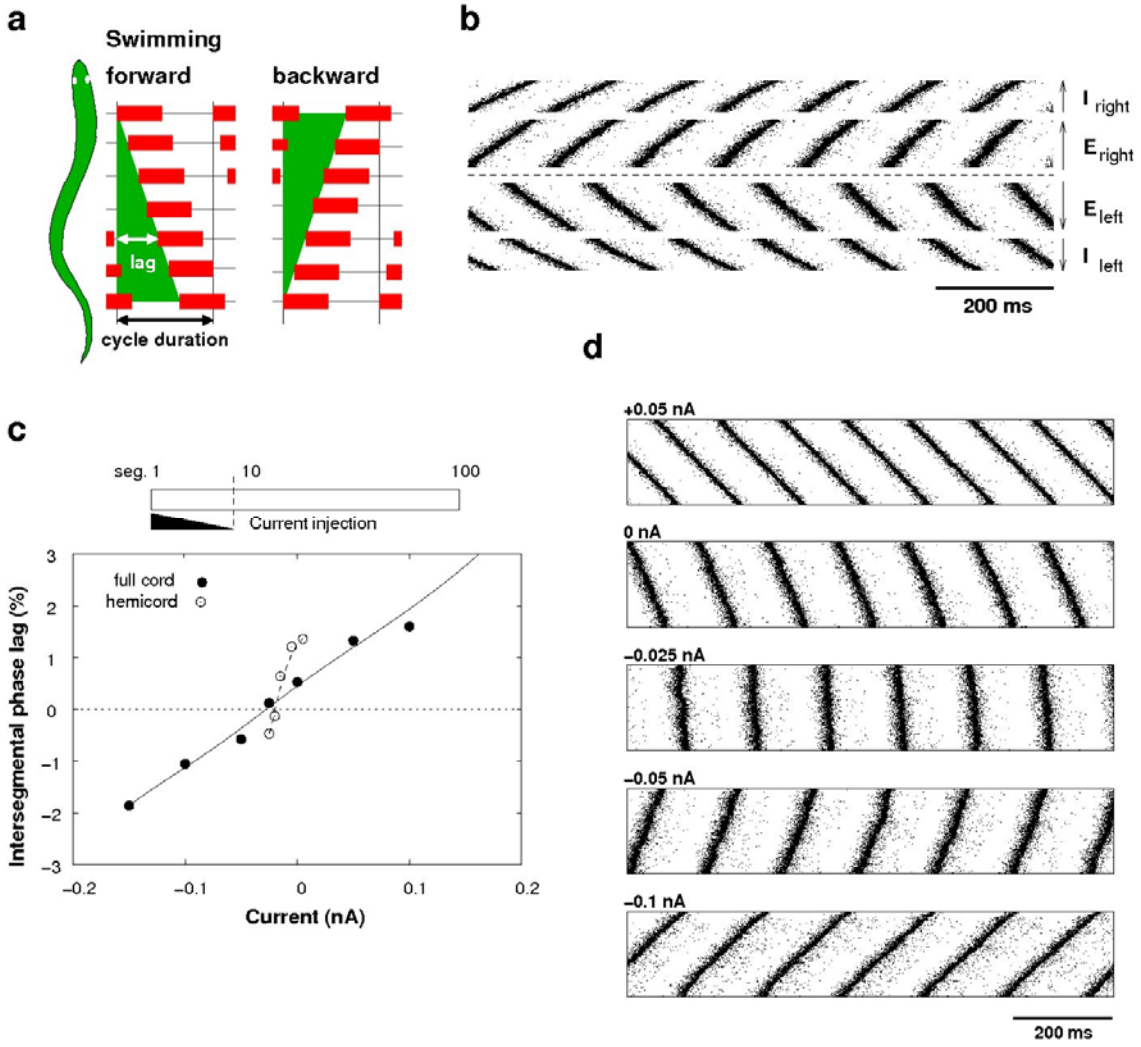
a
Swimming
forward
backward
lag
cycle duration
b
I right
E right
E left
I left
200 ms
c
seg. 1
10
100
Current injection
full cord
hemicord
Intersegmental phase lag (%)
Current (nA)
d
+0.05 nA
0 nA
–0.025 nA
–0.05 nA
–0.1 nA
200 ms

Figure 2.

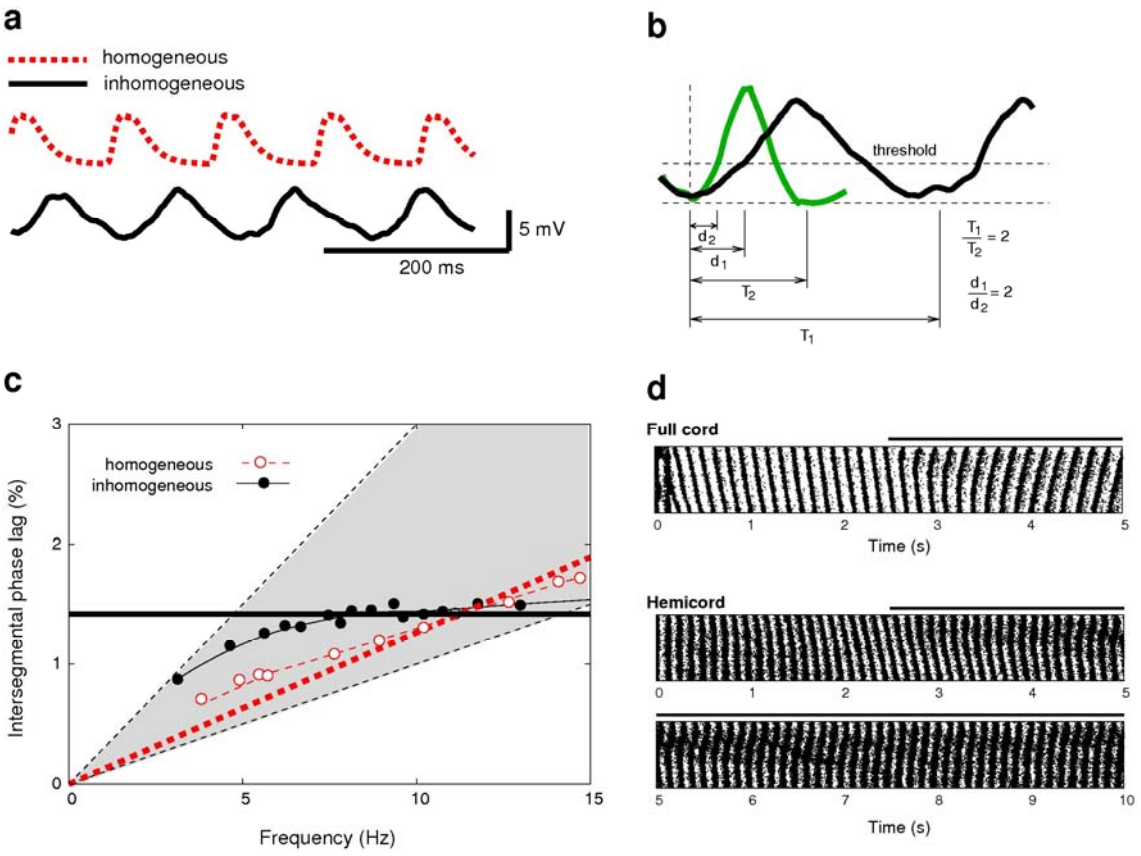
a
homogeneous
inhomogeneous
5 mV
200 ms
b
threshold
d2
d1
T2
T1
T1/T2 = 2
d1/d2 = 2
c
homogeneous
inhomogeneous
Intersegmental phase lag (%)
Frequency (Hz)
d
Full cord
Time (s)
Hemicord
Time (s)

Figure 3.

Paper III

Available online at www.sciencedirect.com
SCIENCE DIRECT
Neurocomputing 69 (2006) 1097–1102
NEUROCOMPUTING
www.elsevier.com/locate/neucom

Modelling self-sustained rhythmic activity in lamprey hemisegmental networks

Mikael Huss[a,*], Lorenzo Cangiano[b,1], Jeanette Hellgren Kotaleski[a,1]

[a]Department of Numerical Analysis and Computing Science, KTH, 100 44 Stockholm, Sweden
[b]Department of Neuroscience, Karolinska Institutet, 171 77 Stockholm, Sweden

Available online 2 February 2006

Abstract

Recent studies of the lamprey spinal cord have shown that hemisegmental preparations can display rhythmic activity in response to a constant input drive. This activity is believed to be generated by a network of recurrently connected excitatory interneurons. A recent study found and characterized self-sustaining rhythmic activity—locomotor bouts—after brief electrical stimulation of hemisegmental preparations. The mechanisms behind the bouts are still unclear. We have developed a computational model of the hemisegmental network. The model addresses the possible involvement of NMDA, AMPA, acetylcholine, and metabotropic glutamate receptors as well as axonal delays in locomotor bouts.
© 2006 Elsevier B.V. All rights reserved.

Keywords: CPG; Self-sustaining activity; Network simulations; Excitatory interneuron

1. Introduction

The neural circuits underlying lamprey swimming have been studied for almost 40 years and are now well understood in many respects. It was long supposed that the left and right spinal cord half-segments (hemisegments) had to be reciprocally connected to yield an alternating rhythm. However, more recent studies on hemicord preparations showed that rhythmic activity is indeed found on the hemisegmental level, even in small preparations of 2.5 hemisegments [3]. Since the hemisegmental bursting persists after blockade of glycinergic transmission [3], it is thought to arise from a purely excitatory network consisting of reciprocally connected excitatory interneurons (EIN), which pass their output activity on to the motoneurons (MN).

Recently, a study was published where these hemisegmental networks were analyzed by electric current injection [4]. It was found that hemicord preparations are able to maintain rhythmic activity for several minutes in response to a brief initial current injection. This suggests that the hemisegmental networks possess a high "re-excitation" capability, which could derive from dense reciprocal connections or strong synaptic conductances. We use results from experimental investigations [2,4] to model, test hypotheses and make predictions about the hemisegmental networks. Here, we are primarily interested in finding out the mechanisms behind the appearance of the sustained rhythm and therefore do not explicitly model its slow termination.

Sustained activity after a brief stimulus has been found in a number of neural systems, particularly working memory. Some mechanisms behind the appearance of sustained activity have been suggested [9], for instance reciprocally coupled networks or brain areas that mutually re-excite each other, bistability in single neurons, or recurrent excitatory connections with slow synaptic (NMDA) conductances that can "carry over" the activity between inter-burst periods. In our case, there was no experimental evidence for single-neuron bistability of the type needed for reverberatory activity, and the small size and homogeneity of the hemisegmental network also ruled out mutually re-exciting areas. The third explanation

*Corresponding author.
E-mail address: hussm@nada.kth.se (M. Huss).
[1]Current affiliation: Dip. di Psichiatria e Neurobiologia, Universita di Pisa, 56126 Pisa, Italy.

0925-2312/$ - see front matter © 2006 Elsevier B.V. All rights reserved.
doi:10.1016/j.neucom.2005.12.053

involving slow NMDA-mediated synaptic conductances seemed reasonable.

In this study, we show that the experimental results from [4] can be reproduced and understood using a computational model. We discuss the involvement of AMPA, NMDA, acetylcholine (ACh), metabotropic glutamate receptors (mGluR), and axonal delays.

Our aim here is to be able to characterize the hemisegmental networks in a detailed way using all available experimental evidence, so that the full segmental network with reciprocal inhibition between the left and right sides can then be simulated with greater confidence. This may also give further insight into the possible advantages of an organization based on self-oscillatory hemisegmental networks.

2. Methods

All simulations were run in GENESIS with a step size of 5 μs. A new model for EIN [5] was used but the model was further simplified, resulting in a model with 6 compartments (one soma, one axon and four dendritic compartments) as compared to 86 in the full model. The physical dimensions of the soma compartments (diameter and length), which were modelled as cylinders, were randomized between 50% and 150% of the experimentally found mean values (27 and 11 μm, respectively). The initial electrical stimulation used in experiments was simulated as a current injection (0.75 nA) delivered uniformly to all neurons. Two neurons were connected with a probability $p = 0.3$. The axonal delays between two neurons were either set to 0 or to a random value between 0 and 20 ms. AMPA, NMDA, ACh, and metabotropic glutamate synapses were used. All synapses were described in terms of rise time constant, decay time constant and conductance, but NMDA synapses were also subject to magnesium block. The rise time and decay constants were, respectively, 5 and 150 ms (NMDA), 3 and 1 ms (AMPA), 10 and 30 ms (ACh), 10 and 10 s (mGluR).

The ratios between the influences of these synaptic components on a single EPSP were varied between simulations. The default conductance settings gave EPSP components as follows: AMPA ~0.8 mV, ACh ~0.5 mV, NMDA ~0.2 mV, mGluR ~0 mV. This gives an EPSP amplitude of 1.5 mV, which is the mean EPSP amplitude in MNs [8]. The simulations were run for 1.5 s, which was deemed sufficient to find out whether bursting would die out or reach steady state.

3. Results and discussion

The first simulations were based on an earlier version [2] of the study in [4], where no specific blockers for NMDA had been applied. The criteria that the model should fulfill to be in accordance with the experiments were the following:

(1) It should display sustained spiking activity throughout the simulation [2]; (2) The spiking should be organized in bursts [2,3]; (3) EPSP sizes should have reasonable values [6–8]; (4) Blocking of AMPA synapses should abolish the spiking activity after the current injection has ended [2]. After the initial model had been built and new experiments performed, an additional criterion was introduced; (5) Self-sustained activity should be achievable even in the absence of NMDA receptors [4].

3.1. Sustained bursting can be obtained with AMPA and NMDA synapses

A simulation that used only NMDA and AMPA synaptic components, and no axonal delays, was able to fulfill the first four criteria we had set up. It shows self-sustaining bursting activity after the electrical stimulation has been removed (Fig. 1), and the activity is highly synchronized.

During the initial period, when stimulation current is applied, the frequency steadily increases. This is due to the combined depolarizing effects of current injection and recurrent synaptic excitation. During this phase, the synaptic NMDA component is summed, so that its conductance will be high at the end of the stimulation period (see Fig. 2 for an example of this from another simulation run). When the stimulation is withdrawn, there is still enough NMDA current to depolarize the cell and carry over the activity to the next action potential. When that action potential is fired, recurrent excitation will (typically) lead to another increase in the NMDA conductance, so that activity is indefinitely maintained. The NMDA conductance will tend to decrease from its highest value at the end of the stimulation period and gradually settle down at a steady-state level where the NMDA peak current for two consecutive spikes is the same. This explains the gradual slowing down of the spiking frequency that is sometimes observed.

AMPA, being a rapidly rising and decaying synaptic component, is inactive during most of the inter-spike interval, but is necessary for complementing the NMDA component and bringing the cells over the firing threshold. AMPA synapses make sure that the firing is synchronized even though the individual cells have different current–frequency response characteristics. If only NMDA synapses and no AMPA synapses are used, the firing will either die out after the current stimulation has been withdrawn, or become so desynchronized that essentially some cell is always firing (not shown).

3.2. A new model with added ACh and mGluR components and axonal delays

New studies [4], performed after the first simulations, showed that the rhythmic activity is still present even after blocking of NMDA receptors. To accommodate the new experimental findings, we constructed a new model that

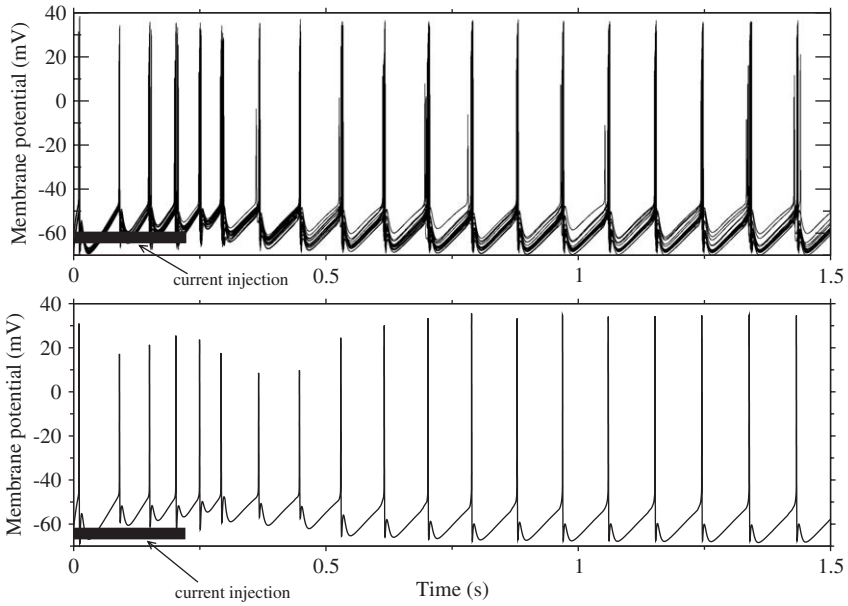

Fig. 1. Voltage traces for 20 randomly selected cells among a total of 200 (top) and an individual cell among these (bottom). The black bars show the period of current stimulation.

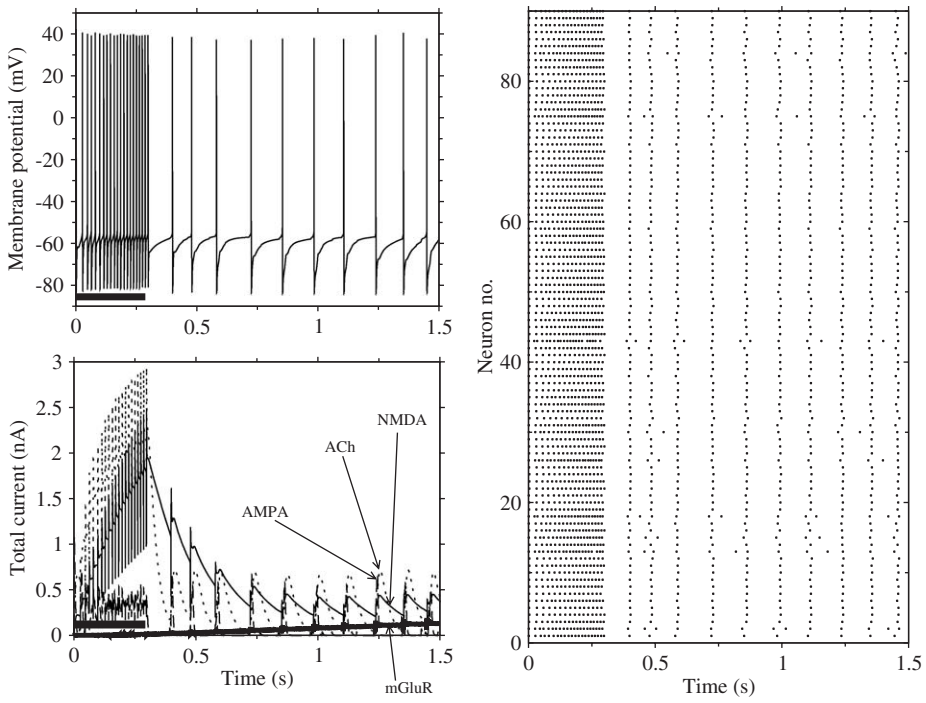

Fig. 2. Sustained oscillatory activity in the new model. Top left, a voltage trace of one of 90 cells used in this simulation. Bottom left, the total current through NMDA, ACh, AMPA and mGluR synapses in the same cell. Black horizontal bars indicate the period during which current was applied. Right, a raster plot showing spike activity in all 90 cells.

incorporated ACh and mGluR synaptic components as well as axonal delays between each pair of cells and fulfilled the five criteria.

We used results from a study on cholinergic synapses in lamprey reticulospinal neurons [7] to estimate the ACh-mediated EPSP in EIN cells. We estimated a rise time constant of 10 ms, a decay time constant of 30 ms and an EPSP proportion of 1/3 for the ACh synaptic contribution.

In lamprey CPG neurons, mGluR1 has been shown to block a hyperpolarizing leak current, which leads to a net depolarization [6]. In the same paper, mGluR1 effects were investigated in dissociated cells, with results suggesting that both the onset of the depolarization and its termination are

on the order of tens of seconds. As a first (and crude) approximation, we modelled the mGluR1 receptor as a synaptic channel with a very low conductance and both rise and decay time constants of 10 s. Simulation results from the new model with ACh and mGluR receptors, in addition to NMDA and AMPA, are shown in Fig. 2. The number of cells needed to obtain self-sustaining activity was about 90. Since typically several hemisegments are needed for locomotor bout expression [4], and each hemisegment has at the very least 20 EIN cells, probably many more [1], this seems anatomically plausible.

We also wanted to see if axonal delays would affect the number of cells needed to generate self-sustaining bursts and/or the degree of synchronization between the spiking cells. We thus added randomized axonal delays to each pair of cells as described in Section 2. This addition slightly lowered the number of cells needed to obtain self-sustaining activity (from 90 to 85), but also increased the mean frequency of the 90-cell network by 30–40% and desynchronized the spiking activity, so that bursts became more "spread out" (Fig. 3). In fact, this less synchronized activity corresponds better to experimental data [4]. The introduction of randomized axonal delays thus enhances model performance, which suggests that the connections can be modelled as randomly coupled over a few hemisegments. Future work could examine alternative, structured connection patterns.

3.3. Sustained bursting can be obtained even if NMDA is blocked

It remains to show that self-sustained activity can appear even without NMDA synapses. With NMDA synapses blocked, the number of cells has to be increased to ~150 in order to regain the self-sustaining activity (Fig. 4). The model predicts that both AMPA, Ach, and mGluR are needed for obtaining bursting if NMDA is blocked. The summation of ACh is not sufficient to bring the cells to the firing threshold after the injected current has been removed. Instead, some cells reach a depolarization level where a fairly small amount of additional mGluR-mediated depolarization is sufficient to nudge the cell above threshold. Due to the slow activation of the mGluR-mediated depolarization, there is often a long delay until the first spike after the current injection has been withdrawn (see Fig. 4). As soon as the mGluR-mediated depolarization brings some of the relatively more sensitive cells to the firing threshold, spiking is propagated through the network by ACh and AMPA synapses. In contrast to the model containing NMDA, the bursting here starts slowly and gradually increases. At $t = 1.5$ s it displays frequencies of around 10 Hz, like in the NMDA case. The summation of the ACh component accounts for the increase in frequency, which seems to settle down at around 10 Hz if the simulation is continued.

In summary, our simulation results suggest that given our single-cell model and a sufficient amount of recurrent excitation (to which the number of cells, connection probability, synaptic strengths and synaptic time constants all contribute), locomotor bouts are easily obtained with a minimum of parameter tuning. As in the experiments, locomotor bouts are obtained in a robust manner as soon as the strength of the initial stimulus crosses a certain threshold. Above this threshold, the resulting bout frequency seems not to depend on initial stimulus strength. The most critical issue is that some synapses must be able to maintain excitatory input between bursts without delivering too much excitation to the system. Thus, the

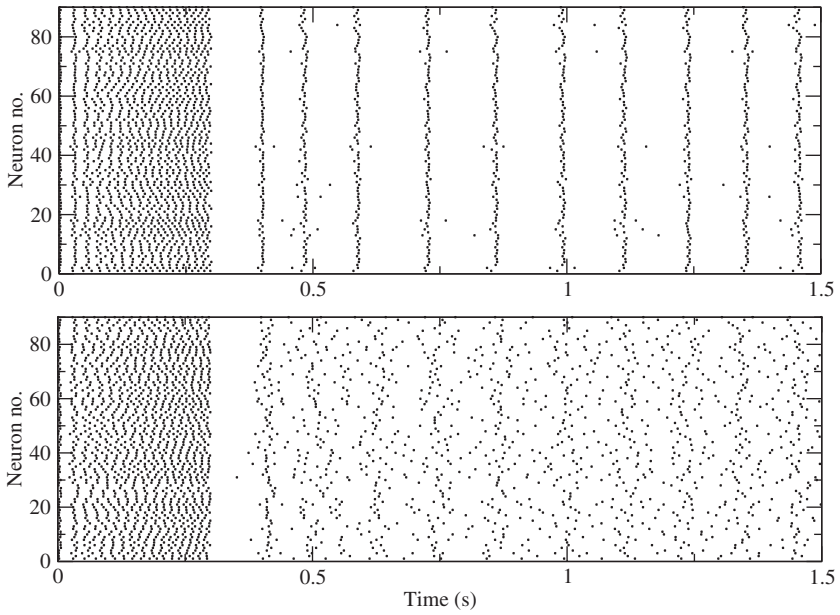

Fig. 3. The effect of introducing random axonal delays in the model. With no axonal delays (top), the neurons are almost perfectly synchronized. With randomized delays (0–20 ms) for each EIN–EIN connection (bottom), firing becomes more desynchronized and the mean firing frequency increases.

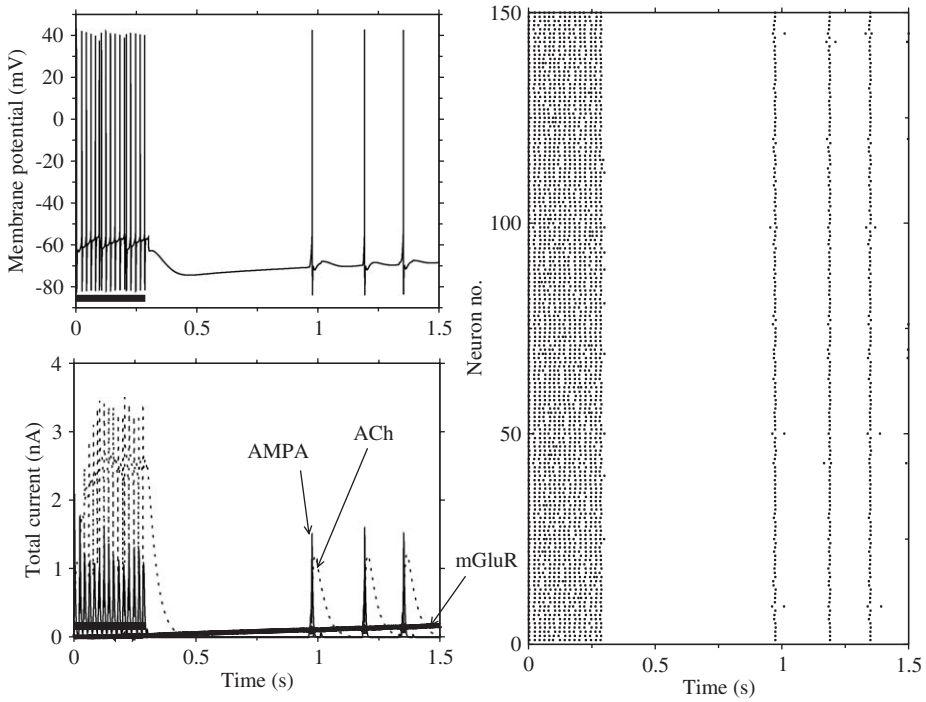

Fig. 4. Sustained oscillatory activity without NMDA synapses. Top left, a voltage trace of one of 150 cells used in this simulation. Bottom left, the total current through ACh, AMPA and mGluR synapses in the same neuron. Black horizontal bars indicate the period during which current was applied. Right, a raster plot showing activity in all 150 cells.

NMDA and mGluR synapses must have conductances and decay time constants that are neither too high nor too low. However, this still gives room for quite a large variation (at least $\pm 20\%$ for the NMDA synapse and more for the mGluR synapse) in these values.

Acknowledgements

This work was supported by the EU grants "Microcircuits" (QLG3-CT-2001-01241) and "Neurobotics" (IST-001917-NEUROBOTICS).

References

[1] J. Buchanan, S. Grillner, S. Cullheim, M. Risling, Identification of excitatory interneurons contributing to generation of locomotion in lamprey: structure, pharmacology, and function, J. Neurophysiol. 62 (1989) 59–69.
[2] L. Cangiano, Mechanisms of rhythm generation in the lamprey locomotor network, Doctoral thesis, Karolinska Institutet, Stockholm, Sweden, 2004.
[3] L. Cangiano, S. Grillner, Fast and slow locomotor burst generation in the hemispinal cord of the lamprey, J. Neurophysiol. 89 (2003) 2931–2942.
[4] L. Cangiano, S. Grillner, Mechanisms of rhythm generation in a spinal locomotor network deprived of crossed connections: the lamprey hemicord, J. Neurosci. 25 (2005) 923–935.
[5] M. Huss, Computational models of lamprey locomotor network neurons, Licentiate thesis, Stockholm, Sweden, 2005.
[6] P. Kettunen, D. Hess, A. El Manira, mGluR1, but not mGluR5, mediates depolarization of spinal cord neurons by blocking a leak current, J. Neurophysiol. 90 (2003) 2341–2348.
[7] D. Le Ray, F. Brocard, C. Bourcier-Lucas, F. Auclair, P. Lafaille, R. Dubuc, Nicotinic activation of reticulospinal cells involved in the control of swimming in lampreys, Eur. J. Neurosci. 17 (2003) 137–148.
[8] D. Parker, Variable properties in a single class of excitatory spinal synapse, J. Neurosci. 23 (2003) 3154–3163.
[9] X. Wang, Synaptic reverberation underlying mnemonic persistent activity, Trends Neurosci. 24 (2001) 455–462.

Mikael Huss (b. 1974) is a Ph.D. student at the Karolinska Institute and the Royal Institute of Technology in Stockholm, Sweden. His thesis research concerns detailed mathematical modelling of neurons and microcircuits in the lamprey spinal cord. The current focus is on understanding how cellular properties affect the characteristics of oscillations generated by small CPG units. In addition to computational neuroscience, Mikael's research interests include machine learning, and he has published papers on network-based algorithms for bioinformatics. Mikael Huss has an M.Sc. degree in biotechnology engineering, a B.A. degree in Chinese and a licentiate degree in computer science.

Lorenzo Cangiano (b. 1970) obtained an M.Sc. degree in Electrical Engineering at the University of Bologna, Italy. He then moved to Sweden for his doctoral studies and earned his Ph.D. at the Karolinska Institute in Stockholm, with an experimental thesis on the neural basis of locomotor rhythm generation in the lamprey spinal cord. Currently, he is a postdoctoral fellow at the University of Pisa, Italy studying the influence of ion channels on the temporal dynamics of night vision in the mouse retina.

Jeanette Hellgren Kotaleski received an M.S. in Medical Sciences from Umeå University in 1989, an M.S. in engineering Physics from Royal Institute of Technology, Sweden, in 1991 and a Ph.D. in computer science in 1998 on work focusing on modeling bursting mechanisms and coordination in motor systems. From 1999 to 2001 she was a postdoc at the Krasnow Institute, VA, USA, modeling biochemical pathways underlying classical conditioning. After returning to Sweden, she is now an associative professor at School of Computer Science and Communication, Royal Institute of Technology. Her main research interests cover modeling of motor systems, including studying the dynamics in intracellular signaling networks involved in learning and synaptic plasticity.

Paper IV

Available online at www.sciencedirect.com
ScienceDirect
Neurocomputing 70 (2007) 1882–1886
NEUROCOMPUTING
www.elsevier.com/locate/neucom

Tonically driven and self-sustaining activity in the lamprey hemicord: When can they co-exist?☆

Mikael Huss*, Martin Rehn

Computational Biology and Neurocomputing, School of Computer Science and Communication, Royal Institute of Technology, 100 44 Stockholm, Sweden

Available online 3 November 2006

Abstract

In lamprey hemisegmental preparations, two types of rhythmic activity are found: slower tonically driven activity which varies according to the external drive, and faster, more stereotypic activity that arises after a transient electrical stimulus. We present a simple conceptual model where a bistable excitable system can exhibit the two states. We then show that a neuronal network model can display the desired characteristics, given that synaptic dynamics—facilitation and saturation—are included. The model behaviour and its dependence on key parameters are illustrated. We discuss the relevance of our model to the lamprey locomotor system.
© 2006 Elsevier B.V. All rights reserved.

Keywords: Lamprey; Dynamical systems; Locomotion; Recurrent excitation

1. Introduction

Activity in central pattern generators is usually thought to be driven by tonic stimulation. However, activity in motor circuits can in some cases sustain itself by positive feedback in the premotor neural circuitry. Evidence for this comes, for example, from the *Xenopus* tadpole, where the isolated spinal cord can generate swimming activity both in response to continuous glutamate agonist application and to a transient touch stimulus [8]. In the latter case, a tadpole whose tail is briefly touched initiates a bout of ''escape swimming''. In the intact spinal cord of the lamprey, another important vertebrate model system for locomotion, fictive swimming is usually only observed in response to tonic stimulation in the form of bath application of glutamate agonists [2]. However, experiments on preparations which have been transected along the midline, so that only half of the spinal cord (the hemicord) is present, have shown both tonically driven activity and self-sustaining unilateral rhythmic activity in response to a transient stimulus. Specifically, D-glutamate application generates a unilateral rhythm with a frequency of 2–10 Hz, while brief electric stimulation can generate fast rhythmic activity (''locomotor bouts'') which initially has a frequency of up to 20 Hz but progressively slows down. The bouts can outlast the initial stimulus by several minutes [2,3]. The D-glutamate induced hemisegmental rhythm has been shown to be related to the lamprey's normal swimming rhythm [2], while the relationship of the locomotor bouts to normal locomotor activity is less clear.

Preparations consisting of just a few hemisegments can display both tonically driven and self-sustaining activity. Since it has been found that blockade of ipsilateral glycinergic inhibition neither abolishes the rhythmic activity in hemisegmental preparations nor changes its frequency [2], the core of the unilateral burst generator is thought to consist of a population of interconnected excitatory interneurons (EINs).

We examine sufficient conditions for the co-existence of tonically driven rhythmic activity and self-sustaining rhythmic activity in the same network by simulations using a simplified neuronal model. The question we want to address is this: if recurrent excitation allows for self-sustaining activity at high firing frequencies, it might be expected that in concert with tonic excitation, it would lead to even higher activity levels, and possible loss of

☆Both authors contributed equally.

*Corresponding author.
E-mail address: hussm@nada.kth.se (M. Huss).

0925-2312/$ - see front matter © 2006 Elsevier B.V. All rights reserved.
doi:10.1016/j.neucom.2006.10.055

rhythmicity. This has not been found to be the case. Rather, tonic activation typically accesses a wide range of activity levels, without triggering stereotypic bouts. How is this possible in a purely excitatory network?

Our approach is based on a conceptual model inspired by dynamical systems theory. We posit that bifurcations occur between cases where the system has either one or three fixpoints, respectively. In the case of one fixpoint, the system will always arrive at a given steady-state frequency regardless of initial conditions. By contrast, in the three-fixpoint case, there will be one stable fixpoint corresponding to low spiking activity, one stable fixpoint corresponding to a fast-spiking state, and an unstable fixpoint in between. Thus, if the system is started from a frequency below that of the unstable fixpoint, the activity will eventually go to zero or to a low frequency, but if it is started from a higher frequency (for instance, by giving a strong enough transient excitatory stimulus), the system will end up in the fast-spiking steady state. When the initial frequency is below the frequency of the unstable fixpoint, the tonic input will determine the steady-state frequency, and this frequency will vary more or less smoothly with the strength of the tonic stimulus. But as soon as the initial frequency is higher than that of the unstable fixpoint, the system will go to a high-frequency steady state which is fairly insensitive to the tonic activation. Can this bistability explain the co-existence of low-frequency tonically driven states and self-sustaining locomotor bouts?

In initial simulations using populations of neurons with static synapses, the networks could not exhibit both self-sustaining bout activity and smoothly varying glutamate-driven activity. With the addition of synaptic dynamics, the two types of firing behaviour could be observed in the same network.

2. Methods

We create a simplified model of an EIN using the formalism introduced by Izhikevich [5]. Our chosen parameter values are $a = 0.01$, $b = 0.2$, $c = -75$, $d = 9$; refer to Izhikevich [5] for explanations of the interpretation of these parameters. The parameter values were chosen to yield cells with realistic current–frequency curves. A more biophysically detailed model, displaying locomotor bouts under various conditions, was presented in Huss et al. [4].

The number of EIN cells in a hemisegment is not known. Buchanan et al. [1] estimated the number to be "at least 20 but possibly much higher", arguing that at least 20 EIN cells are needed to depolarise a motoneuron to the spiking threshold. We choose to use 50 neurons. Each pair of EINs is connected with a probability of 30%. The cells have AMPA- and NMDA-synaptic components. The AMPA synapses, when activated, reach maximum conductance during a single time step (1 ms) with a fast decay, while the conductance of the NMDA synapses reaches a maximum after one time step and decays exponentially according to a parameter τ_{NMDA}, which we vary in the simulations. NMDA synapses are also subject to magnesium block as described in Koch [6] with a simulated magnesium concentration of 1 mM. As a consequence of the magnesium block, the NMDA channel alone cannot sustain locomotor bouts in the absence of external drive; AMPA transmission is also needed, in our model as well as in experiments [3]. Tonic application of D-glutamate is simulated as a constant baseline activation of AMPA and NMDA synapses in equal proportions. Transient electrical stimulation is simulated by delivering a high-frequency synthetic spike train to each neuron in the network. Cell sizes were randomly chosen between 50% and 200% of a reference size, so that the firing response characteristics were different between neurons. A first round of simulations was run with the model as described so far.

Later, two dynamical aspects were added to the synapse model: facilitation and saturation. Facilitating synapses act as high-pass filters, enhancing the transmission of high-frequency spike trains. In our model, facilitating synapses are implemented with two parameters. The first parameter, the "facilitation time", is the time interval within which two spikes must arrive for the synapse to be facilitated. The second parameter, the "facilitation factor", is the enhancement in synaptic transmission that applies to a spike which arrives within the facilitation time following a previous presynaptic spike. Facilitating synapses have been found in lamprey spinal EINs; in one study [7], the synaptic facilitation was found to be stronger the higher the frequency of a presynaptic spike train. Facilitation was most pronounced at higher stimulation frequencies. At 20 Hz, a facilitation factor of 1.6 was observed. Following this, we choose for our model facilitation times corresponding to 20 Hz or higher frequencies, i.e. a facilitation time of 50 ms. Postulating that synaptic facilitation would be further enhanced for higher frequencies than 20 Hz, we choose to study a higher facilitation factor, namely 3.5. In contrast to synaptic facilitation, synaptic saturation low-pass filters synaptic spike trains. One mechanism of synaptic saturation is competition for neurotransmitter binding sites. Our model of synaptic saturation uses a single parameter: the maximum synaptic activation. The synapse model is linear up to the maximum activation, after which the synaptic conductance cannot increase further. In our model, only the NMDA component of a glutamatergic synapse is saturating. Taking into account the functional role of the NMDA channel as an integrator of presynaptic signals, we choose a saturation level corresponding to 140 single synaptic events.

Sample output from the network is shown in Fig. 1. The left subfigure shows rhythmic activity in the tonic, glutamate-driven mode, while the right subfigure shows activity in the bout mode. As can be observed from the spike rasters, the cells in the network show a clear spread in firing frequency, which is due to variations in cell sizes and to the random connectivity of the network (each neuron receives 16.7 ± 3.2 synapses).

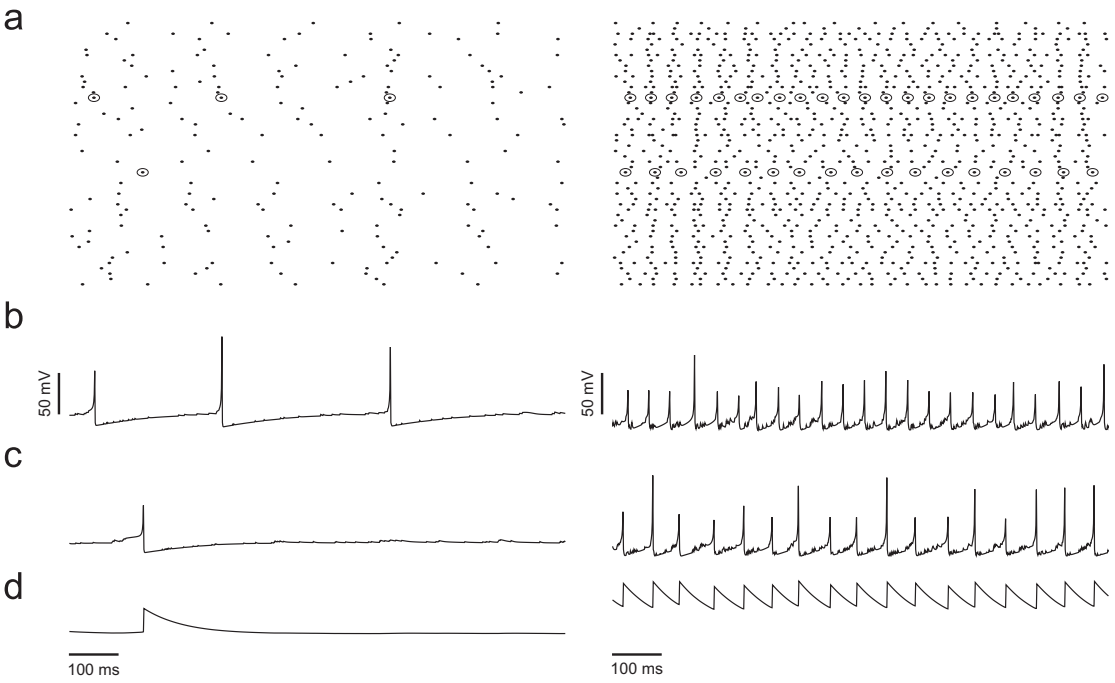

Fig. 1. Sample network output for tonic and bout modes. Both figures consist of the following elements. (a) A raster plot showing spiking activity during one second of simulation time. (b and c) Membrane potential for one of the cells in the net during the same period. (d) The value of the u state variable, describing the membrane recovery in the Izhikevich model, for the cell in (c). Left: tonic mode; bath glutamate stimulation at 0.03 a.u. Network started from rest. Right: no bath stimulation. Network started with an initial electric stimulation corresponding to 30 Hz network activity.

3. Results

Intuitively, it seems unlikely that an excitatory network would display radically different firing modes, like the tonic and bout modes in lamprey hemisegmental preparations. The experimental conditions are precisely the same, except for a glutamate bath chemical stimulation in case of the tonic mode and a transient electrical stimulus in the bout mode. Note that the frequency in the bout mode is much higher, even though the preparation receives no external stimulation after the current stimulus has been removed. Initial simulations using a network model with static synapses did not, for any parameter setting tried, produce a network exhibiting both firing modes. An illustration of a typical result is shown in Fig. 3(left), where τ_{NMDA}, a parameter influencing the overall excitability of the network, was varied. To obtain bifurcation plots showing the system fixpoints, we simulated the network for 10 s, discarded the first four seconds as a transient and varied the initial activity level, the level of tonic stimulation and τ_{NMDA} between simulations. Fig. 3(left) shows a family of bifurcation diagrams. Of the nine plotted diagrams, the four rightmost ones lack unstable points: they have only one steady-state frequency, which varies smoothly with the glutamate level. These correspond to low τ_{NMDA} values, ranging from 30 to 120 ms. Here, the decay of the NMDA current is not slow enough to allow for regenerative, self-sustaining activity. At the opposite end of the spectrum, the diagram for $\tau = 270$ ms shows bout activity for all glutamate levels, as long as the initial activity exceeds about 10 Hz. The $\tau = 240$ ms diagram shows a bistable region for glutamate levels between 0.005 and 0.026. In this range, the activity goes to zero or a very low frequency when started at a low frequency, and to a high-frequency state otherwise. For higher glutamate levels, there is a single fixpoint, and the network will always reach a high frequency. The $\tau = 180-210$ ms cases are similar. $\tau_{\mathrm{NMDA}} = 150$ ms is a borderline case. Here, no unstable fixpoints exist, but there is a narrow region of glutamate concentrations where the steady-state frequency increases rapidly.

Summarising Fig. 3(left), the simulated networks with $\tau < 150$ ms give graded activity in the desired range of 2–10 Hz. Bistability is exhibited when $\tau > 150$; when $\tau > 270$ there are persistent bouts in the absence of glutamate. There is no value of τ where the system exhibits both the desired range of tonic activity and self-sustained bouts.

Next, we introduced synaptic dynamics into the network model. Intuitively, facilitating synapses could be expected to stabilise the self-driven high-frequency bout mode, while leaving a tonic low-frequency mode intact. On the other hand, due to individual variations in the cells' firing rates, the synaptic facilitation mechanism would not be expected to discriminate cleanly between high- and low-frequency firing modes. In our simulation experiments, we nevertheless found a range of facilitation parameters where the bout as well as the tonic firing modes were present. However, with facilitation as the only dynamic mechanism of the model synapses, we found the firing frequencies in the bout mode in excess of what has been observed experimentally. Incorporating also synaptic saturation into

the model, bout frequencies were found to be reduced, while the tonic firing mode was essentially unaffected. Fig. 2 shows the influence of the synaptic dynamics parameters on both tonic and bout steady-state firing frequencies. The left subfigure shows that for short facilitation times, corresponding to requiring high firing rates for facilitation to occur, the bout firing mode cannot be sustained. For long facilitation times, the low-frequency tonically driven mode disappears in the glutamate-driven case. In between, there is a fairly wide range of facilitation times where both modes are present. This range is indicated by a grey rectangle in the figure. Turning to the effects of synaptic saturation (Fig. 2, right), we note that the tonic mode is largely unaffected by changes in this parameter. The bout mode, in contrast, increases its firing frequency along with the synaptic saturation parameter.

Fig. 3(right) shows a state diagram of a network where both tonic and bout firing modes exist. This network has

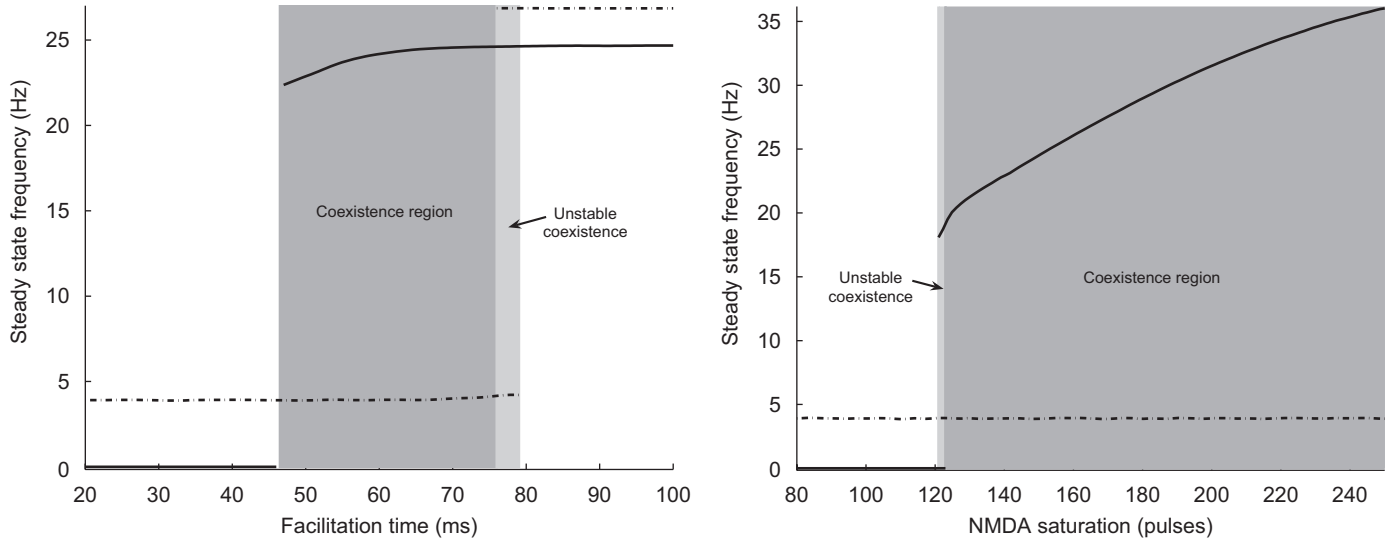

Fig. 2. Effects of varying the synaptic dynamics. Shown in these diagrams is how the steady-state frequencies of our network, in both the tonic and bout modes, vary with the synaptic parameters. Steady-state frequencies for the bout mode with no glutamate added, solid; tonic mode with a fixed glutamate concentration of 0.03 a.u., dash-dotted. Left: changing the facilitation time. Right: changing the saturation parameter for the NMDA receptor. In both subfigures, grey rectangles correspond to x-value ranges where tonic and bout modes co-exist (the lighter shade symbolises ranges where one of the modes was absent for some simulation runs).

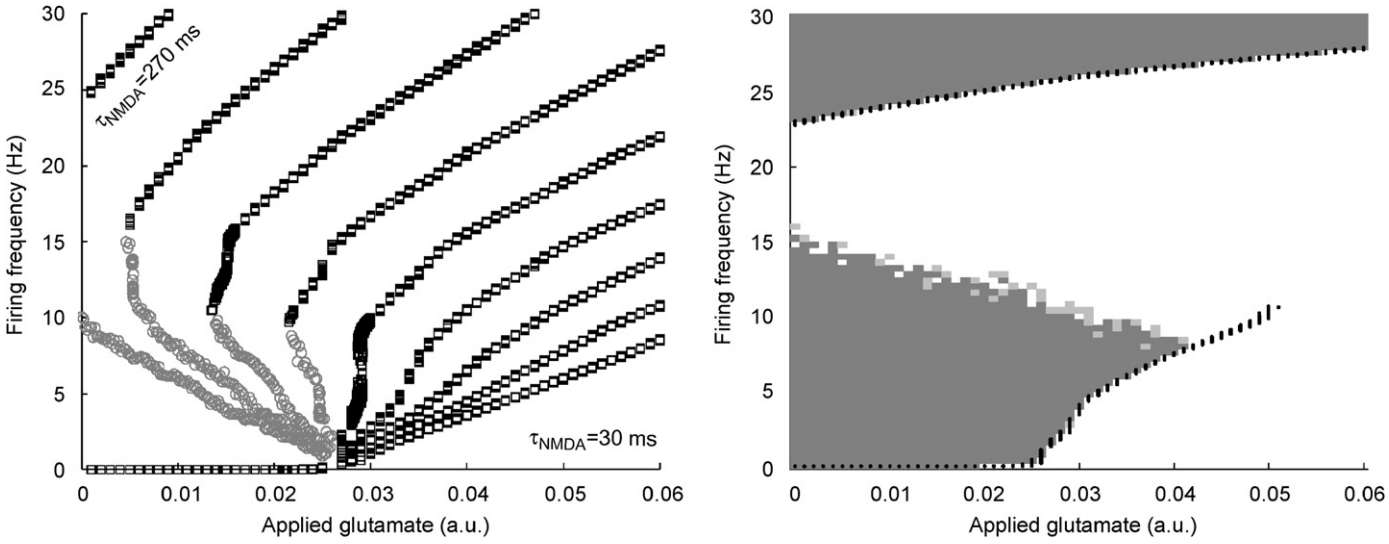

Fig. 3. Network activity states. On the x-axis are bath glutamate concentrations, on the y-axis firing rates of the network. Left: an early network model exhibiting tonic and burst firing modes for different values of a synaptic parameter; the integration time in the NMDA-synaptic components. Squares are stable steady-state firing rates, circles are unstable steady-state firing rates. Right: co-existence of bout and tonic activity in a single network model, incorporating synaptic dynamics. Black points are stable steady-state firing rates. The grey areas correspond to firing rates where the network has a tendency to decrease its firing, white areas to increasing rates.

$\tau_{NMDA} = 180$ ms. The firing frequencies of the tonic mode vary smoothly between approximately 0 and 10 Hz, whereas 2–10 Hz was the range observed in an experimental study [2]. For the bout mode, only the zero-glutamate case has been addressed experimentally [3]. In our simulations we get a frequency of around 22 Hz in this case, while frequencies up to approximately 20 Hz were observed in the experimental study.

4. Conclusions

In this study, we have used a minimal numerical model to study an excitatory network in the lamprey hemicord. Our cell model is the two-state Izhikevich model [5], which is parsimonious in that it can describe a wide variety of neuronal firing behaviour using few parameters. Our synaptic model is slightly more detailed, but still implements synaptic dynamics in a simple fashion with few tunable parameters. With this model, we were able to show that two different firing modes—tonic and self-sustained activity—can co-exist in a simulated excitatory network. Crucially, the addition of frequency-dependent dynamics in the form of synaptic facilitation and saturation was found sufficient to replicate the experimental observations we set out to study.

While we have shown that the bout and tonic modes can co-exist in the same network, an additional explanation for the two distinct behaviours, as experimentally observed, may be a type of activity-dependent feedback or fatigue. According to this explanation, high-frequency bout activity would be attributed to current stimulation having a rapid effect, exciting the network before fatigue has developed. Our model does not at present include a fatigue mechanism; adding one would further increase the robustness of separation between bout and tonic modes.

Little in the model presented here is specific to the lamprey system. In fact, it may be taken as a rather generic model of excitable systems exhibiting sharp transitions between high- and low-activity states, where the low-activity state exhibits a smooth range, while the high-activity state is more stereotypic. In the case of the lamprey, the evolutionary value of such a graded-or-all system may be to allow an all-out high-activity mode, that may be triggered in an escape situation to co-exist with a precisely controllable normal swimming mode.

References

[1] J.T. Buchanan, S. Grillner, S. Cullheim, M. Risling, Identification of excitatory interneurons contributing to generation of locomotion in lamprey: structure, pharmacology, and function, J. Neurophysiol. 62 (1) (1989) 59–69.
[2] L. Cangiano, S. Grillner, Fast and slow locomotor burst generation in the hemispinal cord of the lamprey, J. Neurophysiol. 89 (6) (2003) 2931–2942.
[3] L. Cangiano, S. Grillner, Mechanisms of rhythm generation in a spinal locomotor network deprived of crossed connections: the lamprey hemicord, J. Neurosci. 25 (4) (2005) 923–935.
[4] M. Huss, L. Cangiano, J. Hellgren Kotaleski, Modelling self-sustained rhythmic activity in lamprey hemisegmental networks, Neurocomputing 69 (10–12) (2006) 1097–1102.
[5] E. Izhikevich, Simple model of spiking neurons, IEEE Trans. Neural Networks 14 (6) (2003) 1569–1572.
[6] C. Koch, Biophysics of Computation, Oxford University Press, New York, 1999.
[7] D. Parker, Variable properties in a single class of excitatory spinal synapse, J. Neurosci. 23 (8) (2003) 3154–3163.
[8] A. Roberts, R. Perrins, Positive feedback as a general mechanism for sustaining rhythmic and non-rhythmic activity, J. Physiol. Paris 89 (4–6) (1995) 241–248.

Mikael Huss (b. 1974) is a Ph.D. student at the Karolinska Institute and the Royal Institute of Technology in Stockholm, Sweden. His thesis research concerns detailed mathematical modelling of neurons and microcircuits in the lamprey spinal cord. In addition to computational neuroscience, Mikael's research interests include network-based algorithms for bioinformatics. Mikael Huss has an M.Sc. degree in Biotechnology Engineering, a B.A. degree in Chinese and a licentiate degree in Computer Science.

Martin Rehn received his M.Sc. in Engineering Physics and his licentiate in Computer Science from the Royal Institute of Technology in Stockholm. He is currently pursuing a Ph.D. in Computer Science in the Computational Biology and Neurocomputing Group at that university. His research interests include sensory representation, attractor memories and modelling of cortical circuits.

Paper V

An experimentally constrained computational model of NMDA oscillations in lamprey CPG neurons

Mikael Huss,[1,2] Di Wang,[2] Camilla Trané,[3] Martin Wikström,[2] and Jeanette Hellgren Kotaleski[1,2]

[1]*School of Computer Science and Communication, Royal Institute of Technology, 10044 Stockholm, Sweden*
[2]*Nobel Institute for Neurophysiology, Department of Neuroscience, Karolinska Institutet, 171 77 Stockholm, Sweden*
[3]*School of Electrical Engineering, Royal Institute of Technology, 10044 Stockholm, Sweden*

Rhythmicity is a characteristic of neural networks responsible for locomotion. In many organisms, activation of N-methyl-D-aspartate (NMDA) receptors leads to generation of rhythmic locomotor patterns. In addition, single neurons can display intrinsic, NMDA-dependent membrane potential oscillations when pharmacologically isolated from each other by tetrodotoxin (TTX) application. Such NMDA-TTX oscillations have been characterized, for instance, in lamprey locomotor network neurons. Conceptual and computational models have been put forward to explain the appearance and characteristics of these oscillations. Here, we seek to refine the understanding of NMDA-TTX oscillations by combining new experimental evidence with computational modelling. We find that, in contrast to previous computational predictions, the oscillation frequency tends to increase when the NMDA concentration is increased. We develop a new, minimal computational model which can incorporate this new information. This model is further constrained by another new piece of experimental evidence: that regular-looking NMDA-TTX oscillations can be obtained even after voltage-dependent potassium and high-voltage-activated calcium channels have been pharmacologically blocked. Our model conforms to several experimentally derived criteria that we have set up and is robust to parameter changes, as evaluated through sensitivity analysis. We use the model to re-analyze an old NMDA-TTX oscillation model, and suggest an explanation of why it failed to reproduce the new experimental data that we present here.

Keywords: NMDA, frequency dependence, locomotion

Abbreviations: NMDA - N-methyl-D-aspartate; TTX - tetrodotoxin; TEA - tetraethylammonium; AMPA - alpha-amino-3-hydroxy-5-methyl-4-isoxazolepropionic acid; CPG - central pattern generator; K_{Ca} - calcium-dependent potassium channel; K_V - voltage-dependent potassium channel; Ca_V - voltage-dependent calcium channel

I. INTRODUCTION

NMDA (N-methyl-D-aspartate) induced membrane potential oscillations have been found in many types of neurons in the central nervous system. Notably, such oscillations have been found in spinal cord neurons participating in locomotor pattern generation in many organisms (see for example Grillner and Wallén 1985, Wallén and Grillner 1987, Sillar and Simmers 1994, MacLean *et al.* 1997 and Guertin *et al.* 1998). They have also been observed in many parts of the mammal brain (se Schmidt 1998 for a summary of such findings). Our study examines some aspects of such endogenous NMDA oscillations using neurons in lamprey spinal cord as a model system. These neurons belong to locomotor circuits called *central pattern generators*, where NMDA oscillations are thought to play an important role in generating rhythmic activity. Specifically, applying NMDA or D-glutamate (which activates both AMPA [alpha-amino-3-hydroxy-5-methyl-4-isoxazolepropionic acid] and NMDA type glutamate receptors) in a chemical bath can initiate rhythmic bursting activity in isolated spinal cord and hemicord preparations. We call this type of chemical stimulation *bath application* of e.g. NMDA. It has been shown in several studies (e.g. Grillner and Wallén 1985, Wallén and Grillen 1987) that individual lamprey locomotor neurons can display rhythmic activity – sometimes called *plateau potentials* – in response to co-application of NMDA and TTX (tetrodotoxin), a potent toxin which blocks sodium channels, abolishing action potentials and thus interrupting synaptic communication between neurons. We call these oscillations *NMDA-TTX oscillations*. Taking previously published data (Grillner and Wallén 1985, Wallén and Grillner 1987, El Manira *et al.* 1994, Tegnér *et al.* 1998, Tegnér and Grillner 1999) and our experimental results in this study into account, we find that their amplitude range is about 10-40 mV with frequencies ranging from about 0.06 Hz to 1 Hz.

The presence of NMDA-TTX oscillations shows that there is an intrinsic NMDA-induced rhythmicity at the level of single cells as well as in the locomotor network as a whole. The rhythmicity of the network may reflect the rhythmicity in single cells, or it may arise mainly due to population effects in the network. Whichever factor dominates, it is in any case well-established that the NMDA receptors are important for initiating and shaping the locomotor activity

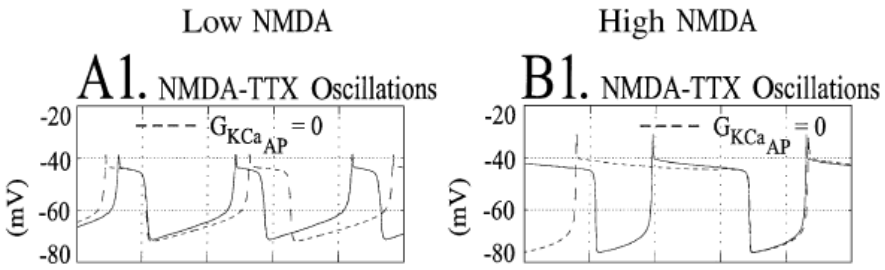

FIG. 1: Plateau lengthening and resulting decrease in frequency when simulated bath NMDA activation is increased in a previous NMDA-TTX oscillation model (reproduced from Tegnér *et al.*, Modulation of Burst Frequency by Calcium-Dependent Potassium Channels in the Lamprey Locomotor System: Dependence of the Activity Level, *J. Comput. Neurosci.* 5: 121-140, 1998, copyright Kluwer Academic Publishers 1998, reproduced with kind permission from Springer Science and Business Media).

(Brodin *et al.* 1985).

A conceptual explanation of the mechanisms behind the appearance of NMDA-TTX oscillations in lamprey has been given in Tegnér *et al.* (1998). This conceptual model is briefly summarized below. First, we note a special characteristic of the NMDA receptor. NMDA receptor channels are subject to a voltage-dependent *magnesium block* (Nowak *et al.* 1984). At hyperpolarized membrane voltages, the block is almost complete, so that little current can pass through the channel; at more depolarized levels, the block is gradually lifted.

1. Following bath NMDA application to a resting lamprey CPG neuron, a (presumably small) subset of NMDA channels that happen to be unblocked by magnesium ions even at the resting potential become activated and depolarize the membrane potential.
2. As the membrane potential is depolarized, the probability of an NMDA channel being Mg^{2+} blocked is decreased, so that even more NMDA receptors can be recruited to depolarize the membrane. In addition, voltage-dependent calcium channels may start to open, resulting in even more inward current and depolarization. This self-amplifying process eventually results in a rapid jump in membrane potential.
3. The rapid depolarization is halted mostly by fast, voltage-dependent, outward potassium (K_V) currents. The balance between the NMDA-induced depolarization and the potassium-channel hyperpolarization results in a depolarized plateau.
4. A portion of the ionic current through NMDA channels is carried by calcium ions, which upon entering the cell can activate outward calcium-dependent potassium (K_{Ca}) channels. These potassium currents are activated with a delay with respect to the NMDA current, since calcium must first accumulate on the inside of the cell membrane. During the plateau, these currents steadily grow in amplitude until they are large enough to terminate the plateau.
5. After a plateau has been terminated, the membrane potential drops down to (approximately) the resting potential. During the inter-plateau phase, the calcium ions that activated K_{Ca} channels are gradually removed from their proximity through diffusion, active transport, buffering, etc. During this process, the K_{Ca} currents decrease until they are small enough to allow the self-amplifying depolarizing process to start again.

Several computational modelling studies have addressed the subject of NMDA oscillations in lamprey spinal cord neurons. Brodin *et al.* (1991) presented the first such model. In further papers (El Manira *et al.* 1994, Tegnér *et al.* 1998, Tegnér and Grillner 1999) this NMDA oscillation model was used to understand more about potential functions of ionic currents such as different types of K_{Ca} channels. While these early models were able to explain the available experimental data and contributed much insight into locomotor circuits, they all had a feature that seemed counterintuitive: in response to an increased NMDA conductance (i.e., a higher concentration of NMDA in the simulated bath), the oscillations became slower. See Fig. 1 for an illustration on this phenomenon in an older model.

The decrease in frequency is connected to the fact that in these models, the depolarized plateau becomes progressively longer the higher the NMDA concentration is. These results are counterintuitive because the opposite effect is observed after induction of fictive swimming in a spinal cord preparation (using NMDA but not TTX): the frequency goes up with increased activation of NMDA receptors (Brodin *et al.* 1985). On the other hand, during fictive swimming, neurons receive phasic synaptic input (Kahn 1982, Russell and Wallén 1983), which makes it difficult to compare NMDA-induced activity during fictive swimming with NMDA-TTX oscillations. The presence of spikes

during fictive swimming is another complicating factor. To find out what kind of concentration-frequency dependence occurs in real lamprey CPG neurons in TTX, we performed experiments where the NMDA concentration was varied and the subsequent effect on TTX oscillation frequency was observed. We found that the frequency dependence is the same as in fictive locomotion (i.e. a higher NMDA concentration gives a higher oscillation frequency) and that the plateau duration is only slightly affected by NMDA concentration. This prompted us to construct a new, simplified computational model of these oscillations. We used additional results from new experiments to further constrain the model; specifically, it was found that NMDA-TTX oscillations could be obtained when high-voltage activated calcium channels and voltage-sensitive potassium channels were blocked. We first built a "biologically minimal" model containing only NMDA and K_{Ca} channels, in addition to a leak current, to make sure that NMDA-TTX oscillations could be simulated with only these components. After we had ascertained this, we proceeded to add simple models of K_V and voltage-dependent calcium (Ca_V) channels, yielding a "full" model which could reproduce additional experimental results and where the concentration-frequency relationship could be addressed.

II. METHODS

A. Experimental protocols

In the experimental parts of the study, we used a protocol described in Wallén and Grillner (1987). In the experiments with potassium and calcium channel blockers, the following drugs were used in addition: nimodipine (1,4-dihydro-2,6-dimethyl-4-(3-nitrophenyl)-3,5-pyridinedicarboxylic acid 2-methoxyethyl 1-methyl ester, (Research biochemicals Inc. (RBI); stock sol: 10 mM in 70% ethanol), ω-conotoxin GVIA (Peptides International; stock sol: 100 μM in H_2O), and tetraethylammonium chloride (TEA, Sigma Inc.).To ascertain that no effects observed with nimodipine were due to the solvent ethanol that is known to modulate NMDA receptors, the effects of ethanol alone were tested at concentrations equivalent to those used in experiments during NMDA-induced TTX resistant membrane potential oscillations. No significant effects on the oscillations were observed.

B. Computational model construction

1. Conceptual approach

As mentioned above, our aim has been to develop a "biologically minimal" model of NMDA-TTX oscillations. Thus, we approximate the neuron as a point neuron (with no axon or dendrites), and neglect ion channels that are not known to be involved in NMDA oscillations. The model was developed in two steps. First, we constructed a model designed to correspond to the minimal set of components necessary to generate NMDA-TTX oscillations. As described elsewhere in this article, we performed experiments with channel blockers to try to isolate these components. After the initial model was built, we added components that were not strictly necessary for generating oscillations, but which experiments have shown are nevertheless involved in shaping NMDA-TTX oscillations in vitro. Using these additional components, it was possible to reproduce even more experimental results.

The initial "minimal" model essentially consisted of four components: an NMDA current, a calcium-dependent potassium current (K_{Ca}), a leak current, and a calcium pool. The minimal model thus obtained was used to simulate NMDA-TTX oscillations in cases where voltage-dependent potassium (K_V) and calcium (Ca_V) channels have been pharmacologically blocked. After this minimal model had been analyzed, we added a generic K_V channel and a generic Ca_V channel. The model thus obtained is used to simulate NMDA-TTX oscillations when K_V and Ca_V channels are unblocked.

The model is conductance-based, but simpler than e.g. many variants of the Hodgkin-Huxley model, because we make several simplifying assumptions regarding the model components. Since the NMDA-TTX oscillations occur on a time scale which is slow compared to the kinetics of most voltage-dependent channels, we make steady-state approximations of the activation of some currents and processes. This also allows us to restrict the number of state variables to two (one for the membrane voltage and one for the effective calcium concentration accessible to K_{Ca} channels in the membrane), so that the state of the system can be completely analyzed in the phase plane. Specifically, we assume that the K_V and the Ca_V channel activations instantaneously reach steady state in response to a change in voltage; the same is true for the magnesium block of the NMDA channel. We also assume that K_{Ca} channels are instantaneously activated by the concentration in the calcium pool. We have tried various versions of the functional shape of the K_{Ca} activation by calcium; in the default setting of the model, this is just a linear function, but similar results can be obtained using a Hill function (not shown in this paper). Finally, the calcium pool is modelled in a simple but standard way, with an influx coming from the NMDA channel (and in the full model, from the Ca_V

channels) and an exponential decay governed by a time constant. Thus, calcium diffusion or transport is not explicitly modelled. All models were implemented and simulated in the XPPAUT package (Ermentrout 2002).

2. Equations and parameters

The model equations were defined as follows:

$$dV/dt = I_{nmda} + I_{kca} + I_{leak} + I_{kv} + I_{cav} \tag{1}$$

where only the first three terms were used in the minimal model. V stands for the voltage state variable and I stands for current, so that I_{nmda} is the current through NMDA channels and so on, and:

$$dC/dt = (i_{nmda} \cdot I_{nmda} + i_{cav} \cdot I_{cav}) - C/\tau \tag{2}$$

where the Ca_V terms were not used in the minimal model. C stands for the calcium concentration state variable. τ is the decay time constant for the calcium pool. i_{nmda} and i_{cav} are influx coefficients for calcium ions through NMDA and Ca_V channels, respectively.

The equations for the different currents are as follows:

$$I_{nmda} = g_{nmda} \cdot mgblock(V) \cdot (E_{nmda} - V) \tag{3}$$

$$I_{kca} = g_{kca} \cdot act_{kca}(C) \cdot (E_k - V) \tag{4}$$

$$I_{kv} = g_{kv} \cdot act_{kv}(V) \cdot (E_k - V) \tag{5}$$

$$I_{cav} = g_{cav} \cdot act_{cav}(V) \cdot (E_{ca} - V) \tag{6}$$

$$I_{leak} = g_{leak} \cdot (E_{leak} - V) \tag{7}$$

Here, g_x stands for the maximum conductance of ion channel x. In particular, the g_{nmda} parameter is the model's equavalent of the bath NMDA concentration in experiments. E_x stands for the equilibrium potential of x ions. Within the above equations, some further functions are introduced. The *mgblock* function models the (steady-state) blockade of the NMDA receptor by magnesium ions. The steady-state magnesium block can be experimentally characterized by a steady-state current-voltage relationship for the NMDA receptor in physiological solution during voltage-clamp conditions. However, since no such data were available for lamprey spinal neurons, we used a simple form for the *mgblock* function, so that its shape could be easily controlled:

$$mgblock(V) = \frac{1}{(1 + e^{\frac{(V - v^m_{half})}{s^m_{half}}})} \tag{8}$$

The rest of the functions relate to the voltage- or concentration-dependent activation of ion channels.

$$act_{kca} = tc \cdot C \tag{9}$$

Here *tc* stands for "transfer coefficient", and just describes how the effective calcium concentration is "translated" into activation of K_{Ca} channels through a linear relationship. We also experimented with using Hill functions with a Hill coefficient of 4, but the results were not improved compared to the simple model used here (not shown).

$$act_{kv}(V) = \frac{1}{(1 + e^{\frac{(V - v^k_{half})}{s^k_{half}}})} \tag{10}$$

$$act_{cav}(V) = \frac{1}{(1 + e^{\frac{(V - v^c_{half}{}^a)}{s^c_{half}{}^a}})} \tag{11}$$

We used g_{nmda} (i.e. the simulated bath NMDA concentration) as the primary parameter of variation. Default parameter values are given in Table 1. Some parameters where changed to illustrate effects of channel blockers or to show how the oscillation shape can be modified; these alternative values are also given in the table, together with a pointer to the relevant figure.

TABLE I: Parameters of the NMDA-TTX oscillation model. mV: millivolts, a.u.: arbitrary units, c.u.: conductance units

Parameter name	Default parameter value	Alternative value(s)
E_{nmda}	0 mV	
E_k	-80 mV	-80 mV to -70 mV [Fig 4d]
E_{ca}	150 mV	
E_{leak}	-70 mV	-70 mV to -60 mV [Fig 4d]
i_{nmda}	0.2 a.u.	
i_{cav}	0.3 a.u.	
τ_{ca}	1 s	
g_{nmda}	0.005 c.u.	0.0025 to 0.01 c.u. [Figs 4a,b]
g_{kca}	20 c.u.	6 to 20 c.u. [Figs 4a,c]
g_{kv}	8 c.u.	0 [Figs 4a,c]
g_{cav}	0.0005 c.u.	0 [Fig 4a]
g_{leak}	0.001 c.u.	
v^m_{half}	-60 mV	
v^k_{half}	-1 mV	
v^{ca}_{half}	-45 mV	
s_m	-(1/0.3) mV	
s_k	-7 mV	
s_{ca}	-5 mV	
tc	0.02 a.u.	

3. Requirements on the model

Based on experimental findings in this study and previous ones, we set up the following criteria that a good model of NMDA-TTX oscillations should fulfill. All of these criteria are defined for a g_{nmda} range $[g^{min}_{nmda}\ 2 \cdot g^{min}_{nmda}]$ where g^{min}_{nmda} is the (approximate) minimum g_{nmda} value that yields oscillations. We chose this interval because the experiment were done from 100 to 200 μM bath NMDA concentrations, and oscillations were not observed for concentrations below 100 μM; so the experiments can roughly be said to characterize a range of approximately $[g^{min}_{nmda}\ 2 \cdot g^{min}_{nmda}]$.

- The model should be able to generate oscillations in the given interval. [1]
- The frequency dependence must be correct: a higher NMDA concentration leads to a higher frequency.[1]

---

[1] Derived from the experimental part of the present study.

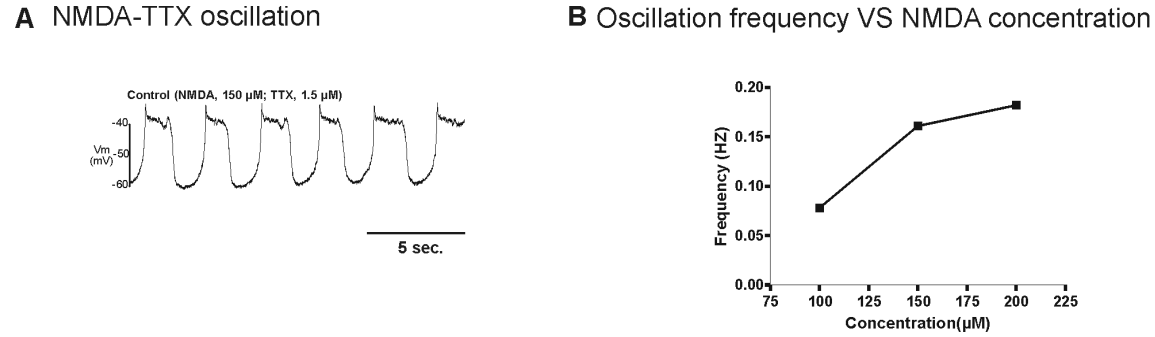

FIG. 2: (a) A representative NMDA-TTX oscillation recorded from a lamprey CPG neuron. (b) The relationship between bath-applied NMDA concentration and oscillation frequency.

- The amplitude of oscillations should be within the physiologically observed range (about 10 to 40 mV). [2]
- The frequency of oscillations should be within the physiologically observed range (about 0.06 to 1 Hz. [2]
- The dependence of plateau length on NMDA concentration should be slight, as observed in our experiments. [1]
- Depolarizing the cell (increasing the resting potential) should yield faster oscillations with a smaller amplitude. [3]
- Blocking K_V should lead to large-amplitude oscillations. [4]
- Blocking K_V and Ca_V should lead to regular-looking NMDA-TTX oscillations. [1]

III. RESULTS

A. The frequency of NMDA-TTX oscillations increases when the bath NMDA concentration is increased

Recordings of NMDA oscillations in TTX were performed for lamprey spinal cord neurons. Before NMDA application, the neurons were held at a resting potential which was sometimes biased by a positive or negative injection current in order to obtained oscillations. NMDA was applied in steps of 50 μM; the lowest dose was 100 μM and the highest was usually 200 μM but 250 μM in some neurons. The detailed results of the experiments will be published separately. There was a consistent positive slope of the dose-response curve; in other words, applying a higher dose of NMDA to the bath gave faster oscillations. However, the dose-frequency relationship sometimes tended to saturate so that, for example the difference between the frequency in 200 μM NMDA and in 150 μM was markedly smaller than the difference between 150 μM and 100 μM (not shown). Also apparent from these recordings was that the length of the plateau did not increase significantly when the NMDA dose was increased; rather, what changes is the length of the interplateau interval, which becomes shorter at higher NMDA doses (not shown). Fig. 2a shows a representative NMDA-TTX oscillation voltage trace for one of the examined neurons. A representative concentration-frequency curves is shown in 2b. Thus, the overall result from this experiment was that, within the concentration range examined, increased bath NMDA concentration leads to a faster NMDA-TTX oscillation, and that – in contrast to simulations – the plateau length is not appreciably lengthened when NMDA concentration is increased.

B. A simplified computational model can reproduce characteristics of NMDA-TTX oscillations

We developed several generations of models described by the kind of equations given in Methods, trying to establish the sufficient requirements for obtaining the observed frequency dependence on NMDA concentration. These initial exploratory efforts suggested that the shape of the *mgblock* function seemed to be important, but due to the many

---

[2] See Grillner and Wallén 1985, Wallén and Grillner 1987, El Manira *et al.* 1994, Tegnér *et al.* 1998, Tegnér and Grillner 1999, and the present study.
[3] Wallén and Grillner 1987
[4] Grillner and Wallén 1985

adjustable parameters in this already simplified model, we sought further constraints on the dynamics of the system apart from those already known from published experiments.

1. *"Normal" NMDA-TTX oscillations are generated in the absence of K_v and Ca_vchannels*

According to the conceptual explanation of NMDA-TTX oscillations outlined in the Introduction, at least NMDA, K_{Ca} and K_V channels, and possibly Ca_V channels, are thought to be involved in generating them. However, oscillations (albeit with a different shape) *can* be generated when K_V channels are blocked by tetraethylammonium (TEA)(Grillner and Wallén 1985), but in this case a high-voltage-activated (HVA) Ca_V dependent mechanism is thought to be responsible for the repolarization phase. We performed channel blocking experiments to find out what would happen if *both* K_V and HVA Ca_V channels were blocked. It was found that, when K_V was blocked by TEA and HVA Ca^{2+} channels were blocked by ω-conotoxin GVIA (specific for N-type channels), and nimodipine (specific for L-type channles), a regular type of NMDA-TTX oscillation (i.e., one with a smaller amplitude and longer plateau than when just K_V is blocked) was recovered. Fig. 3 shows a representative trace; altogether, the experiment was repeated for three neurons. Based on these results, it could be hypothesized that only NMDA channels and K_{Ca} channels may be sufficient to generate NMDA-TTX oscillations, although other calcium channels (e.g. low-voltage activated (LVA)Ca^{2+} channels and P/Q type channels) cannot be ruled out in principle. However, P/Q blockage using ω-agatoxin IVA was tried in a separate experiment (not shown; full manuscript in preparation) and found not to have a significant effect on NMDA-TTX oscillation properties.

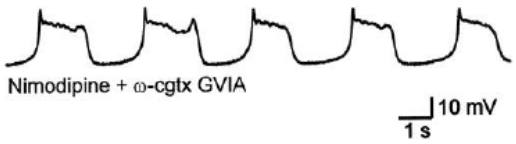

FIG. 3: Normal-looking NMDA-TTX oscillations produced by lamprey CPG neurons during blockage of K_V channels and the two most dominant types of high-voltage activated Ca^{2+} channels.

2. *A biologically minimal model can produce NMDA-TTX oscillations*

Based on the hypothesis that only NMDA and K_{Ca} channels could be sufficient for producing NMDA-TTX oscillations, we developed a minimal model containing only these two types of channel as well as leak channels. A model with parameters as in Table 1 (for those parameters that are applicable) was able to produce simulated NMDA-TTX oscillations with amplitudes and frequencies similar to the experimental trace in Fig. 3. Sample simulation output results is shown in Fig. 4a (upper part). The lower part of Fig. 4a shows the effects of changing the g_{kca} parameter: the plateau length can be varied using this parameter.

After having obtained this minimal model, we freezed its parameters and proceeded to add two voltage-dependent components, K_V and Ca_V. We also assumed that the Ca_V channel could contribute to the effective calcium concentration that is sensed by the K_{Ca} channel. Larval lamprey CPG neurons have at least two types of voltage-activated potassium channels, a slower delayed-rectifier type channel (K_S) and a transient, high-voltage-activated A-type channel (K_t). These have been fairly well characterized at more depolarized membrane potentials, e.g. their time courses during an action potential (Hess *et al.* 2007), but data on the relatively hyperpolarized levels involved in TTX-NMDA oscillations is scarce and noisy. As a rough approximation of the voltage-dependent activation of a lumped K_S/K_t conductance on the relevant membrane potential levels, we used Equation (10) from Methods with the parameters given in Table 1. As for HVA Ca^{2+} channels, larval CPG neurons in lamprey have been shown to have N-, L- and P/Q-type channels (El Manira and Bussières 1997). However these are, according to the cited paper, hardly activated below a membrane potential of -40 mV; in particular the dominating component, the N-type current, only starts to activate at -25 mV. Since there is nevertheless a clear effect of blocking Ca_V channels in addition to K_V channels according to our experiments, we hypothesized that a Ca_V current may still be activated, albeit to a very low degree, at more hyperpolarized potentials. Using an observation by El Manira and Bussières (1997) that some neurons showed a current that started to activate between -60 mV and -50 mV, we postulated a Ca_V conductance with a half-activation potential of -45 mV and a very low conductance density. The effects of setting the K_V and Ca_V parameters in different ways were later assessed through sensitivity analysis (see below).

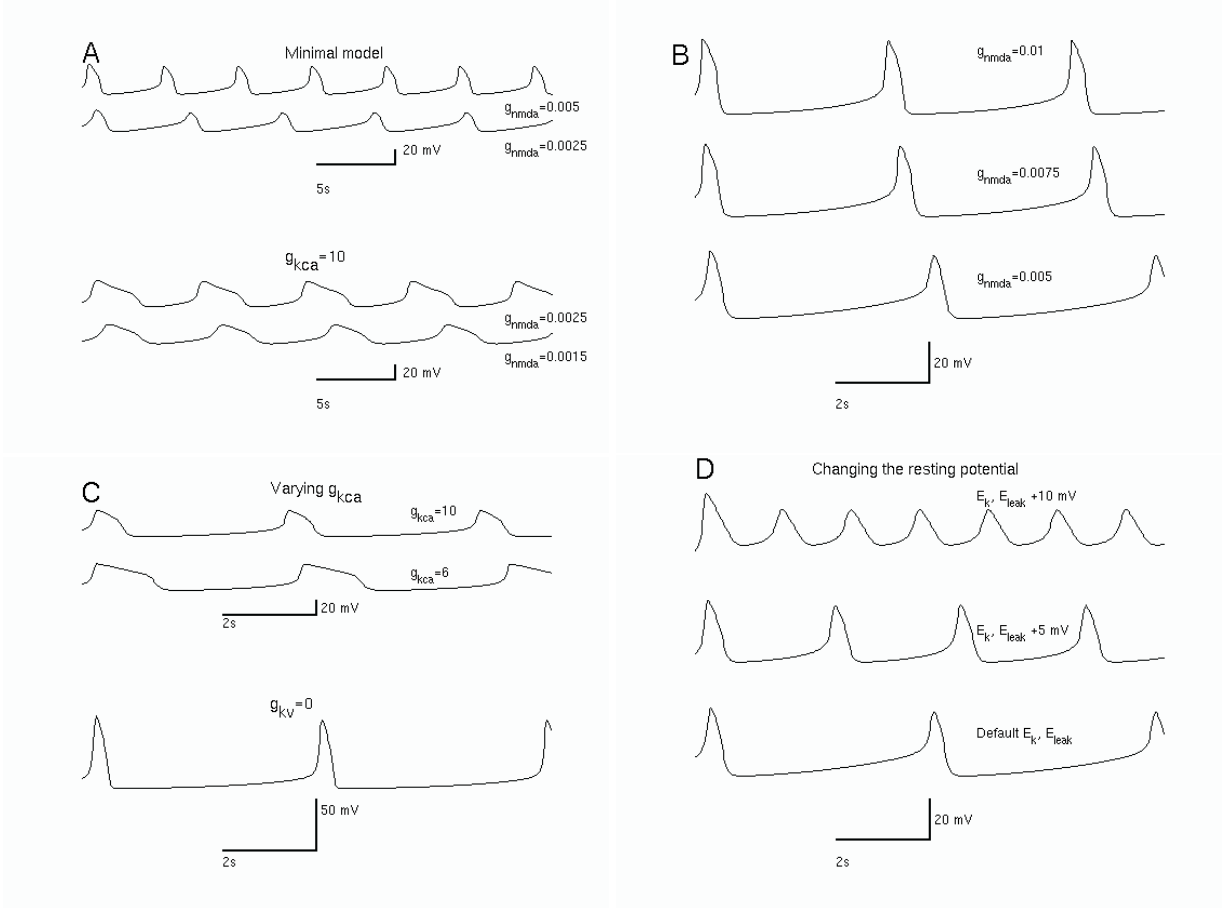

FIG. 4: (A) (upper) NMDA-TTX oscillations generated by the minimal model. (lower) Oscillations generated by the minimal model assuming $g_{kca} = 10$. (B) Oscillations in the full model get increased frequency when the simulated bath NMDA concentration (the g_{nmda} parameter) is increased. (C) (upper) Varying the g_{kca} parameter in the model changes the plateau length of the oscillations. (lower) Simulating TEA application by setting g_k=0 in the model results in large-amplitude oscillations (note scale bar). (D) Changing the resting potential by increasing E_{leak} and E_k results in faster oscillations with smaller amplitudes.

3. The full model reproduces additional experimental results

The full model we obtained by adding the new channels was able to fulfill the criteria we had set up in advance (see Methods). The frequency dependence of the oscillation on the concentration was positive, as in experiments (Fig. 4b); amplitudes and frequencies were in the experimentally observed range; blocking K_V channels gave the characteristic high-amplitude spikes seen in experiments (Fig. 4c, lower trace); and changing the resting potential by depolarizing the model neuron gave oscillations with a higher frequency and a smaller amplitude, again in accordance with experiments (Fig. 4d). When we tried to establish the conditions for obtaining the correct concentration-frequency relationship, we discovered that changing any one parameter could not yield a model with the wrong kind of relationship; at least two variables had to be simultaneously adjusted. Thus, this phenomenon is quite robust in the model. Initial simulations had suggested that the *mgblock* function was important for the phenomenon, but when we substituted a more standard form of steady-state magnesium block function (or expressed in another way, steady-state I-V relationship for the NMDA channel), as based on Ascher and Nowak (1988) and used in e.g. Tegnér *et al.* (1998), the model still displayed the correct frequency dependence.

C. The model is robust to changes in parameter values

1. Amplitude and period sensitivity

We proceeded to make a more formal sensitivity analysis of the full model. To obtain a measure of the quality of a model, parametric sensitivity analysis is frequently used. A common approach to investigate the local sensitivity of a model is to use Metabolic Control Analysis (MCA). MCA was originally developed for metabolic pathways (Heinrich and Rapoport 1974). It has been extended to include sensitivity of amplitudes and periods of autonomously oscillating models (Ingalls 2004). For the model defined in (1) and (2) with parameters p_i given in Table I, the sensitivities of the amplitude and the period are given by the response coefficients

$$R_i^{X_j} = \lim_{t\to\infty} \frac{\delta X_j(t)}{\delta p_i} \tag{12}$$

$$R_i^{T} = \lim_{t\to\infty} \frac{\delta T(t)}{\delta p_i} \tag{13}$$

where X_j denotes the difference between the maximal and minimal value of the potential/concentration in the stationary limit cycle, and T denotes the period of the cycle. To obtain a measure of the relative sensitivity towards individual parametric changes, the response coefficients have been normalized according to

$$R_{i,n}^{X_i} = \lim_{t\to\infty} |\frac{p_i}{X_i(t,p_i)} R_i^{X_i}| \tag{14}$$

$$R_{i,n}^{T} = \lim_{t\to\infty} |\frac{p_i}{T(t,p_i)} R_i^{T}| \tag{15}$$

The results from the local sensitivity analysis can be interpreted as follows. For a 1% modulation of each individual parameter, the normalized response coefficients give the percentage change in amplitude and period, respectively. The local parametric sensitivity analysis of the amplitude and period for the full model where $g_{nmda} = 0.0075$ for a 1% modulation of p_i are shown in Fig. 5. Response coefficients were computed using the Systems Biology Toolbox for MATLAB (Schmidt and Jirstrand 2006). Note that E_{nmda} has been removed from the analysis since its normalized response coefficient would always be zero. Bars show the range of normalized response coefficients obtained for different perturbations, and lines show the mean values.

Examining Fig. 5a, we note that the amplitude is most sensitive to the E_k, v_{half}^{ca} and s_k parameters. However, the relative changes are not especially large: the most sensitive parameter, v_{half}^{ca}, yields about a 2% change in amplitude if changed by 1%. By contrast, the period time can be more sensitively controlled by some parameters. The E_k and s_m parameters both change the period time by about 5% when changed 1% in either direction, while the E_{leak} parameter changes it by approximately 3%. The sensitivity with regard to the s_m parameter shows that the slope of the magnesium block function is important for the resulting period. That E_k and E_{leak} are also important in this regard can be tied to earlier experimental observations (Wallén and Grillner 1987); depolarization of the cell by current injection, which leads to a higher frequency according to the quoted paper, is effectively equivalent to increasing the E_k and E_{leak} parameters (cf. Fig. 4d). In both cases, the holding potential of the cell is depolarized.

2. Admissible parameter intervals

To investigate the effect of global parameter variations we analyzed the full model based on a global search for bifurcations. The range of parameters over which the oscillatory behavior persists (for most initial conditions) was considered. The global parametric sensitivity results for the full model are shown in Table 2. Bifurcation analysis was preformed using the XPPAUT package.

It is evident from this table that most parameters can be changed in rather large parameter ranges while still retaining the oscillations. Although some parameters are close to their upper or lower limits, they can usually be varied quite freely in the other direction. The most constrained parameter appears to be s_k, which can be changed

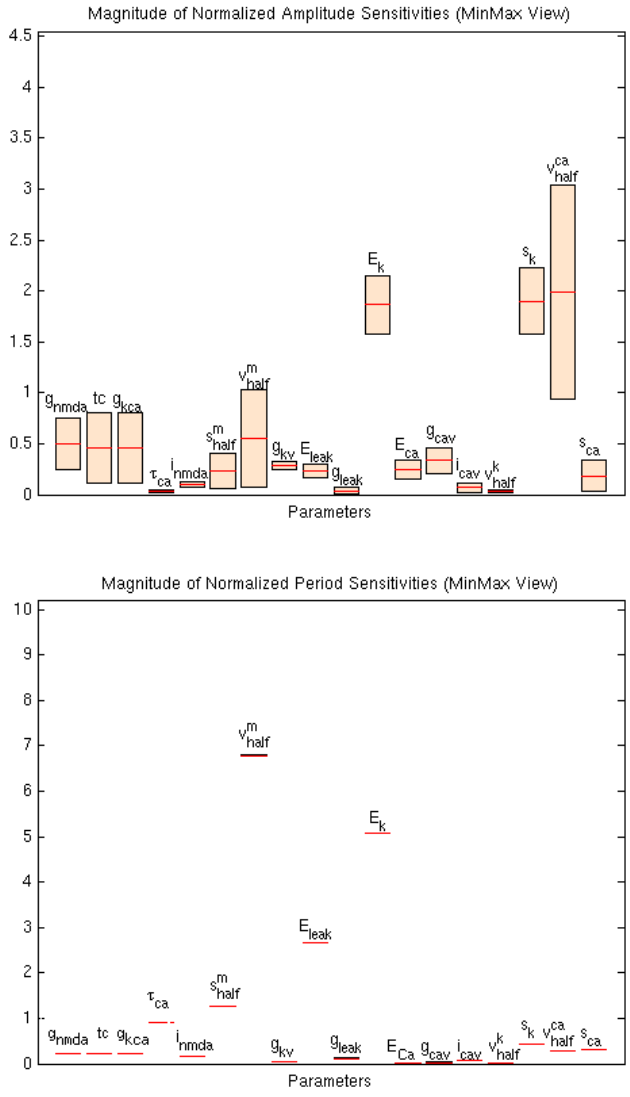

FIG. 5: (a) Normalized sensitivity of NMDA-TTX oscillation frequency on parameters in the model. (b) Normalized parameter sensitivity of oscillation period. In both (a) and (b), the bars show response coefficients obtained for different perturbations, and lines show the mean values.

in a fairly narrow interval between about 0 mV and -7 mV. Thus, the K_V kinetics may be rather important for maintaining the shape of the oscillations; but given the uncertainty of the parameters here, it is more likely that the sensitivity is an artifact of the model. Better steady-state activation data on relatively hyperpolarized levels on the K_V channels should be sought in order to assess their true importance.

3. Modifying the shape of the oscillations

NMDA-TTX oscillations have a wide variety of shapes (see Grillner and Wallén 1985, Wallén and Grillner 1987, El Manira *et al.* 1994, Tegnér *et al.* 1998, Tegnér and Grillner 1999, and the present study). Parameters in our model can be modified to approximate different observed NMDA-TTX oscillations. The plateau length can be regulated most easily by changing e.g. the g_{kca} parameter within the range shown in Table 2 (Fig. 4c, upper traces). As shown by the parametric sensitivity analysis, the amplitude can be manipulated by e.g. changing the E_{leak} and E_k parameters.

D. Phase-plane and dependence on initial conditions

The mechanism underlying the NMDA induced membrane potential oscillations in the full model is a subcritical Hopf bifurcation at $g_{nmda} = 0.00463$. A subcritical Hopf bifurcation is characterized by the coexistence of a stable steady state and a stable limit cycle solution for a certain range of the bifurcation parameter ($g_{nmda} = 0.00428$-0.00463 for the full model). Dependent on the initial conditions the model can thus show either sustained oscillations or a stable behavior for this bifurcation parameter range, as can be seen from the phase plane analysis in Fig. 6. In an experimental context, this would correspond to a bath NMDA concentration just above the minimum concentration needed to obtain oscillations. Due to the difficulties in controlling the local effective concentration of NMDA in a preparation, as well as inherent noise in measurements during experimental conditions, it may be hard to observe this phenomenon in an experiment even if it would actually exist. We did not study whether actual NMDA-TTX oscillations are dependent on initial conditions in this study.

E. Why didn't the previous models capture the correct frequency dependence?

Why, then, didn't the old models - e.g. the one used in Tegnér *et al.* (1998) based on Brodin *et al.* (1991) - show the correct NMDA concentration/frequency behaviour? We concentrate on analyzing an instantiation of the Brodin (1991), as it is a representative example of earlier models. We will call it the "old model" from now on. A newer model (Huss *et al.* 2007) exists and suffers from the same problem, but there the interpretation would be more difficult since the NMDA channels are distributed over the dendritic tree, and many additional parameters are involved. In the old model, all conductances are on the somatic (or axon initial segment) compartment, which simplifies the analysis somewhat.

Running the old model with K_V and Ca_V channels blocked – leaving just NMDA, K_{Ca} and leak channels, as in our minimal model– we discovered that it generated NMDA-TTX oscillations with an exaggerated amplitude (>50 mV), where the plateau was at about -20 mV. Our experiments in this study had shown that the amplitude in this case should be much smaller. Substituting the magnesium block function used in the old model into our minimal model, the same thing happened - the model generated large-amplitude plateaus peaking at approximately -20 mV. The models, in spite of their differences, therefore showed qualitatively similar behaviour in this particular regard.

TABLE II: Admissible parameter ranges for the NMDA-TTX oscillation model

Parameter	Nominal value	Lower limit	Upper limit	Distance%
E_{nmda}	0	-35.91	>100	-
E_k	-80	-85.49	-68.62	6.86
E_{ca}	150	<0	>10000	>100
E_{leak}	-70	-79.25	>0	13.21
i_{nmda}	0.2	0.0002155	0.3534	76.7
i_{cav}	0.3	-0.06716	0.3357	11.90
τ_{ca}	1	0.3759	1.668	62.41
g_{nmda}	0.01	0.00428	> 10	57.20
g_{kca}	20	7.354	30.88	54.40
g_{kv}	8	<0	26.95	>100
g_{cav}	0.0005	<0	>10000	100
g_{leak}	0.001	-0.08666	0.005064	>100
v^m_{half}	-60	-70.16	-57.28	4.53
v^k_{half}	-1	-2.046	>10	>100
$v^c_{half}a$	-45	-68.95	-36.62	18.62
s_m	-1/0.3	-1/0.1446	-1/0.4032	34.4
s_k	-7	-7.11	>0	1.57
s_{ca}	-5	-6.874	3.113	37.48
tc	0.02	0.007354	0.03088	54.40

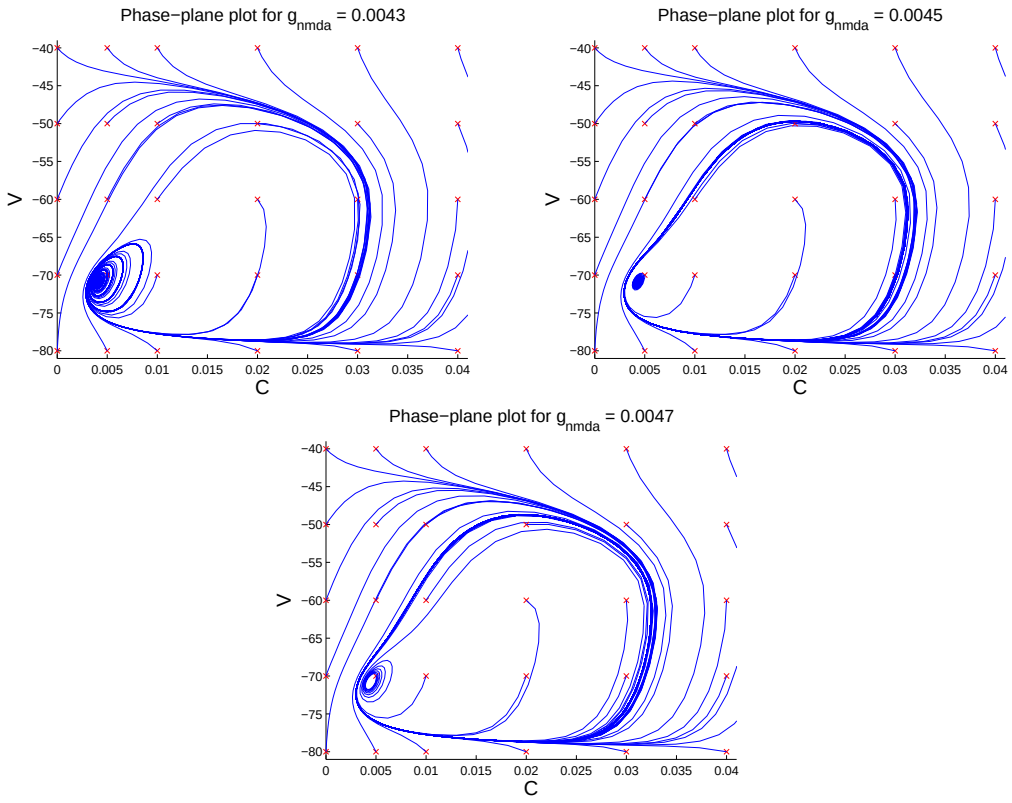

FIG. 6: Phase-plane plot near the bifurcation point of the full model, for $g_{nmda} = 0.0043$, 0.0045 and 0.0047, respectively. Several trajectories starting from different initial conditions are shown. In the $g_{nmda} = 0.0045$ case, a stable fixed point coexists with a stable limit cycle.

Further simulations showed that the given magnesium block function induces a bistability where the minimal model neuron must have either no oscillations or large-amplitude oscillations.

However, this did not yet explain why the old model (and related models) had the incorrect frequency dependence with K_V and Ca_V channels active. By comparing the relative magnitudes of parameters in the two models, we concluded that the "delayed rectifier" conductance in the old model (corresponding to our g_{kv} parameter) was relatively much larger in comparison to the other conductance parameters. By increasing this value substantially in our full model (to $g_k = 200$), while at the same time using the same magnesium block function as in the old model, we observed a negative concentration-frequency relationship in our model.

Thus, the incorrect frequency dependence on bath NMDA concentration in the previous models could be due to a combination of the different magnesium block function and a much higher potassium conductance density. An informal explanation is that both of these factors tend to act as a brake on NMDA activation (the magnesium block function because it is steeper that the one in our model, and the K_V because a higher density of a hyperpolarizing channel will act as a brake on depolarization), and therefore the NMDA conductance in the model must be increased considerably. The large increase in NMDA needed to "overpower" the strong K_V conductance will lead to a relatively large calcium influx, prolonging the resulting plateau.

IV. CONCLUSIONS

We have shown, using experiments, that NMDA-TTX oscillations in lamprey CPG neurons show a positive NMDA concentration-frequency relationship, and that they can be generated even when high-voltage activated calcium channels are blocked. The latter fact suggests the possibility that just NMDA channels and K_{Ca} channels are sufficient to produce these oscillations.

Guided by these experimental results, we have developed an idealized point-neuron model capable of generating NMDA-TTX oscillations similar to those seen in experiments. The model is robust with respect to parameter changes, and effects of channel blockers and other kinds of experimental manipulation can be simulated. By using insights

gained through developing this model, we were able to suggest a plausible reason for why older models tend to show the wrong concentration-frequency dependence.

A primary driver for this work was as a simplified tool for aiding the development of more complex models such as Brodin *et al.* (1991) and Huss *et al.* (2007). By isolating the NMDA-TTX oscillation generating system, it is easier to identify the sufficient conditions for updating more complex models. Indeed, we hope that insights from this paper will be applied by future modellers seeking to better model NMDA receptor mediated activity.

We should mention here that there does exist an earlier computational model of NMDA-TTX oscillations that displays the correct frequency dependence (Moore and Buchanan 1993). Moore and Buchanan used another strategy to build a model of NMDA-TTX oscillations. (Although they just call them "NMDA oscillations" in the paper, they are essentially NMDA-TTX oscillations since no sodium current or any other depolarizing current apart from NMDA is included in the model; they also compare the output of their model with NMDA-TTX oscillations in one of the figures, implicitly suggesting that they should in fact be viewed as NMDA-TTX oscillations.) Although their model has the correct frequency dependence (high NMDA conductance leads to a higher frequency), it gives oscillations with an amplitude of 60 mV or so, which is unrealistically high compared to the maximum value (about 40 mV) observed in experiments. Also, their model does not consider Ca^{2+} or K_{Ca} channels - instead, they postulate a high-voltage activated potassium current with very slow kinetics as the essential hyperpolarizing process in the neuron. Such a current has not been described in lamprey CPG neurons.

As far as extrapolating from NMDA-TTX oscillations to actual locomotor activity, one should be aware that there may be differences between the oscillations in the pharmacologically isolated neurons and in the live network due to experimental conditions. In *in vitro* NMDA-TTX experiments (such as modelled here), the neuron is bathed in NMDA, so that most of its NMDA receptors are likely to be activated (and maybe saturated) at a given time, while in the intact network, the NMDA receptors are transiently activated following action potentials in the presynaptic cells. Keeping these reservations in mind, it is still of interest to examine NMDA-TTX oscillations in single neurons, since they make it possible to infer important details about ion channels in these neurons - information which can be used to better understand the full network. Also, in order to create better and more realistic computer models of the lamprey locomotor network, it is important to make sure that the description of the machinery involved in NMDA oscillations in as accurate as possible.

Our simulations pointed out that the shape of the steady state I-V relationship of NMDA channels in these neurons may be very important for the generation and shape of NMDA-TTX oscillations. In particular, using a conventional form of this relationship, we did not succeed in creating a minimal model that could generate realistic-looking NMDA-TTX oscillations without K_V and Ca_V channels. Experiments to characterize the actual I-V relationship of NMDA channels in dissociated lamprey neurons have been initiated to address this matter.

V. ACKNOWLEDGEMENTS

MH was supported by European Commission grant IST-001917 ("Neurobotics"). JHK acknowledges support from the Swedish Research Council grant VR-M 2005-6423. We thank Ebba Samuelsson, Russell Hill, Peter Wallén, Elling Jakobsen, Sten Grillner, Anders Lansner and Pål Westermark for useful discussions.

VI. REFERENCES

Ascher P and Nowak L. The role of divalent cations in the N-methyl-D-aspartate responses of mouse central neurones in culture. *J. Physiol. Lond.* 399: 247-266, 1988.

Brodin L, Tråvén HG, Lansner A, Wallén P, Ekeberg Ö and Grillner S. Computer simulations of N-methyl-D-aspartate receptor-induced membrane properties in a neuron model. *J. Neurophysiol.* 66: 473-484, 1991.

Brodin L, Grillner S and Rovainen CM. N-Methyl-D-aspartate (NMDA), kainate and quisqualate receptors and the generation of fictive locomotion in the lamprey spinal cord. *Brain Res.* 325: 302-306, 1985.

El Manira A and Bussières N. Calcium channel subtypes in lamprey sensory and motor neurons. *J. Neurophysiol.* 78:1334-1340, 1997.

El Manira A, Tegnér J and Grillner S. Calcium-dependent potassium channels play a critical role for burst termination in the locomotor network in lamprey. *J. Neurophysiol.* 72: 1852-1861, 1994.

Ermentrout, B. Simulating, Analyzing and Animating Dynamical Systems: A Guide to XPPAUT for Researchers and Students. SIAM, Philadelphia, 2002.

Grillner S, Wallén P. The ionic mechanisms underlying N-methyl-D-aspartate receptor-induced, tetrodotoxin-resistant membrane potential oscillations in lamprey neurons active during locomotion. *Neurosci. Lett.* 60: 289-294, 1985.

Guertin PA and Hounsgaard J. Chemical and electrical stimulation induce rhythmic motor activity in an in vitro preparation of the spinal cord from adult turtles. *Neurosci. Lett.* 245: 5-8, 1998.
Heinrich R and Rapoport TA. A linear steady-state treatment of enzymatic chains. Critique of the crossover theorem and a general procedure to identify interaction sites with an effector. *Eur. J. Biochem.* 42:97-105, 1974.
Hess D, Nanou E and El Manira A. Characterization of Na+-activated K+ currents in larval lamprey spinal cord neurons. *J. Neurophysiol.* 97:3484-3493, 2007.
Huss M, Lansner A, Wallén P, El Manira A, Grillner S and Hellgren Kotaleski J. Roles of ionic currents in lamprey CPG neurons: a modeling study. *J. Neurophysiol.* 97:2696-2711, 2007.
Kahn JA. Patterns of synaptic inhibition in motoneurons and interneurons during fictive swimming in the lamprey, as revealed by Cl^- injections. *J Comp Physiol* 147: 189-194, 1982.
Ingalls BP. Autonomously oscillating biochemical systems: parametric sensitivity of extrema and period. *IEE Systems Biology* 1: 62-70, 2004.
MacLean JN, Schmidt BJ, Hochman S. NMDA receptor activation triggers voltage oscillations, plateau potentials and bursting in neonatal rat lumbar motoneurons in vitro. *Eur. J. Neurosci.* 9: 2702-2711, 1997.
Moore L and Buchanan J. The effects of neurotransmitters on the integrative properties of spinal neurons in the lamprey. *J. Exp. Biol.* 175: 89-114, 1993.
Nowak L, Bregestovski P, Ascher P, Herbet P and Prochiantz A. Magnesium gates glutamate-activated channels in mouse central neurones. *Nature* 307:462-465, 1984.
Russell DF and Wallén P. On the control of myotomal motoneurones during "fictive swimming" in the lamprey spinal cord in vitro. *Acta Physiol Scand* 117: 161-170, 1982.
Schmidt, H and Jirstrand M. Systems Biology Toolbox for MATLAB: a computational platform for research in systems biology. *Bioinformatics* 22: 514-515, 2006.
Sillar KT and Simmers A. J. 5-HT induces NMDA receptor-mediated intrinsic oscillations in embryonic amphibian spinal neurons. *Proc. R.Lond. B Biol. Sci.* 255: 139-145, 1994.
Tegnér J and Grillner S. Interactive effects of the GABABergic modulation of calcium channels and calcium-dependent potassium channels in lamprey. *J. Neurophysiol.* 81: 1318-1329, 1999.
Tegnér J, Lansner A and Grillner S. Modulation of Burst Frequency by Calcium-Dependent Potassium Channels in the Lamprey Locomotor System: Dependence of the Activity Level. *J. Comp. Neurosci.* 5: 121-140, 1998.
Wallén P and Grillner S. The effect of current passage on N-methyl–aspartate-induced, tetrodotoxin-resistant membrane potential oscillations in lamprey neurons active during locomotion. *Neurosci. Lett.* 56: 87-93, 1985.
Wallén P and Grillner S. N-methyl-D-aspartate receptor-induced, inherent oscillatory activity in neurons active during fictive locomotion in the lamprey. *J. Neurosci.* Vol. 7: 2745-2755, 1987.

Paper VI

Available online at www.sciencedirect.com
SCIENCE DIRECT®
ELSEVIER
Neurocomputing 58–60 (2004) 431–435
NEUROCOMPUTING
www.elsevier.com/locate/neucom

mGluR-Mediated calcium oscillations in the lamprey: a computational model

Kristofer Hallén[a], Mikael Huss[b,*], Petronella Kettunen[c], Abdeljabbar El Manira[c], Jeanette Hellgren Kotaleski[b]

[a] *Department of Physics and Measurement Technology, Biology and Chemistry, Linköping University, Linköping S-581 83, Sweden*
[b] *Department of Numerical Analysis and Computing Science, Royal Institute of Technology, Lindstedtsv 5, Stockholm S-100 44, Sweden*
[c] *Nobel Institute for Neurophysiology, Department of Neuroscience, Karolinska Institutet, Stockholm S-171 77, Sweden*

Abstract

Slow Ca^{2+} oscillations caused by release from intracellular stores have been observed in neurons in the lamprey spinal cord. These oscillations are triggered by activation of metabotropic glutamate receptors on the cell surface. The pathway leading from receptor activation to the inositol triphosphate-mediated release of Ca^{2+} from the endoplasmatic reticulum has been modelled in order to facilitate further understanding of the nature of these oscillations. The model generates Ca^{2+} oscillations with a frequency range of 0.01–0.09 Hz. A prediction of the model is that the frequency will increase with a stronger extracellular glutamate signal.
© 2004 Elsevier B.V. All rights reserved.

Keywords: mGluR5; Calcium oscillations; Lamprey; Spinal cord

1. Introduction

Calcium is an important intracellular messenger molecule, both in neurons and other cells. Cells at rest have a cytoplasmic Ca^{2+} level around 0.1 μM [3], but the concentration is dynamically regulated and can rise to approximately 1 μM during oscillations [5]. The increase is mainly caused by release of calcium ions from intracellular stores, the most important of which is the endoplasmatic reticulum (ER). Gated channels such

* Corresponding author. Tel.: +46-8-7907784.
E-mail address: hussm@nada.kth.se (M. Huss).

0925-2312/$ - see front matter © 2004 Elsevier B.V. All rights reserved.
doi:10.1016/j.neucom.2004.01.077

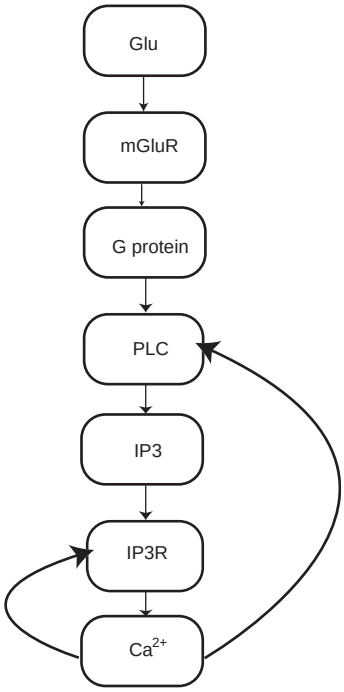

Fig. 1. The main components of the pathway considered in this model.

as the inositol triphosphate (IP3) receptor (IP3R) induce the release of calcium ions from the ER, and ionic pumps work in the other direction to bring Ca^{2+} into the ER.

Intracellular, IP3-mediated calcium oscillations have been observed in the lamprey. These oscillations are dependent on activation of a certain type of metabotropic glutamate receptors (mGluR5, which belong to the group I metabotropic glutamate receptors) on the cell surface [7]. These receptors, in turn, activate G proteins that initiate a biochemical cascade which ends in the binding of IP3 to the IP3R and a subsequent release of calcium from the ER. Fig. 1 shows the main components in the biochemical pathway leading from mGluR5 activation to IP3-induced release of calcium ions from the ER. The actual model contains many more intermediate and parallel reactions, but only the main steps are shown here.

2. Methods

The pathway was modelled using coupled differential equations based on standard biochemical kinetics and adapted from [1]. The equations were initially solved using the XPPAUT package [4]. Binding constants and other parameters were based on values found in the literature. Some of them were modified to improve the qualitative

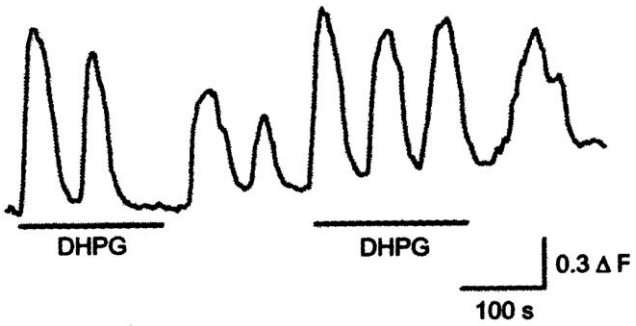

Fig. 2. Experimental response of a neuron to mGluR agonist application, withdrawal and re-application. *x*-axis, time in seconds; *y*-axis, relative intracellular calcium concentration.

behaviour. For instance, the down-regulation of G protein activity is in itself rather slow, but the presence of GTPase-activating proteins (GAPs) increases the rate 1000- to 2000-fold [10]. The model takes into account that PLCβ is such a GAP for the G protein G_q [11].

As for the IP3R, several different models were tried. The best qualitative behaviour in the model, as judged by visual comparison against experimental traces of intracellular calcium concentration levels, was obtained using either the eightstate model described in [12] or the two-variable simplification of this model proposed in [9].

After the full biochemical model had been created using XPP, we implemented it in its entirety into a previously developed compartmental model of a lamprey spinal cord neuron [6]. This was accomplished using the CHEMESIS package [8] together with the GENESIS neural network simulator [2].

3. Results

Our model—depending on the parameter values—gives rise to calcium level oscillations with qualitatively (and sometimes quantitatively) similar behaviour to experimentally observed oscillations.

Fig. 2 (from [7]) shows a typical experimental recording of intracellular Ca^{2+} level oscillations in a lamprey spinal cord neuron. The group I mGluR against DHPG is applied in two distinct steps. When DHPG is removed, the amplitude of the oscillation decays. After re-application of DHPG, the first period of the oscillation has a larger amplitude than the following ones.

Fig. 3 shows a simulation of a similar experimental protocol as the one shown above. Note that the time scales in the simulations are different. However, the oscillatory period in the simulation falls within the observed range for actual lamprey spinal neurons.

It is unknown from experiments whether the intracellular IP3 levels also oscillate during Ca^{2+} oscillations. In our model, the IP3 concentration is oscillatory because of a feedback loop between Ca^{2+} and PLC. If, on the other hand, PLC does not

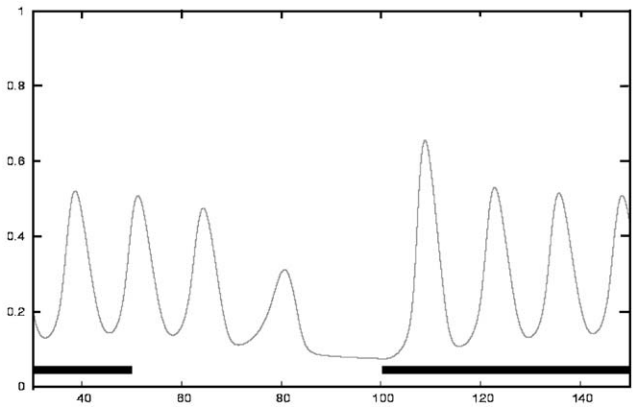

Fig. 3. Computational model's response of a neuron to mGluR agonist application, withdrawal and re-application. *x*-axis, time in seconds; *y*-axis, intracellular calcium concentration in μM. The black bars show the duration of DHPG application and re-application.

require Ca^{2+} for activation, the feedback loop disappears and the IP3 concentration eventually reaches a constant level rather than oscillating. We simulated this scenario and found that the Ca^{2+} oscillations are retained. Thus, the IP3 level does not need to be oscillatory for Ca^{2+} oscillations to occur. Further experiments are needed to find out whether the IP3 levels are indeed oscillatory in lamprey spinal cord neurons.

We also made some exploratory attempts to connect the slow calcium oscillations to the ion channel machinery of the cell. It was shown in [7] that calcium influx through L-type calcium channels is necessary to obtain intracellular Ca^{2+} oscillations. Some of these channels may be open at -60 mV (close to the resting potential of these neurons) which would allow a small but steady influx of calcium ions. We introduced a calcium pool containing calcium that enters through L-type calcium channels at low membrane voltages. The calcium in the pool is degraded with a characteristic time constant. This calcium pool, in the model, replenishes the intracellular calcium with a rate dependent on the concentration difference in the soma and the L-type calcium pool.

With such a model, slow intracellular calcium oscillations are obtained only when the L-type channels are working (results not shown). However, since no experimental evidence exists for the nature of the link between L-type calcium channels and somatic calcium level oscillations, these results must be considered for what they are: suggestions for possible mechanisms and nothing else.

It is known from experiments that intracellular Ca^{2+} oscillations are correlated with a slowing down of the swimming rhythm in the lamprey. We examined if intracellular calcium oscillations could slow down the oscillation rhythm in a single neuron if its calcium-dependent potassium channels were sensitive to intracellular calcium concentration. Indeed, the oscillation frequency was seen to slow down somewhat in simulations using such a mechanism (results not shown). However, experimental evidence seems to indicate that calcium-dependent potassium channels are not involved in this

phenomenon since activation of mGluR5 by DHPG does not induce any change in the resting membrane potential [7].

4. Conclusions

We have built a model to simulate intracellular, mGluR-mediated calcium level oscillations occurring in lamprey spinal cord neurons. It was found that a good qualitative agreement between the model and experimental results can be obtained. The model generates Ca^{2+} oscillations with a frequency range of 0.01–0.09 Hz, as compared to 0.005–0.033 in the actual lamprey neurons. The model also predicts that an increased level of glutamate will increase the frequency of the oscillations.

The biochemical model has been incorporated into a previously developed electrophysiological model of a lamprey spinal neuron. This combined model can be used to probe possible ways that voltage-gated calcium inflow might be connected to intracellular calcium levels, and hypothetical mechanisms by which the intracellular calcium could control the frequency in a spinal interneuronal network.

References

[1] U. Bhalla, R. Iyengar, Emergent properties of networks of biological signaling pathways, Science 283 (1999) 381–387.
[2] J. Bower, D. Beenman, The Book of Genesis, TELOS, 1998.
[3] P. Cullen, J. Lockyer, Integration of calcium and ras signalling, Nature Rev. Mol. Cel. Biol. 3 (2002) 339–348.
[4] B. Ermentrout, Xpp/xppaut homepage, http://www.math.pitt.edu/∼bard/xpp/xpp.html, Web page, last visited 030220.
[5] G. Houart, G. Dupont, A. Goldbeter, Bursting, chaos and birythmicity originating from self-modulation of the inositol 1,4,5-triphosphate signal in a model for intracellular Ca^{2+}, Bull. Math. Biol. 61 (1999) 507–530.
[6] M. Huss, D. Hess, B.L. d'Incamps, A.E. Manira, A. Lansner, J.H. Kotaleski, Role of a-current in lamprey locomotor network neurons, Neurocomputing 52–54 (2003) 295–300.
[7] P. Kettunen, P. Krieger, D. Hess, A.E. Manira, Signaling mechanisms of metabotropic glutamate receptor 5 subtype and its endogenous role in a locomotor network, J. Neurosci. 22 (5) (2002) 1868–1873.
[8] J.H. Kotaleski, K. Blackwell, Modeling the dynamics of second messenger pathways, Neuroscience Databases: A Practical Guide, Kluwer Academic Publishers, Norwell, MA, 2002.
[9] Y. Li, J. Rinzel, Equations for insp3 receptor-mediated [Ca^{2+}] oscillations derived from a detailed kinetic model: a Hodgkin-Huxley-like formalism, J. Theor. Biol. 166 (1994) 461–473.
[10] S. Mukhopadhyay, M. Elliot, Rapid gtp binding and hydrolysis by gq promoted by receptor and gtpase-activating proteins, Biochemistry 96 (1999) 9539–9544.
[11] M. Ross, T. Wilkie, Gtpase-activating proteins for heterotrimeric g proteins: regulators of g protein signaling (rgs) and rgs-like proteins, Annu. Rev. Biochem. 69 (2000) 795–827.
[12] G.D. Young, J. Keizer, A single-pool inositol 1,4,5-trisphosphate-receptor-based model for agonist-stimulated oscillations in Ca^{2+} concentration, Proc. Natl. Acad. Sci. USA 89 (1992) 9895–9899.